This is to certify that the
dissertation entitled

SYNTHESIS AND BIOINORGANIC APPLICATIONS OF MANGANESE CORROLE AND BINUCLEAR METALLOCORROLE

presented by

Fei Yam

has been accepted towards fulfillment
of the requirements for the

Ph.D. degree in CHEMISTRY

Chi K. Chang
Major Professor's Signature

Dec 30, 2008
Date

SYNTHESIS AND BIOINORGANIC APPLICATIONS OF MANGANESE CORROLE AND BINUCLEAR METALLOCORROLE

By

Fei Yam

A DISSERTATION

Submitted to
Michigan State University
in partial fulfillment of the requirements
for the degree of

DOCTOR OF PHILOSOPHY

Chemistry

2009

ABSTRACT

Synthesis and Bioinorganic Applications of Manganese Corrole and Binuclear Metallocorrole

By

Fei Yam

This thesis is concerned with the synthesis of novel corrole macrocycles and the applications of their metal complexes in mediating epoxidation reactions and hydrogen dismutation. Corrole is a porphyrin analogue capable of stabilizing high-valent metal ions. A series of cofacial biscorroles bearing various spacer groups have been synthesized. The dimanganese biscorroles were found to have a surprisingly high activity in catalyzing the dismutation of H_2O_2 to give O_2 and H_2O, similar to the enzymatic reaction of catalase. An asymmetric Mn(III) Mn(V)-oxo transient intermediate was proposed to account for the elevated reactivity. A series of hetero binuclear biscorroles such as [Mn Al] and monomeric Mn(III) corroles equipped with an intramolecular proton donor were synthesized to show that the catalase-like reactivity may be associated with the presence of a Lewis acid and is consistent with a proton-assisted mechanism during the peroxide bond fission. Also synthesized was a series of sterically encumbered Mn-corroles in which both faces of the corrole ring are shielded to enhance the stability of the high-valent Mn(V)-oxo intermediate. Such Mn-corroles were capable of catalyzing epoxidation of olefins by an oxene-transfer reaction analogous to cytochrome P-450

chemistry. The shielding structure also provided a higher level of chemoselectivity in favor of the more exposed or less substituted double bond on the substrate. Furthermore, it was possible to isolate a relatively stable Mn(V)-oxo intermediate with a terphenyl-shielded corrole to permit resonance Raman study for the first time in solution at room temperature. The observed Mn(V)-O^{16} stretching frequency at 952cm^{-1} and that of Mn(V)-O^{18} at 913 cm^{-1} could be interpreted in terms of a Mn(V)≡O triple bond. In another study, iron complexes of the sterically shielded corroles were prepared and the binding of such Fe-corroles to various ligands (such as chloride, nitrosyl and *N*-methylimidazole) were examined. Unfortunately, even with the sterically shielded structure in place, the iron corrole decomposed rapidly in the presence of PhIO or mCPBA oxidant, preventing further investigation of the high-valent intermediate. Finally, the reactivity of Mn-corrole imbedded in supermolecular hydrogel or organogel have been explored. The t-butyl hydroperoxide oxidation of various sulfides in the presence of the Mn-corrole in gel matrix was found to increase selectively the twice-oxidized sulfone at the expense of the less-oxidized sulfoxide, presumably due to diffusion phenomenon within the gel to alter the local concentration of reactants. Thus, the gel matrixes show promises to become a new platform for exploring biomimetic materials.

This thesis is dedicated to my love (Fion) and my family for their support and love.

ACKNOWLEDGMENTS

I would like to express my deepest respect and gratitude to Dr. Chi K. Chang for his help and advice during the course of my graduate study. I thank him for providing me great opportunities to learn at MSU.

I would like to thank Drs. Gregory L. Baker, Babak Borhan and James McCusker for serving as my guidance committee members and for their helpful discussion.

I would also like to thank Drs. Richard Staples and Rui Huang for their help in obtaining X-ray crystal structures that I presented in this dissertation. Dr. Rui Huang is also appreciated for teaching me of running the beach-top GC-MS spectrometer and helping to obtain the MS spectra of some molecules in my graduate study.

Also, I am grateful to the group members in Dr. Chang's research group in Hong Kong, especially to Drs. Hai-Yang Liu and Lam-Lung Yeung for their helpful discussions and friendship.

Friendships from Kin-Sing Lee and Man-Kit Lau are appreciated. I will never forget their understanding and sharing my tears and happiness at MSU. They made my life and study at MSU enjoyable and memorable.

At last, but not the least, I want to thank my family for their invaluable love and support, special appreciation goes to my the one, Fion, for her patience and love. Without them, my life means nothing.

TABLE OF CONTENTS

(Images in this dissertation are presented in color)

LIST OF TABLES

LIST OF FIGURES

ABBREVIATION

$H_3F_{15}C$	5,10,15-tris(pentafluorophenyl)corrole
$H_2F_{20}P$	5,10,15,20-tetrakis(pentafluorophenyl)porphyrin
$H_3F_{23}C$	2,3,7,8,12,13,17,18-octafluoro-5,10,15-tris(pentafluorophenyl)corrole
OEC	2,3,7,8,12,13,17,18-octaethylcorrole
OEP	2,3,7,8,12,13,17,18-octaethylporphyrin
H_6DCA	*1, 8-bis{10-[5,15-bis(pentafluorophenyl)corrolyl]}-anthracene*
H_6DCB	*4, 6-bis{10-[5,15-bis(pentafluorophenyl)corrolyl]}-dibenzyofuran*
H_6DCX	*4, 5-bis{10-[5,15-bis(pentafluorophenyl)corrolyl]}-9,9-dimethylxanthene*
Mn_2DCA	*di-manganese-1, 8-bis{10-[5,15-bis(pentafluorophenyl)corrolyl]}-anthracene*
Mn_2DCB	*di-manganese-4, 6-bis{10-[5,15-bis(pentafluorophenyl)corrolyl]}-dibenzyofuran*
Mn_2DCX	*di-manganese-4, 5-bis{10-[5,15-bis(pentafluorophenyl)corrolyl]}-9,9-dimethylxanthene*
$MnF_{15}C$	Manganese-5,10,15-tris(pentafluorophenyl)corrole
$H_3Br_4F_7C$	*5,15-bis(2,6-dibromo-4-fluorophenyl)-10-(pentafluorophenyl)corrole*
$H_3Br_6F_3C$	*5,10,15-tris(2,6-dibromo-4-fluorophenyl)corrole*
$H_3T_2F_5C$	*5,15-bis(2,4,6-tertphenyl)-10-(pentafluoro-phenyl)corrole*
H_3T_3C	*5,10,15-tris(2,4,6-tertphenyl) corrole*
$MnBr_4F_7C$	Manganese-*5,15-bis(2,6-dibromo-4-fluorophenyl)-10-(pentafluorophenyl)corrole*
$MnBr_6F_3C$	Manganese-*5,10,15-tris(2,6-dibromo-4-fluorophenyl)corrole*

MnT_2F_5C	Manganese-*5,15-bis(2,4,6-tertphenyl)-10-(pentafluoro-phenyl)corrole*
MnT_3C	Manganese-*5,10,15-tris(2,4,6-tertphenyl) corrole*

Chapter 1

Introduction

1-1. Background

Corrole is a tetrapyrrolic macrocycle analogue of porphyrin. The name "corrole" was introduced by Johnson and Price in 1960, as a derivative of corrin (Figure 1-1),[1] and they reported the first synthesis of corrole via photocyclization of 1',8'-dideoxybiladiene-*ac* as shown in Figure 1-2. Corrole was synthesized as a precursor of the corrin ring, which is the chromophore of a cobalamine-vitamin-B_{12} model compound.[2,3]

Corrole Corrin

Figure 1-1. Structures of corrole (i.e. tetradehydrocorrin) and corrin.

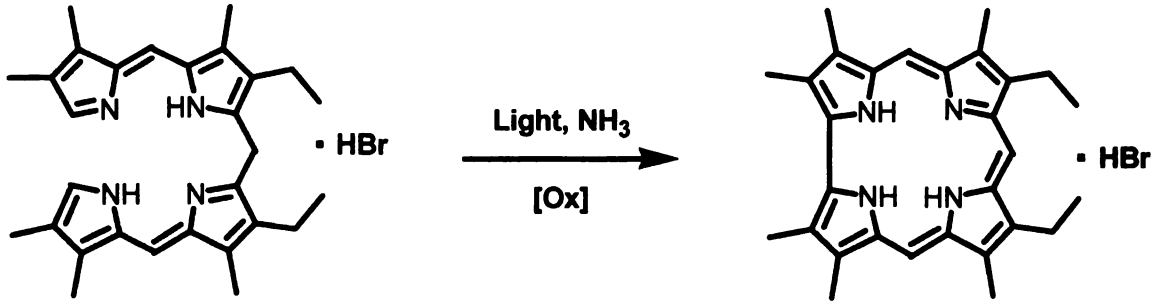

Figure 1-2. Synthesis of 8,12-diethyl-2,3,7,13,17,18-hexamethylcorrole.[2]

The numbering scheme of corrole was derived from that of porphyrin and the only difference between the two rings is the deletion of the position 20 *meso* carbon in corrole. All other carbons are assigned from 1 to 19 and the central nitrogens are numbered from 21 to 24, retaining the same numbering scheme as that in porphyrin (Figure 1-3).

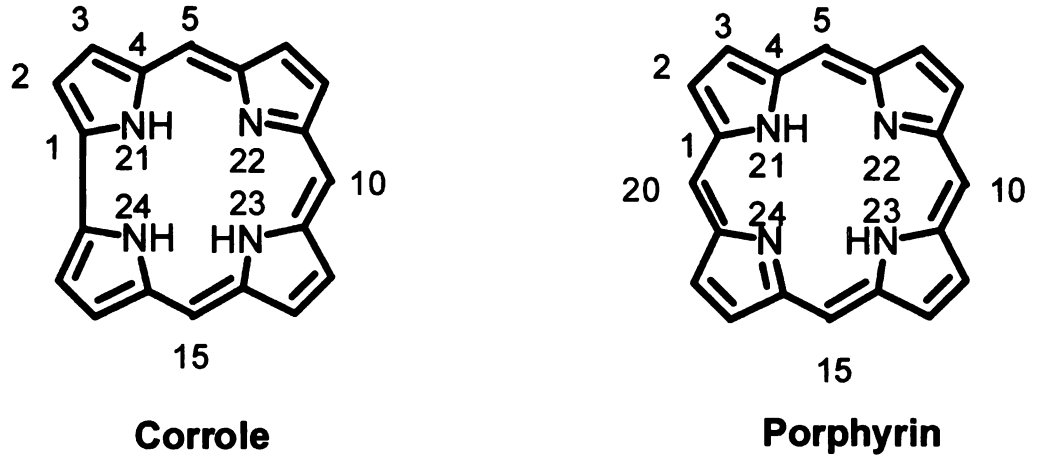

Figure 1-3. Numbering scheme of corrole and porphyrin.

The missing of the *meso* carbon-20 in corrole reduces its symmetry to C_{2v} from D_{4h} of the corresponding porphyrin. The reduction in symmetry imparts the corrole ring many distinct properties not shared by porphyrin.

In porphyrin, the two imino nitrogen atoms are scrambled due to valence tautomers; in corrole, the single imino nitrogen atom is localized at position 22 (or 23), according to the calculations performed by Dyke et al.[7] The 3 N-H hydrogen atoms undergo tautomerism over the 4 nitrogen atoms in the corrole

central core (Figure 1-4). The imino nitrogen located at N22 is more favored than at N21. This is supported by NMR spectra showing higher electron density on ring A and D than on B and C. Using low temperature H-NMR spectrum the activation enthalpy, $\Delta G^{\ddagger}$, of the tautomerization process across the pyrrole rings A-D can be roughly estimated at 11.5kcal/mol, which is comparable to the values found in porphyrins (10-15kcal/mol).[8]

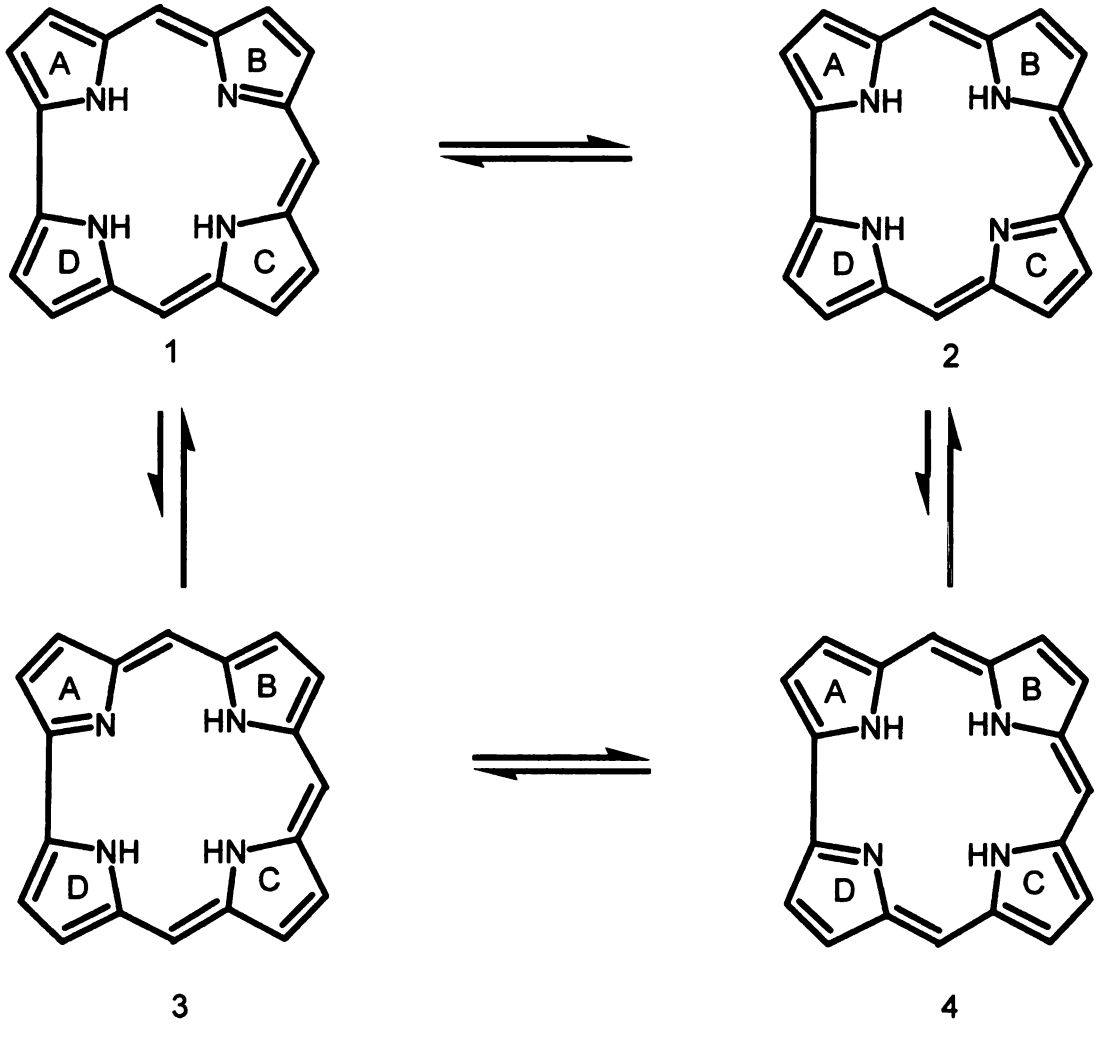

Figure 1-4. Schematic representation of the NH tautomerism in OEC (ethyl substituents omitted)

Similar to porphyrin, corrole is aromatic (18 π-electron chromophore, Figure 1-5)[2~4] with an intense band at around 400nm and several weaker bands in the region of 500-650nm. They are related to the Soret and Q-bands present in porphyrin (Figure 1-6). Free-base corrole (H_3Cor) can be protonated or deprotonated easily to give H_4Cor^+ and H_2Cor^- by CF_3COOH and Et_3N, respectively. The Soret band intensity remains strong in all these forms is an evidence that the conjugation of π-electrons has not been interrupted upon protonation and deprotonation.[4] Corrole also has an intense luminescence band around 600-650nm with a lifetime in nanoseconds.[9]

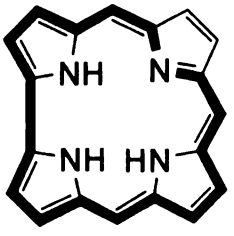

Corrole

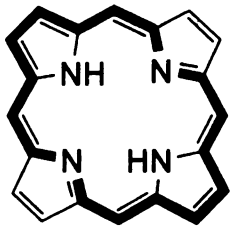

Porphyrin

Figure 1-5. One example of the 18 π-electron skeleton of corrole and porphyrin chromophore.

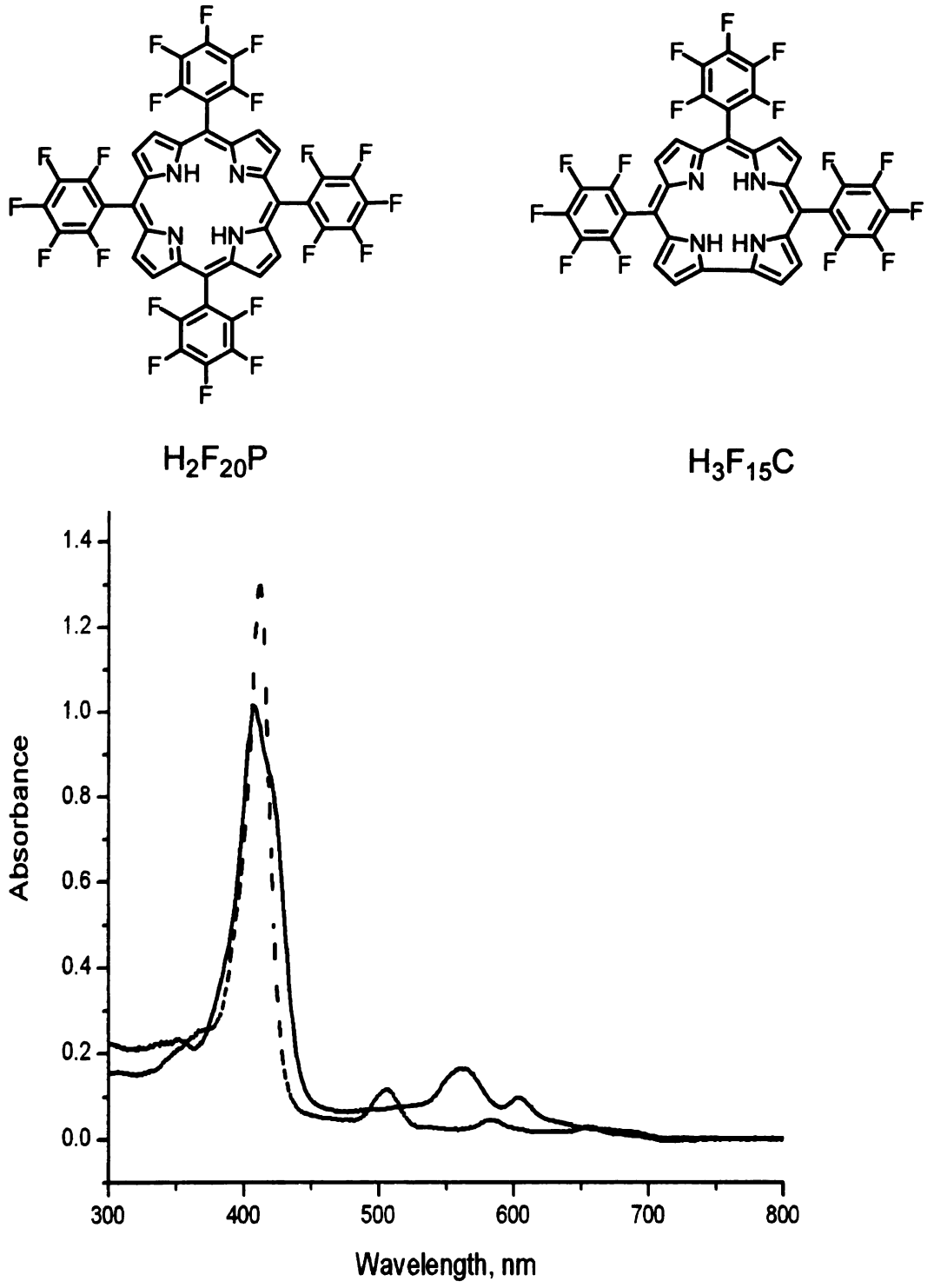

Figure 1-6. Molecular structure and UV-Vis absorption spectra of corrole, $H_3F_{15}C$ (—) and porphyrin $H_2F_{20}P$ (---).

^{1}H-NMR of corrole exhibits a diamagnetic ring current effect similar to that observed in porphyrin. For example in ^{1}H-NMR of $H_2F_{20}P$ and $H_3F_{15}C$, the resonance of inner nitrogen protons of corrole is at δ=-2.25 ppm, which compares well with that of the nitrogen protons of porphyrin at δ=-2.9 ppm.[9]

In terms of chemical stability, corrole tends to be less robust than porphyrin towards oxidative reactions. The free-base octaalkylcorrole undergoes oxidative ring opening to the corresponding biliverdin in the presence of air and light in solution. The decomposition pathway is not fully understood; the proposed mechanism suggests that dioxygen attacks the pyrrole-pyrrole linkage between C1 and C19 on the corrole ring and the oxetane formed can lead to ring cleavage to give biliverdin (Figure 1-7). This reaction highlights the unstable nature of free base corrole.[4,10]

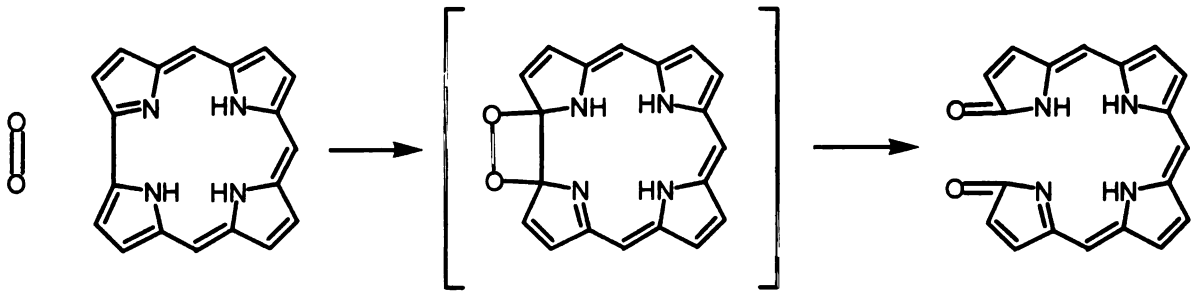

bilverdin

Figure 1-7. Proposed oxidative decomposition reaction of corrole.

1-2. Synthesis

For a long time corrole remained in the shadow of porphyrin until quite recently when novel and facile synthetic routes were discovered. In early 1996, Rosa *et al.* reported the isolation of *meso*-tris(4-tert-butyl-2,6-dinitrophenyl)corrole as an inadvertent by-product from the classical Rothemund synthesis (condensation of pyrrole and benzaldehyde in hot acid).[11] In 1999, several groups working independently reported new synthetic methods for corroles. Gross *et al.* developed the synthesis of 5,10,15-tris-pentafluorophenylcorrole ($H_3F_{15}C$) directly from pyrrole and pentafluorobenzaldehyde in solvent-free condition (Scheme 1-1), now known as the one-pot solvent-free synthesis.[9] The method was used as well to produce *meso*-tris(2,6-difluorophenyl)corrole, *meso*-tris(2,6-dichlorophenyl)corrole, and *meso*-tris(heptafluoropropyl)-corrole.[12~13] This procedure seems to work best for electron-deficient aldehydes. At the same time, these electron deficient substituents render the corrole ring more robust. Indeed, a very stable perfluorinated $H_3F_{23}C$, synthesized more recently in our group, is a good example of such electronic effect (see p.10~11).[14]

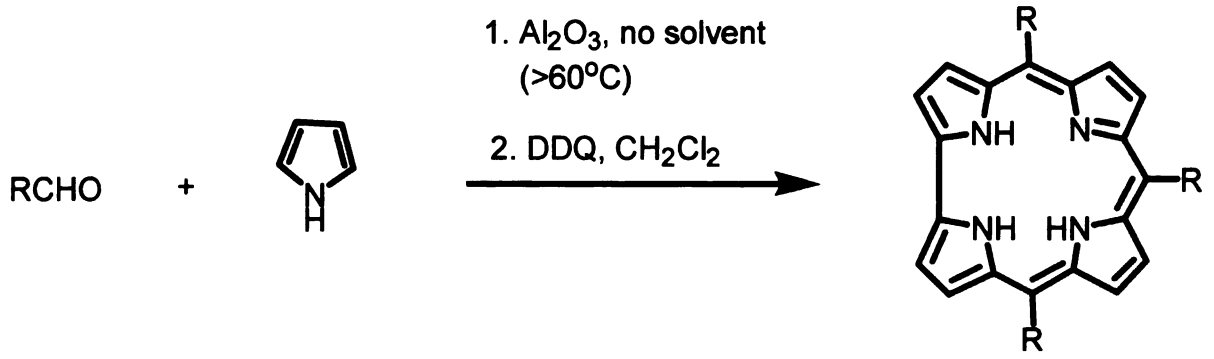

Yield: 1~5%

R= 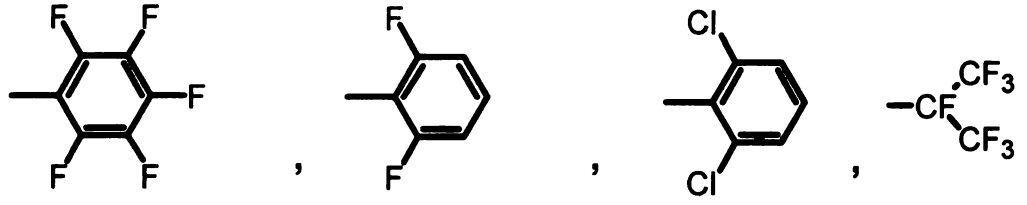

Scheme 1-1. "One-pot solvent-free" synthesis of corroles from electron-withdrawing aldehydes.[9,12~13]

In 1999 also, Paolesse *et al.* prepared a wide variety of free-base triaryl corroles under the standard Rothemund-Adler-Longo reaction condition with glacial acetic acid solvent using a pyrrole/aldehyde molar ratio of 3:1 (Scheme1-2).[15~16]

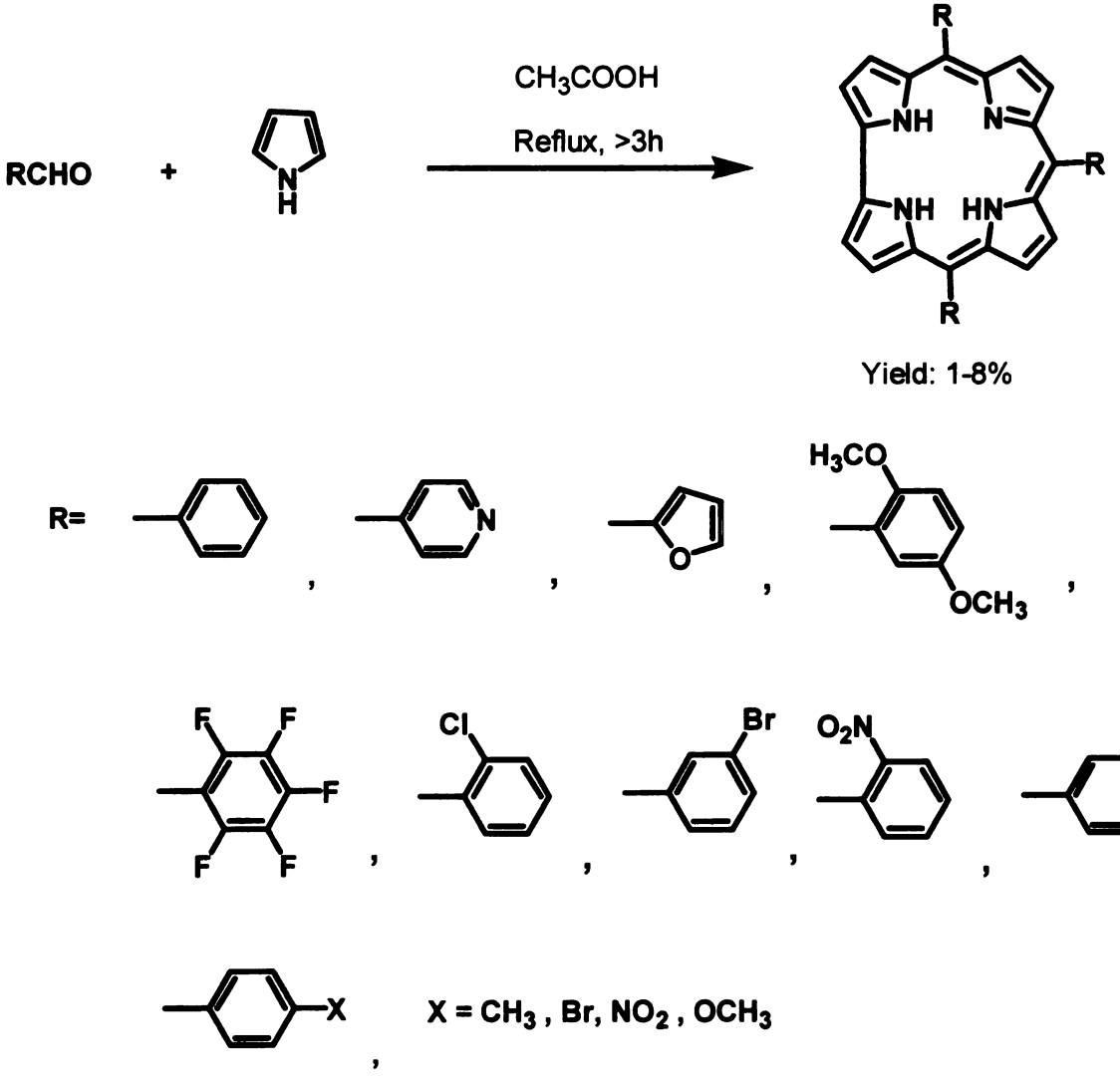

Scheme 1-2. One-pot corrole syntheses in refluxing acetic acid.[15~16]

This procedure is widely applicable except for those 2,6-disubstituented aldehydes such as mesitaldehyde, 2,6-dichlorobenzaldehyde, or 2,6-dimethoxybenzaldehyde.

The one-pot solvent-free method was later modified by Ghosh *et al.*,[17] which turned out to be more general to include both electron-rich and electron-deficient *meta*-substituted aromatic aldehydes (Scheme 1-3). Moreover, the application of the solvent-free method has been extended from pyrrole to 3,4-difluoropyrrole by Ghosh to produce the corresponding β-octafluoro-meso-triaryl corroles.[18]

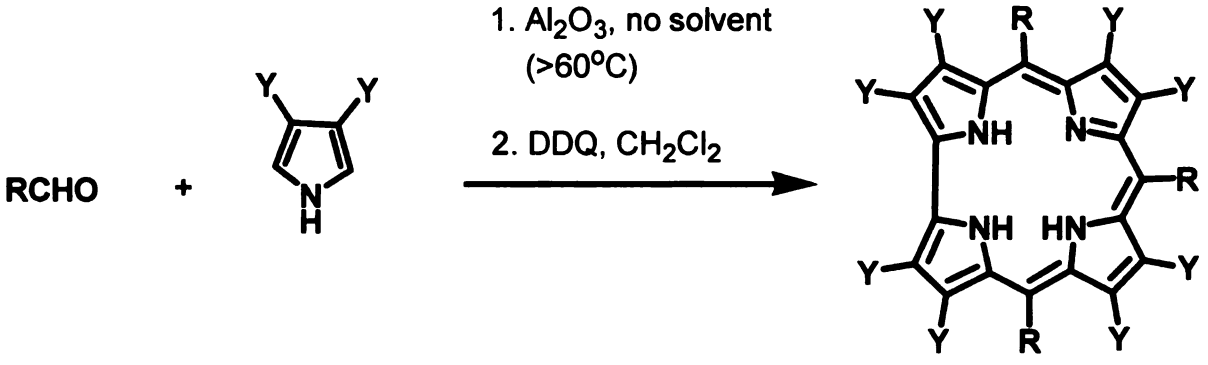

Yield: 3-18%

R= 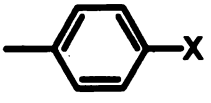 X = OCH_3 , CH_3 , H , Br, CF_3 ; Y = H

,

X = OCH_3 , CH_3 , H , CF_3 ; Y = H

Scheme 1-3. One-pot solvent free corrole synthesis reported by Ghosh.[17~18]

However, the Ghosh modification failed to obtain the condensation product of 3,4-difluoropyrrole and petafluorobenzaldehyde to yield the prized perfluorinated triphenylcorrole ($H_3F_{23}C$). The first report on the synthesis of $H_3F_{23}C$ by Chang *et al.*[14] noted the original condition of one-pot corrole

synthesis was unsuitable for $H_3F_{23}C$ in that a linear bilene intermediate could be isolated, which failed to cyclize, presumably because of the low nucleophilicity of the bilene. Irradiation of this bilene in CH_2Cl_2 under an ammonia atmosphere (the original procedure of Johnson's synthesis of corrole[2~3]) then led to the formation of $H_3F_{23}C$ (Figure 1-8).

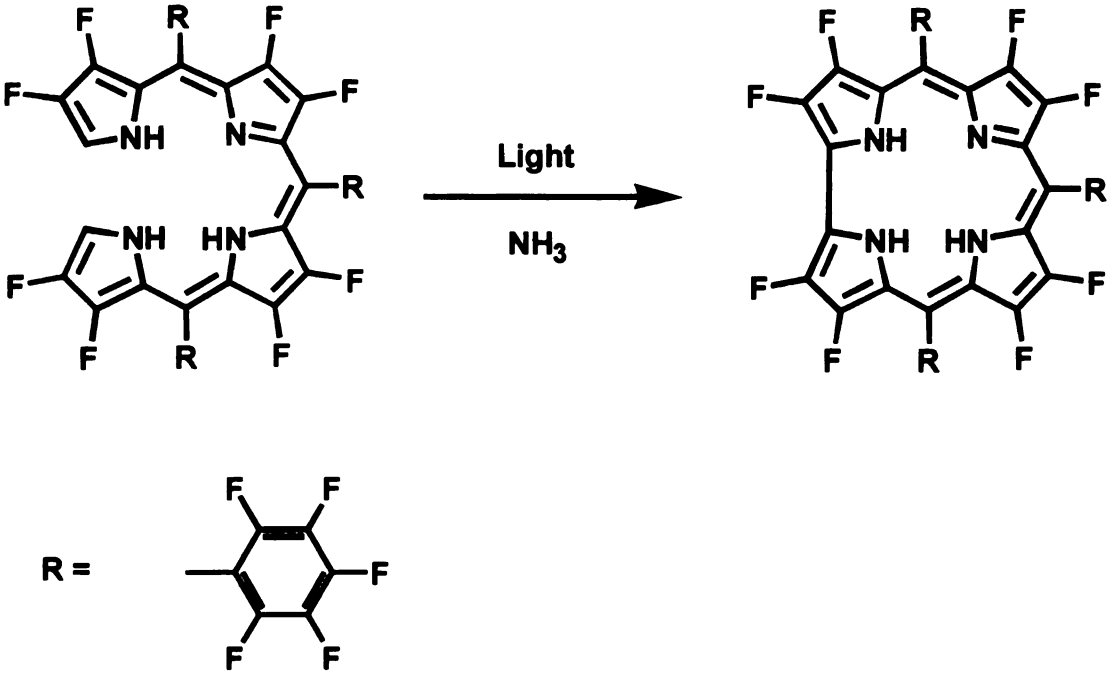

Figure 1-8. Production of perfluorinated corrole $H_3F_{23}C$ from its bilene.

Chang's group also reported that minor modifications in the solvent-free procedure can still give $H_3F_{23}C$ in a low but acceptable yield of 5%.[14]

Recently, Collman and Decréau reported a fast microwave-assisted version of the solvent-free corrole synthesis that improved the yield by about 30% over those observed by Gross and Ghosh. A variety of fluorinated aromatic aldehydes and 4-pyridylcarbaldehyde were condensed with pyrrole giving 13-15% yields of the corresponding *meso*-triaryl corroles by this procedure.[19]

Subsequently, Gryko *et al.* reported the general preparation of various triaryl corroles by a stepwise synthesis.[20~21] This multistep version of the Paolesse one-pot acid-catalyzed synthesis involves the isolation of an aryl dipyromethane, which then condenses with a second aldehyde to produce trans-A_2B-type meso-triaryl corroles. Since then, numerous modifications have been introduced[22~29] and the yield of corrole has been improved from 1-6% [9,15] to over 20%.[28]

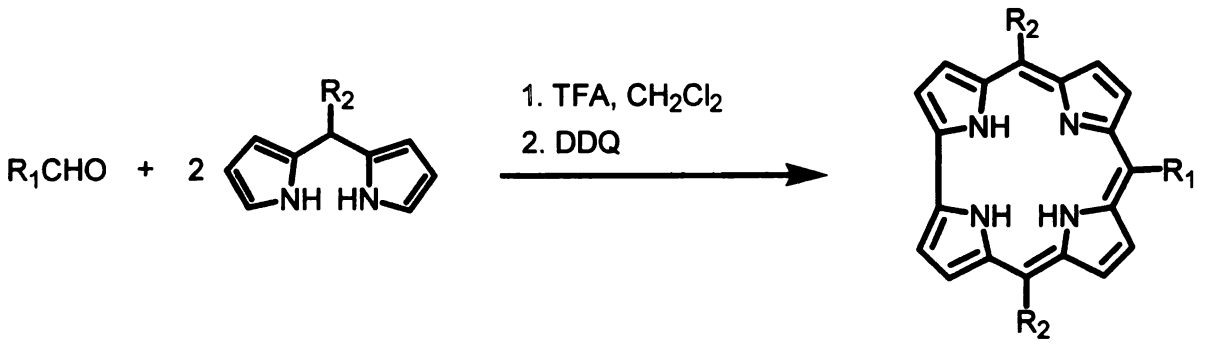

Yield: 8-22%

Scheme 1-4. General synthesis of triarylcorrole from dipyromethane.[20~24]

The past 9 years have seen dramatic developments in corrole synthesis and these advances have changed the state of the art: from lengthy preparation of

multi-pyrrolic intermediates to simple and easy one-pot synthesis; and from a limited selection of meso-triaryl groups (electron-deficient, A_3-type) to a great variety of substituents (electron-deficient, electron rich, 2,6-disubstituted, *trans*-A_2B-type). Furthermore, various substituents can be introduced at the β-positions of pyrrole with acceptable yields. By using these refined methods, free-base corroles and their metal complexes can be prepared in gram quantities, and some free-base corroles have become commercially available. As a result, the properties of their metal complexes have been studied in many fields,[30~39] and such renewed attention has largely increased the number of scientific publications on corroles.[30]

The research on corrole chemistry has identified numberous interesting and unique properties of corroles as well as their metal complexes that may find applications in chemical sensor, catalysis,[41] photodynamic therapy[42] and as building blocks of supramolecular assembly.[43] Since recent advances have basically overcome the synthetic difficulties, the future of corrole research looks promising.

One of the most distinct features of corrole is the presence of three protons in the inner core, which renders it a trianionic ligand. Moreover, the smaller central cavity of corrole stabilizes metal atoms with small ionic radii in high oxidation states, it seems the most stable oxidation number in metallocorrole often being one positive charge higher than its porphyrin analogues, such as

Cu^{III}, Ag^{III}, Mn^{IV} and Fe^{IV}, at least in the formal sense regardless of the exact description of their electronic structure.[33-40] Due to such characters, metallocorrolates might be good models of heme enzymes.[41~43] In my studies, we are interested in mimicking the high valant reactive intermediates that are involved in heme enzyme catalytic cycles such as in cytochrome P-450 monooxygenase[45~48] and dimeric catalase.[49~50] In the following sections, recent advances of iron and manganese corrole complexes are reviewed.

1-3. Iron corrole

Iron corroles have received much attention in recent years, mainly due to their unique properties that are clearly related but distinguishable from those of porphyrins.[41~43] Most importantly, the electronic configuration of iron corrole complex has been studied extensively because of the stable formal oxidation state is often +1 higher than the corresponding iron porphyrin complex. For example, in pyridyl complexes, $(OEP)(Py)_2Fe(II)$ and (OEC)(Py)Fe(III), the oxidation state of iron in porphyrin is +2 whereas in corrole, it is +3; in the phenyl complexes, (OEP)(Ph)Fe(III) and (OEC)(Ph)Fe(IV), the oxidation state of iron in porphyrin is +3 whereas in corrole, it is +4 (Figure 1-9).[51]

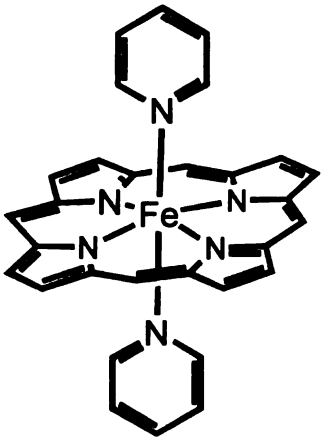

(OEP)(Py)$_2$Fe(II)

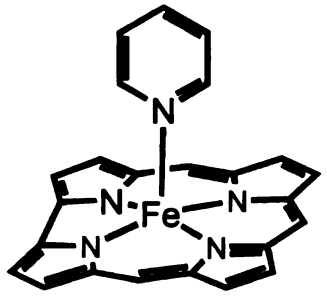

(OEC)(Py)Fe(III)

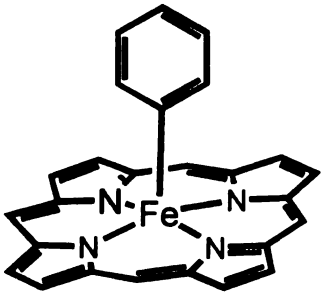

(OEP)(Ph)Fe(III)

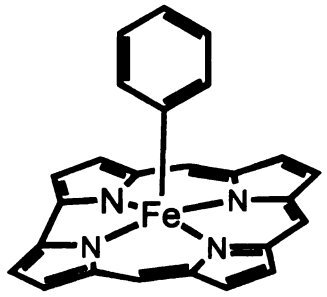

(OEC)(Ph)Fe(IV)

Figure 1-9. The structures of iron porphyrins and iron corroles (ethyl groups are omitted).

In the two cases above, the oxidation state of iron center in corrole is clearly established as +3 (d^5 with S=3/2) and +4 (d^4 with S=1). However, the formal oxidation state of the metal in Fe(X)-corrole (X=F, Cl, Br, I) has been debated either as Fe(IV), suggested by Gross *et al.*[60~63] or as Fe(III)cor$^{+\cdot}$ (corrole cationic radical) suggested by Walker[53~57] and Ghosh[58~59] *et al.*. NMR, EPR, crystal data and DFT calculations suggested the electronic configuration of Fe(X)-corrole complexes should be S_1=3/2 Fe(III), S_2=1/2 (Cor)$^{+\cdot}$, where the macrocycle is a one-electron oxidized radical and is antiferromagnetically

coupled to one of the metal unpaired electrons, thus giving the overall spin state S=1.[53~58]

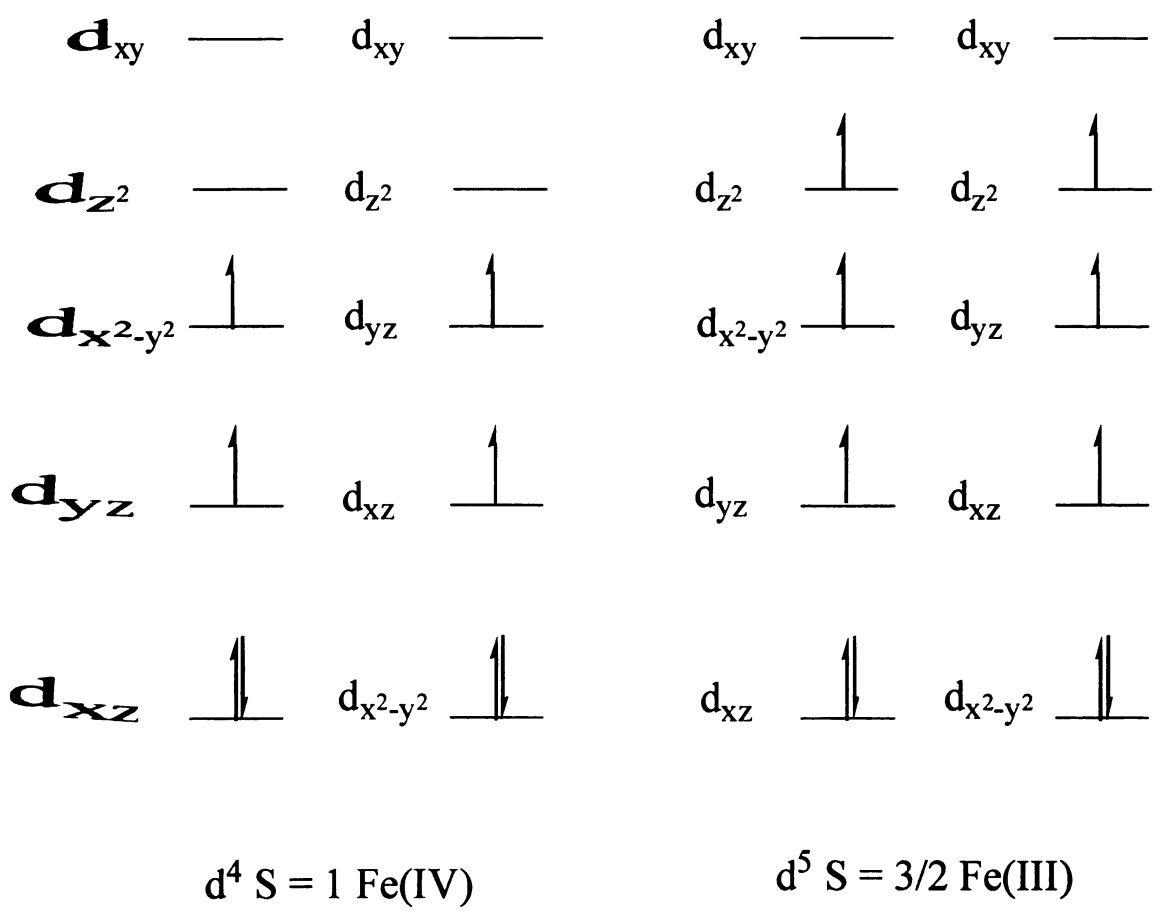

Figure 1-10. Possible electron configurations of iron corrole complexes with formal oxidation state +4 in (OEC)(Ph)Fe(IV), and +3 in (OEC)(Py)Fe(III).[53]

It is not surprising that the formal oxidation state of iron center should depends on the nature of the axial ligand; the strongly basic axial ligands (strong-field) such as oxide or phenyl appear to favor the "true" Fe(IV) center, thus the corrole macrocycle can be considered as purely "-3" anion or "innocent"

trianion ligand. Otherwise, the corrole can be considered as "non-innocent" ligand while weak-field axial ligands such as halogens favored a Fe(III)$Cor^{2-\cdot}$ configuration. Another strong field anionic ligand, CN^-, is thought to favor the Fe(IV) configuration; however, a rapid one-electron reduction occurs and the complex becomes a EPR-active S= ½ spices.[54~55] Another parameter that might affect the formal charge of iron center is the electronic nature of the corrole ligand, which is tunable by substituents on the ring. The relative electron-deficient corrole ring could be considered to be relatively innocent (Figure 1-11).[59]

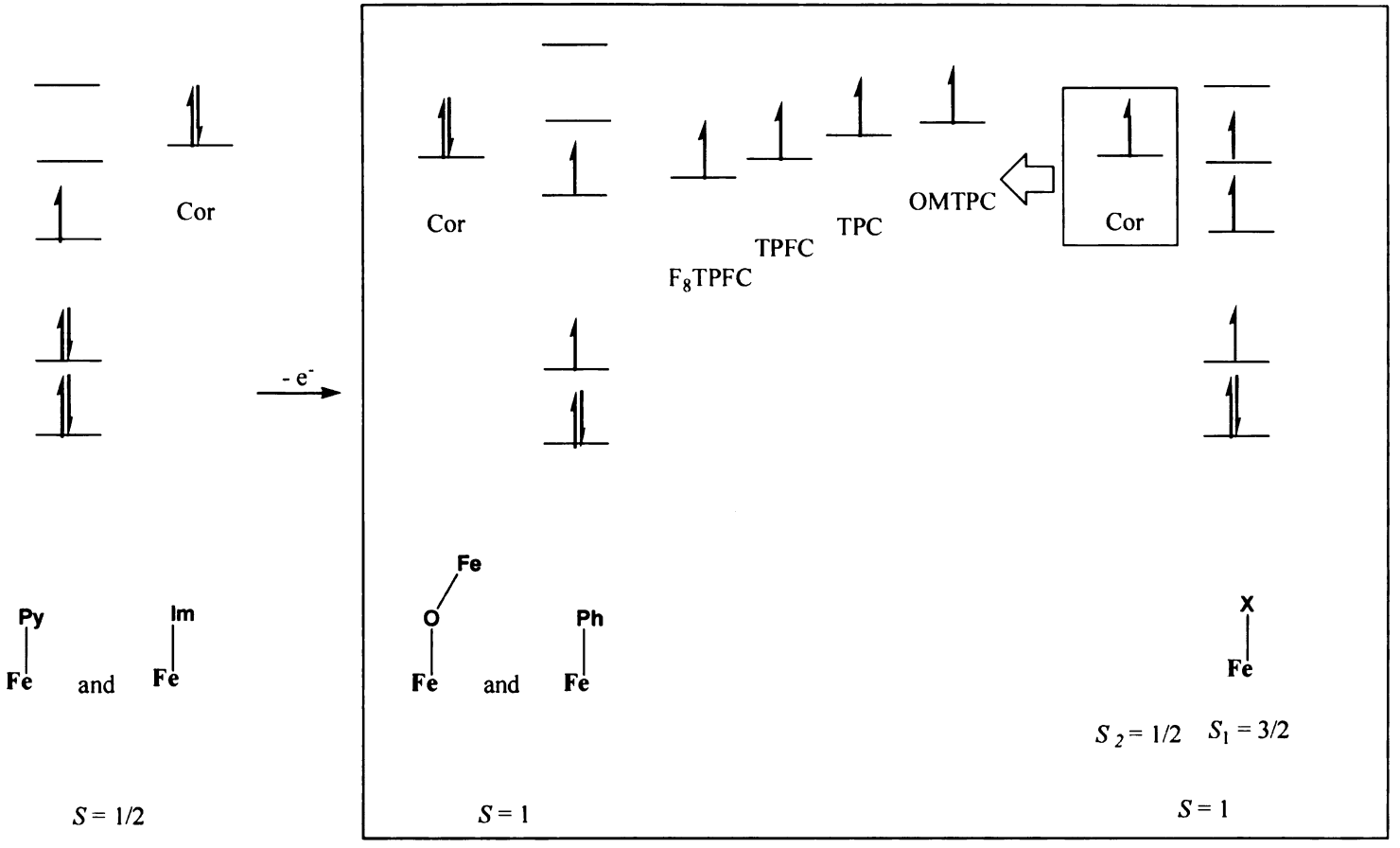

Figure 1-11. A plausible electronic configuration of iron corrole complexes.

The Fe(Cl)-corroles have been used as catalyst to mediate a variety of reactions, such as epoxidation,[61] hydroxylation,[61] cyclopropanation,[60,62] aziridination,[62] and asymmetric sulfoxidation.[63] (Figure 1-12 and 1-13)

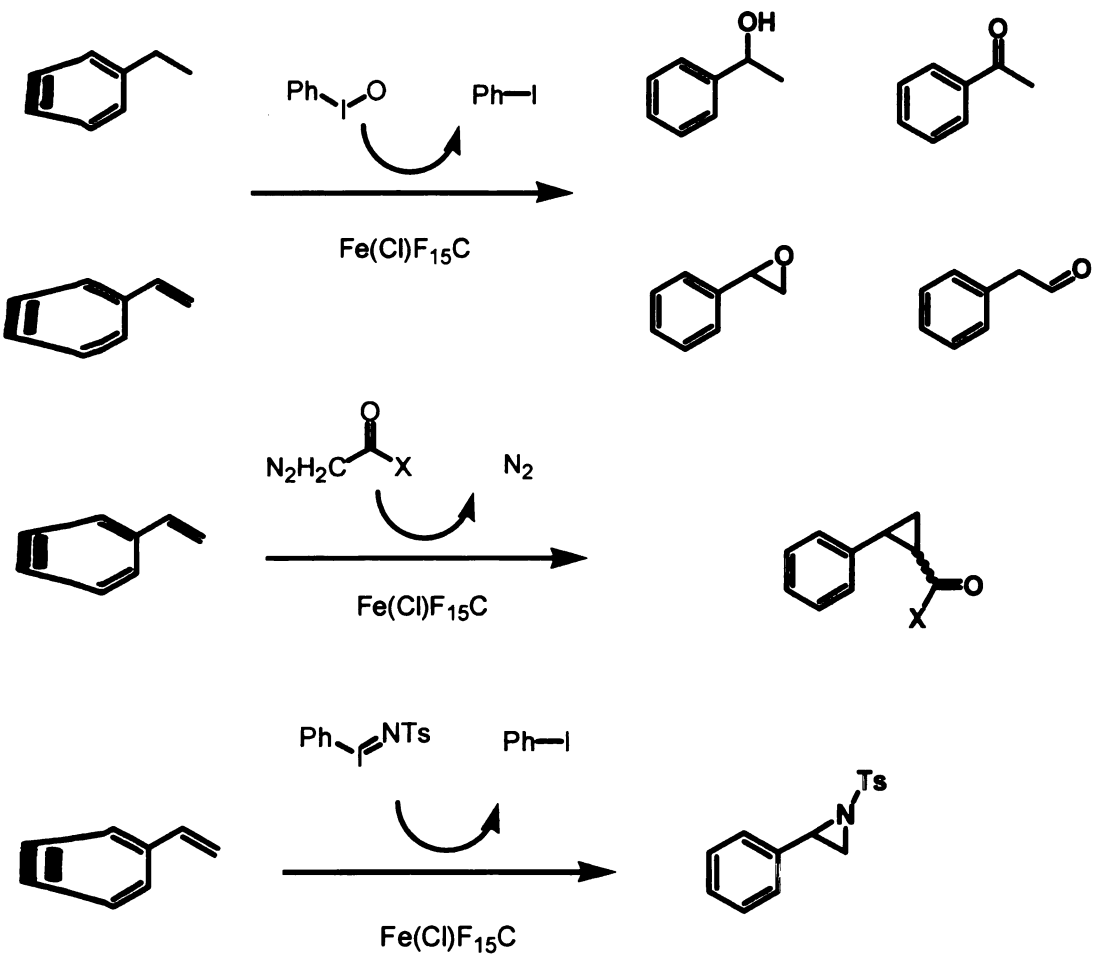

Figure 1-12. Epoxidation, hydroxylation, cyclopropanation, and aziridination catalyzed by $Fe(Cl)F_{15}C$.[60-62]

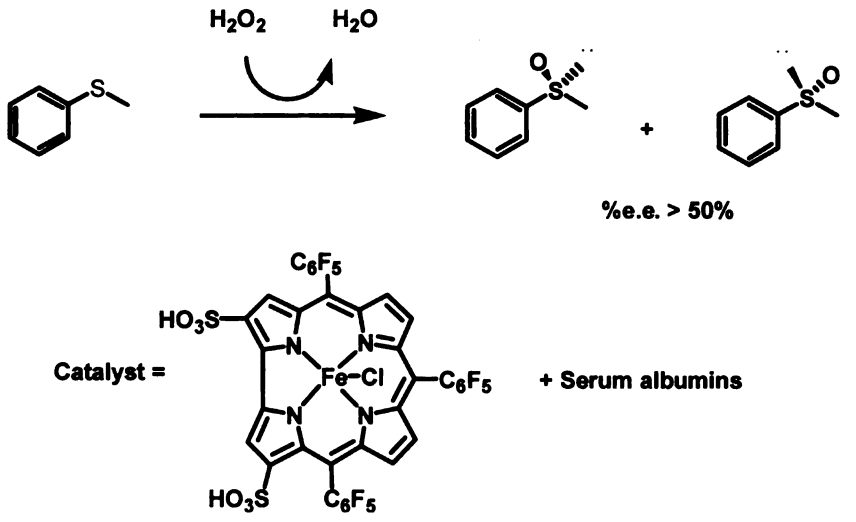

Figure 1-13. Asymmetric sulfide oxidation catalyzed by the bis-sulfonated derivative of $Fe(Cl)F_{15}C$.[63]

In these catalytic reactions most likely a facile one-electron oxidation of the $S_1=3/2$ Fe(III), $S_2=1/2$ $(Cor)^{2-\cdot}$ center to $S_1=1$ Fe(III), $S_2=1/2$ $(Cor)^{2-\cdot}$ has taken place giving rise to a reactive intermediate equivalent to Compound I of the cytochromes P450, peroxideases, and catalases. It should be cautioned[64] that the reported results of epoxidation and hydroxylation are non-reproducible, as the catalyst often completely bleached even in very low oxidant concentration.

Photochemical generation of a highly reactive iron-oxo intermediate, a possible Fe(V)-oxo species, has recently been reported by Newcomb et al.,[65] Laser flash photolysis was employed to induce cleavage of the O-X ($X=ClO_2$, NO_2) bond to produce a highly reactive, high-valent iron-oxo transient that claims to be corrole-iron(V)-oxo species; it slowly converts to its lower energy

iso-electronic isomer, the corrole-iron(IV)-oxo corrole radical cation. The *iron*(V) species has been found very reactive towards cis-cyclooctene and *ethylbenzene*, and is at least 6 orders of magnitude more reactive than that of *the* iron(IV)-oxo corrole radical cation. That is to say the iron(IV)-oxo corrole *radical* cation species has almost no observed oxidation power. The *cis-cyclooctene* oxide yield is 50% based on the Fe(IV)-O-X precursor, and no *reaction* was observed without light.

1-4. Manganese corrole

Manganese corroles have a close relationship to the iron corroles with one less electron in the overall electronic configuration. The neutral Mn(III) corrole is air stable, and binds easily with any neutral ligands such as imidazole, pyridine, MeOH and H_2O to form a 5-coordinated complex. Yet the corrole ligand in these d^4 Mn(III) corrole is "innocent", and the Mn(III) corrole can be reversibly oxidized to Mn(IV)-Cl by dilute hydrochloride acid and conversely, Mn(IV)-Cl can be reduced to Mn(III) by any base such as imidazole or sodium bicarbonate (Figure 1-14).

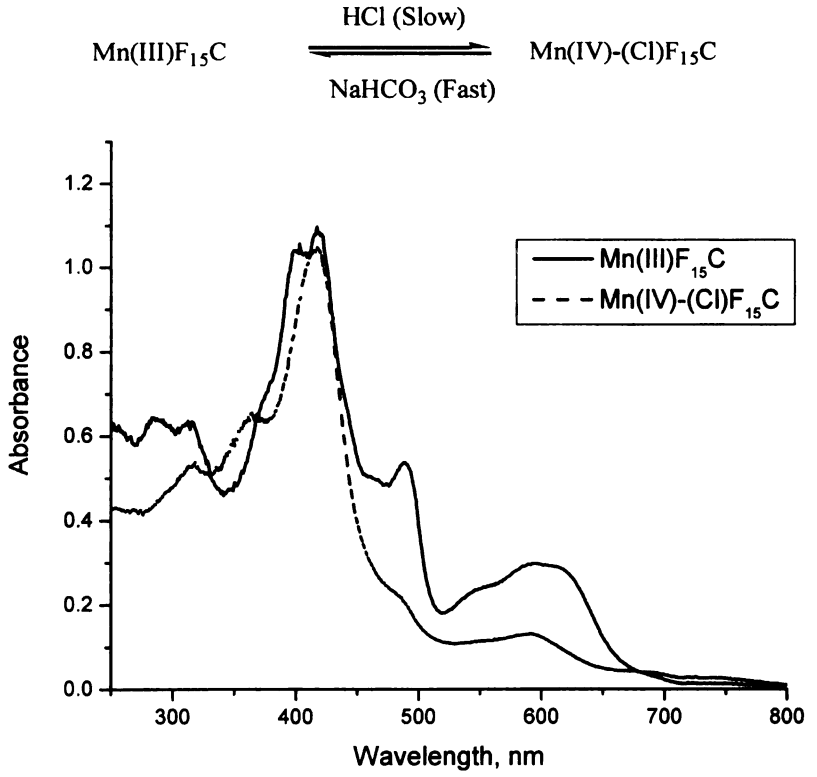

Figure 1-14. UV-Vis spectrum of $Mn(III)F_{15}C$ and $Mn(IV)\text{-}(Cl)F_{15}C$.

The crystal data of different Mn(III) corroles have shown that they are either in 4-coordinated square-planner geometry (perfectly in plane with the N atoms) or 5-coordinated (0.256 ~ 0.292 Å out of the N4 plane).[51,63,68] The 4-coordinated Mn(III) corrole has been assigned a high-spin d^4-configuration, with a magnetic moment of μ_{eff} = 4.78 μ_B;[51] consistent with a *S*=2 spin state. In the presence of an axial ligand, such as pyridine, the magnetic moment μ_{eff} of 5-coordinated Mn(III) corrole depends on the electronic nature of the corrole ring. For those octaalkyl substituted corroles, such as octamethyl corrole, its magnetic moment μ_{eff} is temperature dependent (μ_{eff} = 3.60 μ_B at 293K and μ_{eff} = 3.02 μ_B at 235K). This behavior has been interpreted in terms of antiferromagnetic coupling between an intermediate-spin Mn(II) with *S*=3/2 center and a formally oxidized corrole macrocycle cationic radical (similar to the case of Fe(IV) corrole).[51] An alternative explanation for this behavior is a temperature dependent high-spin to low-spin conversion of the d^4 Mn(III) center caused by coordination of a second pyridine ligand at low temperature.[63] The binding constant of the second pyridine to Mn(III)(Py) corrole is small and has never been measured. Interestingly in electron-deficient corrole such as $F_{15}C$, the 5-corrodinated Mn(III)(L) corrole (L= Ph_3P=O) has a magnetic moment of μ_{eff} = 4.88 μ_B and is temperature independent from 2K to 300K, suggesting a high-spin d^4 Mn(III) center with S=2 spin state.

When Mn(III) corrole is oxidized to Mn(IV)-X corrole, both electron-rich and electron-deficient corrole give a d^3 Mn(IV) center. The magnetic moments of μ_{eff} for (OEC)Mn(IV)-Cl, Mn(IV)-(Br)F_{15}C and (OEC)(Ph)Mn(IV) are 3.87, 3.80 and 3.56 μ_B respectively, and are nearly temperature independent from 150K to 300K.[63,68]

Another oxidation state of manganese corrole is the Mn(V). By reacting Mn(III) corrole with nitrene, as shown in Figure 1-15, the resulting imido Mn(V) corrole seems stable for months under dry inert atmosphere.

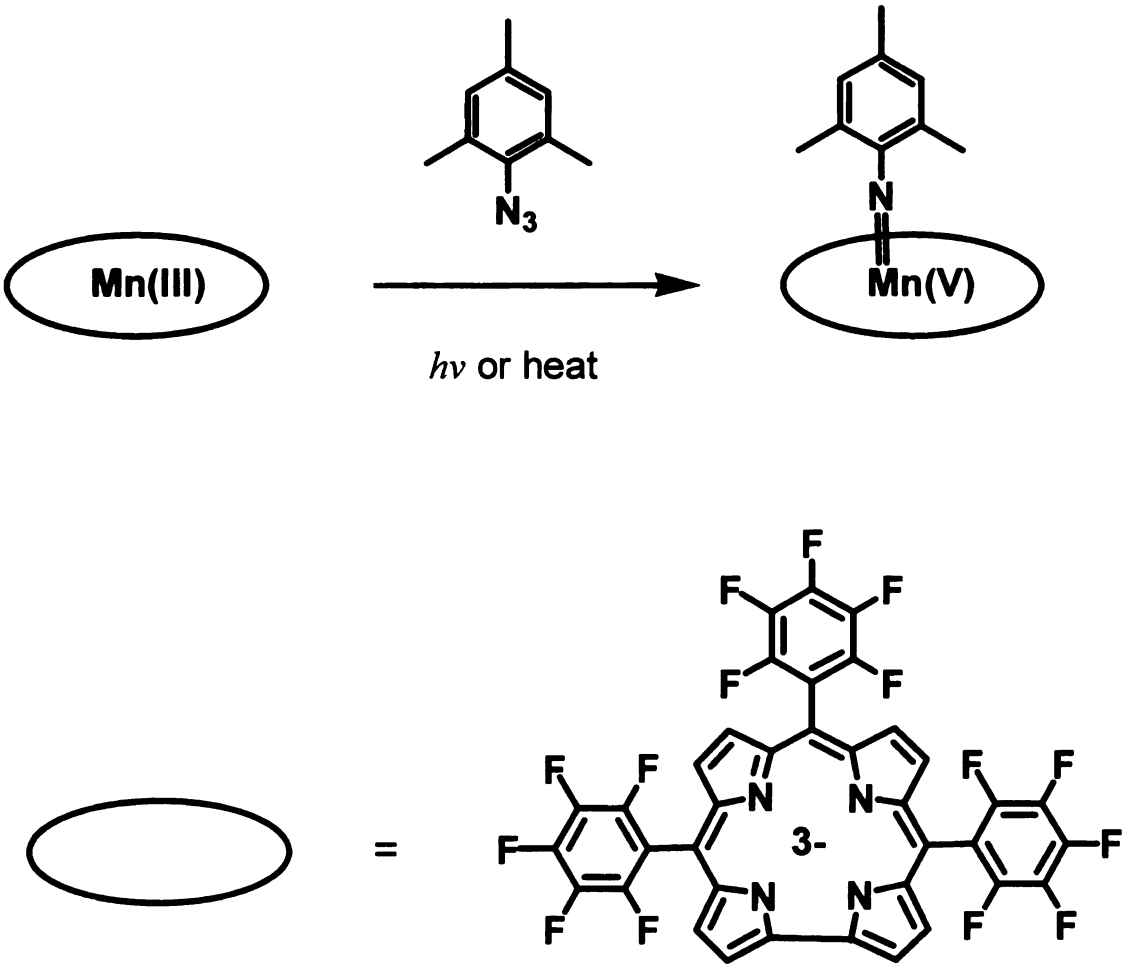

Figure 1-15. Synthesis of stable imido Mn(V) corrole.[66]

The ^{1}H and ^{19}F-NMR spectra of Imido Mn(V) corrole complexes exhibit sharp signals in the same region typical for chemical shifts of free-base corrole, suggesting these Mn(V) corroles have a diamagnetic low-spin d^2 configuration.

More reactions have been reported for Mn(III) corrole than for iron corrole, because of the higher stability of the manganese corrole towards oxidative environment. The most intriguing feature of manganese corrole is that upon reaction with ozone or iodosylbenzene, the green Mn(III) corrole gives a

relative stable, high–valent compound ($t_{1/2}$= 4h in dilute CH_2Cl_2 solution), which is red in color and has been proposed as Mn(V)-oxo species.[67~69] This species can also be produced via photolysis of the Mn-$OClO_2$ corrole complex.[67~68] There have been several catalytic oxidations reported by using Mn(III) corroles as catalyst, such as in epoxidation and sulfur oxidation (Figure 1-16).

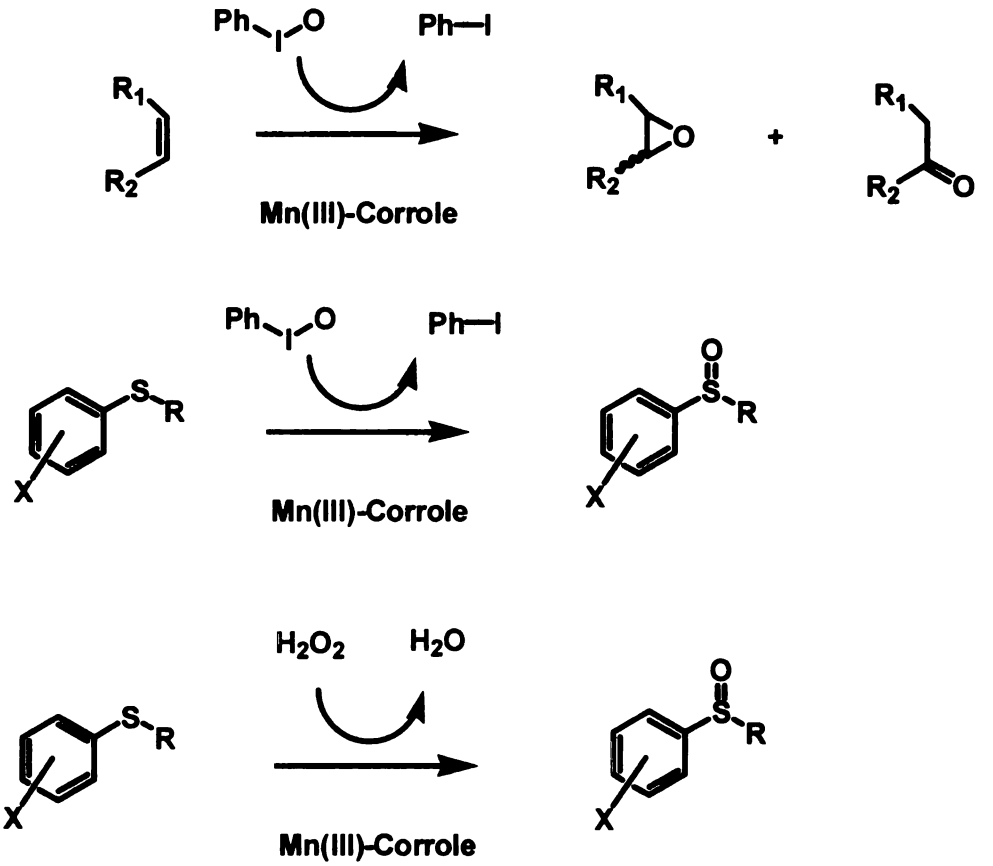

Figure 1-16. Oxidation reactions catalyzed by Mn(III)-corrole.

During the course of these reactions, the green Mn(III) species first turns to red color [from Mn(V)] and turns back to green color, after all the oxidant has been consumed. The Mn(V)-oxo corrole species that has been isolated *via*

ozone or PhIO oxidant was thought to be inactive to oxidize olefins such as styrene;[69] yet later studies by our group[14] and Newcomb *et al.*[67~68] indicated the reactivity of Mn(V)-oxo corrole may be tunable by substituents on the corrole ring. In general, electron-deficient corrole increases the reactivity of the corresponding Mn(V)-oxo species and the most reactive Mn(V)-oxo corrole is the perfluorinated corrole, $(F_{23}C)$Mn(V)-oxo.

A mechanistic study of Mn(III) corrole-catalyzed epoxidation by Collman *et al.*[64] employed three different iodosylarenes as the oxygen source. (Figure 1-17) The overall reaction involved two olefin substrates (styrene and *cis*-cyclooctene), which were competitively epoxidized by an iodosylarene in the presence of a catalyst to afford the epoxides. The ratio of epoxides was used as an indication of the preference of the active intermediate for epoxidizing one substrate over the other. If the Mn(V)-oxo intermediate was the only active epoxidizing species, the product ratio would depend only on the intrinsic reactivity of the oxidant toward the two olefins, and identical selectivity would be expected regardless of the oxygen source. Otherwise, dependence of selectivity on the nature of the oxygen source would require the involvement of the oxygen donor in the product-determining step.

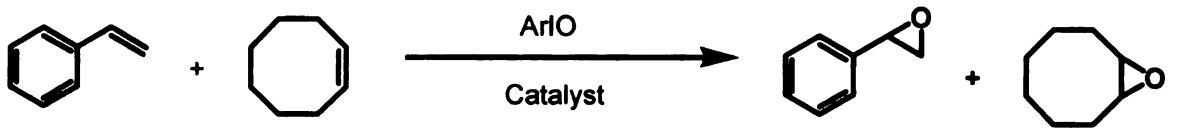

	[cyclooctene oxide]/[styrene oxide]		
Catalyst	PhIO	C_6F_5IO	MesIO
$Mn(Cl)F_{20}P$	2.40	2.45	2.45
$MnF_{15}C$	2.25	1.70	1.80

Figure 1-17. Competitive epoxidations of styrene and *cis*-cyclooctene by three different iodosylarenes.[64]

Their results suggest that the Mn(V)-oxo should not be the only active oxidant in epoxidation, because the cyclooctene oxide/styrene oxide ratio is dependent on the nature of iodosylarenes, which cannot be explained by the participation of a single common active intermediate. Thus, the idosylarenes should be involved in the active intermediate (Figure 1-18).

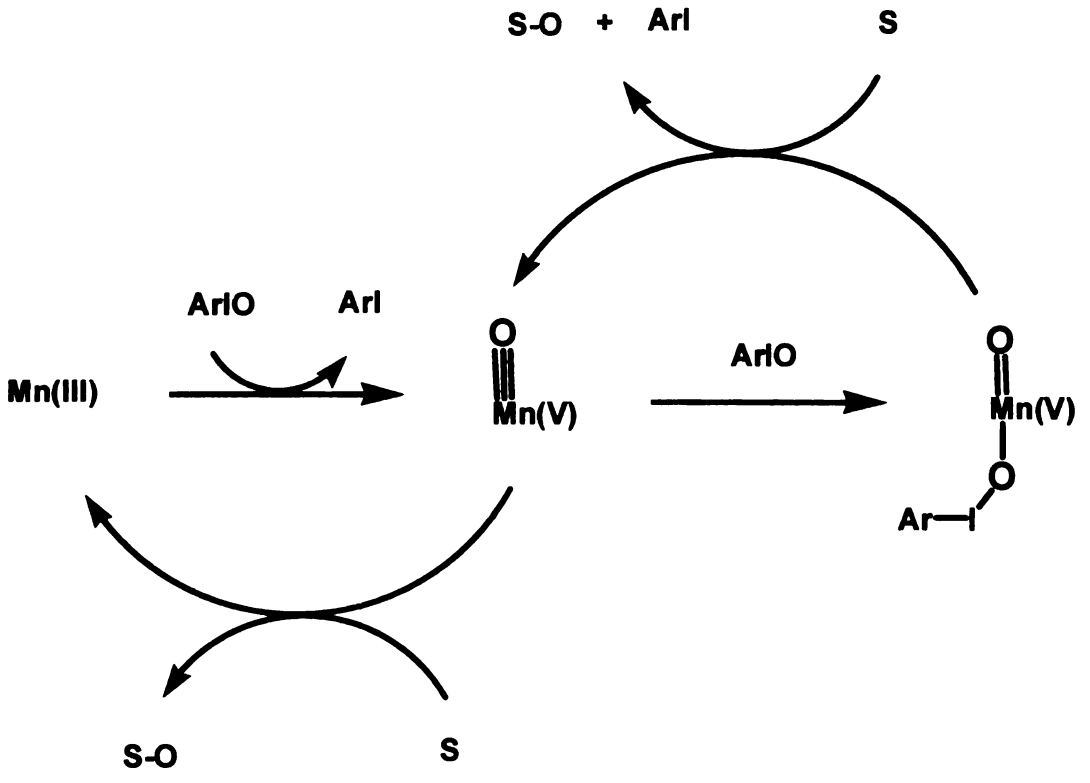

Figure 1-18. Possible mechanism of oxidation reaction catalyzed by Mn(III) corrole with Mn(V) intermediate. (S = substrate)

Additional insight of the role of the Mn-oxo species in epoxidation was provided by Newcomb et al.,[67~68] from kinetic experiments using a laser flash photolysis method to produce the Mn(V)-oxo corrole species. Its reativity towards olefins could not be explained by simple first-order rate equations, which led to the proposal of two possible mechanisms: (1) disproportionation of two Mn(V)-oxo to form a putative Mn(VI)-oxo, which then oxidized the olefins; (2) equilibrium of the "free" Mn(V)-oxo that is active and an inactive "sequested" form.

There seems to be no definitive conclusion at this moment. Suffice it to say the mechanism of epoxidation involving the Mn-oxo species is more complex than

initially assumed, and there could be multiple pathways depending on the electronic nature of corrole, olefin, as well as the method by which the active species is generated.

1-5. Metallocorrole as enzyme biomimetic model

The role of metalloenzymes in biological transformations has attracted intense interest over the past few decades. Due to the complexity of the metalloenzyme systems, chemical models have been commonly employed to understand reactions taken place at the active site of the enzyme. The models are synthetic molecules that contain one or more features present in the enzymatic systems, but are smaller and structurally simpler than the real enzymes. In general, a good enzyme model should fulfill a twofold purpose: firstly it should provide a reasonable simulation of the enzyme reaction, and secondly it should lead to structural and mechanistic insights.[71~72]

As mentioned previously, corrole may have a certain advantage to serve as bioinorganic model compound for heme enzymes model owing to its ability to stablize higher oxidation state of metal center. It perhaps could provide a close look at the high-valent reaction intermediates which are too unstable or too difficult to obtain and study in porphyrin hemes. In the following chapters, novel manganese and iron corrole complexes are described as model for heme enzymes, in particular for cytochrome P-450 monooxygenase and dimeric catalase.

References

1. Johnso, A.W.; Price, R. *J. Chem. Soc.* **1960**, 1649-1653.

2. Johnson. A. W.; Kay. L. T. *J. Chem. Soc.* **1965**, 1620-1629.

3. Johnson, A.W. *pure appl. Chem.* **1970**, 23, 375.

4. Paolesse, R. In *The Porphyrin Handbook*; Kadish, K. M., Smith, K.M., Guilard, R., Eds.; Academic Press: San Diego, CA, 2000; Vol.2, pp 201-232.

5. Erben, C.; Will, S.; Kadish, K. M. In *The Porphyrin Handbook*; Kadish, K. M., Smith, K. M., Guilard, R., Eds.; Academic Press: SanDiego, CA, 2000; Vol. 2, pp 233-300.

6. Guilard, R.; Barbe, J.-M.; Stern, C.; Kadish, K. M. In *The Porphyrin Handbook*; Kadish, K. M., Smith, K. M., Guilard, R., Eds.; Elsevier:San Diego, CA, 2003; Vol. 18, pp 303-349.

7. Dyke, J. M.; Hush, N. S.; Williams, M. L.; Woolsey, I. S. *Mol. Phys.* **1971**, 20, 1149-1152.

8. Boschi, T.; Licoccia, S.; Paolesse, R.; Tagliatesta, P.; Tehran, M. A.; Pelizzi, G.; Vitali, F. *J. Chem. Soc., Dalton Trans.* **1990**, 463~468.

9. Gross, Z.; Galili, N.; Saltsman I. *Angew. Chem., Int. Ed.* **1999**, *38*, 1427~1429.

10. Taradieux, C.; Gros, C. P.; Guilard, R. *J. Heterocycl. Chem.* **1998**, 35, 965~967.

11. Rose, E.; Kossanyi, A.; Quelquejeu, M.; Soleilhavoup, M.; Duwavran, F.; Bernard, N.; Lecas, A. *J. Am. Chem. Soc.* **1996**, *118*, 1567~1568.

12. Gross, Z.; Galili, N.; Simkhovich, L.; Saltsman, I.; Botashansky, M.; BlYser, Y.; Boese, R.; Goldberg, I. *Org. Lett.* **1999**, *1*, 599~600.

13. Simkhovich, L.; Goldberg, I.; Gross, Z. *J. Inorg. Biochem.* **2000**, *80*, 235~240.

14. Liu, H.Y.; Lai, T.S.; Yeung, L.L.; Chang, C.K. *Org. Lett.* **2003**, 5, 617~620.

15. Paolesse, R.; Mini, S.; Sagone, F.; Boschi, T.; Jaquinod, L.; Nurco, D.T.; Smith, K.M. *Chem. Commun.* **1999**, 1307~1308.

16. Paolesse, R.; Nardis, S.; Sagone, F.; Khoury, R.G. *J. Org. Chem.* **2001**, *66*, 550-556.

17. Wasbotten, I.H.; Wondimagegn, T.; Ghosh, A. *J. Am. Chem. Soc.* **2002**, *124*, 8104-8116.

18. Steene, E.; Dey, A.; Ghosh, A. *J. Am. Chem. Soc.* **2003**, *125*, 16300-16309.

19. Collman, J.P.; DecrPau, R.A. *Tetrahedron Lett.* **2003**, *44*, 1207-1209.

20. Gryko, D.T. *Chem. Commun.* **2000**, 2243-2244.

21. Gryko, D. T.; Jadach, K. *J. Org. Chem.*, **2001**, *66*, 4267-4275.

22. Gryko, D. T. *Eur. J. Org. Chem.* **2002**, *11*, 1735.

23. Gryko, D.T.; Piechota, K. *J. Porphyrins Phthalocyanines* **2002**, *6*, 81 – 97.

24. Ka, J.W.; Cho, W.S.; Lee, C.H. *Tetrahedron Lett.* **2000**, *41*, 8121-8122.

25. Brinas, R.P.; BrWckner, C. *Synlett.* **2001**, 442-443.

26. Andrioletti, B.; Rose, E.; J. *Chem. Soc. Perkin Trans. 1* **2002**, 715-720.

27. DecrPau, R.A.; Collman, J.P. *Tetrahedron Lett.* **2003**, *44*, 3323-3323.

28. Gryko, D. T. Koszarna, B. *Synthesis* **2004**, *13*, 2205-2209.

29. Ghosh, A. *Angew. Chem. Int. Ed.* **2004**, *43*, 1918 –1931.

30. Aviv, I., Gross, Z. *Chem. Commun.*, **2007**, 1987-1988.

31. Ramdhanie, B.; Telser, J.; Caneschi, A.; Zakharov, L. N.; Rheingold, A. L.; Goldberg, D. P. *J. Am. Chem. Soc.* **2004**, *126*, 2515-2525.

32. Mandimutsira, B. S.; Ramdhanie, B.; Todd, R. C.; Wang, H. L.; Zareba, A. A.; Czernuszewicz, R. S.; Goldberg, D. P. *J. Am. Chem. Soc.* **2002**, *124*, 15170-15171.

33. Kadish, K. M.; Ou, Z. P.; Shao, J. G.; Gros, C. P.; Barbe, J. M.; Je´roˆme, F.; Bolze, F.; Burdet, F.; Guilard, R. *Inorg. Chem.* **2002**, *41*, 3990-4005.

34. Kadish, K. M.; Shao, J. G.; Ou, Z. P.; Gros, C. P.; Bolze, F.; Barbe, J. M.; Guilard, R. *Inorg. Chem.* **2003**, *42*, 4062-4070.

35. Barbe, J. M.; Canard, G.; Brandes, F.; Je´roˆme, F.; Dubois, G.; Guilard, R. *Dalton Trans.* **2004**, *8*, 1208-1215.

36. Steene, E.; Wondimagegn, T.; Ghosh, A *J. Phys. Chem. B* **2001**, *105*, 11406-11411.

37. Steene, E.; Wondimagegn, T.; Ghosh, A. *J. Inorg. Biochem.* **2002**, *88*, 113-120.

38. Cai, S.; Walker, F.A.; Licoccia, S. *Inorg. Chem.* **2000**, *39*, 3466-3478.

39. Zakharieva, O.; Schuenemann, V.; Gerdan, M.; Licoccia, S.; Cai, S.; Walker, F.A.; Trautwein, A.X. *J. Am. Chem. Soc.* **2002**, *124*, 6636-6648.

40. Cai, S.; Licoccia, S.; D'Ottavi, C.; Paolesse, R.; Nardis, S.; Bulach, V.; Zimmer, B.; Shokhireva, T.K.; Walker, F.A. *Inorg. Chim. Acta* **2002**, *339*, 171-172.

41. Kadish, K.M.; Smith, K.M.; Guilard, R. (Eds.), *The Porphyrin Handbook*, vol. 6, Academic Press, Boston, MA, **2000**. and reference there in.

42. Kadish, K.M.; Smith, K.M.; Guilard, R. (Eds.), *The Porphyrin Handbook*, vol. 14, Academic Press, Boston, MA, **2000**. and reference there in.

43. Kadish, K.M.; Smith, K.M.; Guilard, R. (Eds.), *The Porphyrin Handbook*, vol. 2, Academic Press, Boston, MA, **2000**. and reference there in

44. Kadish, K.M.; Erben, C.; Ou, Z.; Adamian, V.A.; Will, S.; Vogel, E.; *Inorg. Chem.* **2000**, 39, 3312-3319.

45. "*Cytochrome P450: Structure, Mechanism, and Biochemistry*", Groves, J. T., 3rd ed.; Ortiz de Montellano, P. R., Ed.; Kluwer Academic/Plenum Publishers: New York, **2005**; pp 1-43.

46. Collman, J.P.; Zhang, X.; Lee, V.J.; Uffelman E.S.; Brauman. J.I. *Science* **1993**, *261*, 1404~1411.

47. Meunier, B. *Chem. Rev.* **1992**, *92*, 1411-1456.

48. Mansuy, D. *Coord. Chem. Rev.* **1993**, *125*, 129-141.

49. Tommos, C., Babcock G. T., *Acc. Chem Res,* **1998**, *31*, 18-25.

50. Dismukes G. C. *Chem. Rev.*, **1996**, *96*, 2909-2926.

51. Vogel, E.; Will, S.; Schulze, A.; Tilling, L.; Neumann, J.; Lex, E.; Bill, A.X.; Trautwein, K.; Wieghardt, K. *Angew. Chem., Int. Ed.* **1994**, *33*, 731–735.

52. "Iron Porphyrin Chemistry---A Ten-Year Update," Walker, F. A.; Simonis, U. In Encyclopedia of Inorganic Chemistry; Ed. 2; King, R. B., Ed.; Wiley & Sons, Ltd.: Chichester; **2005**; pp. 2390-2521.

53. Walker, F.A.; Licoccia S.; Paolesse, R, *Journal of Inorganic Biochemistry* **2005**, *100*, 810–837.

54. Cai, S.; Walker, F.A.; Licoccia, S. *Inorg. Chem.* **2000**, *39*, 3466–3478.

55. Walker, F.A. *Inorg. Chem.* **2003**, *42*, 4526–4544.

56. Cai, S.; Licoccia, S.; Walker, F.A. *Inorg. Chem.* **2001**, *40*, 5795–5798.

57. Zakharieva, O.; Schünemann, V.; Gerdan, M.; Licoccia, S.; Cai, S.; Walker, F.A.; Trautwein, A.X. *J. Am. Chem. Soc.* **2002**, *124*, 6636–6648.

58. Steene, E.; Wondimagegn, T.; Ghosh, A. *J. Phys. Chem. B,* **2001**, *105,* 11406–11413.

59. Ghosh, A.; Steene, E. *J. Inorg. Biochem.* **2002**, *91,* 423–436.

60. Simkhovich, L.; Mahammed, A.; Goldberg, I.; Gross, Z. *Chem. Eur. J.* **2001**, *7*, 1041–1055.

61. Gross, Z.; Simkhovich, L.; Galili, N. *Chem. Comm.* **1999**, 599–600.

62. Simkhovich, L.; Gross, Z. *Tetrahedron Lett.* **2005**, *42,* 8089–8092.

63. Mahammed, A.; Gross, Z. *J. Am. Chem. Soc.* **2005**, *127*, 2883–2887.

64. Collman J. P.; Zeng L. and Decréau R. A. *Chem. Commun.* **2003**, 2974.

65. Harischandra, D.N.; Zhang, R.; Newcomb, M. *J. Am. Chem. Soc.* **2005**, *127*, 13776–13777.

66. Edwards, N. Y.; Eikey, R. A.; Loring, M. I.; Abu-Omar, M. M. *Inorg. Chem.* **2005**, *44*, 3700-3708.

67. Zhang, R.; Horner, J. H.; Newcomb, M. *J. Am. Chem. Soc.* **2005**, *127*, 6573-6582.

68. Zhang, R., Harischandra, D.N., Newcomb, M. *CHEM-EUR J.* **2005**, *11*, 5713.

69. Gross, Z.; Golubkov, G.; Simkhovich, L. *Angew. Chem. Int. Ed.* **2000**, *39*, 4045.

70. Ou, Z. P.; Erben, C.; Auret, M.; Will, S.; Rosen, D.; Lex, J.; Vogel, E.; Kadish, K. M. *J. Porphyrins and Phthalocyanines* **2005**, *9*, 398-402.

71. Denisov, I.G.; Makris, T.M.; Sligar, S.G.; Schlichting I. *Chem. Rev.* **2005**, *105*, 2253.

72. *"Cytochrome P450: Structure, Mechanism, and Biochemistry"*, 3rd ed; Ortiz de Montellano, P.R. Ed.; Kluwer Academic/Plenum Publishers: New York. **2005**.

Chapter 2

Cofacial biscorrole as catalase model

2-1. Introduction

In living cells, catalases protect organisms from oxidative damage by serving as scavenger to remove the appreciable levels of hydrogen peroxide produced during O_2 metabolism. By some estimates, as much as 10% of O_2 consumed in cellular respiration may be reduced to hydrogen peroxide,[1] which is readily converted to hydroxyl radical and hydroxide ion by a variety of one-electron reductants commonly found in cells. The resulting hydroxyl radical is an indiscriminate potent oxidant capable of oxidizing all cellular components it comes in contact. In this sense, the catalases provide the first line of defense against oxidative stress and associated degenerative diseases, including possibly forestalling the onset of cancer and aging.[2~3] Many of these enzymes are hemoproteins and those of the bacterial origin contain manganese as a cofactor.[1] Among these enzymes, the cooperation of two or even more metal centers helps to reduce the activation energy of multi-electron transfer, to increase the substrate's affinity for the catalyst, and also to activate the bound substrate. The determination of each of these factors is important for understanding the action of enzymes.

To mimic the catalase functions, cofacial macrocycles with rigid spacer group could be used as a model to probe the H_2O_2 dismutation. The synthesis of

cofacial diporphyrins and their application to model enzymes including oxygenases and catalases have been firmly estabilished.[4-19] Spacer moieties such as anthracene, dibenzofuran and xanthene have been employed to provide an appropriate space between the two macrocycle planes. The spacer group often affects the reactivity of the metal diporphyrins. It has been demonstrated that in cofacial porphyrin studies, DPX with xanthene spacer group has a high reactivity whereas DPB with a dibenzofuran spacer group is nearly unreactive towards H_2O_2, due to unfavorable inter-planar geometry.[19]

In recent years, corrole macrocycles as an alternative platform of bioinorganic models are gaining considerable attention. Corrole stabilizes higher oxidation states of certain metals[20-25] at its core; for example, the first oxidation potential of its Mn complex is much lower than that of porphyrin. Kadish and Guilard *et al.*[26~30] reported the synthesis, electrochemistry, and some binding properties of *meso* unprotected cofacial cobalt biscorroles possessing anthracenyl, biphenylenyl, dibenzofuran, dibenzothiophene and xanthene spacer groups. While the etioporphyrin-type substitution patterns used in their study are generally unstable under oxidizing conditions for porphyrins because of the unprotected *meso* positions,[26-27] it is even worse for the case of corrole macrocycle which undergoes ring opening and cleavage of the C1, C19-double bond by dioxygen addition to from a biliverdin structure (Figure 1-7, page 6). The introduction of four phenyl rings at β-pyrrole positions (position 2, 3, 17 and 18) by Guilard *et al.*[28-30] was reported to resist the dioxygen attack at the C1, C19 double bond.

The synthesis of the 2,3,17,18-tetraaryl-substituented biscorrole was rather lengthy (Figure 2-1), which limited the studies of their properties. An alternative approach to develop a cofacial corrole for studying multi-electron transfer in oxdative environment is needed as the corrole has to survive in harsh conditions such as in the presence of H_2O_2. Recent advances[21,24] in corrole chemistry indicated that electron-withdrawing groups can greatly improve the stability of corrole ring towards oxidative conditions; these results prompted us to study the synthesis of meso-substituted pentafluorophenyl biscorroles, and their application in catalase modelling.

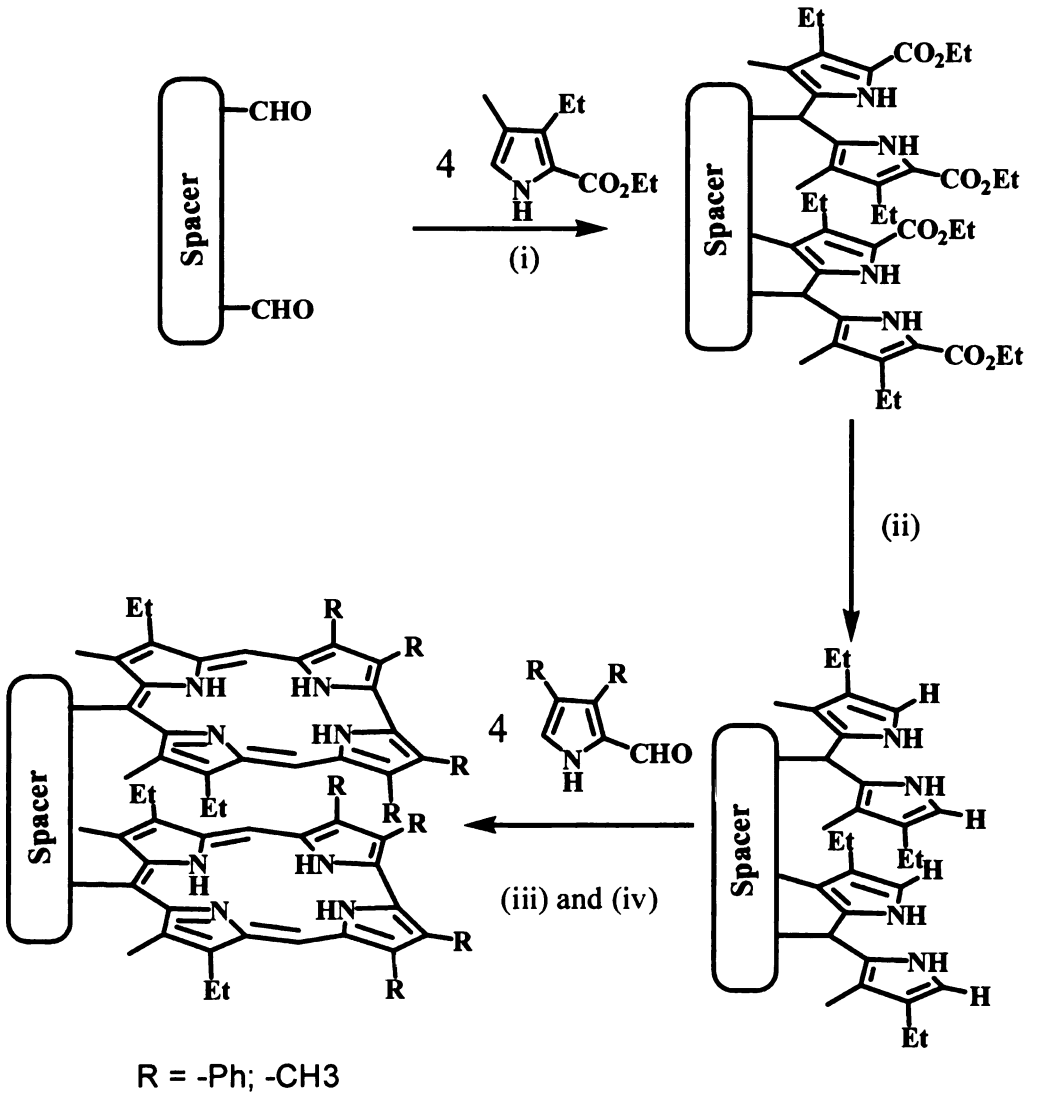

(i). HCl, CH_3OH

(ii). NaOH, diethyleneglycol, 100°C, 90min then 190°C

(iii). HBr/CH_3CO_2H, 4h; (iv). $NaHCO_3$, *p*-chloranil, N_2H_4 (50% in H_2O)

Figure 2-1. Synthetic scheme of cofacial biscorrole reported by Kadish and Guilard *et al.*[30]

In this chapter, we report a facile one-step synthesis of cofacial biscorroles, **5~7** (Scheme2-1), by reacting dialdehydes, **2~4**, with pentafluorophenyl dipyrromethane, **1**, to give reasonable yields (~10%) of the dimers in one step. Also a catalase-like H_2O_2 dismutation with high turn-over number by our di-manganese metallocorroles is demonstrated.

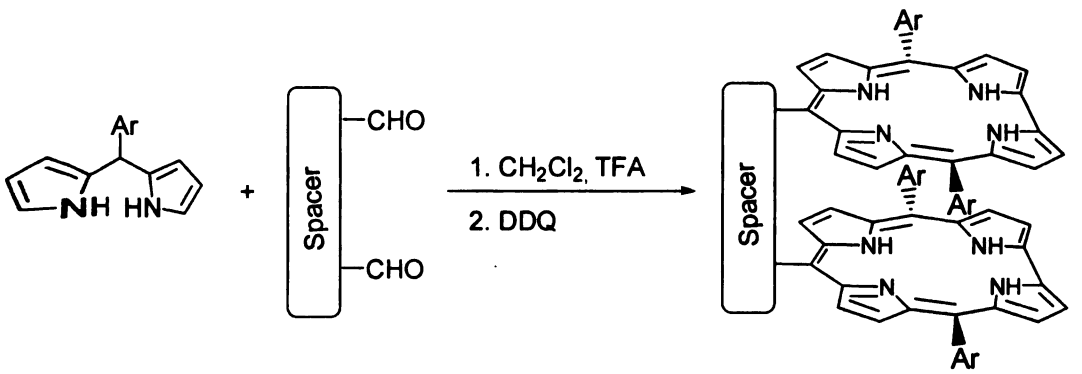

Yield: 8-15%

Ar: C_6F_5, **1** Spacer: Anthracene, **2**
Dibenzofuran, **3**
Xanthene, **4**

Ar: C_6F_5

Spacer: Anthracene (H_6DCA), **5**
Dibenzofuran (H_6DCB), **6**
Xanthene (H_6DCX), **7**

Scheme 2-1. One-step synthesis of cofacial biscorrole, **5~7**.

2-2. Results and Discussion

Synthesis

Referring to Scheme 2-2, the one-pot synthesis of dialdehyde dibenzofuran **3** began with a regioselective dilithiation of the commercially available dibenzofuran. The dilithium derivative was then treated with dry DMF followed by hydrolysis of the intermediate diimine salt. The dialdehyde 9,9-dimethylxanthene **4** was synthesized from its precursor, xanthone. Xanthone was first dimethylated by trimethylaluminum to generate 9,9-dimethylxanthene, **4a**, as a pale yellow oil in over 90% yield. The compound **4a** was then di-formaylated in the same fashion as described above for dibenzofuran. A longer reaction time for the dilithiation step was required for larger scales of over ten grams. All of these transformations were clean, high yielding (>85%) and easy to purify.

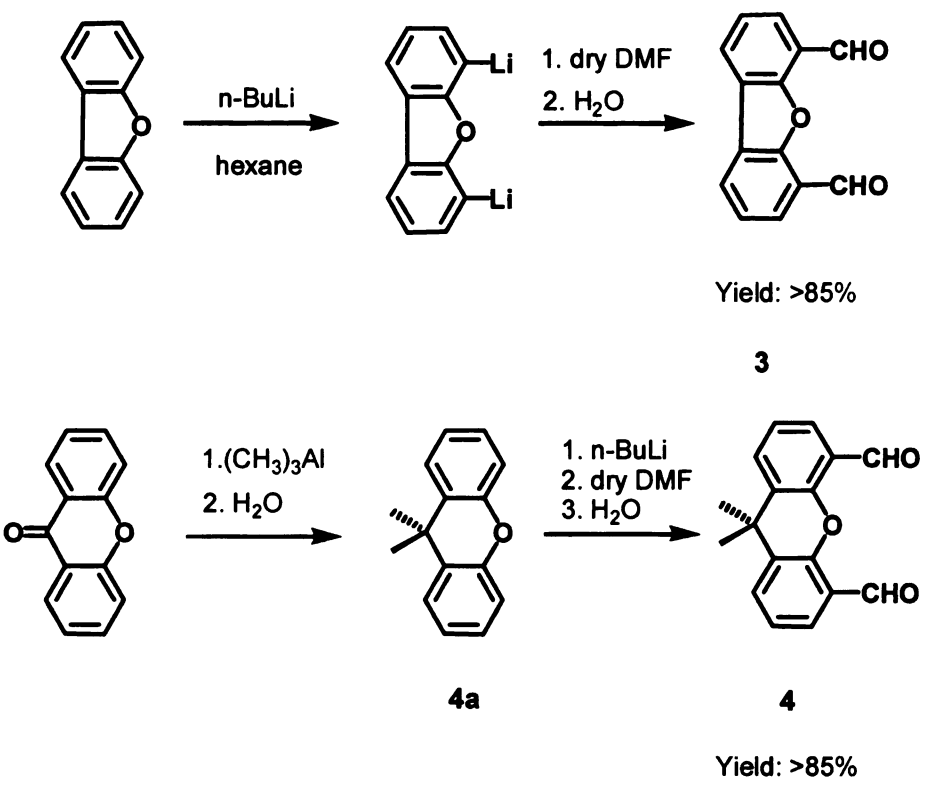

Scheme 2-2. Synthesis of dialdehyde **3** and **4**.

The xanthene bridged cofacial dicorrole, **7** (H_6DCX), was initially synthesized by a modified Rothemond reaction using 4mmol dialdehyde, **4**, 16mmol dipyrromethane, **1**, and 30μL TFA, in 600mL CH_2Cl_2, and this result was reported in 2004.[36] However, this reaction using high dilution conditions took 3 days to obtain 3% yield of the dimer and ~8% of the 4-formyl, 5{10-[5,15-bis(pentafluorophenyl)-corrolyl]}-9,9-dimethylxanthene, **7a**, which presumably is the intermediate before the dimer formation (Scheme 2-3). The separation of **7** and **7a** could be achieved by chromatography on silica gel; the R_f of **7** is 0.8 (1:2 CH_2Cl_2/hexane) whereas the R_f of **7a** is ~0.2. By this procedure, the

biscorroles, H_6DCA **5** and H_6DCB **6**, with anthracene or dibenzofurane as spacer group could not be obtained.

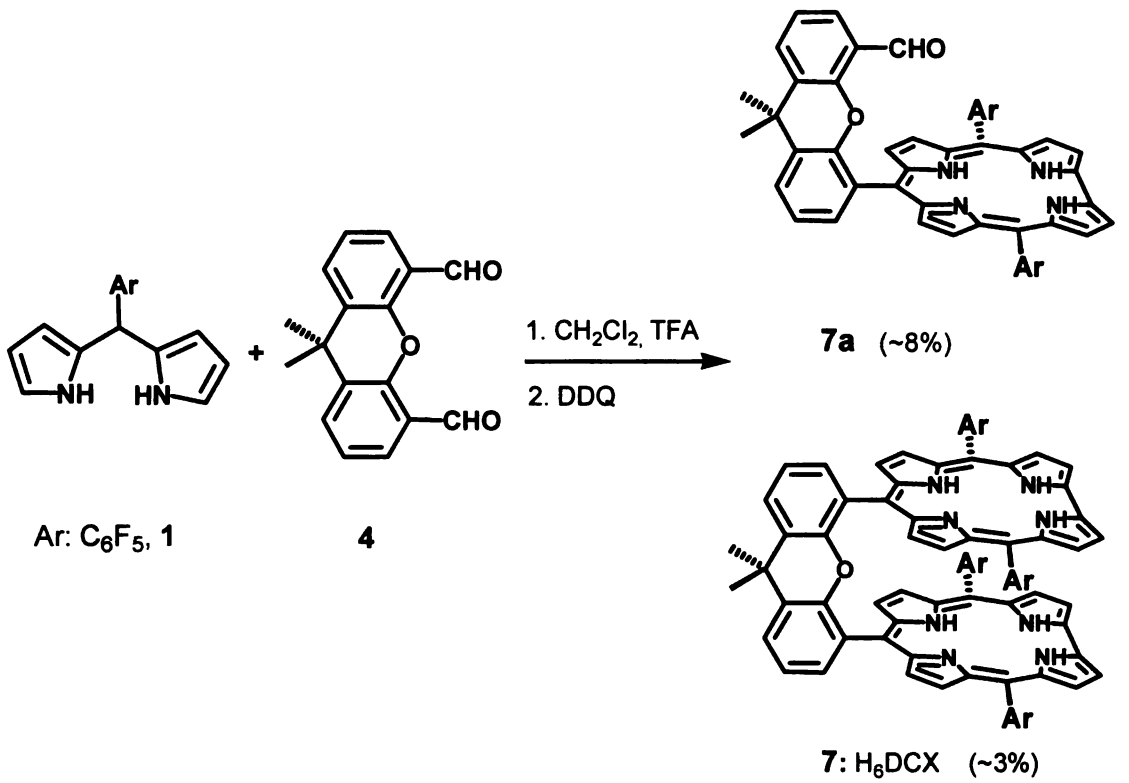

Scheme 2-3. Synthesis of **7** and **7a** with diluted reaction condition.

As reported by Gryko *et al.*,[31-32] a concentrated reaction mixture and high dipyrromethane/acid ratio could give higher yields of corroles in a short period of time, with some corroles achieving ~20% yield in 15 minutes. These reports prompted us to optimize the reaction conditions for our biscorrole synthesis. By varying the ratio of dipyrromethane/dialdehyde/acid (TFA) and their concentration in different reaction time (Table 2-1), H_6DCX was achieved over 11% isolated yield, with only 2% of **7a**. By using this optimized reaction

condition, H_6DCA and H_6DCB were synthesized at 8% and 11% yields, respectively.

Table 2-1. Optimization of H_6XDC synthesis.

4, mmol	**1**, mmol	CH_2Cl_2	TFA	Rx'n time	% yield of **7**
1	4	30 mL	30 uL	4hr	4.2
1	4	30 mL	30 uL	10hr	3.8
1	4	60 mL	30 uL	4hr	11.8
1	4	60 mL	30 uL	6hr	9.8
1	4	60 mL	30 uL	10hr	10.2
1	4	120 mL	30 uL	4hr	6.8
1	4.4	60 mL	30 uL	4hr	11.2

The free base biscorroles can be easily metalated using manganese salts in refluxing pyridine and methanol mixture (1:1) to give dimanganese corrolate complexes **8**, **9** and **10** (Scheme 2-4).

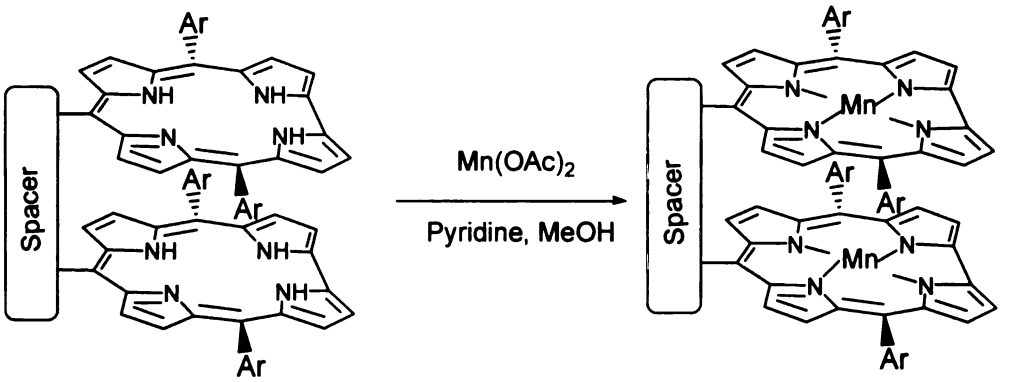

Yield: ~80%

Spacer: Anthracene (Mn_2DCA), **8**
Dibenzofuran (Mn_2DCB), **9**
Xanthene (Mn_2DCX), **10**

Scheme 2-4. Synthesis of **8** ~ **10**

When metalation of H_6DCX with 0.8 equivalent of manganese metal salt was performed, this reaction gave a separable mixture of Mn_2DCX (**10**), H_3MnDCX (**11**) and unreacted H_6DCX. The stability of H_3MnDCX is moderate, it tends to decompose under light and air. HRMS analysis (Figure 2-2) confirmed the structure of MnH_3DCX (MS^+=1518, M^+), along with its methanol complex MnH_3DCX-CH_3OH (MS^+=1551) and there is no indication of the presence of Mn_2DCX (MS^+=1571, M^+).

The MnH_3DCX was used as the precursor of heterometal biscorrole. The second metal insertion was preformed immediately after the MnH_3DCX was purified by TLC to afford a variety of heterometal biscorrole (Figure 2-3). The molecular structures of AlMnDCX (**12**) and CuMnDCX (**13**) were also confirmed by HRMS.

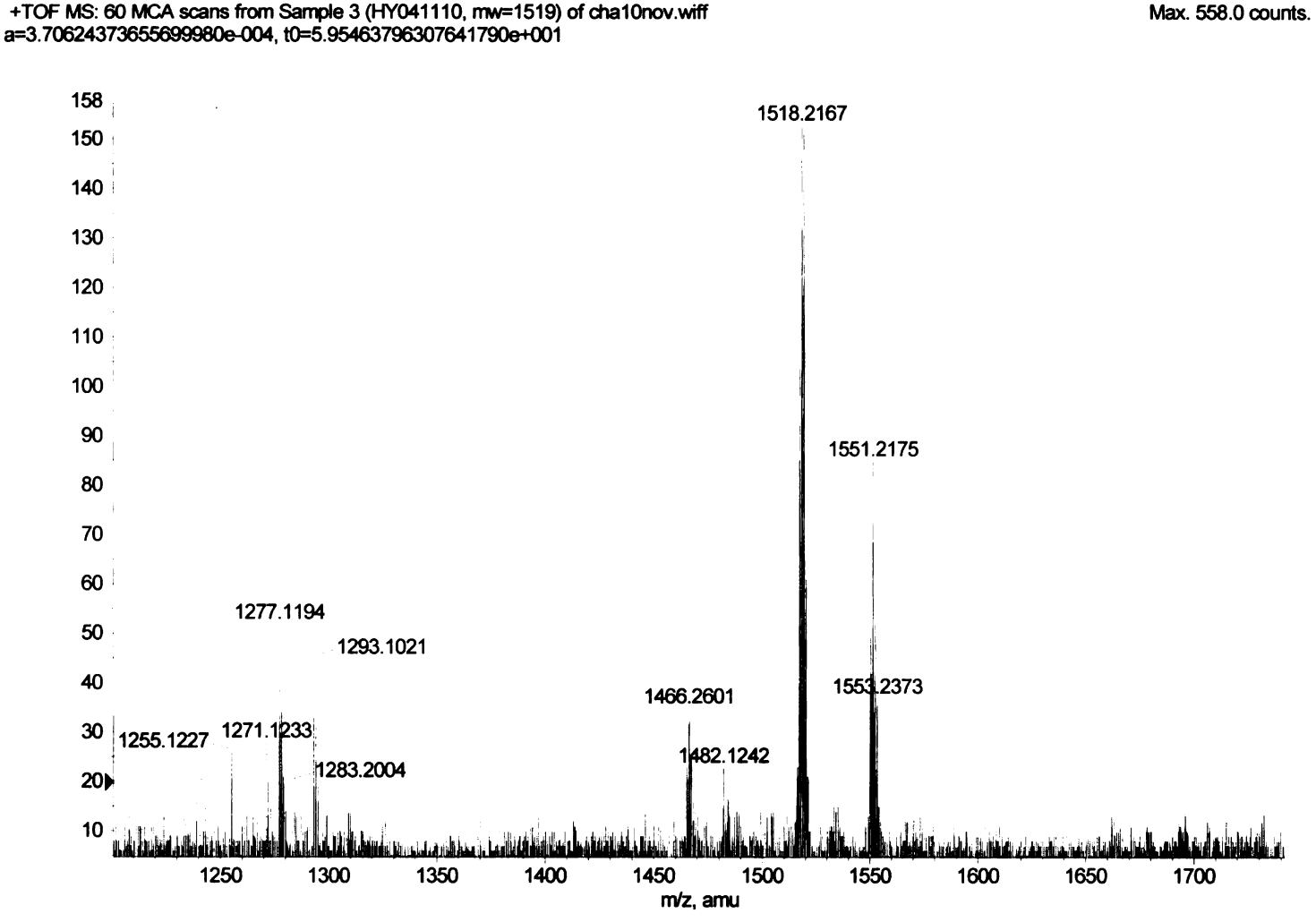

Figure 2-2. HRMS (MALDI-TOF) of MnH_3DCX (**11**).

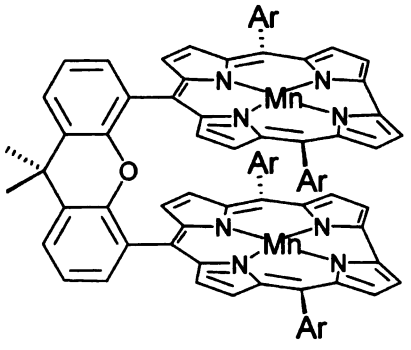

10: Mn_2DCX

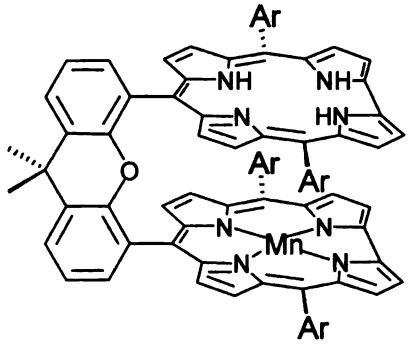

11: MnH_3DCX

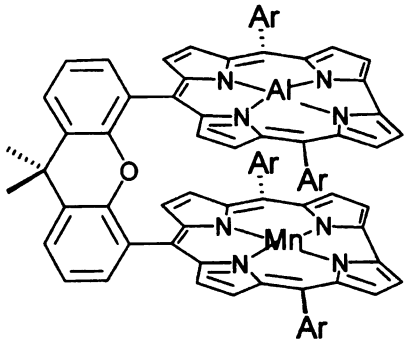

12: AlMnDCX

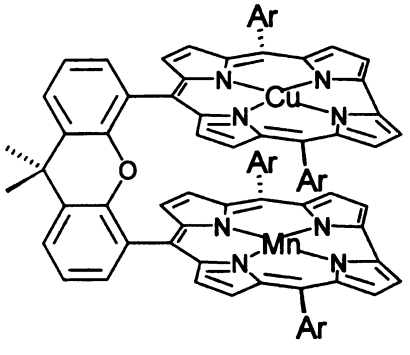

13: CuMnDCX

Figure 2-3. Structure of heterometal biscorroles, **10~13.**

Compound **7a**, with an unreacted aldehyde group on the xanthene spacer, can be modified to different functional groups to make available other model compounds to test the proton-coupled reaction in H_2O_2 dismutation. The transformations are shown in Scheme 2-4 and 2-5. The aldehyde group on **7a** was reduced to alcohol by $LiAlH_4$ to obtain **14** with ~75% yield. Compound **14** was very polar on silica gel (R_f=0.1 eluted with CH_2Cl_2).

The aldehyde unit can also be converted to nitrile by reacting with an excess amount of $NH_2OH{\cdot}HCl$ in refluxing formic acid to obtain **16** with ~85% yield. The polarity of **7a** and **16** were very similar on silica gel; a complete reaction was necessary to avoid the separation of **7a** and **16**.

The nitrile group on compound **17** was efficiently converted to amidine or amidinium salts by using the Weinreb's amide transfer reagent.[34] This reagent was prepared by reacting 1:1 ratio of ammonium chloride and trimethylaluminum in toluene at 5°C for 1~2 hours. **18** was purified by washing with dilute HCl and water, and recrystallization from CH_2Cl_2/hexane solution.

In our hands, neither acid nor basic hydrolysis of compound **16** or **17** could convert the –CN group to its corresponding $-CO_2H$ group. Thus one of the aldehyde in compound **4** was oxidized to carboxylic acid to produce compound **4b** before the corrole ring formation. It should be noted that during the basic

hydrolysis of **4a** to **4b** the refluxing must be carried out under nitrogen; the presence of air gave dicarboxylic xanthene, likely via air oxidation.

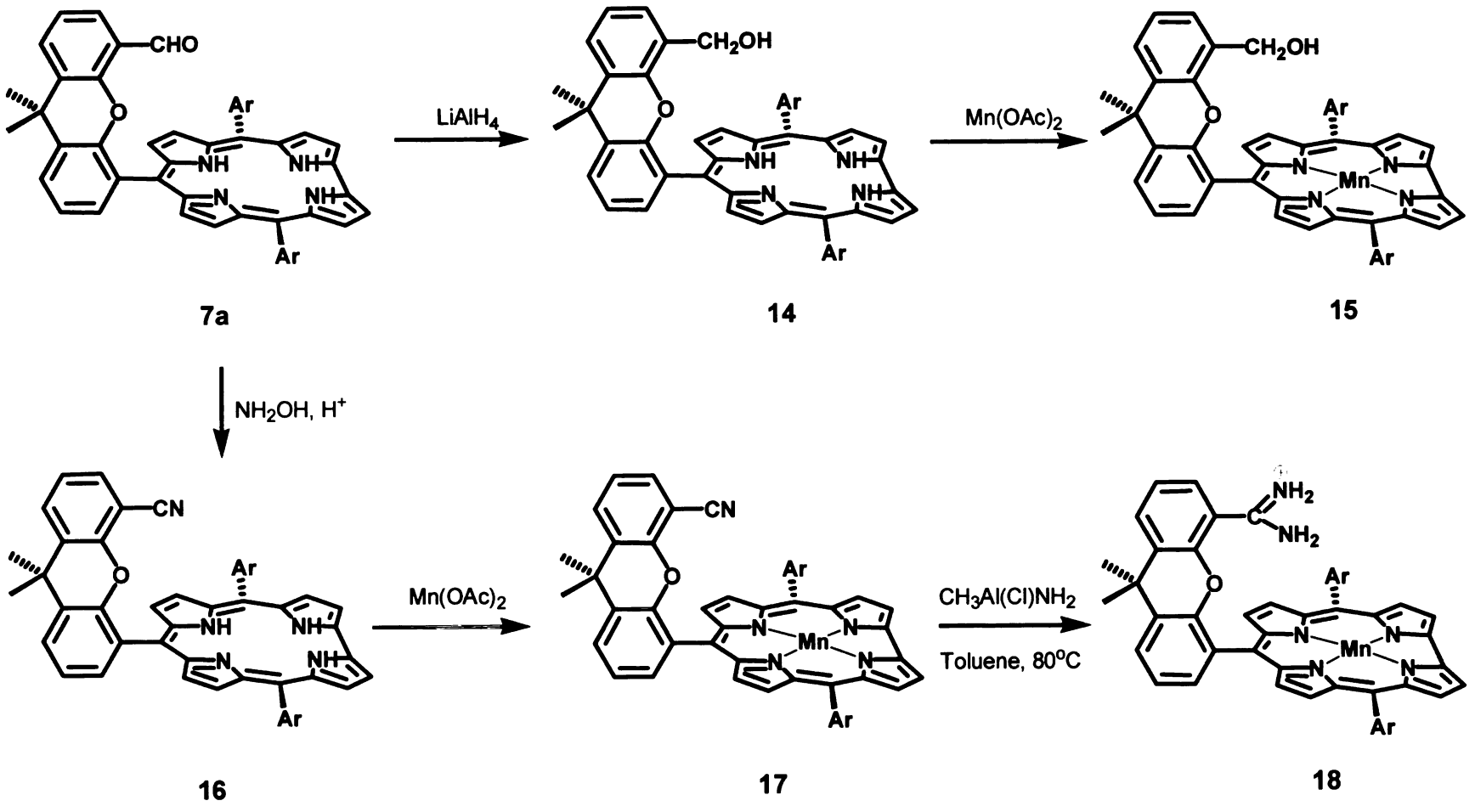

Scheme 2-5. Synthesis of **14~18**.

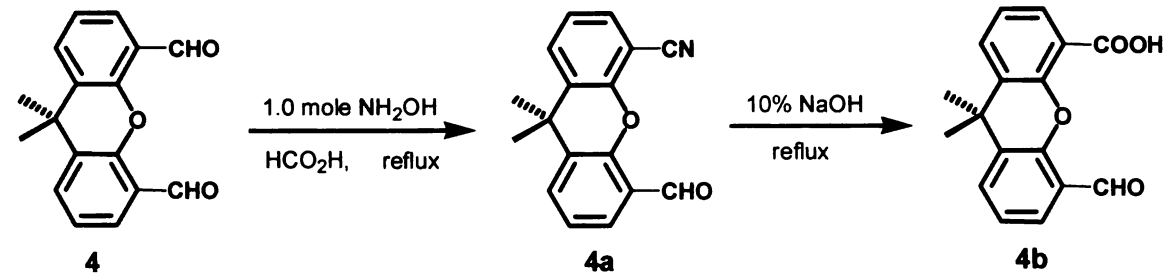

4 4a 4b

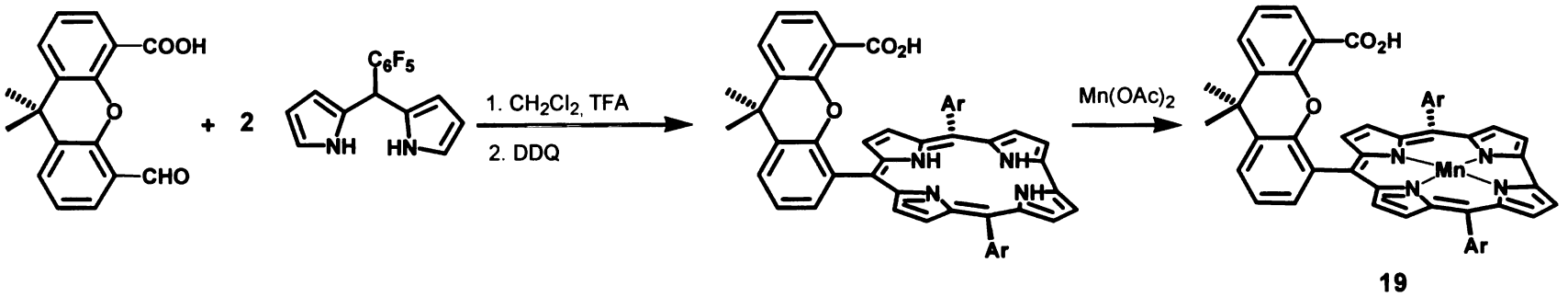

19

Scheme 2-6. Synthesis of **19**.

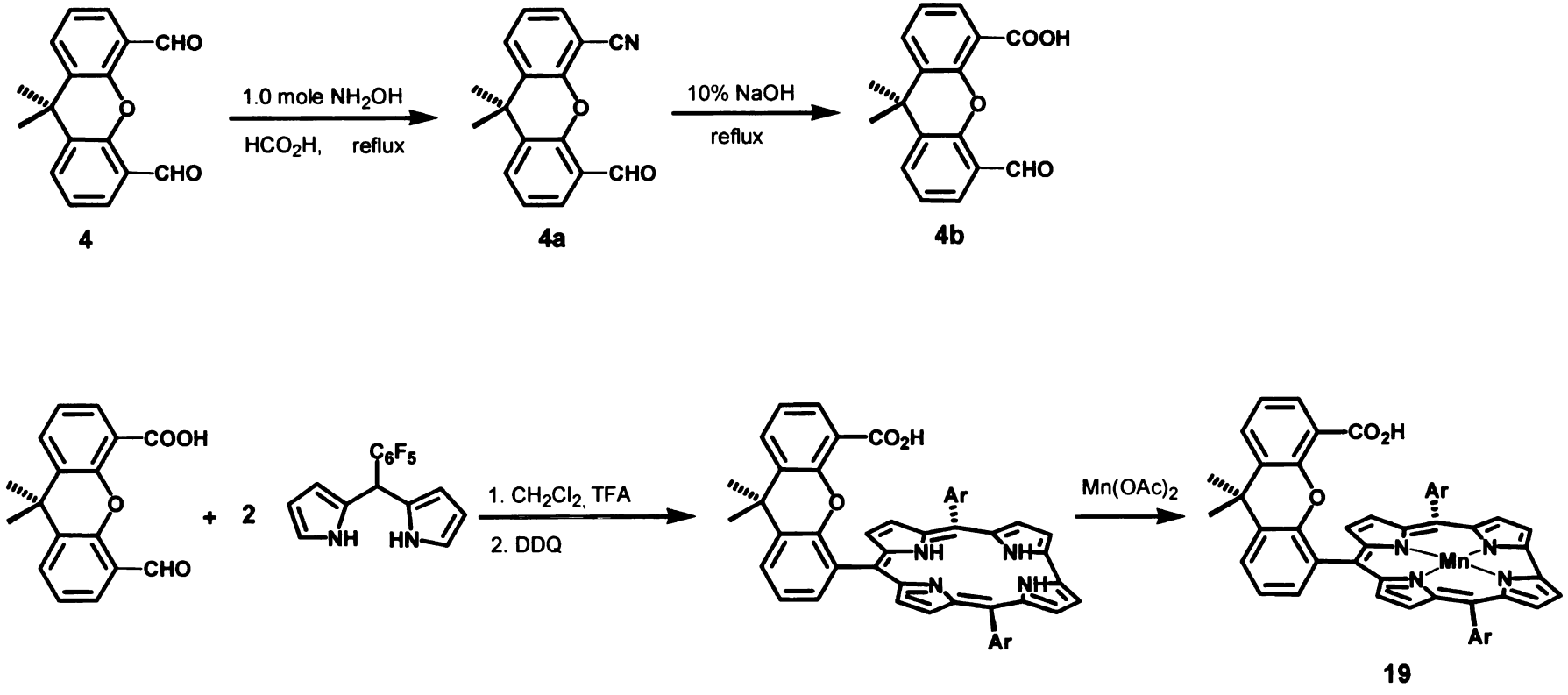

Scheme 2-6. Synthesis of **19**.

Crystal structure

Single crystals of H_6DCX were grown in a layer diffusion of methanol and $CHCl_3$ solution of H_6DCX. And The X-ray structure of H_6XDC, **7**, is shown in side-view in Figure 2-4. Overall the two corrole planes are essentially parallel, with a general concave or bowed curvature of the individual pyrrole rings splayed out from the inter-corrole void.

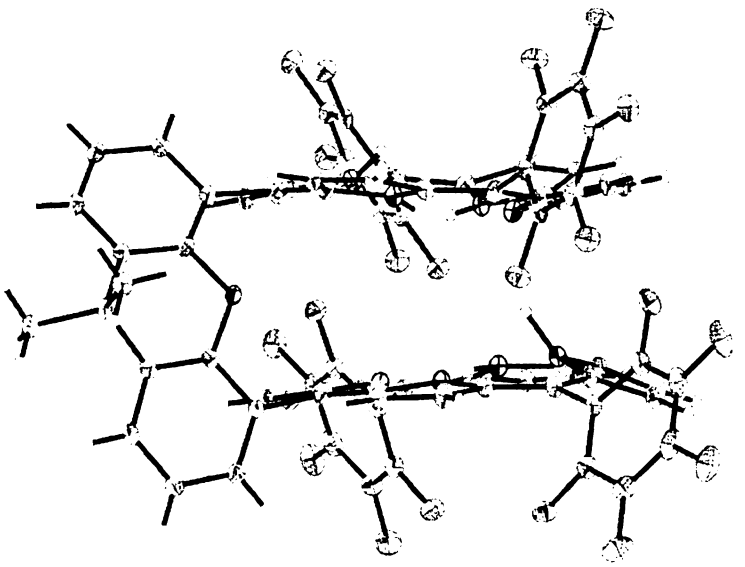

Figure 2-4. Side view of the molecular structure of H_6XDC. Thermal ellipsoids enclose 30% probability. One Solvent molecule (CH_3OH) is omitted for clarity.

The six acidic protons of the eight corrole nitrogens in the crystal structure of H_6DCX are found to be localized, so that the 6 N-H and 2 N: positions are not crystallographically disordered. The reason for this is that a specific set of hydrogen bonds is formed by the compound, both intra-molecularly and to a methanol of solvation. The distance between two N-4 centroids is 3.59Å, and the mean plane separation calculated from the average distance of one N-4 centroid to the opposite N-4 plane is 3.43Å. The dihedral angle between the

two N-4 planes is 18.8°. This apparent deviation from parallel orientation may be exaggerated by the fact that one pyrrole ring in one corrole is tipped down to the other ring to form an intra-molecular N-H---N hydrogen bond. The degree of non-planarity in the two corroles can be estimated by the mean deviations of 0.14Å and 0.16Å respectively of all corrole ring non-H atoms. The bridging dimethylxanthene acts as a hinged spacer group. The central pyran ring has a boat conformation, which creates a dihedral angle of 31° between the two fused aryl substituents. While the geometric arrangement created at the hinge is consistent with Cs mirror symmetry, this is not found in the solid state due to the asymmetry of packing with the methanol solvent of crystallization, which interacts with just one half of the biscorrole unit.

Optical properties

The UV/vis spectra of biscorroles typically exhibit an intense Soret absorption at around 400nm (Figure 2-5) in dichloromethane, showing a large blue-shift (~13nm) compared to that of free-base 10-phenyl-5,15-bispentafluoro-phenylcorrole. This phenomenon is well-known for cofacial diporphyrins.[5~6, 11~12,] The fluorescence of H_6DCX, H_6DCA and H_6DCB were significantly quenched from the level of monomeric corroles, (Figure 2-6) which is generally an indication of the tight space of these cofacial biscorroles.

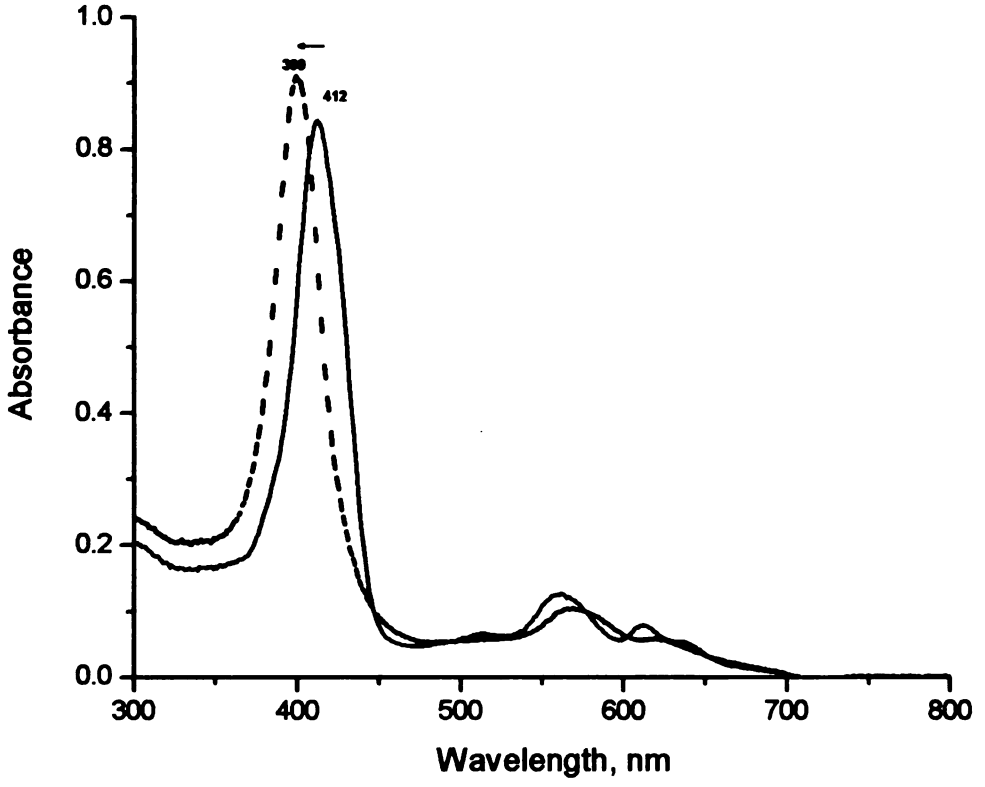

Figures 2-5. UV-Vis spectra of H_6DCX (—) and 10-phenyl-5,15-bispentafluorophenylcorrole (—) in CH_2Cl_2. (This Image is presented in color)

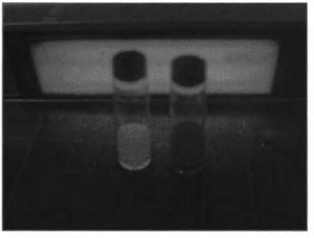

Figure 2-6. Fluorescence of $H_3F_{15}C$ (left) and H_6DCX (right). (This Image is presented in color)

Catalases model

As mentioned earlier, catalases take the first line of defense against oxidative stress of H_2O_2 that may be produced during metabolism. The chemical model to mimic catalase must be able to accomplish two important features: fast rate and propensity to scavenge appreciable levels of peroxide. The catalase-like activity of Mn_2DCX was initially reported by us in 2004.[36] With two additional cofacial dicorroles **5** and **6** and their di-Mn biscorrole complexes **8** and **9** made available, we have a full set of models to study the H_2O_2 dismutation. The catalase-like activity of Mn_2DCA **8**, Mn_2DCB **9**, and Mn_2DCX **10** were monitored by measuring the volume of oxygen gas evolution with catalyst/H_2O_2 ratio of 1:1000 under heterogeneous condition at the presence of phase transfer catalyst and 1,5-dicyclohexylimidazole as axial ligand. The 1,5-dicyclohexyl substituents on the imidazole providing a bulkiness of this axial ligand which ensured that coordination of the axial ligand did not occur inside the two Mn-corrole planes but from the outside of the dimer. Dioxygen stoichiometry was established by measuring the release of gas with a calibrated burette. The released volume of O_2 gas was found to satisfy the 2:1 H_2O_2:O_2 stoichiometric ratio implied by equation 2-1, which is characteristic of dismutation:

$$2H_2O_2 + \text{Catalase} \rightarrow 2H_2O + O_2 + \text{Catalase} \quad \text{(Eqn. 2-1)}$$

Catalytic activities expressed in turnover numbers (TON) for Mn_2DCA **8**, Mn_2DCB **9**, and Mn_2DCX **10** are listed in Table 2-2. For all of these catalysts, the first 1000 folds of H_2O_2 gave almost a quantitative yield of O_2 and all completed within first 2 hours. And during the catalytic cycles, a color change of the catalyst phase ($CHCl_3$) is observable if the stirring speed is low.

Table 2-2. Turnover numbers (TON) for oxygen release from H_2O_2 dismutation (L=1,5-dicyclohexylimidazole).

Entry	Catalyst	TON [c]
1	Mn_2DCA, **8**, + L	1760 ± 105
2	Mn_2DCB, **9**, + L	1470 ± 150
3	Mn_2DCX, **10**, + L	1960 ± 140
4	$MnF_{15}C$ + L	20 ± 5
5	$MnF_{15}C$ [a] + L	25 ± 5
6	Mn_2XDC, **10** [b]	310 ± 40

[a] mole ratio of $MnF_{15}C$ is doubled; [b] Absent of 1,5-dicyclohexylimidazole; [c] the overall turn-over number is calculated after 24 h when the catalyst become inactive towards H_2O_2.

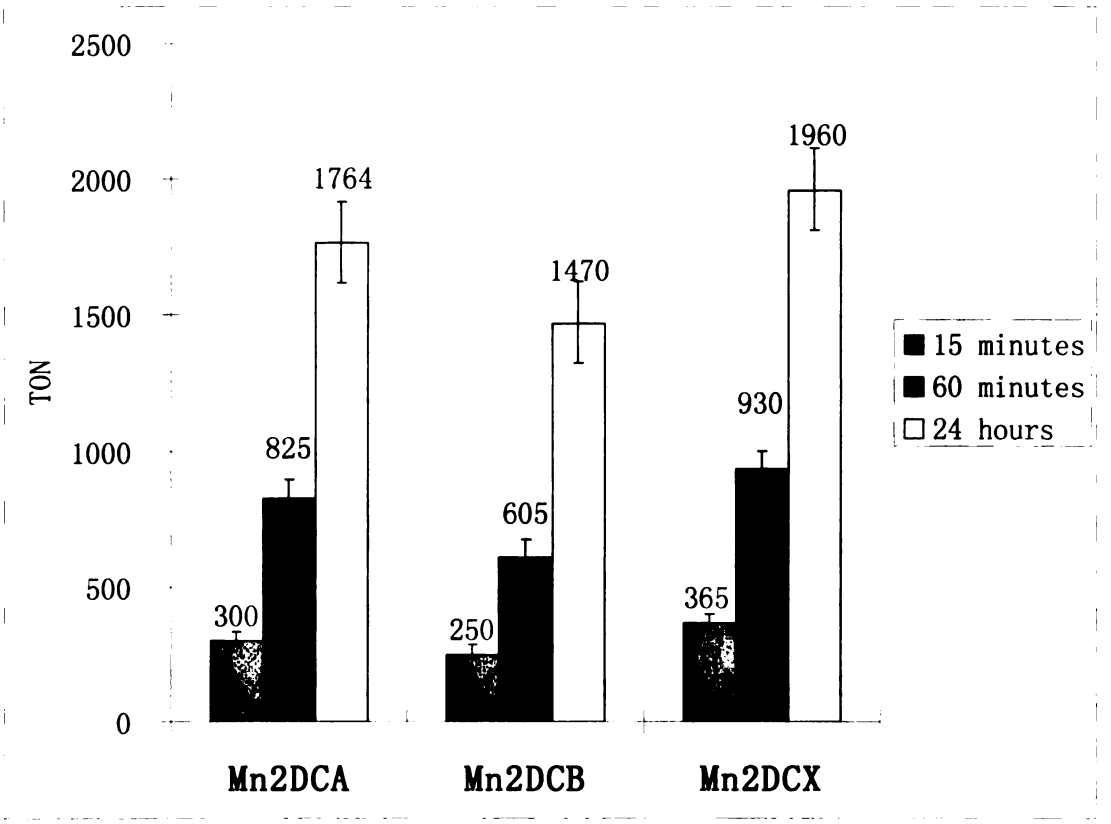

Figure 2-7. Turn over number of catalyst **8**, **9** and **10**.

Several control experiments were performed to verify the significance of the foregoing results. A negligible oxygen evolution was observed in the absence of catalyst, only 0.2 mL (0.008 mmol) of oxygen was released after 3hrs. The reference compound, monomeric $MnF_{15}C$ (entry 4) failed to increase the oxygen evolution from the level of the absence of catalyst, and showed no significant improvement to the TON even when the concentration of $MnF_{15}C$ was doubled (entry 5). And in the absence of the axial 1,5-dicyclohexylimidazole ligand (entry 6), the O_2 evolution was significantly lower, indicating the axial ligand is important for the reaction. The TON of Mn_2DCB is ~25% lower compare to that of the Mn_2DCA and Mn_2DCX, and this may be due to the longer distance of the two Mn centers when spaced by

dibenzofurane. However, the catalase-like activity of Mn_2DCB is still significantly higher than its diporphyrin analog, which is nearly inactive towards H_2O_2 dismutation.[19]

The rate of O_2 evolution in the heterogeneous condition is strongly dependent on the stirring speed and concentration of the phase transfer catalyst. Another set of H_2O_2 dismutation experiments was performed in acetonitrile using Mn_2DCX as catalyst. In these homogeneous tests, the H_2O_2/catalyst ratio was set from a range of 500:1 to 62.5:1, and the O_2 evoluted from the first five minutes was recorded. A *pseudo*-first order reaction of O_2 production was obtained (Figure 2-8), indicating only one molecule of the di-Mn-bis-corrole is involved in the dismutation reaction of H_2O_2. In such homogeneous system, the catalyst appeared to decompose quickly, and the overall TON in homogeneous test is limited to the range of 500 to 800, depending on the H_2O_2/catalyst ratio.

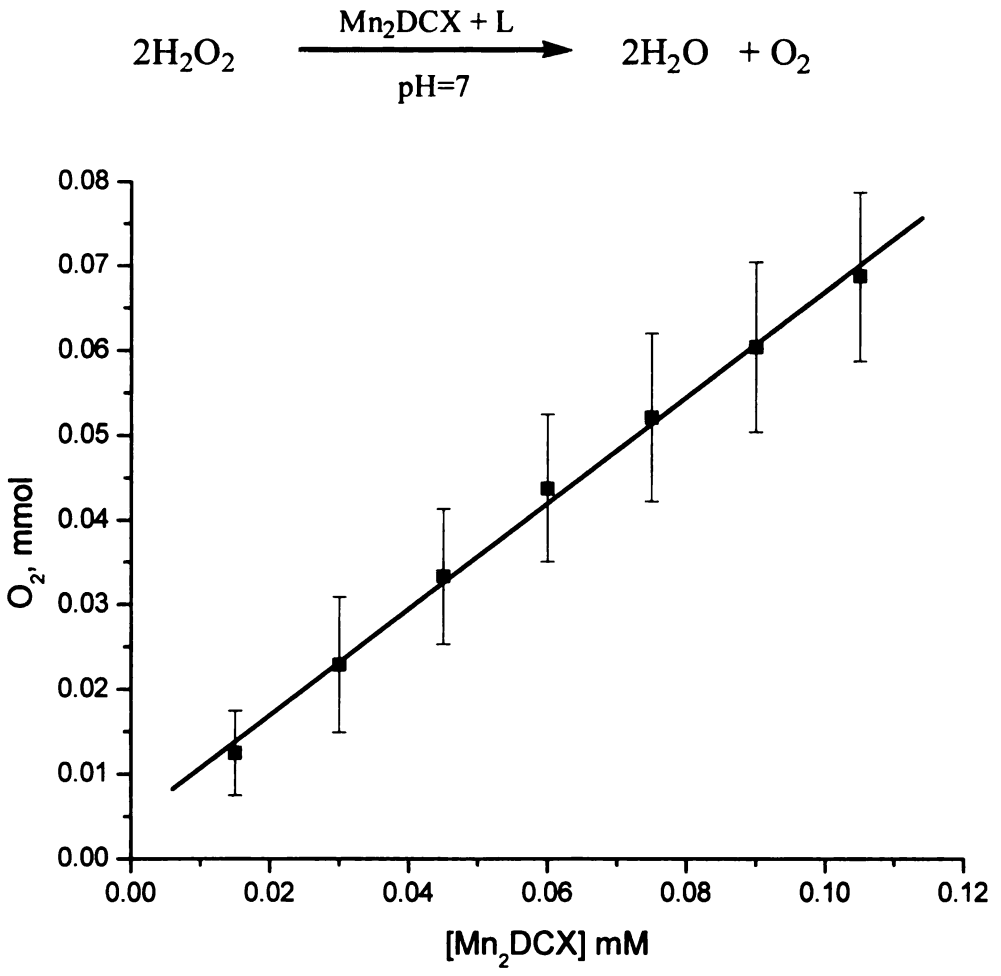

Figure 2-8. The initial phase of oxygen evolution collected in the first 5min in Mn_2DCX catalyzed H_2O_2 dismutation.

Some natural catalases have been found to be sensitive to pH,[1] thus another set of experiments were performed to find out the pH dependence of the di-Mn-biscorrole using Mn_2DCX as model compound. In these experiments, the reaction was carried out in 1mL of CH_2Cl_2 and 1mL of aqueous buffer solution

at different pH. The results of TON for O_2 released in the first 60 minutes in different pH catalyzed by Mn_2DCX are given in Table 2-3 and Figure 2-9.

Table 2-3. TON for O_2 releases in the first 60 minutes catalyzed by Mn_2DCX.

Entry	pH	TON
1	3	1560 ± 85
2	4	1440 ± 70
3	5	1240 ± 70
4	7	930 ± 35
5	8	1110 ± 55
6	10	1290 ± 65

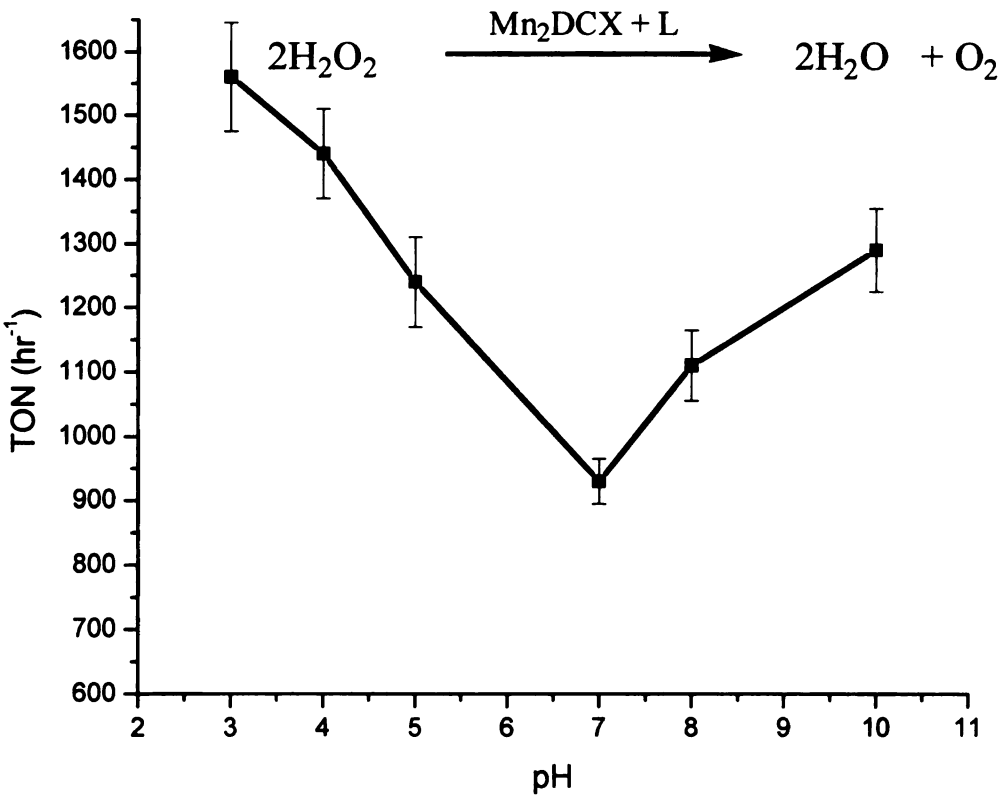

Figure 2-9. pH dependence of O_2 released in the first one hour.

The results clearly indicate a faster dismutation occuring at either acidic or basic conditions. This may suggest acid or base catalysis although the faster rate at basic condition may be due to the activity of axial ligand as OH^- may coordinate to the metal center.

The mechanism of enzymatic H_2O_2 dismutation has not been fully defined. The commonly agreed pathway involves two H_2O_2 molecules incorporated in the dinuclear manganese center. In our models, the monomeric manganese

corrole complex does not show any catalase-like activity whereas the di-manganese biscorrole complexes exhibit a superior activity. And during the catalytic cycle, the green Mn(III) catalyst could turn brownish-red if the stirring is stopped, which appears to be an Mn(V)-oxo species. Moreover, the presence of an axial ligand is crucial in enhancing the rate and turnover of dismutation. Also, the turnover rate depends on the pH.

All these results lead us to propose a possible mechanism for the H_2O_2 dismutation catalyzed by di-Mn-biscorroles. (Scheme 2-7) Taking into consideration of the difference observed in a corresponding diporphyrin system that is significantly less reactive, we suggest that the involvement of an asymmetric Mn^{III}/Mn^{V} intermediate is crucial in the catalytic cycle. Whereas in the diporphyrin system Mn^{III}/Mn^{III} μ-oxo dimer is well known as a stable compound, the Mn^{IV}/Mn^{IV} μ-oxo dimer in corrole has never been detected. It is likely that the coordinated H_2O_2 molecule undergoes a O-O bond cleavage by using the second Mn(III) site as a Lewis acid to help polarize the O-O bond to facilitate the formation of a Mn(V)-oxo intermediate. The Mn(V)-oxo can then be readily reduced by another H_2O_2 molecule.

The cleavage of the first coordinated H_2O_2 to generate Mn(V)-oxo as well as the second H_2O_2 to produce O_2 could benefit from general acid/general base catalysis, which seems to agree with the pH profile. The robustness of the catalyst might have benefited from the fast decompostion rate of the (Mn)-

H_2O_2-(Mn) complex without incurring the accumulation of any highly reactive intermediate.

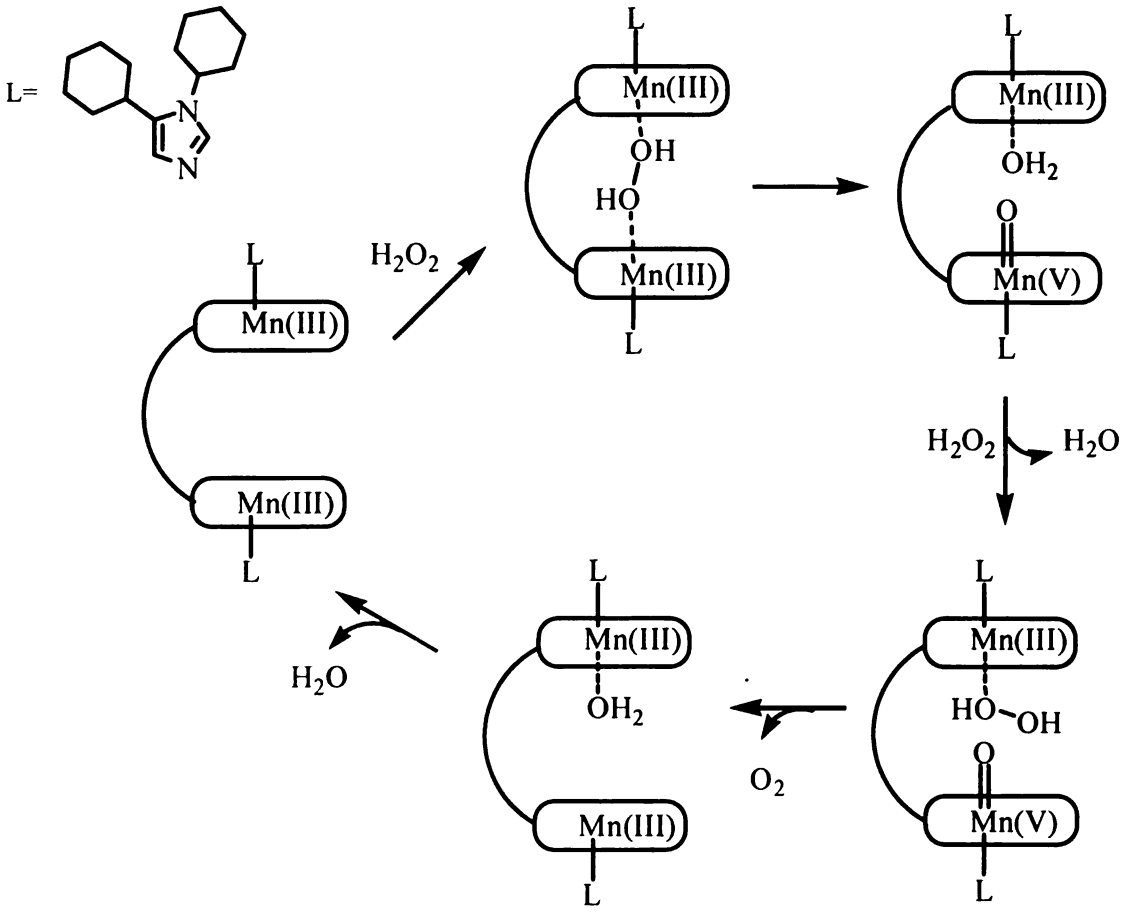

Scheme 2-7. Proposed mechanism that involves Mn^{III}/Mn^{V} intermediate.

In contrast to the porphyrin system in which the easily formed Mn(III)-O-Mn(III) is a thermodynamic sink, the proposed formation of the asymmetric [Mn(V)-oxo Mn(III)] intermediate could account for the difference of monomeric Mn(III) corrole versus cofacial biscorrole, and between the di-manganese biscorrole and diporphyrin. The difference may be understood by the closed-

shell electronic structure requirement for linear L_5M-X-ML_5 dinuclear transition metal complexes (where L_5 is porphyrin or corrole plus an axial ligand).[37] The configuration of the μ–oxo dimanganese in porphyrin is d^4-d^4 with two 3-center π bonds in the linear Mn^{3+}-O-Mn^{3+} unit. In the corresponding corrole system, the metals would be in the +4 oxidation state and the d^3-d^3 configuration would not satisfy the closed-shell requirement (Scheme 2-8).

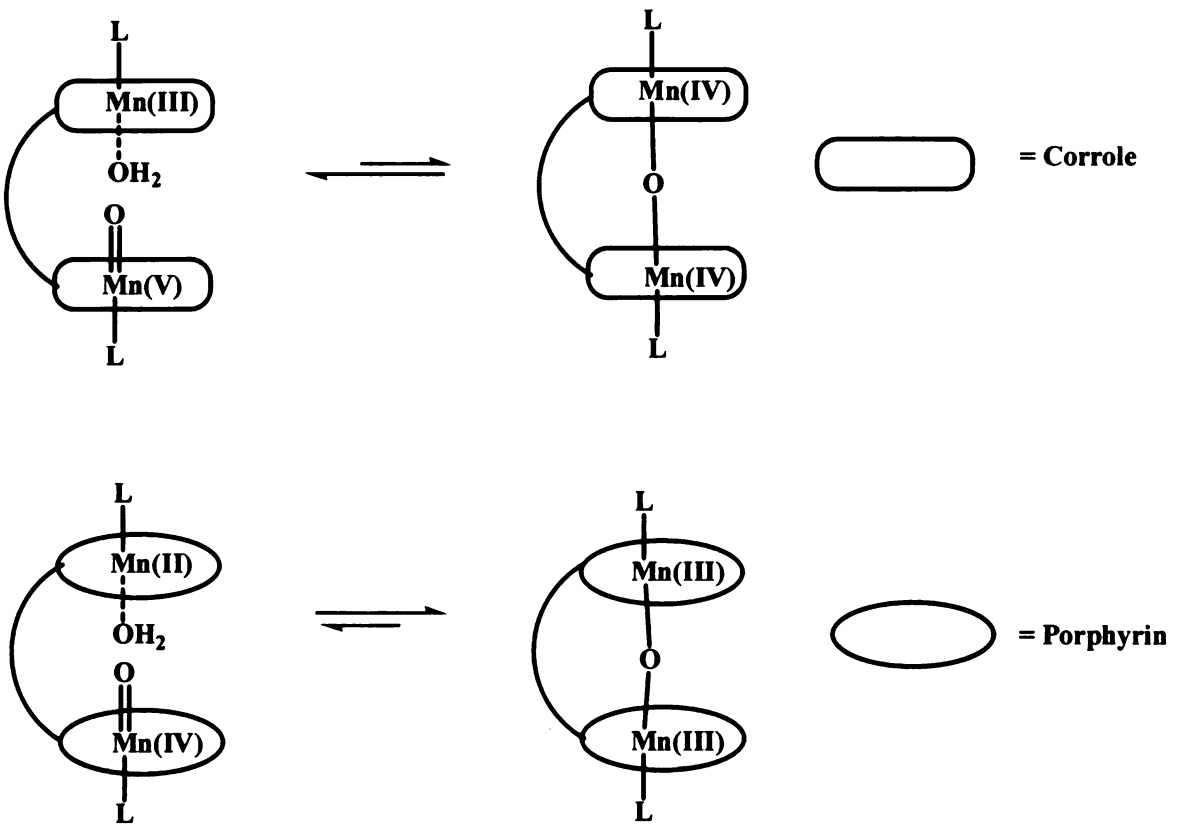

Scheme 2-8. formation of diMn-μ–oxo complexes in corrole and porphyrin.

In order to verify this mechanism, heterometal dicorrole complexes, compound **11~13** were synthesized and used for comparison. The result was summarized at Table 2-4. In this set of experiments, the reaction condition is heterogeneous and buffered with 1mL of buffer solution (pH=7).

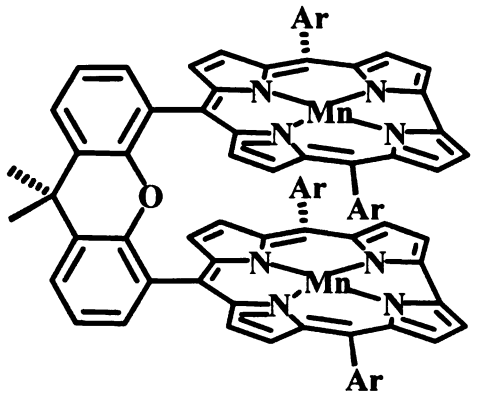

10: Mn_2DCX

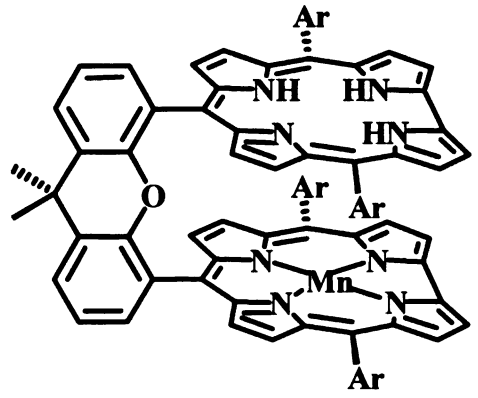

11: MnH_3DCX

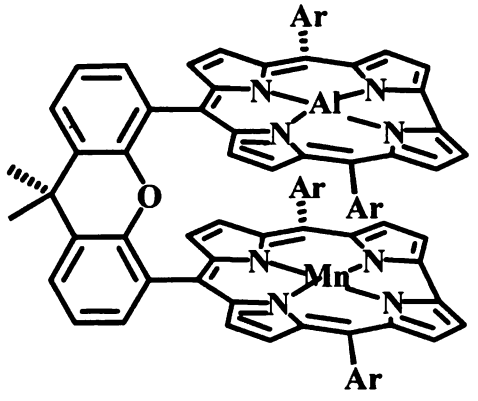

12: AlMnDCX

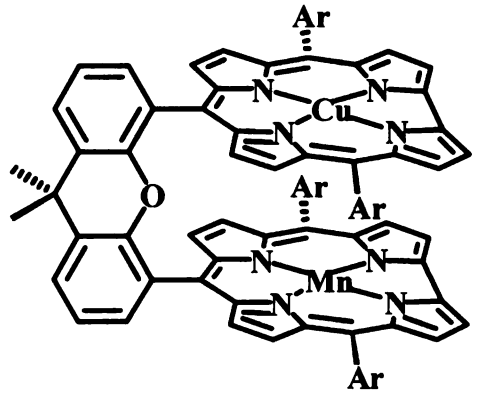

13: CuMnDCX

Table 2-4. Turnover numbers (TON) for Oxygen Release from H_2O_2 dismutation.

Entry	Catalyst	TON
1	Mn_2DCX, **10**	1960 ± 140
2	H_3MnDCX, **11**	250 ± 75
3	AlMnDCX, **12**	680 ± 45
4	CuMnDCX, **13**	85 ± 20

When one manganese metal is replaced with aluminium, which has a stronger Lewis acid character, the TON is still high, whereas with the MnCu dimer, or in the absence of the second metal center, lower TON are observed. The result argues for having the second manganese metal in the dimanganese biscorrole to behave like a Lewis acid to polarize the O-O bond in peroxide, facilitating the bond cleavage. These results suggest that a monomeric Mn-catalyst could still be active in H_2O_2 dismutation, but another Lewis acid site or an intramolecular Bronsted acid must be present at close proximity.

The role of intramolecular Bronsted protons in the dismutation reaction by monomeric Mn-corrole has also been examinated. Four monomeric Mn-corroles, **15**, **17~19** (Figure 2-10), bearing different functional groups have been synthesized and tested; the pKa values of these compounds are 15 (compound **15**, $-CH_2OH$), 9.5 (compound **18**, $-C(NH_2)=N^+H_2$) and 4 (compound **19**, -COOH). The results are summarized in Table 2-5. In this set of experiments, the reaction condition is heterogeneous and buffered with 1mL of buffer solution (pH=4).

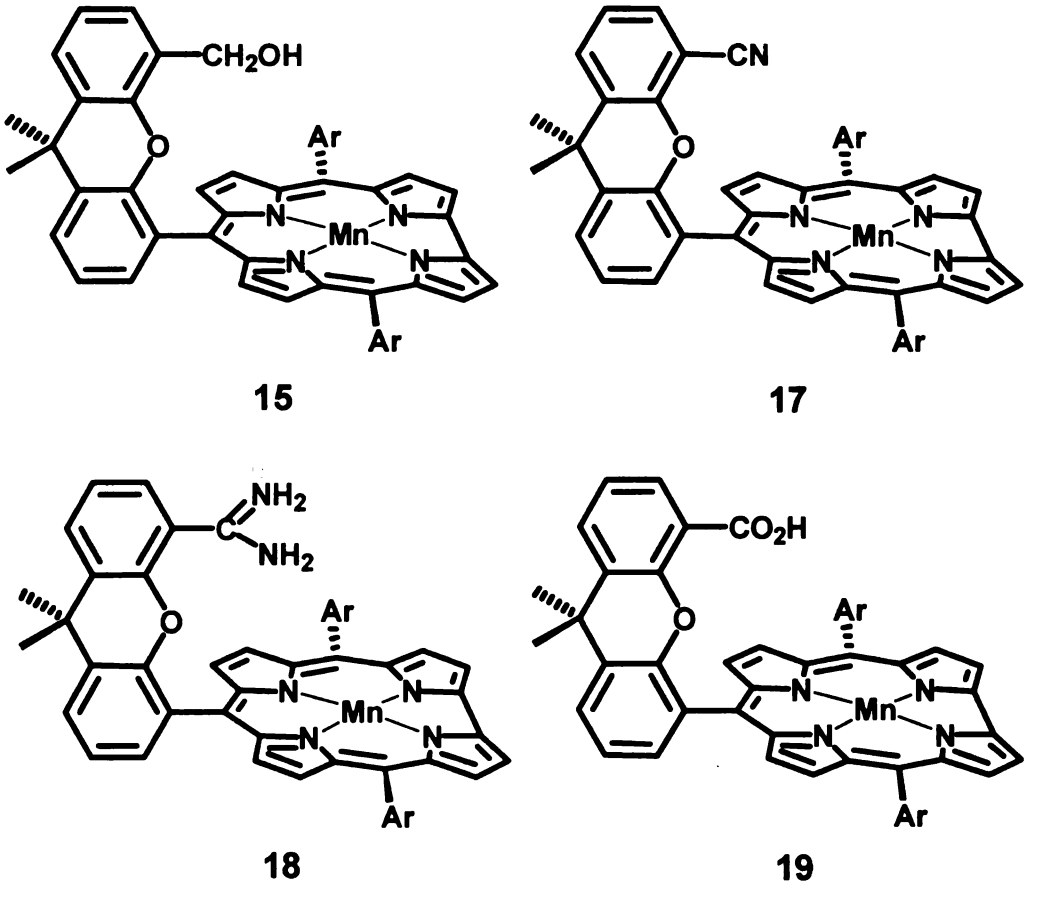

Figure 2-10. Structure of compound **15**, and **17~19**.

Table 2-5. Turnover numbers (TON) for Oxygen Release from H_2O_2 dismutation at pH=4.

Entry	Catalyst	TON
1	**15**	130 ± 10
2	**17**	20 ± 10
3	**18**	490 ± 45
4	**19**	530 ± 20

The turnover numbers in Table 2-5 indicate that the presence of intramolecular acidic proton (entry 3 and 4) can render the unreactive monomeric Mn-corrole more reactive in H_2O_2 dismutation reaction. The cyano group of **17** (entry 2) has no effect and **17** remains as inactive as simple Mn-corrole ($MnF_{15}C$ in Table 2-2 entry 4). Moreover, that the TON of $MnF_{15}C$ stayed the same in more acidic condition (pH=3) shows the importance of the intramolecular carboxylic acid and admidinium groups in compound **18** and **19**, as they should also serve as anchor to coordinate the second H_2O_2 molecule and facilitate the dismutation and release O_2 gas.

2-3. Conclusion

In conclusion, we have synthesized and characterized three different types of cofacial biscorrole and their di-Mn(III) complexes as well as the heterometal corrole complexes (Al-Mn and Cu-Mn-biscorrole). We also demonstrated the surprisingly high activity of di-manganese biscorrole towards H_2O_2 dismutation, suggesting that cofacial biscorrole is a superior platform for modeling the biomimetic multi-electron transfer process. An asymmetric Mn(III) Mn(V)-oxo intermediate was proposed to be responsible for the high activity. We further demonstrated the crucial role of an intramolecular acidic proton in H_2O_2 dismutation reaction.

2-4. Experimental

Instrumentation

UV-VIS Spectra were obtained on a Varian Cary 50 UV-Visible spectrophotometer with samples dissolved in CH_2Cl_2 unless otherwise stated. Mass spectra were recorded by a Finngan TSQ-7000 mass spectrometer. NMR spectra were recorded using a Varian 300 MHz spectrometer. Chemical shift (ppm) were reported with respect to $CDCl_3$, C_6D_6, or d_6-acetone supplied by Cambridge Isotope Laboratories.

Preparation of 5-(pentafluorophenyl)dipyrromethane (1)

Pyrrole (100 mL, 1.44 mol) and pentafluorobenzaldehyde (7.8g, 0.04 mol) were mixed and degassed by nitrogen for 5 minutes. Trifluoroacetic acid (TFA) (0.31 mL, 4.00 mmol) was added to initiate the reaction. The reaction mixture was stirred for 5 to 10 minutes. A potion of 5mL triethylamine was used for neutralizing TFA. The reaction mixture was then extracted by using diethyl ether and washed with water and brine. The product was purified by using a silica gel column with cyclohexane / ethylacetate / triethylamine (8:2:0.1 v/v/v) as the eluent to yield 7.8g (63%) pale yellow powder : ^{1}H-NMR ($CDCl_3$): δ, ppm 8.10 (br, s, 2H, NH), 6.725 (d, 2H), 6.182 (d, 2H), 6.043 (t, 2H), 5.943 (s, 1H), ^{19}F-NMR (282.31mHz): -141.695 (2F), -155.875 (1F), -161.298 (2F). MS (FAB) : m/z=311.9 (M^+), 312.07 calculated for $C_{15}H_9F_5N_2$.

Preparation of 4,6-diformyl-dibenzofuran (3).

Dibenzofuran (24g, 0.142mol) was dissolved in 150mL of dry hexane. N,N,N,N-tetramethylethylenediamine (TMEDA, 54mL, 0.36 mol), freshly distilled over NaOH, was then added. The solution was degassed with a stream of nitrogen for 10 min. 2.5M n-BuLi in hexane (160mL, 0.4mol) was then added slowly, in *ca.* 20 min. The mixture was heated to reflux for 15 min and allowed to cool to room temperature. After cooling to 0°C in an ice-water bath, DMF (freshly distilled over CaH_2 under vacuum, 60 mL, 0.78mol) was added dropwise. The mixture was stirred at 0°C for 10 more min; afterward, it was allowed to warm to room temperature before being poured into 8 L of water. The creamy colored solids were collected by filtration, thoroughly washed with water and heptane, and dried (27.2g, 85%): ^{1}H-NMR ($CDCl_3$), δ 10.72 (2H, s, CHO), δ 8.25 (2H, d), δ8.05 (2H, d), δ 7.57 (2H, t). MS (FAB): m/z=224(M^+), 224.05 calculated for $C_{14}H_8O_3$.

Preparation of 4,5-diformayl-9,9-dimethylxanthene (4).

Xanthone (50.0g, 0.255mol) was suspended in 300mL anhydrous toluene under nitrogen atmosphere. The apparatus was evacuated and filled with nitrogen three times and then cooled to 0°C in an ice bath while trimethylaluminum solution (2.0M in toluene, 350mL, 0.70mol) was added slowly over 50 min. the resulting solution was allowed to warm to room temperature over in *ca.* 3 hrs and stirred further for 16 hrs. The reaction mixture was transferred into a manually stirred mixture of 250 mL of

concentrated HCl and 5 L of ice, via a cannula. The organic phase was separated, dried over $MgSO_4$, filtered, and concentrated by rotary evaporated to afford 51.8g (97%) of **4a** as a yellow oil, which was used without further purification. 9,9-dimethylxanthene **4a** (29.4g, 0.14mol) was dissolved in 1.2 L anhydrous heptane under nitrogen atmosphere. of N,N,N,N-tetramethylethylenediamine (TMEDA, 60mL, 0.40mol), freshly distilled over NaOH, was then added. The solution was degassed with a stream of nitrogen for 10 min. 2.5M n-BuLi in hexane (160mL, 0.4mol) was then added slowly, in *ca.* 20 min. The mixture was heated to reflux for 15 min and allowed to cool to room temperature. After cooling to 0°C in an ice-water bath, DMF (freshly distilled over CaH_2 under vacuum, 60 mL, 0.78mol) was added dropwise. The mixture was stirred at 0°C for 10 more min; then, it was allowed to warm to room temperature before being poured into 8 L of water. The creamy colored solids were collected by filtration, thoroughly washed with water and heptane, and dried: ^{1}H-NMR ($CDCl_3$), δ 10.68 (2H, s, CHO), δ 7.80 (2H, d), δ7.69 (2H, d), δ 7.24 (2H, t), δ 1.67(6H, s, CH_3); MS (FAB): m/z=266(M^+), 251(M^+-CH_3), 266.09 calculated for $C_{17}H_{14}O_3$.

General procedure for preparation of cofacial biscorrole

Pentafluorophenyl dipyrromethane **1** (1.25g, 4.0mmol) and an dialdehyde **2~4** (1.0 mmol) were dissolved in 60mL anhydrous dichloromethane and degassed with a stream of N_2 for 5min. 30uL of TFA was added and the mixture was allowed to stir for 4 hours in room temperature. The reaction mixture was then

diluted to 300 mL with CH_2Cl_2. A total amount of 910 mg DDQ (4 mmol) dissolved in 20mL of toluene was added in 4 portions, in *ca.* 10 min. The reaction mixture was stirred for further 20 min and passed though a silica gel column, eluting with by CH_2Cl_2. The crude product was further purified by column chromatography.

Preparation of 1, 8-bis{10-[5,15-bis(pentafluorophenyl)corrolyl]}-anthracene (5).

The crude product was purified by column chromatography (SiO_2, 1:2 CH_2Cl_2/hexane, 0.1% THF) to afford pure H_6DCA, the solubility of H_6DCA is low in CH_2Cl_2. Recrystallization from $CHCl_3$ and methanol gave deep green powders, 141mg (9.8% yield). ^{1}H-NMR (C_6D_6), δ 8.97 (1H, s), δ 8.489 (1H, s), δ 8.407~8.425 (2H, d), δ 8.108~8.118 (8H, br), δ 8.020~8.082 (4H, d), δ 7.764 (4H, br) δ 7.715~7.728 (2H, d), δ 7.572~7.603 (2H, dd); ^{19}F-NMR ($CDCl_3$), -136.55 (4F, br), -138.781 (4F, br), -153.576 (4F, t), -162.188 (4F, m), -164.227 (4F, br); MS (FAB): m/z=1435($M+1^+$), 1434.23 calculated for $C_{76}H_{30}F_{20}N_8$. UV/vis (CH_2Cl_2): $\lambda_{max,}$ nm: 399(0.95), 567(0.115), 635(0.05).

Preparation of 4, 6-bis{10-[5,15-bis(pentafluorophenyl)corrolyl]}-dibenzyofuran (6).

The crude product was purified by column chromatography (SiO_2, 1:2 CH_2Cl_2/hexane) to afford pure H_6DCB, recrystallization from CH_2Cl_2 and methanol gave deep violet powders, 144mg (10.1% yield). ^{1}H-NMR (C_6D_6), δ

8.365~8.383 (4H, d), δ 8.201 (2H, br), δ 8.166 (4H, br), δ 8.089~8.106 (4H, d), δ 8.042 (2H, br), δ 7.809 (2H, d), 7.628~7.667 (2H, t) ^{19}F-NMR ($CDCl_3$), -135.553(4F, br), -137.651(4F, br), -152.664 (4F, t), -161.920 (4F, m), -162.584 (4F, br); MS (FAB): m/z=1425 ($M+1^+$), 1424.21 calculated for $C_{74}H_{28}F_{20}N_8O$. UV/vis (CH_2Cl_2): $\lambda_{max,}$ nm: 405 (0.95), 572 (0.11), 636 (0.09).

Preparation of 4, 5-bis{10-[5,15-bis(pentafluorophenyl)corrolyl]}-9,9-dimethylxanthene (7).

The crude product was purified by column chromatography (SiO_2, 1:3 CH_2Cl_2/hexane) to afford H_6DCX, recrystallization from CH_2Cl_2 and methanol gave violet needle crystals, 175mg (11.9% yield). ^{1}H-NMR ($CDCl_3$), δ 8.417~8.432 (4H, d), δ 8.046 (4H, s, br), δ 7.952~7.968 (4H, d), δ 7.843~7.890 (6H, m), δ 7.258~7.281 (4H, m), δ 2.190 (6H, s, CH_3); ^{19}F-NMR ($CDCl_3$), -136.887(4F, br), -138.771(4F, br), -153.883 (4F, t), -162.100 (4F, m), -164.317 (4F, br); MS (FAB): m/z=1467($M+1^+$), 1466.25 calculated for $C_{77}H_{34}F_{20}N_8O$. UV/vis (CH_2Cl_2): $\lambda_{max,}$ nm: 399(0.91), 569(0.105), 635(0.06).

***General procedure for preparation of* di-manganese(III) biscorrole.**

0.034 mmol of bicorrole and 50 mg of NaOAc was dissolved in 20 mL of dichloromethane/methanol (1:1). $MnCl_2{\bullet}4H_2O$ (20mg, 0.101mmol) was then added and the resulting solution was heated to reflux for 20 min. The progress of reaction was monitoring by a UV-vis spectrometer and TLC. The solution was washed with water, dried over $MgSO_4$ and the solvent was evaporated.

The crude product was purified by column chromatography on silica to afford pure di-manganese(III) biscorrole

Preparation of di-manganese-1, 8-bis{10-[5,15-bis(pentafluorophenyl)-corrolyl]}-anthracene, Mn_2DCA, (8).

The crude product was purified by column chromatography (SiO_2, 1:1 CH_2Cl_2/hexane with 1% EtOAc), recrystallization from CH_2Cl_2 and hexane to afford **8** (44 mg, 82% yield) as dark green powder. MS (FAB): m/z=1539($M+1^+$), 1538.06, calculated for $C_{76}H_{24}F_{20}Mn_2N_8$. UV/vis ($CH_2Cl_2$): $\lambda_{max,}$ nm: 395 (1.11), 590 (0.21).

Preparation of di-manganese-4, 6-bis{10-[5,15-bis(pentafluorophenyl)-corrolyl]}-dibenzyofuran, Mn_2DCB (9)

The crude product was purified by column chromatography (SiO_2, 2:1 CH_2Cl_2/hexane with 1% EtOAc), recrystallization from CH_2Cl_2 and hexane to afford **9** (40 mg, 75% yield) as dark green powder. MS (FAB), m/z=1529($M+1^+$), 1528.04, calculated for $C_{74}H_{22}F_{20}Mn_2N_8O$. UV/vis ($CH_2Cl_2$): $\lambda_{max,}$ nm: 398 (0.99), 588 (0.17).

Preparation of di-manganese-4, 5-bis{10-[5,15-bis(pentafluorophenyl)-corrolyl]}-9,9-dimethylxanthene, Mn_2DCX (10)

The crude product was purified by column chromatography (SiO_2, 1:1 CH_2Cl_2/hexane with 1% EtOAc), recrystallization from CH_2Cl_2 and hexane to

afford pure **10** (42 mg, 79% yield) as dark green powder. MS, (FAB): m/z=1571($M+1^+$), 1570.08, calculated for $C_{77}H_{28}F_{20}Mn_2N_8O$. UV/vis ($CH_2Cl_2$): $\lambda_{max,}$ nm: 397 (1.04), 588 (0.190).

Preparation of manganese-4, 5-bis{10-[5,15-bis(pentafluorophenyl)-corrolyl]}-9,9-dimethylxanthene, H_3MnDCX (11)

7 (200mg, 0.136mmol) and 200 mg of NaOAc was dissolved in 100 mL of pyridine/methanol (1:1) and reflux under N_2. $MnCl_2 \bullet 4H_2O$ (20 mg, 0.101mmol) dissolved in 5 mL methanol was then added to the refluxing solution in 3 potion and the resulting solution was reflux for 30 min. The progress of reaction was monitoring by UV-vis and TLC. The solution was washed with water, dried over $MgSO_4$ and the solvent was evaporated. Then purified by column chromatography (SiO_2, 1:1 CH_2Cl_2/hexane) to recover the unreacted H_6DCX (95mg, 45%). The mixture of H_3MnDCX and Mn_2DCX was separated on a TLC developed by 1:1 mixture of CH_2Cl_2/hexane with 1% EtOAc to afford crude H_3MnDCX. The crude product was then recrystallization from CH_2Cl_2/hexane to afford pure **11** as dark green powder (55mg, 28% yield). HRMS (MALDI-TOF): m/z=1518.2167(M^+), 1518.1682 calculated for $C_{77}H_{31}F_{20}MnN_8O$. UV/vis (CH_2Cl_2): $\lambda_{max,}$ nm: 398 (1.015), 404 (0.98), 588 (0.293).

Preparation of* copper-manganese-*4,5-bis{10-[5,15-bis(pentafluoro-phenyl)corrolyl]}*-9,9-dimethylxanthene, *CuMnDCX (13)

11 (20mg, 0.013 mmol) and 20 mg of NaOAc was dissolved in 10 mL dichloromethane/methanol (1:1). $Cu(OAc)_2 \bullet 4H_2O$ (10mg, 0.04mmol) was then added and the resulting solution was stirred under room temperature for 30 min. The progress of reaction was monitoring by UV-vis and TLC until the polar H_3MnDCX no longer exist. The solution was washed with water, dried over $MgSO_4$ and evaporated to afford crude **13**. The crude **13** was then recrystallization from chloroform/hexane to afford deep green powder, (19mg, 95% yield). HRMS, (MALDI-TOF): m/z=1578.2155 ($M+1^+$) 1578.0843 calculated for $C_{77}H_{28}F_{20}CuMnN_8O$. UV/vis ($CH_2Cl_2$): $\lambda_{max,}$ nm: 402 (1.08), 588 (0.253).

Preparation of* aluminium-manganese-*4,5-bis{10-[5,15-bis(pentafluoro-phenyl)corrolyl]}*-9,9-dimethylxanthene, *AlMnDCX (12)

11 (20mg, 0.013 mmol) and was dissolved in 10 mL dried toluene. 2M solution of trimethylaluminum in toluene (50µL, 0.1mml) was then added and the resulting solution was stirred under N_2 at room temperature for 1hour. The reaction was stopped by adding 1 mL water and 2mL of THF. The solution was washed with water, dried over $MgSO_4$ and evaporated to afford crude **12**. The crude **12** was then recrystallization from THF/hexane to afford deep green powder (12mg, 62% yield). HRMS, (MALDI-TOF): m/z=1614.3471 ($M+THF-1^+$),

1614.1838 calculated for $C_{77}H_{28}F_{20}AlMnN_8O+C_4H_8O$. UV/vis ($CH_2Cl_2$): λ_{max}, nm: 402 (1.32), 588 (0.267).

Preparation of di-cobalt dimer (10b).

7 (50mg, 0.034 mmol) was heated to reflux under air in chloroform/methanol (1:1) with 26 mg triphenylphosphine (0.1mmol) and $Co(OAc)_2 \bullet 4H_2O$ (25mg, 0.1mmol) refluxing for 15 min. The progress of reaction was monitoring by a UV-vis spectrometer and TLC. The resulting solution was concentrated and purified by column chromatography to afford 49mg of pure **10b**. (70% yield). ^{1}H-NMR ($CDCl_3$), δ 8.146~8.160 (4H, d), δ 7.875~7.890 (4H, d), δ 7.763~7.789 (2H, d), δ 7.643~7.690 (6H, m), δ 7.258~7.281 (4H, m), δ 2.019 (6H, s, CH_3); MS (FAB): m/z=1578(M^+), 1578.07 calculated for $C_{77}H_{28}F_{20}Co_2N_8O$.

***Preparation of* di-copper(III) dimer (10c).**

7 (50mg, 0.034 mmol) and 50 mg of NaOAc was dissolved in 20 mL dichloromethane/methanol (1:1). $Cu(OAc)_2 \bullet 4H_2O$ (25mg, 0.1mmol) was then added and the resulting solution was stirred at room temperature for 10 min until the color of the solution became deep red. The solution was washed with water, dried over $MgSO_4$ and evaporated to afford crude **10c**. The crude **10c** was then recrystallized in chloroform/methanol to afford deep red crystals (51mg, 94% yield). ^{1}H-NMR ($CDCl_3$), δ 7.514 (2H, d), δ 7.493 (2H, d), δ 7.458 (2H, d), δ 7.110~7.135 (2H, t), δ 7.021~7.046 (2H, dd), δ 6.847~6.890 (8H, dd,

br), δ 6.681~6.696 (4H, d), δ 1.762 (6H, s, CH_3); MS (FAB): m/z=1588(M^+), 1586.09 calculated for $C_{77}H_{28}F_{20}Cu_2N_8O$.

Preparation of 4-formayl, 5{10-[5,15-bis(pentafluorophenyl)corrolyl]}-9,9-dimethylxanthene (7a).

4,5-diformayl-9,9-dimethylxanthene, **4** (1g, 3.76mmol) and pentafluorophenyl dipyrromethane, **1** (2.3g, 7.37mmol) were dissolved in 500mL of CH_2Cl_2 and 30 uL of TFA was added and the mixture was allowed to stir for 2 days at room temperature. DDQ (1.5g, 6.6mmol) was added in 3 portions. The mixture was stirred for a further 30 min and passed though a silica gel column eluting with CH_2Cl_2. The crude product was further purified by column chromatography (1cm of neutral alumina and ~10 cm of SiO_2) to afford pure **7a** (330mg, 9.6% yield). ^{1}H-NMR ($CDCl_3$), δ 9.090~9.104 (2H, d), δ 8.620 (4H, s, br), δ 8.544 (2H, d), δ 7.868~7.961 (2H, dd), δ 7.720 (1H, s, CHO), δ 7.681~7.720 (1H, d), δ 7.523~7.557 (1H, t), δ 7.313~7.336 (1H, t), δ 7.023~7.074 (1H, t), δ 1.906 (6H, s, CH_3); MS (FAB): m/z=866(M^+), 866.17 calculated for $C_{47}H_{24}F_{10}N_4O_2$.

Preparation of 4-nitril, 5{10-[5,15-bis(pentafluorophenyl)corrolyl]}-9,9-dimethylxanthene (16).

86 mg of **7a** (0.1 mmol) was dissolved in 20mL of 98% formic acid with NH_2OH*HCl (10mg, 0.14mmol) and refluxed for 30 minutes under N_2. 20 mL of $CHCl_3$ was added after the reaction mixture was cooled down to room

temperature. The solution was then washed with water and brine. The organic layer was dried over $MgSO_4$ and evaporated to afford crude **16**. The crude product was then purified by chromatography (SiO_2, with 1:1 CH_2Cl_2/hexane, R_f of **16**=0.4 and R_f of **7a** = 0.3) to afford **16** as deep violet powders. (68mg, 85% yield) ^{1}H-NMR ($CDCl_3$), δ 9.095~9.110 (2H, d), δ 8.615 (4H, br), δ 8.564 (2H, d), δ 7.865~7.965 (2H, dd), δ 7.681~7.720 (1H, d), δ 7.525~7.555 (1H, t), δ 7.316 (1H, t), δ 7.026~7.075 (1H, t), δ 1.917 (6H, s, CH_3); MS (FAB), m/z=863(M^+), 863.17 calculated for $C_{47}H_{23}F_{10}N_5O$.

Preparation of manganese-4-nitril, 5{10-[5,15-bis(pentafluoro-phenyl)corrolyl]}-9,9-dimethylxanthene (17).

The same manganese insertion reaction procedure as the preparation of di-Mn dimer was used. The crude product was purified by column chromatography (SiO_2, 1:1 CH_2Cl_2/hexane with 1% EtOAc), to afford pure **17** (22 mg, 85% yield) as dark green powder. MS (FAB): m/z=914 ($M\text{-}1^+$), 915.09 calculated for $C_{47}H_{20}F_{10}MnN_5O$. UV/vis (CH_2Cl_2): λ_{max}, nm: 395 (1.11), 590 (0.21).

Preparation of Weinreb's amide transfer reagent [34]

Ammonium chloride (54mg, 1mmol) was suspended in 10 mL of dried toluene in a 2-necked flask under N_2 with stirrer and cooled to 0°C. A solution of 2M trimethylaluminium in toluene (0.5mL, 1mmol) was added slowly to the solution. The reaction mixture was allowed to stir at 0°C until no more

methane gas evolved from the reaction. The reaction mixture was then warmed to room temperature and was stirred for additional 30 min.

Preparation of manganese-4-admido, 5{10-[5,15-bis(pentafluoro-phenyl)corrolyl]}-9,9-dimethylxanthene (18).

17 (92mg, 0.1mmol) was dissolved in 20 mL of dried toluene, a solution of the Weinreb's reagent (1.5mL, 0.15mmol) was added and the reaction mixture was heated to 80°C under N_2 for 1 hour, the completion of the reaction is monitored by TLC. The reaction mixture was then cooled down to room temperature and was washed with water and diluted HCl (0.1M). The solution was dried over $MgSO_4$ and then evaporated to afford **18** (82mg, 89% yield). MS (FAB) m/z=934 (M^+, 100%), 932.12 calculated for $C_{47}H_{23}F_{10}MnN_6O$.

Preparation of 5-formyl-9,9-dimethylxanthene-4-carboxylic acid (4b).

4 (532 mg, 2mmol) and $NH_2OH{\bullet}HCl$ (146mg, 2.1mmol) was dissolved in 50 mL of formic acid, and the solution was refluxed for 1 hour under N_2. The reaction mixture was cooled down to room temperature and 50mL of $CHCl_3$ was added. The mixture was then washed with water and brine. The organic layer was dried over $MgSO_4$ and evorpated to dryness to afford crude **4a** and used without further purification. MS (FAB) m/z=263(M^+), 263.09 calculated for $C_{17}H_{13}NO_2$. 300mg of crude **4a** was suspended in 20 mL of 10% sodium hydroxide and refluxed under N_2, the reaction was stopped when most of the suspended powder were dissolved. The solution was then cooled to room

temperature and neutralized with HCl. Precipitations were collected by filtration to give crude **4b** which was used without further purification. MS (FAB): m/z=283 ($M+1^+$, 100%), 268($M-CH_3^+$, 85%), 282.09 calculated for $C_{17}H_{14}O_4$.

Preparation of 4-carboxlic, 5{10-[5,15-bis(pentafluorophenyl)corrolyl]}-9,9-dimethylxanthene (19a).

A solution of dipyrromethane **1** (624mg, 2mmol) and aldehyde **4b** (300mg, 1.1mmol) dissolved in 50mL CH_2Cl_2 was deaerated by N_2 for 5min. TFA (35uL) was added and the reaction was allowed to stirred at room temperature for 2 hr. The reaction mixture was diluted to 800mL by CH_2Cl_2 and a solution of DDQ (1.36g, 6mmol) in 20 mL toluene was added dropwise in *ca.* 10 min. The reaction mixture was allowed to stir at room temperature for another 30 min after the addition of DDQ. The reaction mixture was passed through a silica gel column eluting with CH_2Cl_2 and the solvent was evaporated to dryness. The residue was redissolved (CH_2Cl_2:EtOAc 2:1) and pass through a silica gel column to afforded corrole **19a**. ^{1}H-NMR (C_6D_6), δ 8.644~80652 (2H, d), δ 8.506~8.515 (2H, d), δ 8.390~8.399 (2H, d), δ 8.198~8.206 (2H, d),δ 7.860~7.878 (1H, dd), δ 7.551~7.569 (1H, dd), δ 7.355~7.370 (1H, t), δ 6.990 (2H, br), δ 6.589 (1H, t), δ 1.921 (6H, s, CH_3); MS (FAB): m/z=883 ($M+1^+$), 882.17 calculated for $C_{47}H_{24}F_{10}N_4O_3$.

Preparation of manganese-4-carboxyl, 5{10-[5,15-bis(pentafluorophenyl)-corrolyl]}-9,9-dimethylxanthene (19)

The same manganese insertion reaction procedure as the preparation of di-Mn dimer was used. The crude product was purified by column chromatography (SiO_2, 1:1 CH_2Cl_2/EtOAc), to afford pure **19.** MS (FAB): m/z=935 ($M+1^+$), 934.08 calculated for $C_{47}H_{21}F_{10}MnN_4O_3$. UV/vis ($CH_2Cl_2$): $\lambda_{max,}$ nm: 395 (0.99), 590 (0.19).

Determination of H_2O_2 dismutation activity

Dismutation reactions were carried out at 295K in a 5-mL conical reaction vial with a side port, equipped with a magnetic stir bar and a capillary gas delivery tube linked to a graduated burette filled with water. The reaction vial was charged with 0.5μmol of the catalyst, 25μmol of 1,5-dicyclohexylimidazole, 4μmol of benzyldimethyltetradecylammonium chloride, 1mL dichloromethane, and 1mL of buffer. The solution was stirred to ensure gas pressure to reach equilibrium. An aliquot of ~35% H_2O_2 (100μL) was added to the reaction mixture via syringe through the side port, the oxygen evoluted was collected in the burette. The H_2O_2 addition was repeated as the amount of O_2 gas approached its theoretical amount; for Mn dimers, the addition was repeated 4 times. The turnover number was calculated by the number of moles of O_2, assuming the O_2 gas is ideal gas, over the number of moles of catalyst, the overall turnover number was calculated when the catalyst was no longer

active. The identity of the oxygen gas was confirmed independently by using the alkaline pyrogallol test.

X-ray data collection and structure refinement

Crystals were grown by layer diffusion of chloroform and methanol solutions or of chloroform and octane solutions. Data were collected at 293 K and structures were solved by the direct method using NRCVAX program package. All non-hydrogen atoms were refined anisotropically. The hydrogen atoms of interest were located from difference map and refined positionally when appropriate. The crystallographic data for the structures are summarized in Appendix.

References

1. Dismukes G. C. *Chem. Rev.*, **1996**, 96, 2909-2926. and reference there in.

2. Collman, J. P., Wagenknecht, P. S., Hutchinson, J.E. *Angew. Chem., Int. ed. Engl.* **1994**, 33, 1537.

3. Tommos, C., Babcock G. T., *Acc. Chem Res,* **1998**, 31, 18-25.

4. Chang, C.K.; Abdalmuhdi, I. *J. Org. Chem.* **1983**, 48, 5388-5390.

5. Chang C.K.; Liu H.Y.; Abdalmuhdi, I. *J. Am. Chem. Soc.* **1984**, 106, 2725-2726.

6. Chang, C.K.; Abdalmuhdi, I. *Angew. Chem., Int. Ed. Engl.* **1984**, 23, 164-165.

7. Liu H.Y.; Abdalmuhdi, I.; Chang, C.K.; Anson, F.C. *J. Phys. Chem.* **1985**, 89, 665-668.

8. Ni, C.L.; Abdalmuhdi, I.; Chang C.K.; Anson, F.C. *J. Phys. Chem.* **1987**, 91, 1158-1162.

9. Proniewicz, L.M.; Odo, J.; Goral, J.; Chang C.K.; Nakamoto, K. *J. Am. Chem. Soc.* **1989**, 111, 2105-2110.

10. Collman, J.P.; Hutchison, J.E.; Lopz, M.A.; Guilard, R. *J. Am. Chem. Soc.* **1992**, 114, 8066-8073.

11. Collman, J.P.; Hutchison, J.E.; Ennis, M.S.; Lopz, M.A.; Guilard, R. *J. Am. Chem. Soc.* **1992**, 114, 8074-8088.

12. Collman, J.P.; Hutchison, J.E.; Lopz, M.A.; Tabard, A.; Guilard, R.; Seok, W.K.; Ibers, J.A.; L'Her, M. *J. Am. Chem. Soc.* **1992**, 114, 9869-9877.

13. Guilard, R.; Lopez, M.A.; Tabard, A.; Richard, O.; Lecomte, C.; Brandes, S. Hutchison, J.E.; Collman, J.P. *J. Am. Chem. Soc.* **1992**, 114, 9877-9889.

14. Collman, J.P.; Ha, Y.; Wagenknecht, P.S.; Lopz, M.A.; Guilard, R. *J. Am. Chem. Soc.* **1993**, 115, 9080-9088.

15. Guilard, R.; Brandes, S.; Tardieux, C.; Tabard, A.; L'Her, M.; Miry, C.; Gouerac, P.; Knop, Y.; Collman, J.P. *J. Am. Chem. Soc.* 1995, 117, 11721-11729.

16. Le Mest, Y.; L'Her, M.; Hendrick, N.H.; Kim, K.; Collman, J.P. *Inorg. Chem.* 1992, 31, 835-847.

17. Le Mest, Y.; L'Her, M.; Sailard, J.Y. *Inorg. Chim. Acta* **1996**, 248, 181.

18. Chang, C.J.; Loh, Z.H.; Shi, C.; Anson, F.C.; Nocera, D.G. *J. Am. Chem. Soc.* **2004**, 126, 10013-10020.

19. Chng L. L., Chang, C. J., Nocera D. G., *J. Org. Chem.* **2003**, 68, 4075-4078.

20. Simkhovich, L.; Iyer, P.; Goldberg, I.; Gross, Z.; *Chem. Eur. J.*, **2002**, *8*, 2595.

21. Andrioletti, B.; Rose, E.; *J. Chem. Soc., Perkin Trans. 1*, **2002**, 715.

22. Jérôme, F.; Barbe, J.M.; Gros, C.P.; Guilard, R.; Fischer, J.; Weiss, R.; *New J. Chem.* **2001**, 25, 93.

23. Simkhovich, L.; Galili, N.; Saltsman, I.; Goldberg, I.; Gross, Z. *Inorg. Chem.* **2000**, 39, 2704-2705.

24. Kadish, K.M.; Erben, C.; Ou, Z.; Adamian, V.A.; Will, S.; Vogel, E.; *Inorg. Chem.* **2000**, 39, 3312-3319.

25. Jérôme, F.; Billier, B.; Barbe, J.M.; Espinosa, E.; Dahaoui, S.; Lecomte, C.; Guilard, R. *Angew. Chem. Int. Ed.* **2000**, 39, 4051-4055.

26. Guilard, R.; Gros, C.P.; Bolze, F.; Jérôme, F.; Ou, Z.P.; Shao, J.G.; Fischer, J.; Weiss, R.; Kadish, K.M. *Inorg. Chem.* **2001**, *40*, 4845-4856.

27. Guilard, R.; Jérôme, F.; Barbe, J.M.; Gros, C.P.; Ou, Z.P.; Shao, J.; Fischer, J.; Weiss, R.; Kadish, K.M. *Inorg. Chem.* **2001, *40***, 4856-4865.

28. Kadish, K.M.; Ou, Z.P.; Shao, J.G.; Gros, C.P.; Barbe, J.M.; Jérôme, F.; Bolze, F.; Burdet, F.; Guilard, R. *Inorg. Chem.* **2002**, *41*, 3990-4005.

29. Barbe, J.M.; Burdet, F.; Espinosa, E.; Gros, C.P.; Guilard, R. *J. of Porphyrins and Phthalocyanines*, **2003**, 365-400.

30. Kadish, K.M.; Shao, J.G.; Qu, Z.P.; Gros, C.P.; Bolze, F.; Barbe J.M.; Guilard, R. *Inorg. Chem.* **2003**, 42, 4062-4070.

31. Gryko, D. T.; Jadach, K. *J. Org. Chem.*, **2001**, *66*, 4267-4275.

32. Gryko, D. T. Koszarna, B. *Synthesis* **2004**, *13*, 2205-2209.

33. Yam, F. Mphil. Thesis, Hong Kong University of Science and Technology, **2004** Chapter 3.

34. Levin, L.; Turos, E.; Weinreb, S.M. *Syn. Comm.* **1982**, *12*, 989-990.

35. Garigipati, R.S. *Tetrahedron Lett.* **1990**, *31*, 1969-1970.

36. Yam, F.; Liu, H.Y.; Yeung, L.L.; Chang, C.K. poster presented at the *Internationational conference of porphyrins and phthalocyanines,* **2004**.

37. Lin, Z.Y; Hall, M.B. *Inorg. Chem.* **1991**, *30*, 3817-3822.

Chapter 3

Sterically hindered metallocorrole as cytochrome P-450 model

3-1. Introduction

Cytochromes P-450 perform hydroxylation of alkanes and epoxidation of alkenes often with high chemo- and stereoselectivity.[1] The use of iron porphyrins as cytochrome P-450 models has aided the understanding of enzyme mechanisms as well as finding novel applications in synthesis with custom-made catalysts.[2] The use of synthetic manganese (III) porphyrins for such proposes has also been firmly established.[3~4] While the reaction intermediates, the high-valent metal-oxo species, are generally too reactive to be studied directly, the Mn(V)-oxo porphyrin intermediate has been identified and spectroscopically characterized.[5~10] Even so, the low stability of Mn(V)-oxo porphyrins has limited the detailed study of the oxygen atom transfer reactions.

Manganese corroles have also been shown to catalyze epoxidations.[11~14] Since the trianionic corrole macrocycle is thought to stabilize high valence metal center, manganese corroles may offer special advantages with regard to the pursuit of the reactive intermediate. Indeed, a red species produced from idosylbenzene (PhIO) and Mn(III) corroles has been tentatively assigned as Mn(V)-oxo corrole by Gross and our group.[11,14] Yet the reactivity of the Mn(V)-

oxo towards olefins is generally low, and it has been discussed in Chapter 1 that the Mn(V)-oxo complex may not be the only active intermediates in catalytic epoxidation reactions.[15~16]

In the present study, we designed a series of corroles bearing sterically bulky substituents at the *meso* positions (Figure 3-1), which may hinder bimolecular contacts of corrole complexes and thus increasing the stability of the Mn(V)-oxo species. The preparation, spectroscopy properties and reactivities of these Mn(V)-oxo corroles are described in this chapter.

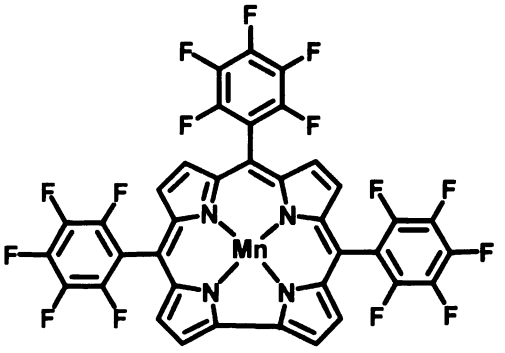

$MnF_{15}C$, 1a

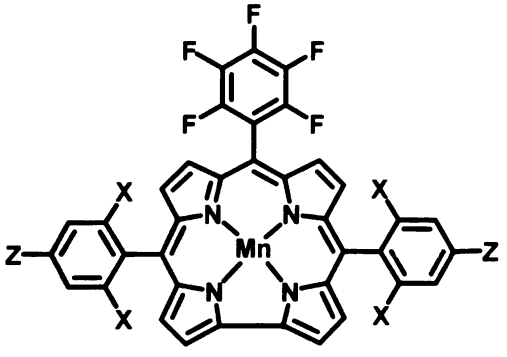

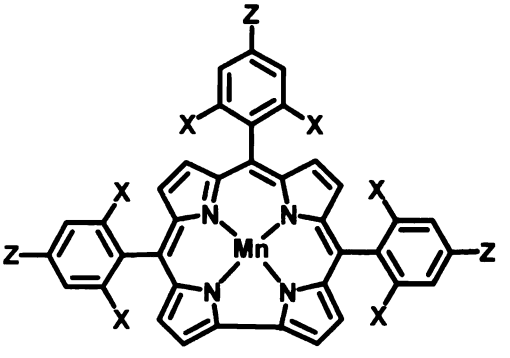

	X	Z
$MnBr_4F_7C$, 6	Br	F
MnT_2F_5C, 7	Ph	Ph

	X	Z
$MnBr_6F_3C$, 8	Br	F
MnT_3C, 9	Ph	Ph

Figure 3-1. Structure of Mn(III) corrole complexes used in this study.

3-2. Results and Discussion

Synthesis

The prerequisite aldehydes, 2,6-dibromo-4-fluorobenzaldehyde and 2,4,6-triphenylbenzaldehyde, were synthesized in high yields according to a literature procedure. (Scheme 3-1) [18]

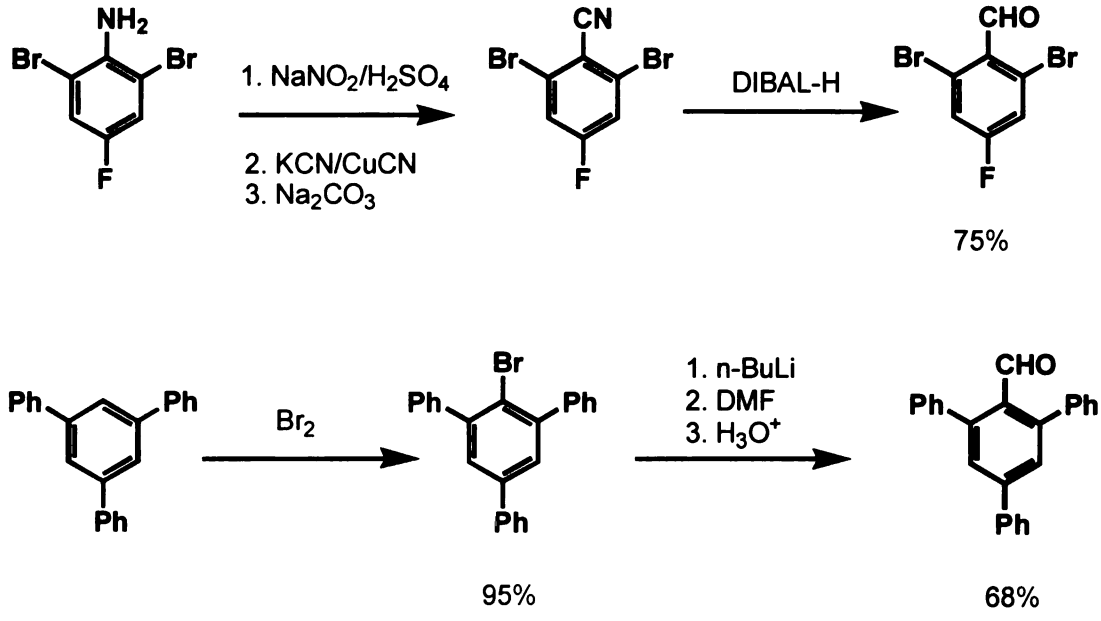

Scheme 3-1. Synthesis of 2,6-dibromo-4-fluorobenzaldehyde and 2,4,6-triphenylbenzaldehyde

The synthetic challenge of bulky encumbered corrole is to overcome the low yield; for example, the tris-2,6-dichlorophenyl corrole has a 1% reported yield by the solvent free method.[11] To synthesize the corrole **2~5**, we use a stepwise approach, giving 3~8% overall yields in optimized reaction conditions (Scheme 3-2). Thus, the dipyrromethanes were synthesized by reacting the corresponding 2,6-disubstituted aldehyde with 40 folds of pyrrole and ~0.1 molar ratio of trifluoroacetic acid;[19] the yields in this step were generally fair

(50~65%). A second aldehyde was then to condense in 2:1 molar ratio with the dipyrromethane under a modified Gryko's condition, (high concentration).[20] The reactivity of the second aldehyde critically affects the yield of corrole formation. For example, the A_2B type corroles (B = pentafluorophenyl) $H_3Br_4F_7C$, **2** and $H_3T_2F_5C$, **3** gave >15% yields whereas the steric hindered A_3 type corroles, $H_3Br_6F_3C$, **4** and H_3T_3C, **5** gave only ~6% yields in the second step. In comparison, a porphyrin analogue of H_3T_3C, the bis-pocket porphyrin reported by Suslick *et al.*[21] in 1983, has <1% overall yield when the reaction is carried out in refluxing propionic acid.

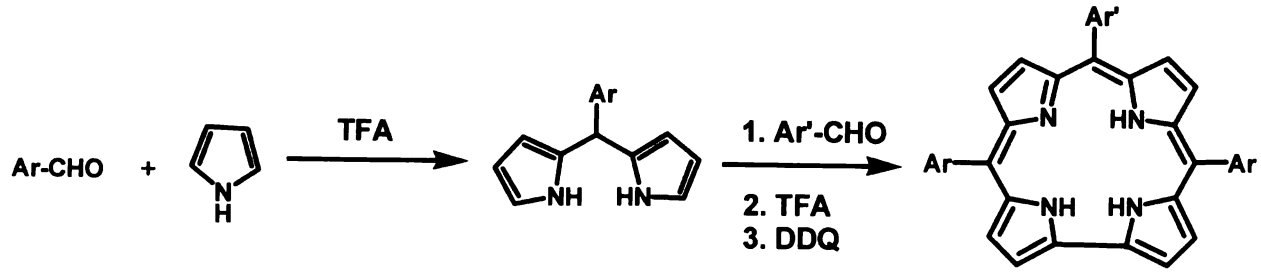

A_2B type corrole

Corrole	Ar	Ar'
$H_3Br_4F_7C$, 2	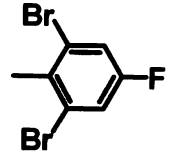	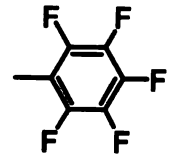
$H_3T_2F_5C$, 3	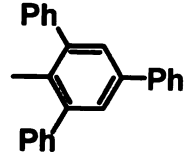	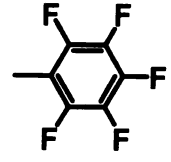

A_3 type corrole

Corrole	Ar = Ar'
$H_3F_{15}C$, 1	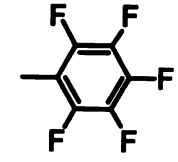
$H_3Br_6F_3C$, 4	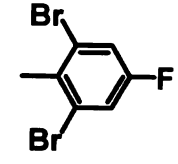
H_3T_3C, 5	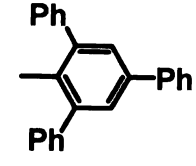

Scheme 3-2. Synthesis of sterically encumbered corroles.

Crystal structure

The solid-state structure of the terphenyl-containing corrole H_3T_3C, **5** has been characterized by X-ray diffraction (Figure 3-2). Single crystals of **5** were grown in a layer diffusion of methanol and $CHCl_3$ solution of **5**. From the side-view of the crystal structure the three terphenyl substituents at the *meso* positions have two sets of torsion angles, the terphenyl groups on C5 and C15 positions have 110° whereas the terphenyl on C10 position has 118° with reference to the corrole plane, and these terphenyl groups are projecting the two ortho-phenyl groups above and below the corrole plane to cover the corrole center. And because corrole has only 3 *meso* positions, there is a wide-open gap between C1-C19 which may provide an opening for the substrate to come in contact with the reactive metal-oxo center.

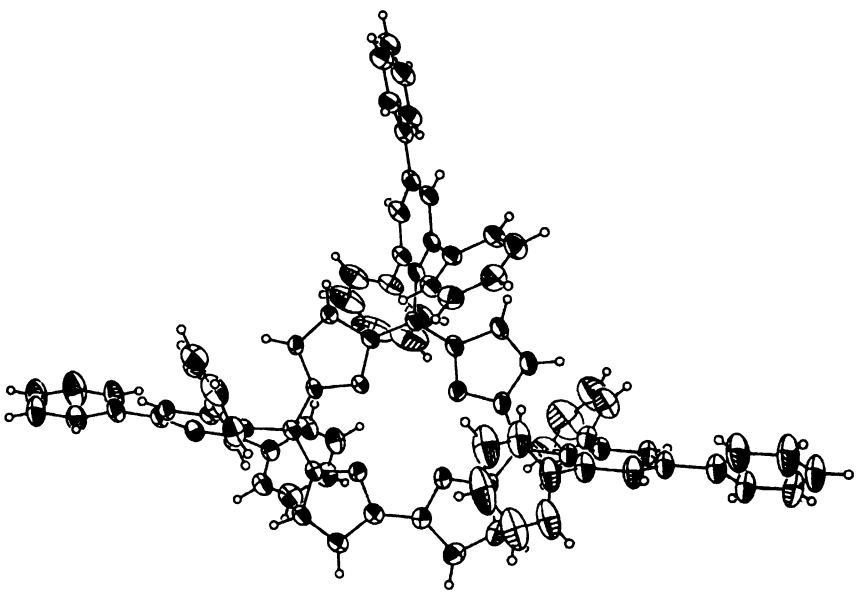

Figure 3-2. Top view of molecular structure of H_3T_3C (**5**). Thermal ellipsoids enclose 50% probability. One solvent molecule (CH_3OH) is omitted for clarity.

Ligand binding of Mn-corrole

The insertion of manganese into sterically hindered corroles was notably slower than that of the less bulky $H_3F_{15}C$ (**1**); thus, a longer refluxing time in pyridine and methanol mixture was necessary to afford the corresponding Mn(III)-corrole at >80% yield. The sterically hindered Mn(III)-corroles exhibit typical absorption bands in UV-Vis spectra, similar to other less bulky Mn(III)-corroles.

The binding of Mn-corroles with *N*-methylimidazole was studied; upon addition of *N*-methylimidazole the absorption band at ~490 nm increased, and the Soret band split into two bands, as shown in Figure 3-3. The Job's plot of [L]/{[L]+[Mn]} showed a maximum at about 0.5, indicating a 1:1 binding stoichiometry.[28] The obtained binding constants for different Mn(III)-corroles are summarized in Table 3-1. The binding constant decreases as the bulkiness of the corrole increases, with the most hindered MnT_3C, **9** showing a 20-fold decrease in binding affinity versus that of the unhindered $MnF_{15}C$, **1a** this tendency may also attributed by the electronic effects of the corrole rings, as the electron density of the corrole rings increase as the bulkiness increase. Note that the binding constants of pyridine are at least 4 orders of magnitudes less than that of the *N*-methylimidazole (K_{py}=~$0.1M^{-1}$), but the electron-rich 4-(*N*,*N*-dimethyl)aminopyridine (DMAP) has a much higher binding constant (~10^3 M^{-1}).

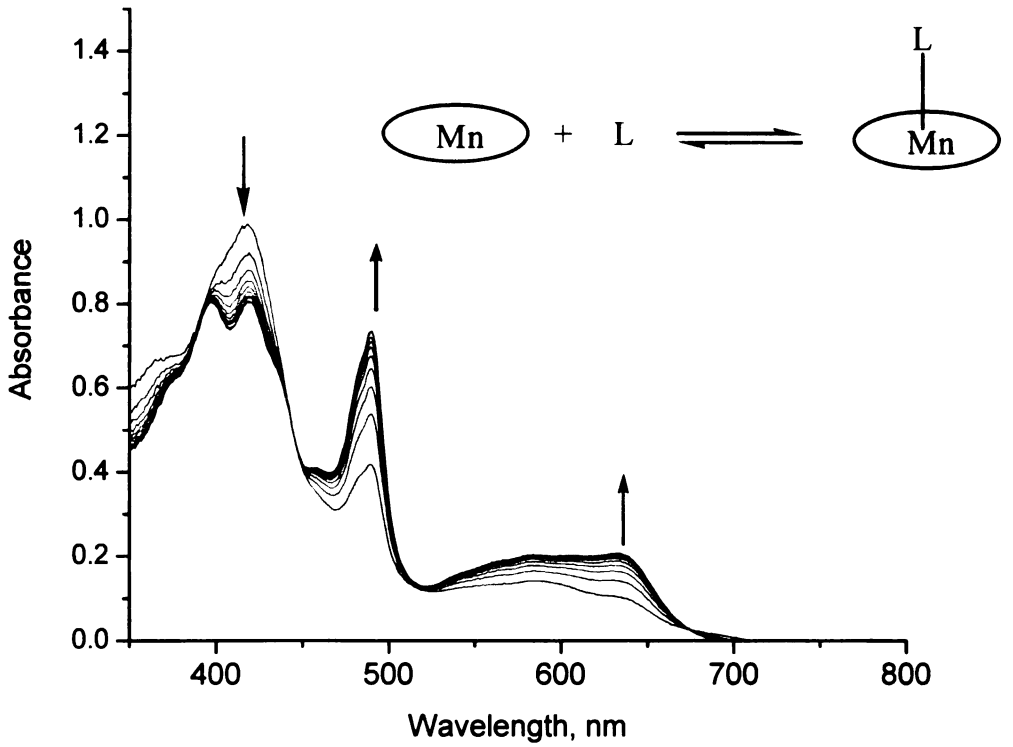

Figure 3-3. The UV-Vis spectrum of Mn(III)Br_6F_3C, **8** titrated with *N*-methylimidazole.

Table 3-1. The binding constant of *N*-methylimidazole and Mn(III)-corroles in CH_2Cl_2.

Mn-corrole	**Binding constant (M^{-1})**
$MnF_{15}C$, **1a**	7×10^4
$MnBr_6F_3C$, **8**	2×10^4
MnT_3C, **9**	3×10^3

Shape selective epoxidation revealed by the bulky corroles

Previously, Suslick,[21-23] Collman,[24] and Chang[25] et al. used the sterically encumbered metalloporphyrins (with descriptive names such as bis-pocket porphyrins and picnic basket porphyrins) to demonstrate shape-selective epoxidation and hydroxylation. Generally, there are three types of tests for shape selectivity: (i) intramolecular competition between two sites in a molecule, (ii) intermolecular competition between two contrasting molecules, and (iii) intermolecular competition between *cis* and *trans* isomers. In this study, we have used all three types of test to examine the effectiveness of our bulky corroles as chemoselective catalyst.

Intramolecular competition

For this test, we studied the catalytic epoxidation of a series of non-conjugated dienes, compounds **10~13** (Figure 3-4) and compared the relative reactivity of the terminal versus the more substituted internal double bonds (Scheme 3-7). The catalytic epoxidation of olefins was performed with the Mn(III) corroles and iodosylbenzene as oxygen donor (the ratio of catalyst : oxidant : diene = 1 : 500 : 2000). Control epoxidation reactions were carried out with m-chloroperbenzoic acid (mCPBA) and the sterically unhindered Mn(III)-corrole, $MnF_{15}C$.

The results are summarized in Figure 3-5, where the data of m-chloroperbenzoic acid (mCPBA) is included as reference. The new sterically

encumbered Mn(III)-corrole catalysts, $MnBr_6F_3C$ and particularly MnT_3C demonstrate a very good selectivity toward the terminal double bond.

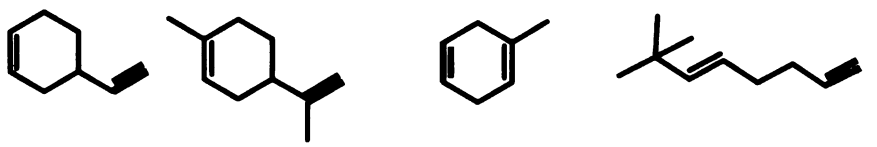

11 **12** **13** **14**

Figure 3-4. The nonconjugated dienes used in intramolecular competition of epoxidation, with the less hindered double bonds shown by bold line.

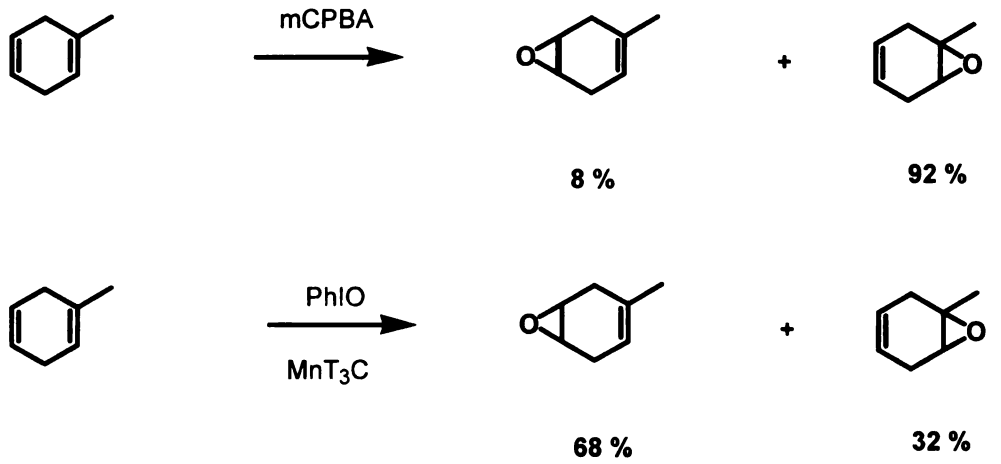

Scheme 3-7. Epoxide product ratios for the reaction of mCPBA and $PhIO/MnT_3C$.

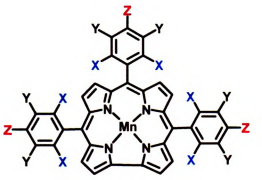

Mn(III) corrole	X	Y	Z
$MnF_{15}C$, 1a	F	F	F
$MnBr_6F_3C$, 8	Br	H	F
MnT_3C, 9	Ph	H	Ph

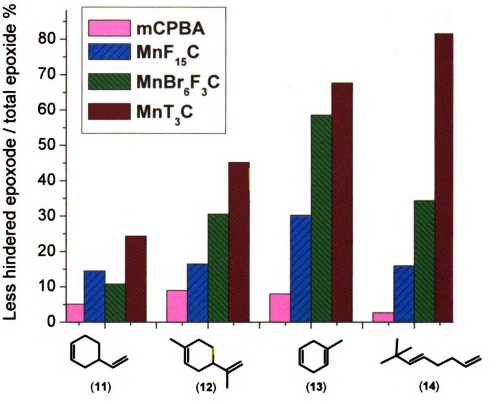

Figure 3-5. Shape-selective epoxidation of dienes by bulky Mn(III)-corrole catalysts and PhIO, with epoxides obtained by mCPBA serving as benchmarks. All Mn-corrole reactions were carried out under the same conditions: 0.5μmol of Mn-corrole, 1mmol of diene substrates, 0.5 mmol of PhIO. 2 hours at 293K. Products were analyzed using gas chromatography against authentic samples of epoxide. Yields of epoxidation were 40~80% based on the PhIO for all reactions. (This Image is presented in color)

In all cases, the bulky corrole catalysts enhanced the epoxidation to take place at the less hindered double bond; in the case of 7,7-dimethyl-1,5-octadiene (**14**) MnT_3C showed a remarkable preference for epoxidation at the terminal postion (>80%).

Limonene (**12**) and its structural analogue 4-vinylcyclohexene (**11**) are useful chiral starting materials for organic syntheses. Epoxidation of these molecules usually gives almost exclusively ring epoxidation products. While this pattern was not reversed, our sterically encumbered catalyst MnT_3C greatly enhance the epoxidation of the external double bond raising its ratio from 5~8% to 25~46%.

For 1-methylcyclo-1,4-hexadiene (**13**) the differentiation of the two double bonds makes an interesting case. Here, even the unhindered $MnF_{15}C$ seems to enhance the epoxidation of the less substituted double bond. This may be attributable to a *cis-trans* type of selectivity to be discussed later.

These regioselectivities can be further increased by addition of axial ligands, a phenomenon which has also been observed in the case of porphyrins. [26~27] The results are summarized in Table 3-2. In these reactions, the condition was the same as mentioned above, but 500 folds of *N*-methylimidazole (MeIm) was added as axial ligand. The selectivity of unhindered double bond generally increased after the addition of axial ligand, especially in the case of

epoxidation of 1-methylcyclo-1,4-hexadiene (**13**) and 7,7-dimethyl-1,5-octadiene (**14**), in which even the unhindered $MnF_{15}C$ (**1a**) gave 58% and 44% epoxidation product at the less hindered double bond (entry 7 & 10). For the most hindered MnT_3C, **9** epoxidation at the less hindered double bond in 7,7-dimethyl-1,5-octadiene (**14**) was 95% (entry 12).

Table 3-2. Regioselectivity of Mn-corroles in the presence of *N*-methylimidazole (MeIm) as axial ligand.

			% of less hindered Epoxide	
Entry	**Diene**	**Catalyst**	**Without MeIm**	**With MeIm**
1	**11**	$MnF_{15}C$, **1a**	15	15
2	**11**	$MnBr_6F_3C$, **8**	11	15
3	**11**	MnT_3C, **9**	24	31
4	**12**	$MnF_{15}C$, **1a**	17	20
5	**12**	$MnBr_6F_3C$, **8**	30	31
6	**12**	MnT_3C, **9**	45	49
7	**13**	$MnF_{15}C$, **1a**	30	58
8	**13**	$MnBr_6F_3C$, **8**	59	69
9	**13**	MnT_3C, **9**	68	77
10	**14**	$MnF_{15}C$, **1a**	16	44
11	**14**	$MnBr_6F_3C$, **8**	34	66
12	**14**	MnT_3C, **9**	82	95

A plausible explanation proposed earlier by Chang *et al.*[26] for the general improvement by axial ligand is that the binding of the ligand in the highly crowded environment would restrict the rotational freedom of the terphenyl rings against the macrocycle plane leading to a comparatively more restrictive pocket on the other side for efficient molecular recognition. This explanation implied a 6-coordinated Mn-oxo as the active intermediate in the reaction mechanism.

Another plausible explanation of this axial ligand effect may be related to the in-plane structure of the six-coordinate L-Mn-O, giving the meso-substituents more influence at the transition state geometry. Based on the X-ray structure of the 5-coordinated nitrene complexes F_{15}CMn(V)(NMes)[44] and (TBP_8Cz)Mn(V)(NMes)[29] (TBP_8Cz=octakis(*p-tert*-butylphenyl)corrolazine), the Mn core sits above the mean plane of the four pyrrole N-atoms by 0.55Å and 0.51 Å, respectively. By extrapolation, the Mn in the 5-coordinated Mn-oxo intermediate should also be out of plane to render the bulky substitutes less effective in shielding the reactive center.

Intermolecular competition

For the test of intermolecular competition we studied the relative rate of epoxidation of two alkenes, 1-hexene and *cis*-cyclooctene, in a 1:1 mole ratio mixture. This set of experiments should be able to demonstrate the selectivity of Mn-corroles towards terminal double bond versus a cyclic *cis*-olefin. Control

epoxidation reactions were carried out with mCPBA, the unhindered $MnF_{15}C$ and its corresponding Mn porphyrin, Mn-Cl(F_{20}TPP) [F_{20}TPP=5,10,15,20-tetrakis-(penta-fluorophenyl)porphyrin]. Normally, one would expect a greater reactivity towards the more electron-rich *cis*-cyclooctene than towards 1-hexene. It is true for the control experiments carried out by mCPBA: a molar ratio of 1:2:2 (mCPBA:1-hexene:cis-cyclooctene) gave almost exclusively epoxidation at the *cis*-cyclooctene (>99%).

Surprisingly, the unhindered $MnF_{15}C$ demonstrated a five-fold increase of 1-hexene oxide (1-hexene oxide/total epoxide = 0.1) comparing to that of its porphyrin analog Mn-Cl(F_{20}TPP). It is not totally clear why this is the case. The modestly hindered $MnBr_6F_3C$ failed to increase the selectivity much as compared to that of the unhindered $MnF_{15}C$, showing that the ortho-dibromo groups may not be big enough barriers towards *cis* double bond. This phenomenon was also observed in the intramolecular competition of 4-vinylcyclohexene (**11**).

A high selectivity is observed in the case of the most bulky MnT_3C, giving a 35:65 ratio of 1-hexene oxide : *cis*-cyclooctene oxide.

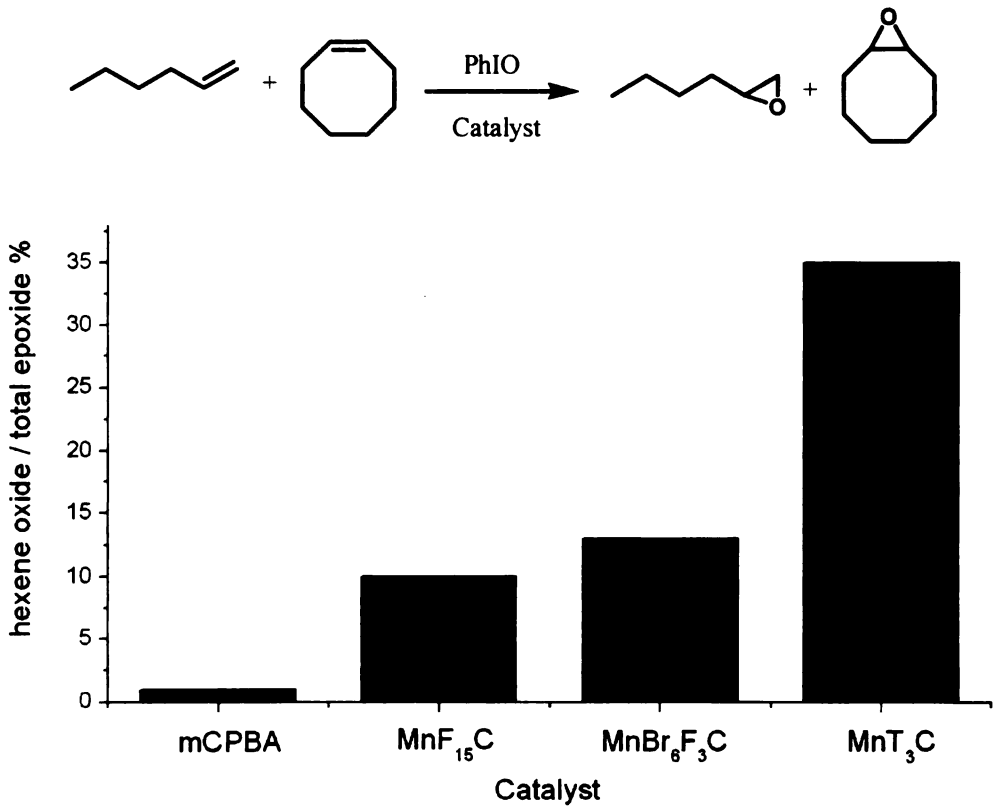

Figure 3-6. The epoxide product distribution of intermolecular competition. All reactions were using the same conditions: 0.5μmol of Mn-corrole/porphyrin, 1mmol of 1-hexene and 1mmol of *cis*-cyclooctene substrates, 0.5 mmol of PhIO. 2 hours at 293K. Products were analyzed using gas chromatography with authentic samples of epoxide. Yields of epoxidation were 40~80% based on the PhIO for all reactions.

***cis*- versus *trans*-olefins**

In addition to the foregoing comparisons, we also studied the selectivity of Mn-corroles towards *cis* and *trans* double bonds. The relative rate of epoxidation was studied in a 1:1 mixture of *cis*-methylstyrene and *trans*-methylstyrene reacting with PhIO and Mn-corrole catalysts in a ratio of 1000:1000:500:1. The reaction was carried out in a NMR tube for 2 hours using $CDCl_3$ as solvent. The ratio of unreacted *cis* and *trans*-methylstyrene was determined by the peak area ratio of the allic protons in H-NMR. This experiment gave a 6:4 ratio of the *trans*:*cis*-methylstyrene remaining in the solution. Admittedly, the error bar of this experiment was fairly large (±10%), possibly because of the poor mixing during the reaction. Thus, another experiment was designed by looking at the decay of the reactive species.

As reported by our group previously,[14] the Mn(V)-oxo species can be isolated by flash chromatography from the reaction of PhIO and Mn(III)-corroles, and the reactivity of this species towards alkenes increases by electron-withdrawing groups on the corrole ring. We used the modestly hindered $MnBr_6F_3C$, which has both steric effects and electron-withdrawing groups, as a model catalyst to determine the reaction rate towards *cis* and *trans* double bonds. The Mn(V)-oxo species was synthesized and isolated according to references 11 and 14. The absorbance decay plots of the {Mn(V)-oxo}Br_6F_3C were studied at λ=350nm in the presence of a huge excess (10^5 folds) of *cis*-methylstyrene and *trans*-methylstyrene, respectively. The reaction was carried

out in toluene at 35°C, because of the rather slow rate at room temperature ($t_{1/2}$ > 4 hours without substrate).

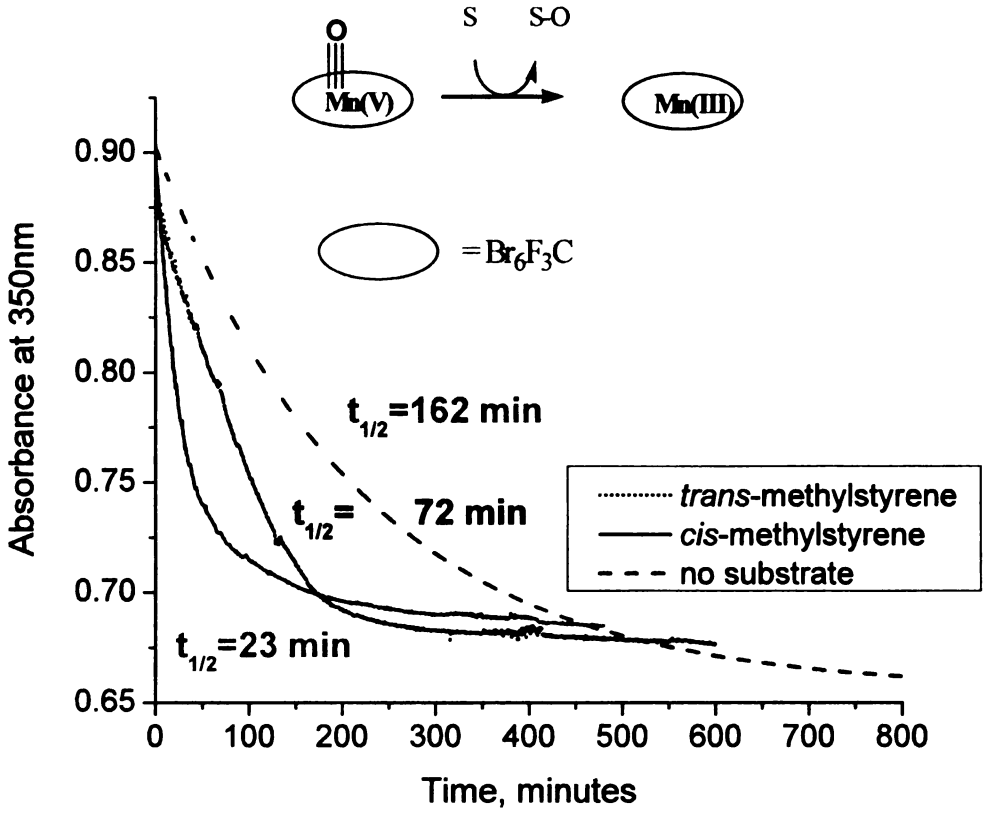

Figure 3-7. Decay plots at λ=350nm of {Mn(V)-oxo}Br_6F_3C at 10 sec. time interval of each data point. All reactions were carried out in freshly distilled dry toluene at 35°C. The *cis* and *trans*-methylstyrene bought from Aldrich® were purified by flash chromatography on SiO_2 to remove any trace of antioxidants. (The decay curve without substrate was smoothed by a five-point average.) (This Image is presented in color)

The half-lifes ($t_{1/2}$) of Mn(O)$F_{15}C$ and Mn(O)Br_6F_3C are listed in Table 3-3. Mn(O)T_3C was not used in this set of experiments, because the reaction rate was too slow ($t_{1/2}$ > 300 minutes with substrates). The $t_{1/2}$ of Mn(O)Br_6F_3C

showed a large difference between *cis*-methylstryene (23 minutes) and *trans*-methylstyrene (72 minutes), indicating the ortho-dibromo groups are effective to differentiate *cis/trans* double bonds. The unhindered $Mn(O)F_{15}C$ also showed a slightly lower $t_{1/2}$ in *cis*-methylstyrene than that of the *trans*-methylstyrene. The product of such oxygen atom transfers is the epoxide, which has been independently verified with a higher concentration of the Mn(V)-oxo solution.

Table 3-3. The half-life of Mn(V)-oxo-corroles.

	$t_{1/2}$ (minutes)		
Mn(V)-oxo-corroles	**Without substrates**	***cis*-methylstyrene**	***trans*-methylstyrene**
$Mn(O)F_{15}C$	120	21	32
$Mn(O)Br_6F_3C$	162	23	72

The epoxidation mechanisms of metallophyrins have been extensively discussed in the literature.[1~4, 40~43] The general features of the metal-catalyzed epoxidations are the following: the initial olefin approach to the active site that leads to epoxidation may be similar for many otherwise dissimilar metal-oxo species.[2] Groves and Nemo first proposed a side-on approach of olefins to porphyrin ferryl (Fe=O) species to account for *cis*-olefins being epoxidized faster than *trans*-olefins.[40] Such an approach should maximize the interactions

between the olefin π orbitals and the Fe=O π antibonding orbitals, where the approach of trans-olefins were repulsed by the porphyrin plane. This postulate has provided a useful working model in the design of metalloporphyrins and other transition metal-based epoxidation catalysts.[41] An alternative head-on approach of olefins to encumbered porphyrin chromium-oxo[42] and dioxoruthenium[43] has also been proposed to account for the more severe steric effect. These two approaches of olefins should also be viable to explain the *cis-trans* selectivity that appeared in the case of our bulky corrole catalysts.

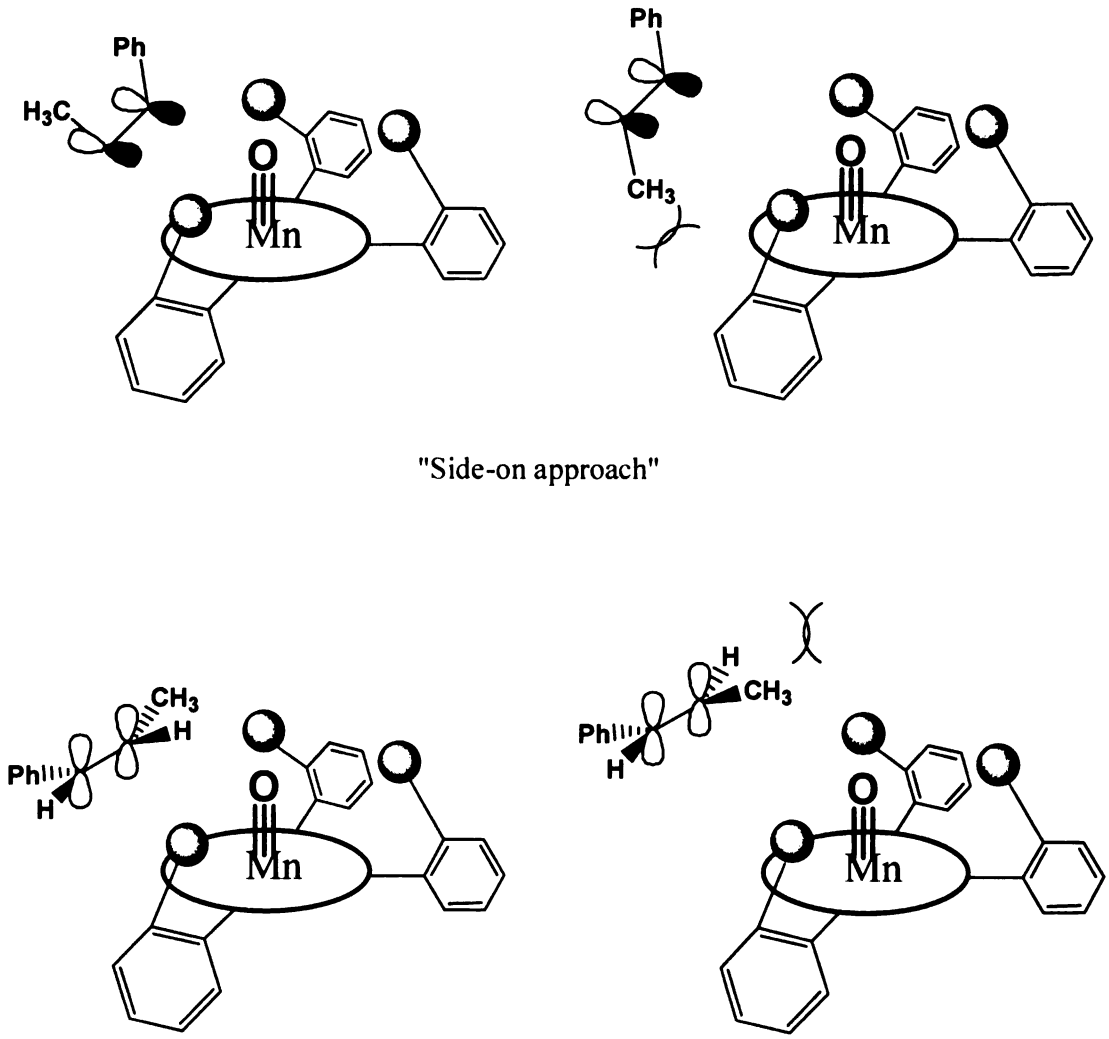

Figure 3-8. "Side-on" and "Head-on" approach of olefins to Mn corrole.

Resonance Raman studies of the corrole Mn(V)-oxo species

Mn(V)-oxo corroles have been characterized by NMR and UV-vis spectroscopy. [14, 16, 29] However, further study on this reactive species is limited by its stability.In our hands, while the Mn(V)(O)$F_{15}C$ seemed to be stable in dilute solution, it decompose at higher concentration and returned to the Mn(III)$F_{15}C$. This could be attributable to a bi-molecular disproportionation reaction. The higher stability of the bulky Mn(V)-oxo-T_3C prompted us to study the properties of the Mn-O bond by using Resonance Raman spectroscopy.

The Mn(V)-oxo-T_3C, **5b** was synthesized by reacting MnT_3C, **5a** with PhIO in CH_2Cl_2 or CD_2Cl_2 solution, followed by flash chromatography on SiO_2. The ^{1}H-NMR spectrum of this species in CD_2Cl_2 solution shows sharp ^{1}H resonances of the β-H's on corrole ring in the normal aromatic region (δ 8~9 ppm), indicating **5b** is diamagnetic, similar to the Mn(V)-oxo corroles [14, 16] and Mn(V)-oxo corrolazine [28~29] reported previously.

The ^{18}O labeled Mn(V)-oxo **5c** was prepared by stirring a solution of **5b** in CH_2Cl_2 with H_2O^{18} (95%) under Ar for 1 hour to give a product that is identical to **5b** except its RR spectrum showing a new peak with *ca.*70% exchanged (*vide infra*). Previous reports on Mn porphyrins have shown that ^{18}O exchange with water is one of the hallmarks of an Mn(V)-oxo-porphyrin intermediate.[30~34]

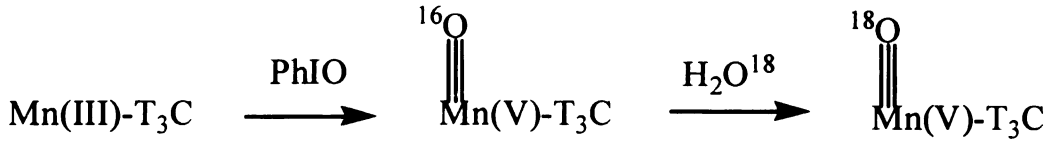

5a **5b** **5c**

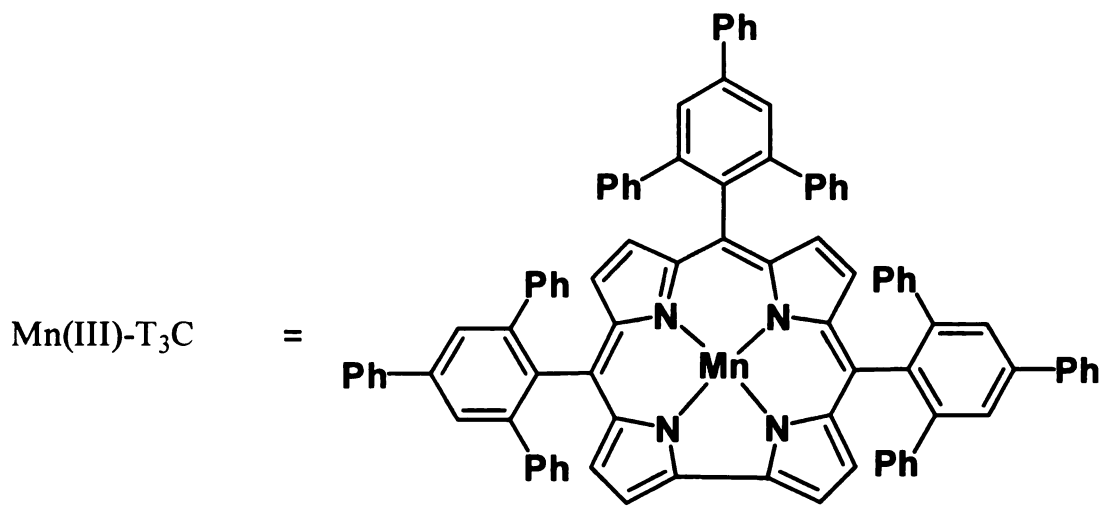

Scheme 3-8. Syntheses of Mn(V)-oxo-T_3C **5b** and **5c**.

The Resonance Raman (RR) spectra of **5a**, **5b** and **5c** were obtained with excitation near the absorption maxima of the Soret band (413 nm). The direct evidence for the Mn(V)-oxo species was shown in Figure 3-9. Excitation of **5b** near the absorption maxima of the Soret band led to the appearance of a new strongly enhanced Raman band at 952 cm^{-1} [Figure 3-9(b)]. This new band is attributed to the stretching mode of the Mn-oxo bond, *v* (MnO). It shifts to 913 cm^{-1} when oxo group is exchanged with O^{18} [Figure3-9(c)]. The Mn-O isotopic

shift of 39 cm^{-1} after O^{18}-O^{16} exchange is comparable to the shift (43cm^{-1}) observed in the case of Mn(V)-oxo-corrolazine. [29] The wavelength observed and its isotopic-shift suggests that the Mn(V) and the oxygen atom is triply bonded, i.e. Mn(V)≡O. A recent report on Mo(V)≡O corroles, shows a *v* ($Mo^{16}O$)=969 cm^{-1} and the *v* ($Mo^{18}O$)=924 cm^{-1} which have a -45cm^{-1} shift.[39] Another Mn(V)≡O complex that has been characterized by vibrational spectroscopy (RR, IR) belongs to a tetraamide macrocycle, for which *v*($Mn^{16}O$)=981~970cm^{-1} and *v*($Mn^{18}O$)=942~933 cm^{-1}.[35~36] Similar vibrational properties have been determined for the iso-electronic Mn(V)≡N and Cr(IV)≡N in five-coordinated porphyrin complexes having a triply bonded axial nitrido ligand.[37] Moreover, five-coordinate Mn(IV)-oxo porphyrins give the IR and RR bands of Mn(IV)=O at the characteristically low frequency of ~755 cm^{-1}, indicating a double bond character.[38] To our knowledge, this is the first RR study of a corrole-based Mn≡O species.

Table 3-4. Stretching wave-number of metal-X (X=O; N) multiple bond

Metal	X	Ligand	Wave-number (cm^{-1})	Bond order
Mn(V)	O	Corrole	952(^{16}O); 913(^{18}O)	3
Mo(V)	O	Corrole	969(^{16}O); 924(^{18}O) [39]	3
Mn(V)	O	Corrolazine	979(^{16}O); 938(^{18}O) [29]	3
Mn(V)	O	Tetraamide	981(^{16}O); 942(^{18}O) [35~36]	3
Mn(V)	N	Porphyrin	1049 [37]	3
Cr(IV)	N	Porphyrin	1017 [37]	3
Mn(IV)	O	Porphyrin	757(^{16}O); 726(^{18}O) [38]	2

Complexes **5b** and **5c** are capable of oxidizing styrene at a relatively slow rate. Thus, a solution of **5c** in CH_2Cl_2 with ~$1X10^5$ fold of styrene was allowed to react overnight in Ar, the amount of styrene oxide (^{16}O and ^{18}O) were determined by GC-MS, the presence of ^{18}O-labeled styrene oxide gave a strong evidence that **5c** is a reactive intermediate.

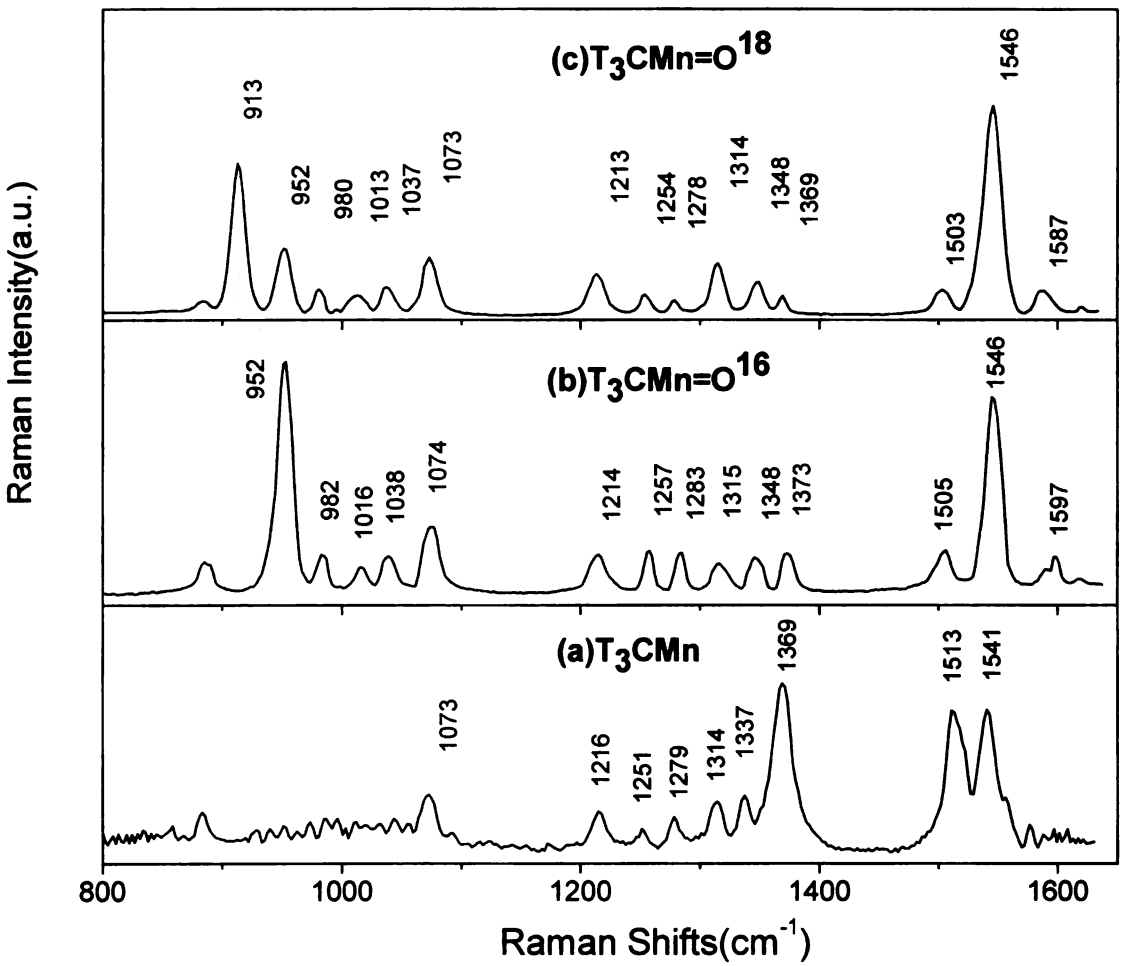

Figure 3-9. Resonance Raman (RR) spectra of (a). MnT_3C, (b) $Mn(V)(^{16}O)T_3C$, and (c). $Mn(V)(^{18}O)T_3C$ excited at 413.1 nm (60mW).

3-3. Conclusion

By using the sterically bulky Mn(III) corroles as models to study the catalytic epoxidation reactions, our result clearly indicate that the ortho-substituents on the meso-phenyl ring impart the Mn-corroles shape selectivities for substrates, including terminal double bond versus internal double bond; straight-chain double bond versus cyclic *cis*- double bond; and *cis* double bond versus *trans* double bond. In addition, the selectivity of epoxidation reaction could be enhanced by an axial ligand. The sterically bulky Mn(III) corroles also increase the stability of its corresponding Mn(V)-oxo species by preventing bi-molecular disporprotionation. Resonance Raman spectra of Mn(V)-oxo-T_3C gave evidence that the Mn(V) center is triply bonded to the oxygen atom.

3-4. Experimental section

Instrumentation

UV-VIS Spectra were obtained on a Varian Cary 50 Scan UV-Visible Spectrophotometer with samples dissolved in CH_2Cl_2 unless otherwise stated. Mass spectra were recorded by a Finngan TSQ-7000 mass spectrometer. NMR spectra were recorded using a Varian 300 MHz spectrometer. Chemical shifts (ppm) were reported with respect to $CDCl_3$ or d_6-Acetone, Cambridge Isotope Laboratories.

Preparation of 2,6-dibromo-4-fluobenzonitrile (6a).

Sodium nitrite (15.18 g, 0.22 mmol) was added portionwise to a magnetically stirred concentrated sulfuric acid (100 ml) at 0 °C. The resulting mixture was allowed to warm to 55 °C and then held at room temperature. This nitrosyl sulfuric acid was then added dropwise to an acetic acid (110 ml) solution of 2,6-dibromo-4-fluoroaniline (53.6 g, 0.2 mmol) at 20 °C. After stirring for 1 h the diazonium solution was added dropwise to a mechanically stirred solution containing KCN (65.12 g, 1 mol), CuCN (21.49g, 240 mmol), and Na_2CO_3 (340 g, 3.2 mol) in 1 l of water at 0 °C. When the addition was complete, the mixture was stirred at room temperature for 1 h. The mixture was then filtered, washed with water and dried. The resulting crude product was dissolved in benzene and the insoluble solid was removed by filtration. Benzene was removed under reduced pressure and the residue was chromatographed on

silica gel eluting with CH_2Cl_2 and hexanes (1:1) to afford 35.9 g (71%) of nitrile. M.p. 103-105 °C; ^{1}H-NMR (300 MHz, $CDCl_3$): δ 7.41 (2H, d); MS (70eV, EI): m/z=278.0 (M+), 278.85 calculated for $C_7H_2Br_2FN$.

Preparation of 2,6-dibromo-4-fluorobenzaldehyde (6).

To a solution of nitrile (2.78 g, 10 mmol) in 20 ml CH_2Cl_2 was added DIBAL-H (1 M solution in hexane, 12 ml, 12 mmol) at 0 °C under argon. The solution was stirred at room temperature for 4 h and then poured into 30 ml 6 N HCl in an ice bath. After stirring for 1h, the mixture was extracted with CH_2Cl_2. The dichloromethane solution was dried over anhydrous sodium sulfate and then the solvent was removed under reduced pressure. The crude product was purified by flash chromatography on silica gel eluting with CH_2Cl_2 and hexanes (1:1) to give 2.54 g (90%) of aldehyde **6**. M.p. 85-86 °C; ^{1}H NMR (300 MHz, $CDCl_3$): δ 10.20 (1H, s, CHO), 7.43 (2H, s, phenyl); MS (EI): m/z=282.0 (M^+), 281.85 calculated for $C_7H_3Br_2FO$.

Preparation of 2,4,6-triphenylbenzaldehyde (7).

2,4,6-triphenylbenzene (66g, 0.22mol) was dissolved in 500mL of CS_2 with stirring. 24.0mL of Br_2 (24mL, mol) was then added and allow the reaction to stand for 12 hours. The solution was then pour into 500 mL of methanol and evaporated to nearly dryness by a steam of air. The solid was washed thoroughly with methanol and recrystallization from hot ethanol to afford colorless needle crystals as 1-bromo-2,4,6-triphenylbenzene (80.5g, 96%). 1-

Bromo-2,4,6-triphenylbenzene (6g, 15.6mmol) was dissolved in 250mL dry Et_2O with stirring under nitrogen. When most of the solids dissolved, the flask was allowed to cool down to 0°C for 15 minutes. A solution of 2.5M nBu-Li (10mL, 25mmol) was then added over 1 minute and the reaction mixture was stirred for 6 more minutes (total 7 minutes, do not over-heat). 5 mL DMF (dried over activated 4A molecular sieve for 1 night and then distilled under vacuum) was then added dropwise and after stirring for 5 min, the reaction mixture was poured into 200mL ice/water mixture and allow the Et_2O to evaporate. The solids (pare yellow) was redissolved into CH_2Cl_2 and was purified by chromatography on silica gel eluting first with CH_2Cl_2/hexane (1:3) until triphenylbenzene was washed out and then with CH_2Cl_2 (2:3>1:1) to yield the 2,4,6-triphenylbenzaldehyde (3.5g, 66%). ^1H NMR (300 MHz, $CDCl_3$): δ 9.916 (1H, s, CHO), 7.604~7.636 (2H, dd); 7.557 (2H, s); 7.330~7.403 (13H, br). MS (EI): m/z=335 (M^+), 334.14 calculated for $C_{25}H_{18}O$.

General procedure for the synthesis of corrole 2~5.

To a 100mL round-bottom flask, pyrrole (25 ml, 0.35 mol) and the corresponding aldehyde (0.01 mol) were mixed and degassed by nitrogen for 5 minutes. Trifluoroacetic acid (TFA) (0.15 ml, 2.00 mmol) was added to initiate the reaction. The reaction mixture was stirred for 15 to 20 minutes. A potion of 5mL triethylamine was used for neutralizing TFA. The reaction mixture was then extracted by diethyl ether and washed with water. After evaporation of the diethyl ether under vacuum, the unreacted pyrrole was removed vacuum distillation. The purified product was isolated by using silica gel column with hexane/ethylacetate/triethylamine as the eluent to yield 40~60% of the corresponding dipyrromethane. To the sample of dipyrromethane (6mmol) an aldehyde (2.5mmol) dissolved in 50mL CH_2Cl_2, TFA (35uL) was added and the reaction was allowed to stirred in room temperature for 4~6hr. The reaction mixture was diluted to 1L with CH_2Cl_2, a solution of DDQ (1.36g, 6mmol) in 20 mL toluene was added slowly in *ca.* 15 min, and the reaction mixture was stirred in room temperature for a further 30 min. Then the reaction mixture was purified as described below.

Preparation of 5,15-bis(2,6-dibromo-4-fluorophenyl)-10-(pentafluoro-phenyl)corrole (2).

The reaction mixture was filtered and evaporated to dryness and then redissolved (CH_2Cl_2:hexane, 1:2) and pass through a silica gel column. Subsequent chromatography (silica; CH_2Cl_2:hexane, 1:4) afforded the pure

corrole **2**. ^{1}H-NMR ($CDCl_3$): δ = 7.780 (d, 4H); 8.377 (dd, 2H); 8.446 (dd, 2H); 8.538 (d, 2H); 8.977 (d, 2H). MS (FAB): m/z=967 (M^+), 967.79 calculated for $C_{37}H_{15}Br_4F_7N_4$.

Preparation of 5,10,15-tris(2,6-dibromo-4-fluorophenyl)corrole (3).

The reaction mixture was filtered and evaporated to dryness. The reaction mixture was redissolved (CH_2Cl_2:hexane, 1:2) and pass through a silica gel column. Subsequent chromatography (silica; CH_2Cl_2:hexane, 1:3) afforded corrole **3** with some unidentified impurities. Another chromatography (neutral alumina; CH_2Cl_2:hexane, 1:3; then 1:1) afforded the pure corrole **3**. ^{1}H-NMR ($CDCl_3$): δ = 7.755 (d, 2H); 7.766 (d, 4H); 8.315 (d, 2H); 8.344 (d, 2H); 8.475 (d, 2H); 8.929 (d, 2H). MS (FAB): m/z=1054 (M^+), 1053.65 calculated for $C_{37}H_{17}Br_6F_3N_4$.

Preparation of 5,15-bis(2,4,6-tertphenyl)-10-(pentafluoro-phenyl)corrole (4).

The dipyrromethane was used without further purification after vacuum distillation of pyrrole. The reaction mixture was filtered and evaporated to dryness. The reaction mixture was redissolved (CH_2Cl_2:hexane, 1:2) and pass through a silica gel column. Subsequent chromatography (silica; CH_2Cl_2:hexane, 1:3) afforded the pure corrole **4** ^{1}H-NMR (300mHz, $CDCl_3$): δ = 6.524 (d, 4H); 6.554 (d, 8H); 7.035 (dd, 8H); 7.480 (t, 2H); 7.582 (t, 4H);

7.948 (d, 4H); 7.971 (s, 4H); 8.066 (d, 2H); 8.349 (d, 2H); 8.574 (d, 2H); 8.616 (d, 2H). MS (ESI), m/z=1073.4 (M^+), 1072.36 calculated for $C_{75}H_{45}F_5N_4$.

Preparation of 5,10,15-tris(2,4,6-tertphenyl) corrole (5).

The dipyrromethane was used without further purification after vacuum distillation of pyrrole. The reaction mixture was filtered and evaporated to dryness. The reaction mixture was redissolved in CH_2Cl_2 and pass through a silica gel column. Subsequent chromatography (silica; CH_2Cl_2:hexane, 1:3, then 1:2) afforded corrole **5** with some unidentified impurities. Recrystallization from CH_2Cl_2:hexane afforded the pure corrole **5**. Single crystals of H_3T_3C were grown in a layer defusion of methanol and $CHCl_3$ solution of H_3T_3C. ^{1}H-NMR (300mHz, $CDCl_3$): δ = 6.339 (dd, 4H); 6.471 (dd, 2H); 6.488 (d, 8H); 6.570 (dd, 4H) 6.949 (d, 8H); 7.480 (t, 3H); 7.581 (t, 6H); 7.938 (d, 6H); 7.949 (s, 6H); 8.1866 (d, 4H); 8.397 (d, 2H); 8.447 (d, 2H). MS (FAB): m/z=1211.8 ($M+1^+$), 1210.50 calculated for $C_{91}H_{62}N_4$.

General procedure for preparation of manganese(III) corrole

Free-base corrole (0.05mmol) and 50 mg of NaOAc was dissolved in 50 mL of dichloromethane/methanol (1:1). $MnCl_2{}^{\bullet}4H_2O$ (20mg, 0.101mmol) was then added and the resulting solution was heated to reflux for 20~50 min. The progress of reaction was monitoring by a UV-vis spectrometer and TLC. The solution was washed with water, dried over $MgSO_4$ and the solvent was

evaporated *in vacuo*. The crude product was purified by a column chromatography on silica to afford manganese(III) corroles.

Preparation of manganese-5,15-bis(2,6-dibromo-4-fluorophenyl)-10-(pentafluorophenyl)corrole ($MnBr_4F_7C$, 6).

The titled compound was obtained by the general procedure and recrystallization from hexane to obtain dark green powder. MS (FAB): m/z= 1020 ($M+1^+$), 1019.71 calculated for $C_{37}H_{12}Br_4F_7MnN_4$.

Preparation of manganese-5,15-bis(2,4,6-tertphenyl)-10-(pentafluorophenyl)corrole $Mn(T_2F_5C$, 7)

The titled compound was obtained by the general procedure and recrystallization from hexane to obtain dark green powder. MS (FAB): m/z= 1125 ($M+1^+$), 1124.27 calculated for $C_{73}H_{42}F_5MnN_4$.

Preparation of manganese-5,10,15-tris(2,6-dibromo-4-fluorophenyl)-corrole ($MnBr_6F_3C$, 8).

The titled compound was obtained by the general procedure and recrystallization from hexane to obtain dark green powder. MS (FAB): m/z= 1105 (M^+), 1105.57 calculated for $C_{37}H_{14}Br_6F_3MnN_4$.

Preparation of manganese-5,10,15-tris(2,4,6-tertphenyl) corrole (MnT_3C, 9).

The titled compound was obtained by the general procedure and recrystallization from hexane to obtain dark green powder. MS (FAB): m/z= 1263 ($M+1^+$), 1262.41 calculated for $C_{91}H_{59}MnN_4$.

Resonance Raman Spectroscopy

The near-UV line 413.1 nm in resonance with the Soret band for resonance Raman excitation was from a krypton ion laser (Innova 400, coherent). The laser power was *c.a.* 60 mW. A spinning quartz cell was used to prevent heating from laser beam. Scattered light was collected at 90° and dispersed by a Spex Model 500 M monochromator spectrometer equipped with liquid nitrogen cooled CCD detector.

X-ray data collection and structure refinement

Crystals were grown by layer diffusion of chloroform and methanol or of chloroform and octane solutions. Data were collected at 293 K and structures were solved by the direct method using the NRCVAX program package. All non-hydrogen atoms were refined anisotropically. The hydrogen atoms of interest were located from difference map and refined positionally when appropriate. The crystallographic data for the structures are summarized in Appendix.

References

1. Groves, J. T. In "*Cytochrome P450: Structure, Mechanism, and Biochemistry*", 3rd ed.; Ortiz de Montellano, P. R., Ed.; Kluwer Academic/Plenum Publishers: New York, **2005**; pp 1-43.

2. Collman, J.P.; Zhang, X.; Lee, V.J.; Uffelman E.S.; Brauman. J.I. *Science* **1993**, *261*, 1404-1411.

3. Meunier, B. *Chem. Rev.* **1992**, *92*, 1411-1456.

4. Mansuy, D. *Coord. Chem. Rev.* **1993**, *125*, 129-141.

5. Groves, J. T.; Lee, J.; Marla, S. S. *J. Am. Chem. Soc.* **1997**, *119*, 6269-6273.

6. Jin, N.; Groves, J. G. *J. Am. Chem. Soc.* **1999**, *121*, 2923-2924.

7. Jin, N.; Bourassa, J. L.; Tizio, S. C.; Groves, J. T. *Angew. Chem., Int. Ed.* **2000**, *39*, 3849-3851.

8. Nam, W.; Kim, I.; Lim, M. H.; Choi, H. J.; Lee, J. S.; Jang, H. G. *Chem. Eur. J.* **2002**, *8*, 2067-2071.

9. Zhang, R.; Newcomb, M. *J. Am. Chem. Soc.* **2003**, *125*, 12418-12419.

10. Zhang, R.; Horner, J. H.; Newcomb, M. *J. Am. Chem. Soc.* **2005**, *127*, 6573-6582.

11. Gross, Z.; Galili, N.; Saltsman, I. *Angew. Chem., Int. Ed.*, **1999**, **38**, 1427-1429.

12. Collman, J.P.; Decréau, R.A. *Tetrahedron Lett.*, **2003**, **44**, 1207-1208.

13. Gross, Z.; Simkhovich, L.; Galili, N. *Chem. Commun.*, **1999**, 599-600.

14. Liu H.Y.; Lai T.S.; Yeung L.L.; Chang C.K. *Org. Lett.* **2003**, 5, 617-620.

15. Collman J. P.; Zeng L.; Decréau R. A. *Chem. Commun.* **2003**, 2974-2975.

16. Zhang, R., Harischandra, D.N., Newcomb, M. *CHEM-EUR J.* **2005**, *11*, 5713.

17. Aviv, I.; Gross, Z. *Chem. Commun.*, **2007**, 1987-1988.

18. Worden, L.R.; Kaufman, K.D.; Smith, P.J.; Widiger, G.N. *J. Chem Soc. (C).*, **1970**, 227-230.

19. Littler, B.J.; Miller, M.A.; Hung, C.H.; Wagner, R.W.; O'Shea, D.F.; Boyle, P.D.; Lindsey, J.S. *J. Org. Chem.* **1999**, 64, 1391-1396.

20. Gryko, D. T. Koszarna, B. *Synthesis* **2004**, *13*, 2205-2209.

21. Suslick, K.S. Fox, M.M. *J. Am. Chem. SOC.* **1983,** *105,* 3507-3510.

22. Suslick, K.S. in: *comprehensive Supramolecular Chemistry*, Vol. 5, J.M. Lehn (ED.), Elsevier, London **1996**, p. 141. and reference there in.

23. Bhyrappa, P.; Young, J.K.; Moore, J.S.; Suslick, K.S. *J. Am. Chem. Soc.* **1996**, *118*, 5708-5711.

24. Collman, J.P.; Zhang, X.; Hembre, H.; Brauman, J.I. *J. Am. Chem. Soc.* **1990**, *112*, 5356-5357.

25. Chang, C.K.; Yeh, C.Y.; Lai, T.S. *Macromol. Symp.* **2000**, *156*, 117-124.

26. Lai., T.S.; Lee, S.K.S.; Yeung, L.L.; Liu, H.Y.; Williams, I.D.; Chang, C.K. *Chem. Commum.* **2003**, 620-621.

27. Liu, S.Q.; Pecaut, J.; Marchon, J.C. *Eur. J. Inorg. Chem.* **2002**, 1823.

28. Lansky, D.E.; Mandimutsira, B.; Ramdhanie, B.; Clausen, M.; Penner-Hahn, J.; Zvyagin, S.A.; Telser, J.; Krzystek, J.; Zhan, R.Q.; Ou, Z.P.; Kadish, K.M.; Zakharov, L.; Rheingold, A.L.; Goldberg, D.P. *Inorg. Chem.* **2005**, *44*, 4485-4498.

29. Mandimutsira, B.S.; Ramdhanie, B.; Todd, R.C.; Wang, H.; Zareba, A.A.; Czernuszewicz, R.S.; Goldberg, D.P. *J. Am. Chem. Soc.* **2002**, *124*, 15170-15171.

30. Jin, N.; Bourassa, J. L.; Tizio, S. C.; Groves, J. T. *Angew. Chem., Int. Ed.* **2000**, *39*, 3849-3851.

31. Jin, N.; Groves, J. T. *J. Am. Chem. Soc.* **1999**, *121*, 2923-2924.

32. Groves, J. T.; Lee, J.; Marla, S. S. *J. Am. Chem. Soc.* **1997**, *119*, 6269-6273.

33. Bernadou, J.; Fabiano, A.-S.; Robert, A.; Meunier, B. *J. Am. Chem. Soc.* **1994**, *116*, 9375-9376.

34. Nam, W.; Kim, I.; Lim, M. H.; Choi, H. J.; Lee, J. S.; Jang, H. G. *Chem.-Eur. J.* **2002**, *8*, 2067-2071.

35. Workman, J. M.; Powell, R. D.; Procyk, A. D.; Collins, T. J.; Bocian, D. F. *Inorg. Chem.* **1992**, *31*, 1548-1550.

36. Collins, T. J.; Powell, R. D.; Slebodnick, C.; Uffelman, E. S. *J. Am. Chem. Soc.* **1990**, *112*, 899-901.

37. Campochiaro, C.; Hofmann, J. A., Jr.; Bocian, D. F. *Inorg. Chem.* **1985**, *24*, 449-450.

38. Czernuszewicz, R. S.; Su, Y. O.; Stern, M. K.; Macor, K. A.; Kim, D.; Groves, J. T.; Spiro, T. G. *J. Am. Chem. Soc.* **1988**, *110*, 4158-4165.

39. Czernuszewicz, R.S.; Mody, V.; Adelajda A.; Zareba, A.A.; Zaczek, M.B.; Gałeüzowski, M.; Sashuk, V.;Grela, K.; Gryko, D.T. *Inorg. Chem.* **2007**, 46, 5616-5624.

40. Groves, J.T.; Nemo, T.E. *J. Am. Chem. Soc.* **1983**, *105*, 5786-5791.

41. Groves, J.T.; Han, Y.; Van Engen, D. *J. Chem. Soc. Chem. Commun.* **1990**, 436-437.

42. He, G.X; Mei, H.Y.; Bruice, T.C. *J. Am. Chem. Soc.* **1991**, *113*, 5644-5650.

43. Liu, C.J.; Yu, W.Y.; Che, C.M; Yeung, C.H. *J. Org. Chem.* **1999**, *64*, 7365-7374.

44. Edwards, N. Y.; Eikey, R. A.; Loring, M. I.; Abu-Omar, M. M. *Inorg. Chem.* **2005**, *44*, 3700-3708.

Chapter 4

Preparation of some iron complexes of the sterically encumbered corroles

4-1. Introduction

As discussed in chapter 1, the electronic configuration of most iron corroles containing a halogen axial ligand (e.g. Fe(Cl)-corrole) can be described as Fe(III)-corrole cationic π radical.[3,23-33] It would seem that a 1-electron oxidation of the Fe(III)-corrole cationic π radical could afford a species equivalent in oxidation state and/or electronic configuration to the active Compound I of cytochrome P-450, peroxidases and catalases.[2~3] It is on this premise that iron corroles are extremely interesting.

Recently, photochemical generation of a high valent iron-oxo intermediate has been reported by Newcomb *et al.*, using laser flash photolysis of the O-X (X=ClO_2, NO_2) ligand on iron corrole.[12] However, when Fe(Cl)-corrole chemically reacts with oxidants (mCPBA, PhIO, NaOCl or H_2O_2) it usually bleaches rapidly in solution, even at very low oxidant concentration.[13~15] A common pathway of metalloporphyrin decomposition in catalytic cycle is the self oxidation via a bimolecular reaction. The series of corroles bearing sterically bulky substituents reported in chapter 3 (Figure 4-1), perhaps may stabilize the corrole ring by preventing bimolecular contacts of corrole complexes.

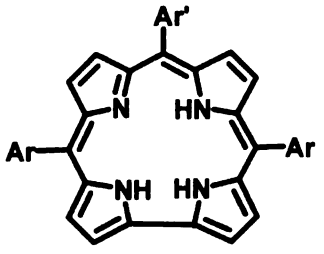

A_2B type corrole

Corrole	Ar	Ar'
$H_3Br_4F_7C$, 2	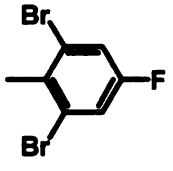	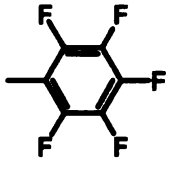
$H_3T_2F_5$, 3	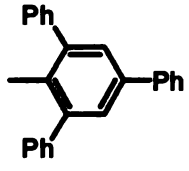	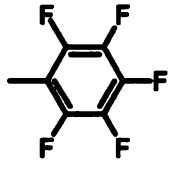

A_3 type corrole

Corrole	Ar = Ar'
$H_3F_{15}C$, 1	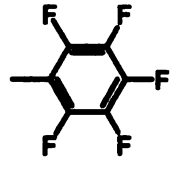
$H_3Br_6F_3C$, 4	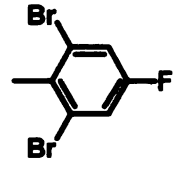
H_3T_3C, 5	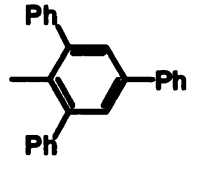

Figure 4-1. Sterically hindered corroles.

4-2. Results and discussion

Synthesis and UV-Vis spectra

The iron insertion to corroles is usually accomplished by refluxing with a methanolic solution of $FeBr_2$ (Scheme 4-1). However, the sterically hindered corroles, such as $H_3T_2F_5C$ and H_3T_3C, require the heating with iron carbonyl (Scheme 4-2). For the sterically less hindered corroles, the $Fe(III)L_2$ (L=MeOH; H_2O; Et_2O or pyridine) complex initially formed and readily convert to their μ-oxo dimers in the presence of moisture and air. The rate of this process, as expected, is sensitive to the bulkiness of the corrole ring; for example, the $FeL_2F_{15}C$ (L=pyridine) readily converts to its μ-oxo dimer during work up (by partition in CH_2Cl_2 and H_2O) whereas the $FeL_2Br_6F_3C$ can be extracted into CH_2Cl_2 and seems to be stable for days. Reaction of FeL_2-corrole with diluted HCl acid gives the stable Fe(Cl)-corrole which reverts to its μ-oxo form easily by washing a CH_2Cl_2 solution with dilute NaOH.

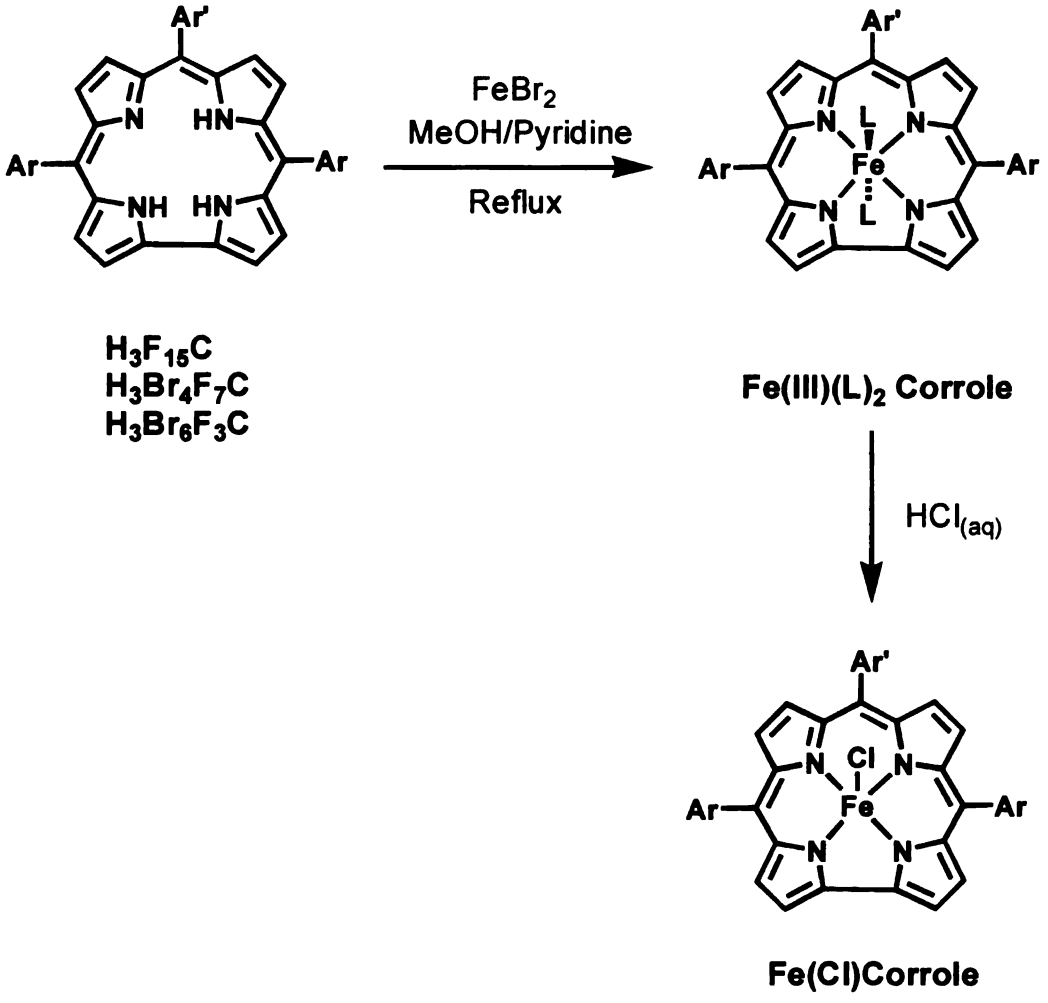

Scheme 4-1. Usual iron insertion for less hindered corroles.

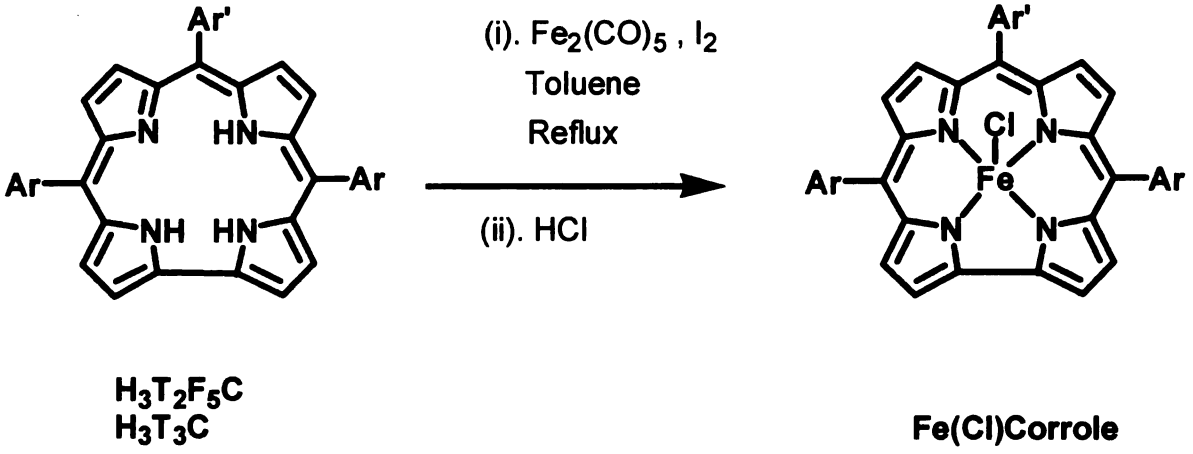

Scheme 4-2 Iron insertion for terphenyl substituted corroles.

Thus, anion on Fe(X)-corrole (X=anion) is exchangeable by reacting the μ-oxo dimer or the 6-coordinated FeL_2-corrole with another acid (Scheme 4-3).

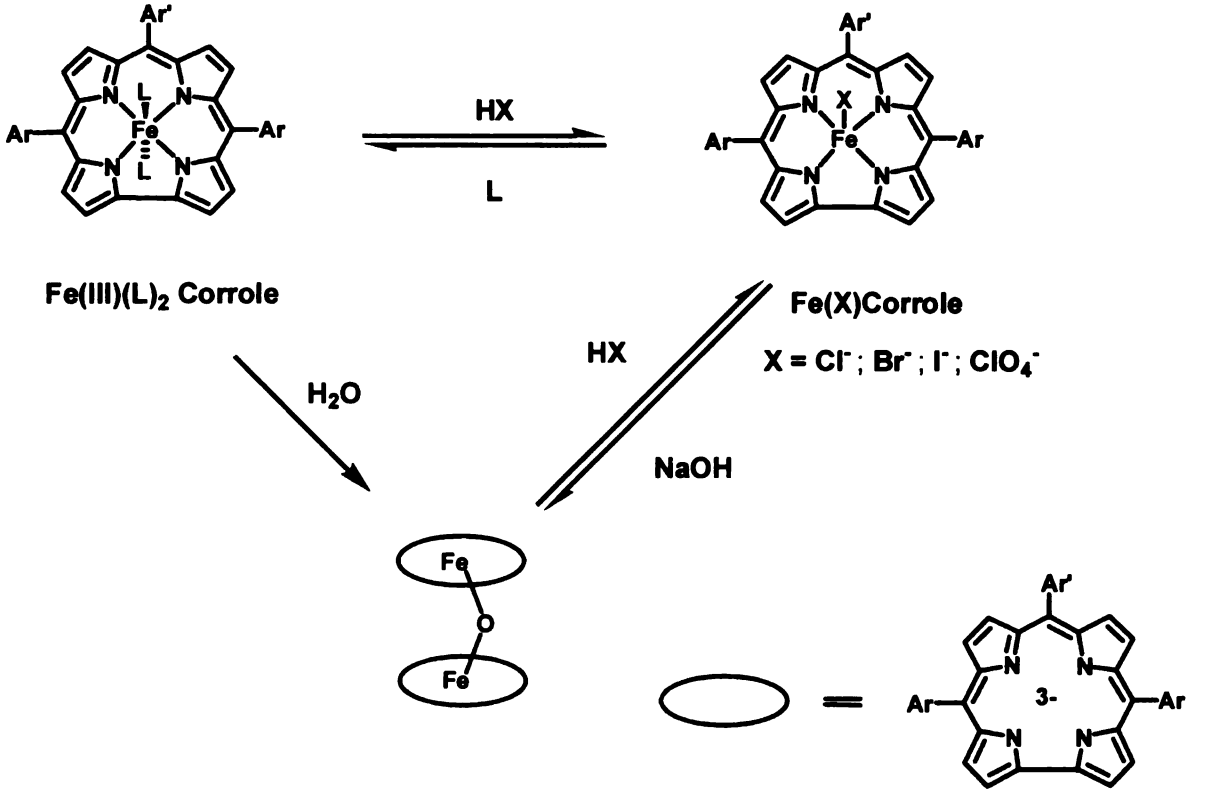

Scheme 4-3. Synthetic routes of different iron corroles.

Interestingly, the reaction of the μ-oxo dimer and 40 $\%_{w/w}$ NaOH yields a compound that has a UV-Vis spectrum similar to that of the six-coordinate FeL_2-corrole, and this compound spontaneously converts back to μ-oxo dimer during attempted isolation. In contrast, the reaction of Fe(Cl)-corrole and $NaOCH_3$ in CH_3OH yields a compound which has a different UV-Vis spectrum from that of the six-coordinate FeL_2-corrole; it is most likely a five-coordinated $Fe(OCH_3)$-corrole, which is stable under anhydrous condition.

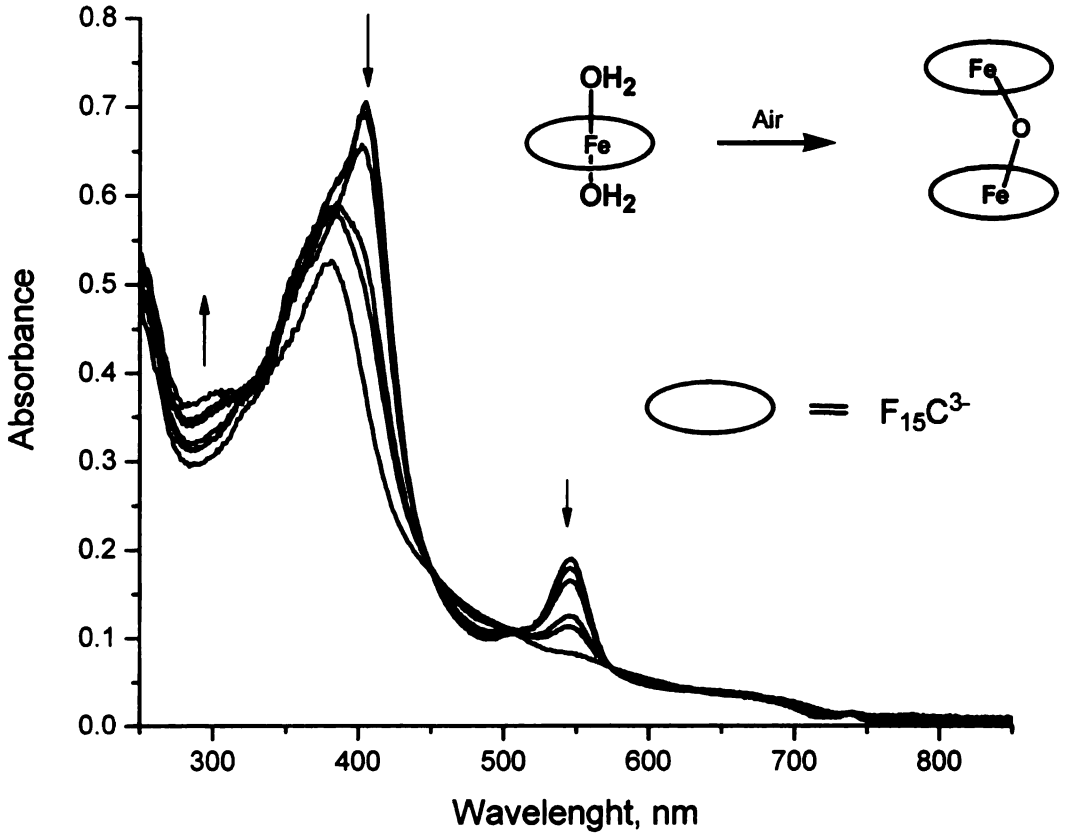

Figure 4-2. Spontaneous conversion of $Fe(H_2O)_2(F_{15}C)$ to $(FeF_{15}C)_2O$.

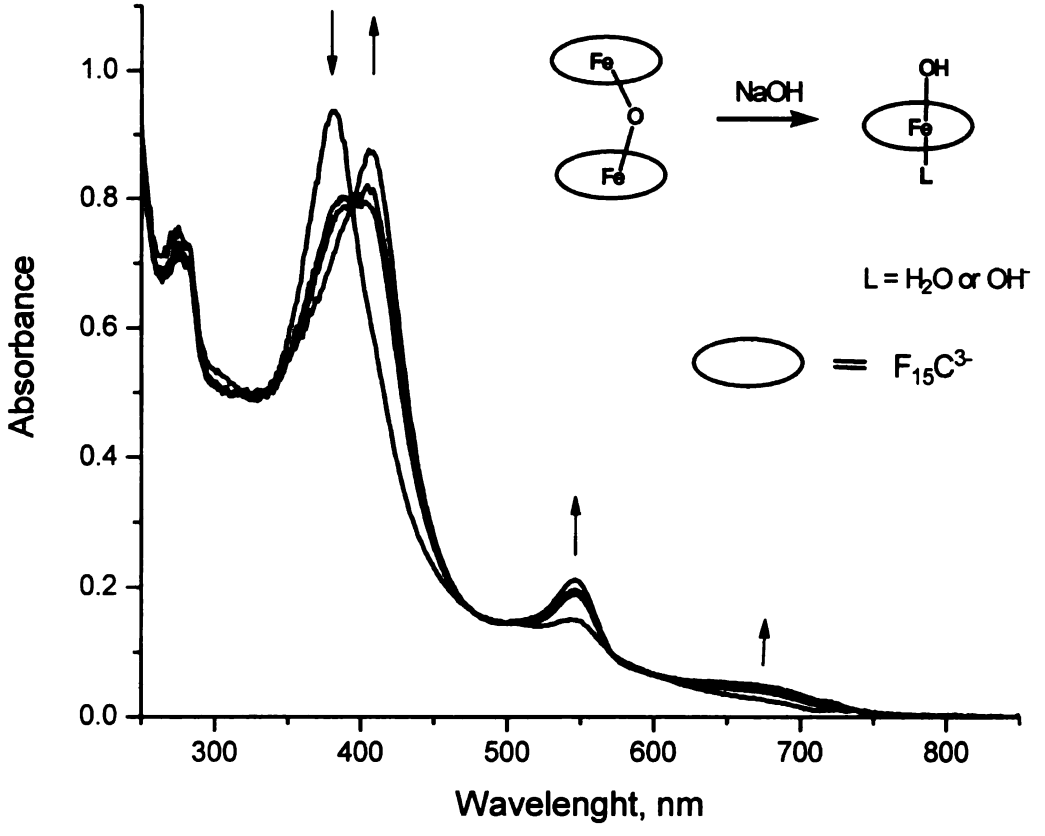

Figure 4-3. UV-Vis spectrum change upon adding NaOH to $(FeF_{15}C)_2O$.

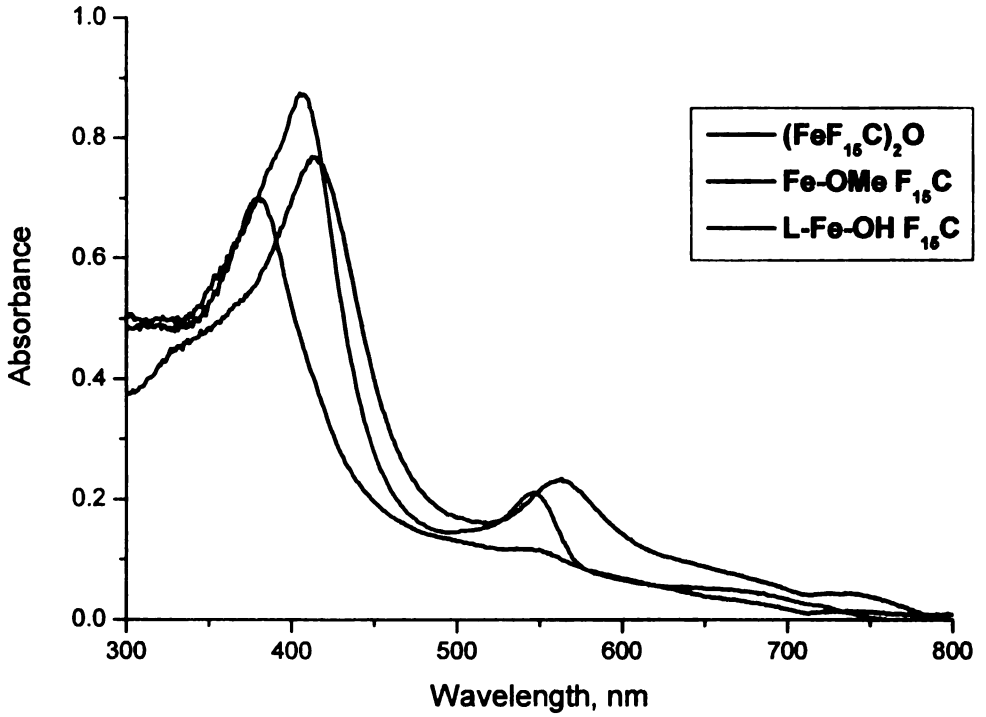

Figure 4-4. UV-Vis spectra of $(FeF_{15}C)_2O$; $Fe(OCH_3)(F_{15}C)$ and L-$Fe(OH)(F_{15}C)$. (This Image is presented in color)

Crystal structure

The solid-state structures of the $Fe(Cl)Br_4F_7C$ (Figure 4-5) and $Fe(Br)T_3C$ (Figure 4-6) have been characterized by X-ray diffraction. The crystal structure of the latter confirms the shielding of the iron center by the two ortho-phenyl groups above and below the corrole plane. The corrole rings in both cases are buckled. The Fe-X bond and the iron out-of-plane distances are listed in Table 4-1.

Table 4-1. Structural data of $Fe(Cl)Br_4F_7C$ and $Fe(Br)T_3C$.

	$Fe(Cl)Br_4F_7C$	**$Fe(Br)T_3C$**
Distance of Fe-X (Å)	2.230	2.459
Distance of Fe-N_4 mean plane (Å)	0.403	0.326

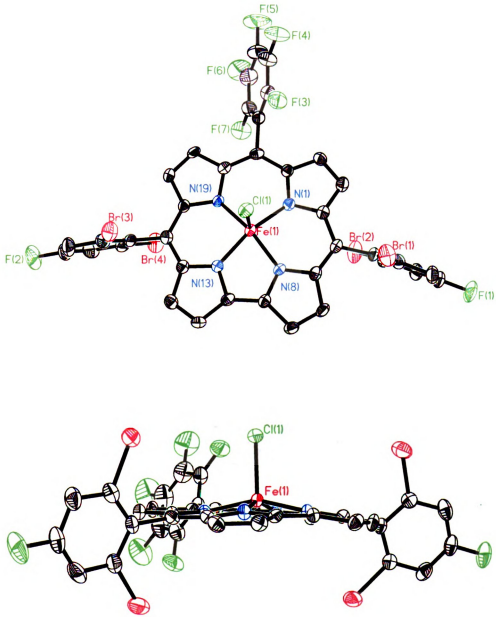

Figure 4-5. Top-view and side-view of the molecular structure of $Fe(Cl)Br_4F_7C$. Thermal ellipsoids enclose 50% probability. (This Image is presented in color)

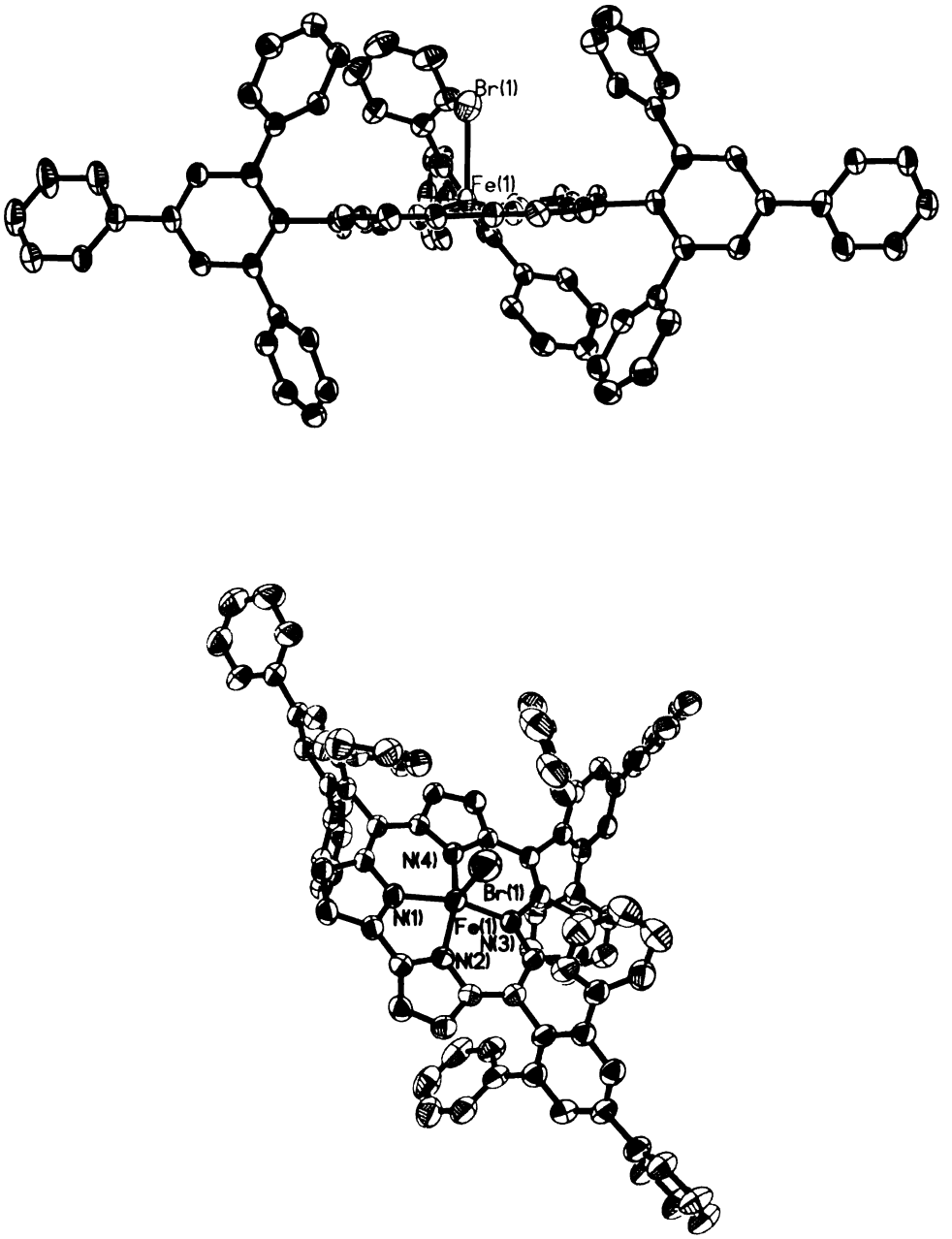

Figure 4-6. Side-view and top-view of the molecular structure of $Fe(Br)T_3C$. Thermal ellipsoids enclose 35% probability. (This Image is presented in color)

Synthesis and characterization of Fe(III)NO corrole

A nitrosyl complex of iron(III)-corrole can be made by reacting the Fe(Cl)corrole with $NaNO_2$.[19~22] The resulting nitrosyl complex is generally deep red in color and diamagnetic. The interaction between Fe and the coordinated NO is often considered to have a charge transfer character, i.e. the bonding between Fe(III) and NO can be represented as $Fe^{II}(NO^+)$. However, the electrons in these complexes are delocalized and perhaps better represented by using the Feltham/Enemark designation[18] $\{FeNO\}^n$, where n is the sum of the metal d electrons and NO antibonding π^*-electron. Thus, $\{FeNO\}^6$ is the case of Fe(III)(NO). In the present case, Fe(Corrole)(NO) will be referred to any Fe(III)-corrole-NO complexes without assignment of the metal oxidation state.

The nitrosyl complex exhibits a very intense N-O stretch band in IR, and the wavenumber of ν_{N-O} is a function of the electronic nature of the corrole ring. As shown in Table 4-2, the ν_{N-O} is highest with the most e-withdrawing corrole ($F_{15}C$) and the lowest with the most e-donating hosts (last two entries), reflecting the electron density of the d_{x2-y2} orbital available for the metal → ligand backbonding. Large backbonding weakens the π-bond of NO and reduces its bond order whereas less backbonding gives larger N≡O triple bond character.

Table 4-2. Nitrosyl stretching frequencies, of different $Fe(Ar_3C)(NO)$ (thin film)

$Fe(Ar_3C)(NO)$	ν N-O (cm^{-1})
$Fe(F_{15}C)(NO)$	1801
$Fe(Br_4F_7C)(NO)$	1796
$Fe(Br_6F_3C)(NO)$	1794
$Fe(T_2F_5C)(NO)$	1794
$Fe(T_3C)(NO)$	1782
Fe(OEC)(NO) [21]	1767
Fe(TMOPC)(NO) [19]	1761

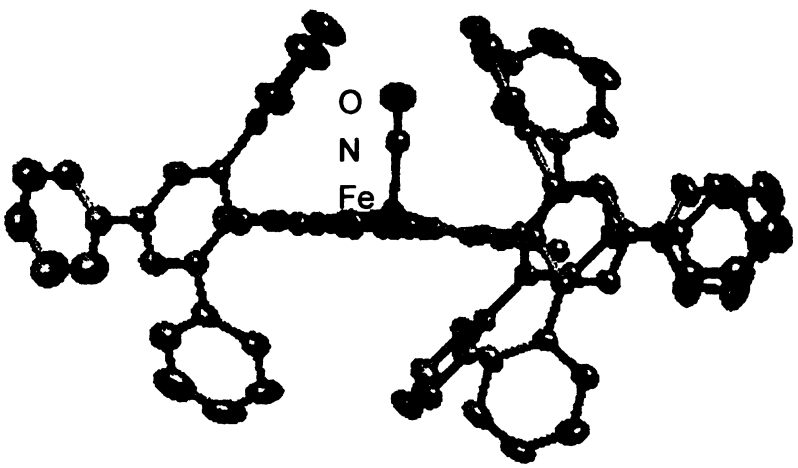

Figure 4-7. Side-view of the molecular structure of of $Fe(T_3C)(NO)$. Thermal ellipsoids enclose 50% probability. (bond angle of Fe-N-O = 176.3°).

Coordination of MeIm to Fe(Cl)T_3C

The binding of Fe(Cl)-corrole with *N*-methylimidazole (MeIm) was studied to probe the steric effect. As shown in Figure 4-8, with the unhindered Fe(Cl)$F_{15}C$, upon addition of MeIm the Soret band shifted from ~380nm to ~425nm, a band at ~550nm initially increased and then decreased, and another absorption band at ~605nm increased in proportional to the concerntration of MeIm. The lack of true isosbestic points suggests more than one end product is involved, i.e. the formation of 5- and 6-coordinate complexes. On the other hand, when the sterically encumbered corrole Fe(Cl)T_3C was titrated with MeIm (Figure 4-9), the absorption band at ~605nm did not appear even at much higher MeIm concentrations employed for that of the Fe(Cl)$F_{15}C$, giving mostly a 5-coordinated Fe(MeIm)-corrole. In looking at the comparison of UV-Vis spectra of 5- and 6-coordinated Fe-corroles (Figure 4-10), the absorption band at 550nm belongs to the 5-coordinated Fe(L)-corrole, and the absorption band at ~605nm comes from the 6-coordinated Fe$(L)_2$corrole.

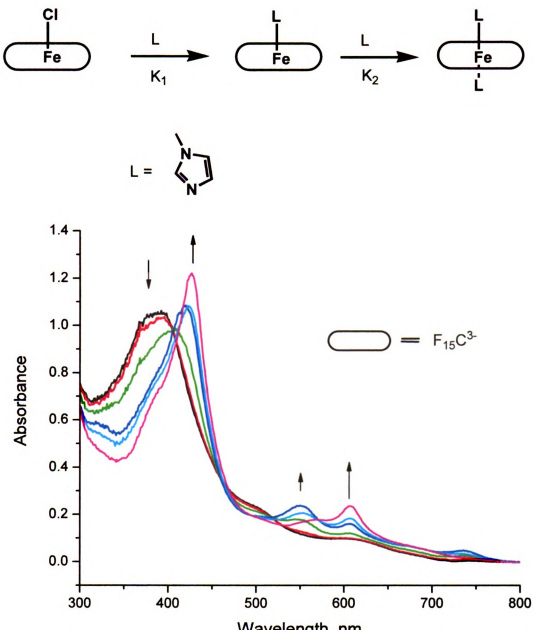

Figure 4-8. UV-Vis spectral changes of $Fe(Cl)F_{15}C$ (0.03μmol) during titration with MeIm; the aliquote amount being roughly 2.5 μmol to give a final [MeIm]= 25μmol. (This Image is presented in color)

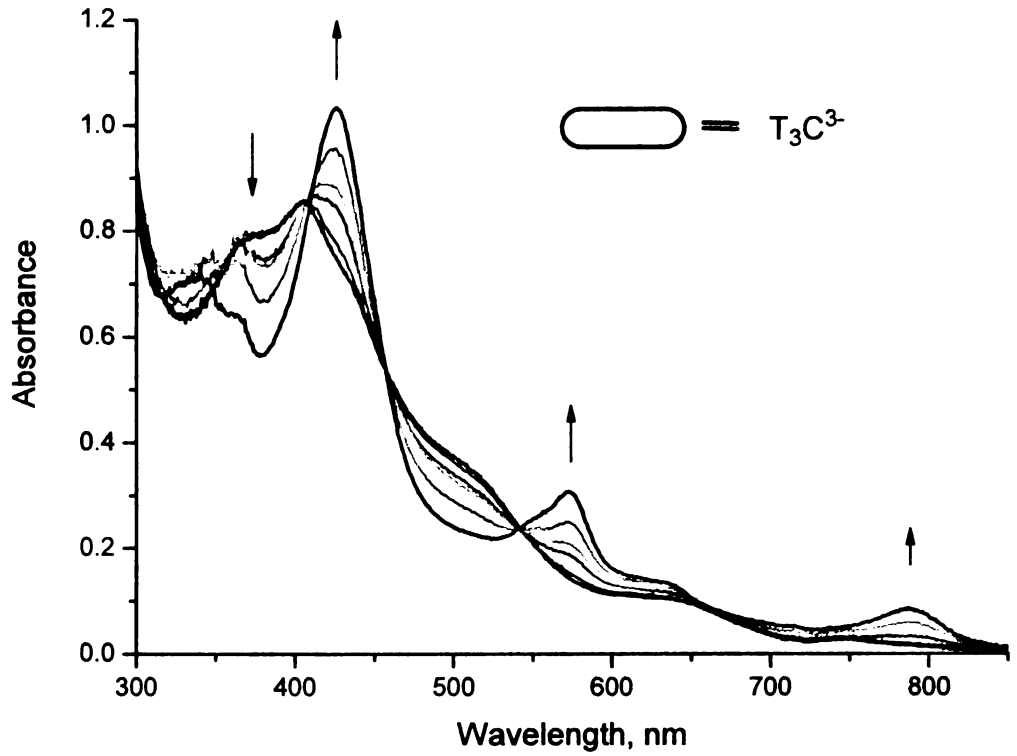

Figure 4-9. UV-Vis spectral changes of Fe(Cl)T_3C (0.04μmol) during titration with MeIm; the final [MeIm]≈370μmol. (This Image is presented in color)

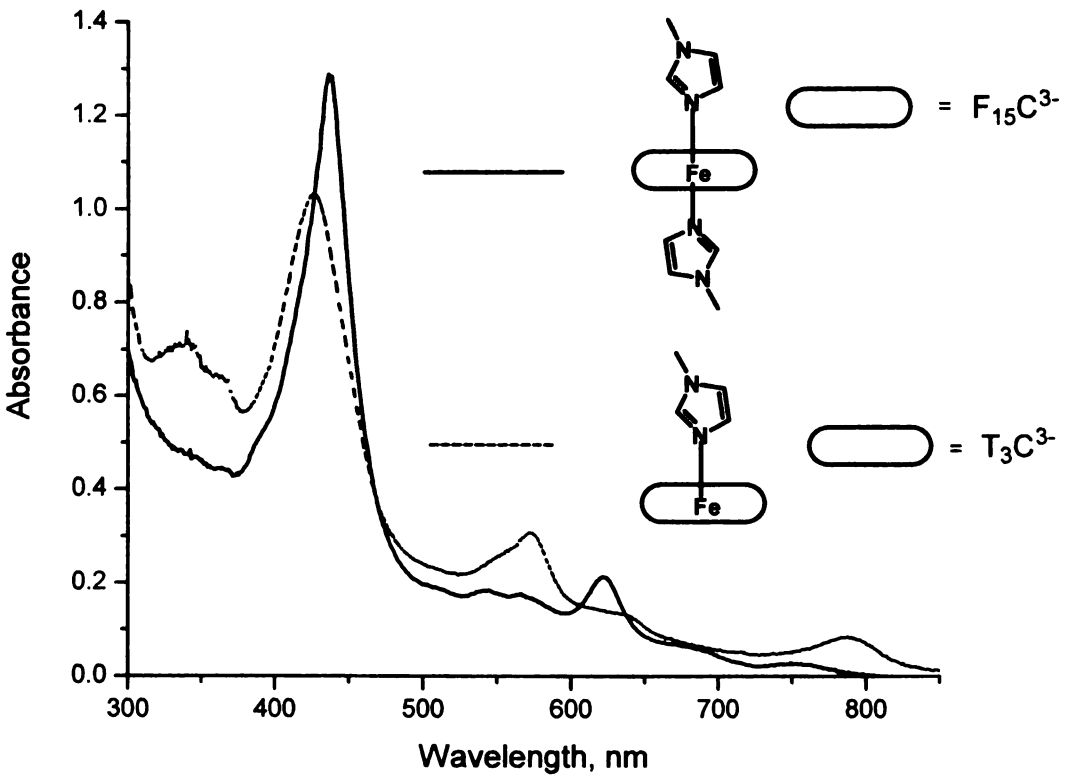

Figure 4-10. Comparison of UV-Vis spectra of 5- and 6-coordinated Fe-corroles. (This Image is presented in color)

Reaction of Fe(Cl)T_3C and PhIO

At the beginning of this work, we presumed that the sterically encumbered iron corrole should be more stable towards oxidants because of the shielding of the iron center to hinder bimolecular oxidation. Unfortunately, we did not observe a significant difference between Fe(Cl)T_3C and Fe(Cl)$F_{15}C$ in their reaction with PhIO in CH_2Cl_2 solution and the iron catalysts completely bleached in minutes. The same situation happened when mCPBA or NaOCl were used as oxidant. The reactive intermediate (in whatever form) formed under these conditions seems to have the propensity to attack the corrole ring possibly by a unimolecular mechanism that leads to decomposition of the corrole ring.[34]

To summarize, several iron corroles with electronic withdrawing groups and sterically encumbered structure have been synthesized. The binding of iron corrole to different ligands (halogen, oxides, nitric oxide and *N*-methylimidazole) were studied. Unfortunately, even with the sterically shielded corrole T_3C, the stability of its iron complex towards oxidant was too low for characterization.

4-3. Experimental

Instrumentation

IR spectra were obtained on a Nicolet IR/42 FTIR spectrophotometer. UV-VIS Spectra were measured on a Varian Cary 50 UV-Visible spectrophotometer with samples dissolved in CH_2Cl_2 unless otherwise stated. Mass spectra were recorded by a Finngan TSQ-7000 mass spectrometer. NMR spectra were recorded using a Varian 300 MHz spectrometer. Chemical shifts (ppm) were reported with respect to $CDCl_3$ or d_6-acetone, supplied by Cambridge Isotope Laboratories.

General procedure of iron insertion to less sterically hindered corroles (Method A)

Free-base corrole (0.05mmol) was dissolved in 20 mL of pyridine/methanol (1:1). $FeCl_2{}^{\bullet}4H_2O$ (60mg, 0.30mmol) was then added and the resulting solution was heated to reflux for 20~50 min under N_2 atmosphere. The progress of reaction to form the red-colored $Fe(L)_2$-corroles was monitoring by UV-vis and TLC. After cooled down to room temperature, the reaction mixture was added to 200mL of CH_2Cl_2 and then washed with water, dried over $MgSO_4$ and the solvent was evaporated. The crude product was purified by column chromatography on silica gel and then washed with HCl (2N) until the color of the iron corrole solution became yellowish-green. The solution was dried over $MgSO_4$ and the solvent was evaporated to obtain Fe(Cl)corrole.

General procedure of iron insertion to sterically hindered corroles (Method B).

Free-base corrole (0.015mmol) was dissolved in 100 mL of toluene under N_2 atmosphere. Iron pentacarbonyl (82μL, 0.6mmol) and I_2 (40mg, 0.15mmol) was added and the resulting solution was heated to reflux for 2hr. The progress of reaction was monitoring by UV-vis and TLC. After cooled down to room temperature, the solution was wash with water, dried over $MgSO_4$ and the solvent was evaporated to give Fe-corrole likely as the iodide. The crude material was washed with dil. NaOH (2N) and HCl (2N) subsequently. Further purification was accomplished by recrystallization from CH_2Cl_2 and hexane solution.

General procedure to obtain nitrosyl iron corrole complexes.

A solution of Fe-Cl-corrole (0.05mmol) in 25mL of dichloromethane was stirred vigorously with 1mL of saturated aqueous solution of sodium nitrite for 2 hour. The organic layer was washed with water and dried over Na_2SO_4, and the solvent was evaporated in vacuo. The residue was chromatographed on neutral alumina (Brockman activity I) eluting with CH_2Cl_2. The first red fraction was collected and evaporated to dryness. Recrystallization from hexane gave pure Fe(NO)-corrole (45~60% yield).

Preparation of ferric-chloride-5,15-bis(2,6-dibromo-4-fluorophenyl)-10-(pentafluorophenyl)corrole [Fe(Cl)Br_4F_7C].

The titled compound was obtained by the method A and recrystallization from hexane to obtain a dark brown powder. Crystals were grown by slow evaporation of $CHCl_3$ and octane solution of Fe(Cl)Br_4F_7C. MS (FAB): m/z= 1020 (M-Cl^+), 1055.67 calculated for $C_{37}H_{12}Br_4ClF_7MnN_4$.

Preparation of ferric-chloride-5,10,15-tris(2,6-dibromo-4-fluorophenyl)corrole [Fe(Cl)Br_6F_3C].

The titled compound was obtained by either method A or method B and recrystallization from hexane to obtain a dark green powder. MS (FAB): m/z= 1106 (M-Cl^+), 1141.53 calculated for $C_{37}H_{14}Br_6ClF_3FeN_4$.

Preparation of ferric-chloride-5,15-bis(2,4,6-tertphenyl)-10-(pentafluorophenyl)corrole [Fe(Cl)T_2F_5C].

The titled compound was obtained by the method B and recrystallization from hexane to obtain a dark green powder. MS (FAB): m/z= 1125 (M-Cl^+), 1160.17 calculated for $C_{73}H_{42}F_5ClMnN_4$.

Preparation of ferric-chloride-5,10,15-tris(2,4,6-tertphenyl) corrole [Fe(Cl)T_3C].

The titled compound was obtained by the method B and recrystallization from hexane to obtain dark green powder. MS (FAB): m/z= 1264 ($M-Cl^+$), 1299.31 calculated for $C_{91}H_{59}ClMnN_4$.

X-ray crystallographic data collection and structure refinement

Crystals were grown by layer diffusion of chloroform and methanol or of chloroform and octane solutions. Data were collected at 293 K and structures were solved by the direct method using the NRCVAX program package. All non-hydrogen atoms were refined anisotropically. The hydrogen atoms of interest were located from difference map and refined positionally when appropriate.

In the crystal data of Fe(T_3C)(NO), solvent molecules were found to reside in the lattice void, which is presumably octane resulting from crystallization. Attempts to model these solvents and or redefine as CH_2Cl_2; $CHCl_3$ failed to generate a chemically sensible model. The SQUEEZE (Sluis, P.V.D.; Spex, A.L. *Acta. Cryst.* **1990**, *A46*,194.) function of PLATON (Spex, A.L. *J. Apply. Cryst.* **2003**, *36*, 7-13.) was used to eliminate the contribution of the electron density in the void from the intensity data. The total solvent area volume was found to be 1377 $Å^3$, with electron count of about 237 electrons. This corresponds to approximately three molecules of octane residing in the cell. Although the electron count is slightly higher than calculated, the large volume

suggests that this void is mostly consumed by octane and not the other potential solvent, dichloromethane. The calculate F(000) and density was calculated for the cell containing three molecules of octane per cell or 1.5 per molecule of interest. The refinement was carried out on the new reflection file generated by PLATON.

The crystallographic data for the structures are summarized in Appendix.

References

1. Denisov, I.G.; Makris, T.M.; Sligar, S.G.; Schlichting I. *Chem. Rev.* **2005**, *105*, 2253.

2. *"Cytochrome P450: Structure, Mechanism, and Biochemistry"*, 3rd ed; Ortiz de Montellano, P.R. Ed.; Kluwer Academic/Plenum Publishers: New York. **2005**.

3. "Iron Porphyrin Chemistry---A Ten-Year Update," Walker, F. A.; Simonis, U. In Encyclopedia of Inorganic Chemistry; Ed. 2; King, R. B., Ed.; Wiley & Sons, Ltd.: Chichester; **2005**; pp. 2390-2521.

4. Schlichting, I.; Berendzen, J.; Chu, K.; Stock, A. M.; Maves, S. A.; Benson, D. E.; Sweet, R. M.; Ringe, D.; Petsko, G. A.; Sligar, S. G. *Science* **2000**, *287*, 1615-1622.

5. Davydov, R.; Makris, T. M.; Kofman, V.; Werst, D. E.; Sligar, S. G.; Hoffman, B. M. *J. Am Chem. Soc.* **2001**, *123*, 1403.

6. Groenhof, A. R.; Ehlers, A. W.; Lammertsma, K. *J. Am. Chem. Soc.* **2007**, *129*, 6204-6209.

7. Groves, J. T.; McClusky, G. A. *J. Am. Chem. Soc.* **1976**, *98*, 859-861.

8. Groves, T.; McClusky, G. A.; White, R. E.; Coon, M. J. *Biochem. Biophys. Res. Commun.* **1978**, *81*, 154-160.

9. Schőneboom, J. C.; Cohen, S.; Lin, H.; Shaik, S.; Thiel, W. *J. Am. Chem. Soc.* **2004**, *126*, 4017-4034.

10. Schőneboom, J. C.; Lin, H.; Reuter, N.; Thiel, W.; Cohen, S.; Ogliaro, F.; Shaik, S. *J. Am. Chem. Soc.* **2002**, *124*, 8142-8151.

11. Ogliaro, F.; Harris, N.; Cohen, S.; Filatov, M.; De Visser, S. P.; Shaik, S. *J. Am. Chem. Soc.* **2000**, *122*, 8977-8989.

12. Harischandra, D.N.; Zhang, R; Newcomb, M. *J. Am. Chem. Soc.* **2005**, *127*, 13776–13777.

13. Groves, J. T.; Haushalter, R. C.; Nakamura, M.; Nemo, T. E.; Evans, B. J. *J. Am. Chem. Soc.* **1981**, *103*, 2884-288.

14. Collman, J.P., Zeng, L., Decreau, R.A. *Chem. Commun.*, **2003**, 2974-2975.

15. Harrison, H. R.; Hodder, O. J. R.; Crowfoot Hodgkin, D. *J. Chem. Soc. B* **1971**, 640.

16. Anderson, B. F.; Bartczak, T. J.; Crowfoot Hodgkin, D. *J. Chem. Soc. Perkin Trans. 2* **1974**, 977.

17. Harischandra, D.N.; Zhang, R; Newcomb, M. *J. Am. Chem. Soc.* **2005**, *127*, 13776–13777.

18. Enemark, J.H.; Feltham, R.D. *Coord. Chem. Rev.* **1974**, *13*, 339.

19. Joseph, C.A.; Lee, M.S.; Iretskii, A.V.; Wu, G.; Ford, P.C. *Inorg. Chem.* **2006**, *45*, 2075.

20. Simkhovich, L.; Goldberg, I.; Gross, Z. *Inorg. Chem.* **2002**, *41*, 5433.

21. Autret, M.; Will, S.; Caemelbecke, E.V.; Lex, J.; Gisselbrecht, J.P.; Gross, M.; Vogel, E.; Kadish, K.M. *J. Am. Chem. Soc.* **1994**, *116*, 9141.

22. Caemelbecke, E.V.; Will, S.; Autret, M.; Adamian, V.A.; Lex, J.; Gisselbrecht, J.P.; Gross, M.; Vogel, E.; Kadish, K.M. *Inorg. Chem.* **1996**, *35*, 184.

23. Walker, F.A. *Inorg. Chem.* **2003**, *42*, 4526–4544.

24. Cai, S.; Walker, F.A.; Licoccia, S. *Inorg. Chem.* **2000**, *39*, 3466–3478.

25. Cai, S.; Licoccia, S.; Walker, F.A. *Inorg. Chem.* **2001**, *40*, 5795–5798.

26. Steene, E.; Wondimagegn, T.; Ghosh, A. *J. Phys. Chem. B* ***2001***, *105*, 11406–11413.

27. Ghosh, A.; Steene, E. *J. Inorg. Biochem.* ***2002***, *91*, 423–436.

28. Zakharieva, V. Schu¨nemann, M. Gerdan, S. Licoccia, S. Cai, F.A. Walker, A.X. Trautwein, *J. Am. Chem. Soc.* ***2002***, *124*, 6636–6648.

29. Simkhovich, L.; Mahammed, A.; Goldberg, I.; Gross, Z. *Chem. Eur. J.* ***2001***, *7*, 1041–1055.

30. Gross, Z.; Simkhovich, L.; Galili, N. *Chem. Comm.* **1999**, 599–600.

31. Simkhovich, L.; Gross, Z. *Tetrahedron Lett.* ***2001****, 42,* 8089–8092.

32. Mahammed, A.; Gross, Z. *J. Am. Chem. Soc.* ***2005****, 127*, 2883–2887.

33. Walker, F.A.; Licoccia S.; Paolesse, R, *Journal of Inorganic Biochemistry 100* (**2006**) 810–837.

34. For unimolecular decomposition in iron porphyrins, please see: Sono, M.; Roach, M.P.; Coulter, E.D.; Dawson, J.H. *Chem. Rev.* ***1996****, 96*, 2841.

Chapter 5

Organogel-based corrole as cytochrome P-450 model

5-1. Introduction

A gel is an apparently solid, jelly-like material formed from a colloidal solution, mainly liquid plus a small amount of gelator (0.1-10 wt %). In addition to the currently more prevalent polymer gels, the discovery and design of small organic molecules capable of gelating aqueous solvents is a rapidly expanding area of research,[1-4] in particular due to their possible practical applications of tissue engineering.[1] drug delivery,[5-9] screening biomolecules,[10] wound healing,[11] and pollutant capture and removal.[12] The gel is usually formed by heat or ultrasonication until the solution turned into clear, isotropic fluids followed by cooling the solution to below the gelation transition temperature (T_{gel}), i.e., the temperature below which the flow is no longer observed over long periods. The frequent way to test a gel formation is turn the gel containing small vial or test tube upside down, if no flow is observed, the solution is said to be gelled (Figure 5-1).

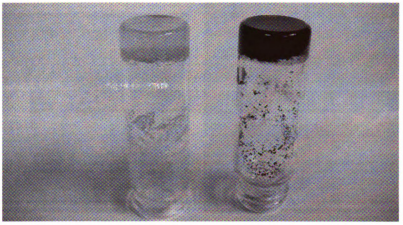

Figure 5-1. Fmoc-FF organogel (toluene) (left) and $MnF_{15}C$ imbedded organogel (right).

The gelation phenomenon is thought to arise from the fibers of gelators (nano to micrometer scale) becoming entangled and forming three-dimensional coss-linking frameworks capable of trapping solvent via surface tension.[13-16] Unlike polymer gels, the gels formed by low-molecular-weight organic molecules are supported by self-assembling of molecules from noconvalent interactions. In addition, the cross links between fibers are also noncovalent. One consequence of this is that small molecule gels are often thermally reversible. After the gelation process, the gelators in the gel are linked in complex, three-dimensional networks; for example, the rod like networks and the interconnected fibers shown in Figure 5-2,[17] which immobilize the liquid component to a variable extent by surface tension. There are several types of gel depends on the types of liquid trapped inside the gel upon gelation, in this research we mainly focused on hydrogel and organogel that traps water and toluene, respectively.

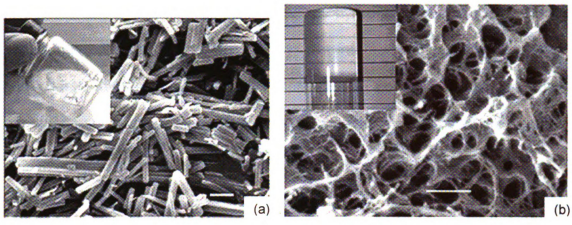

Figure 5-2. Scanning electron micrographs of fibers formed by L-DHL (lanosta-8,24-dien-3β-ol/24,25-dihydrolanosterol) in diisooctylphthalate (DIOP). (a) Short, thick fibers formed by 10 wt % L-DHL/DIOP (b) Interconnected fiber networks in 10 wt % L-DHL/DIOP system after adding 0.004 wt % EVACP (ethylene/vinyl acetate copolymer) to promote branching. (b) is a gel, as shown in the inserted picture. (Reproduced from ref 17.)

Hydrogel

Small-molecular-weight hydrogels are formed via the self-assembly or nanoscale aggregation of small organic molecules, which are related to, but fundamentally different from, the polymer hydrogel and small-molecular-weight organogels.[3] For most currently used hydrogelators, they share a common structure behavior which contains hydrophilic head; flexible hydrophobic tail; rigid spacer and flexible linkers in between.[3] In general, the gelation process is a balance between crystallization and solubilization, therefore, the gelators require different functional groups in the molecule that provide both functionalities, for example in forming hydrogels, the organic gelators are amphiphilic with hydrophobic groups to enhance aggregation and hydrophilic groups to provide solubility.

In addition to the structure amphiphilicity, the hydrogelators also should have strong intermolecular interactions such as π-π interactions, hydrogen bonding, and charge interactions among the molecules to confer the fiber structure formation and the three-dimensional networks as the matrices of hydrogels.[4]

Organogel

Unlike the formation of hydrogel in which hydrophobic attractions of gelators is a major driving force for aggregation in water,[23] aggregation of gelators in organogel must result from a different set of interactions,[24-26] where forces are mainly from dipolar interactions and possibly, specific intermolecular hydrogen bonding or metal-coordination. These interactions must be strong enough to balance the entropy loss from the reductions in the translational and rotational freedom of motion.[2, 18] The organic phase entrapped in a gel network has greater variety, the liquid can be e.g. polysiloxanes, parafins, alcohols, aromatics and chlorinated molecules, nematic and smectic liquid-crystalline materials, electrolytes, polymerizable liquid, and others containing an enormous range of functional groups.[2, 18-22]

There is no general structure requirement for organogelators as in hydrogelators; several reviews[2,18,19] introduced different classes of organogelator including fatty acid derivatives, steroid derivatives, anthryl derivatives, steroid and condensed aromatic ring derivatives, amino acid

derivatives, etc., as these compounds are capable of gelating a wide variety of organic liquids via the interactions discussed above at.

Heme models imbedded in gel matrix

The first example of the fusion of gel and a heme enzyme was reported by Xu *et al.*[27] Revealing that the immobilized enzyme in a varieties of hydrogels shows superactivity in organic solvent (toluene) relative to unconfined enzyme in water. This result indicates the hydrogel is able to provide an aqueous microenvironment to carry out enzymatic reactions in organic solvent.

It has been well documented that the presence of proton donor or polar groups around the heme active site can affect the activities of hemoproteins.[28-30] Chang *et al.*[31-32] have previously synthesized a series of heme models modified by a range of groups with different polarity at or near the active site. From studies on these models, it is concluded that dipolar forces and hydrogen bonding should play a significant role in regulating the oxygen affinities of heme proteins.

The same series of heme model compounds have recently been incorporated into a supermolecular hydrogel, and these imbedded hemes demonstrate high catalytic activities in organic media, which are significantly higher than that of the heme model alone. The catalytic activity of the hydrogel-based model in toluene reached about 90% of the nascent activity of horseradish peroxidases

(HRP) in water.[33-34] Thus, hydrogel provides an excellent platform for achieving artificial enzyme where self-assembled nanofibers of aminoacids allow the of heme model compounds to function as the nature prosthetic group.

Given the excellent performance of the enzyme mimetic system made by supermolecular hydrogel prompted us to evaluate whether supermolecular hydrogel could also serve as a platform to study cytochromes P-450 activities. We also turned our sight from porphyrin to corrole. Manganese and iron corroles in particular share many properties with the metallo prophyrins. However, poor stability in oxidativen environment has been a major disadvantage preventing metallocorroles to be good cytochromes P-450 models. In our previous study, imbedding manganese corrole on functionalized silica gel by covalent bond suffiently increased the overall turnover number from 100 to over 500 in catalytic epoxidation, presumably due to less self-oxidation by immobilization.[35]

Using the supermolecular hydrogel or organogel as immobilizing materials should be attractive. The non-covalent bond interaction between gel and corrole ring also allows the recovery of the expensive catalyst.

5-2. Results and Discussion

The model reaction of interest is the oxidation of methyl phenyl sulfide by t-butylhydrogenperoxide (TBHP) catalyzed by metalloporphyrin or metallocorroles (Eqn. 4-1). The initial catalytic turnover numbers of iron and manganese porphyrin, $Mn(Cl)F_{20}P$ and $Fe(Cl)F_{20}P$, and the corrole analogs, $MnF_{15}C$ and $Fe(Cl)F_{15}C$ are shown in Table 5-1. The activities of catalyst in hydrogel/buffer are nearly 10 times less reactive than that in toluene, and almost zero activity in aqueous media, which seems surprising and unexpected. However, by analyzing the phase equilibrium of reactants and products between the hydrophobic toluene solution and the hydrophilic hydrogel, we recognized the fact that the products, i.e. sulfone and sulfoxide, have a higher polarity than sulfide, and thus have a slow rate of diffusion from the hydrogel matrices to the toluene solvent, which may account for the reduced activity.

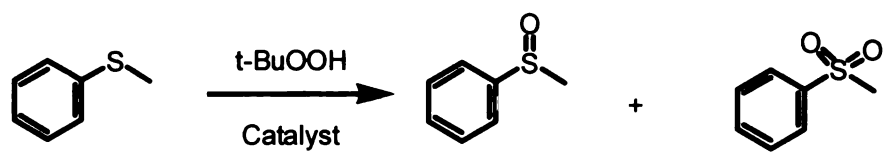

Eqn. 4-1

Catalyst:

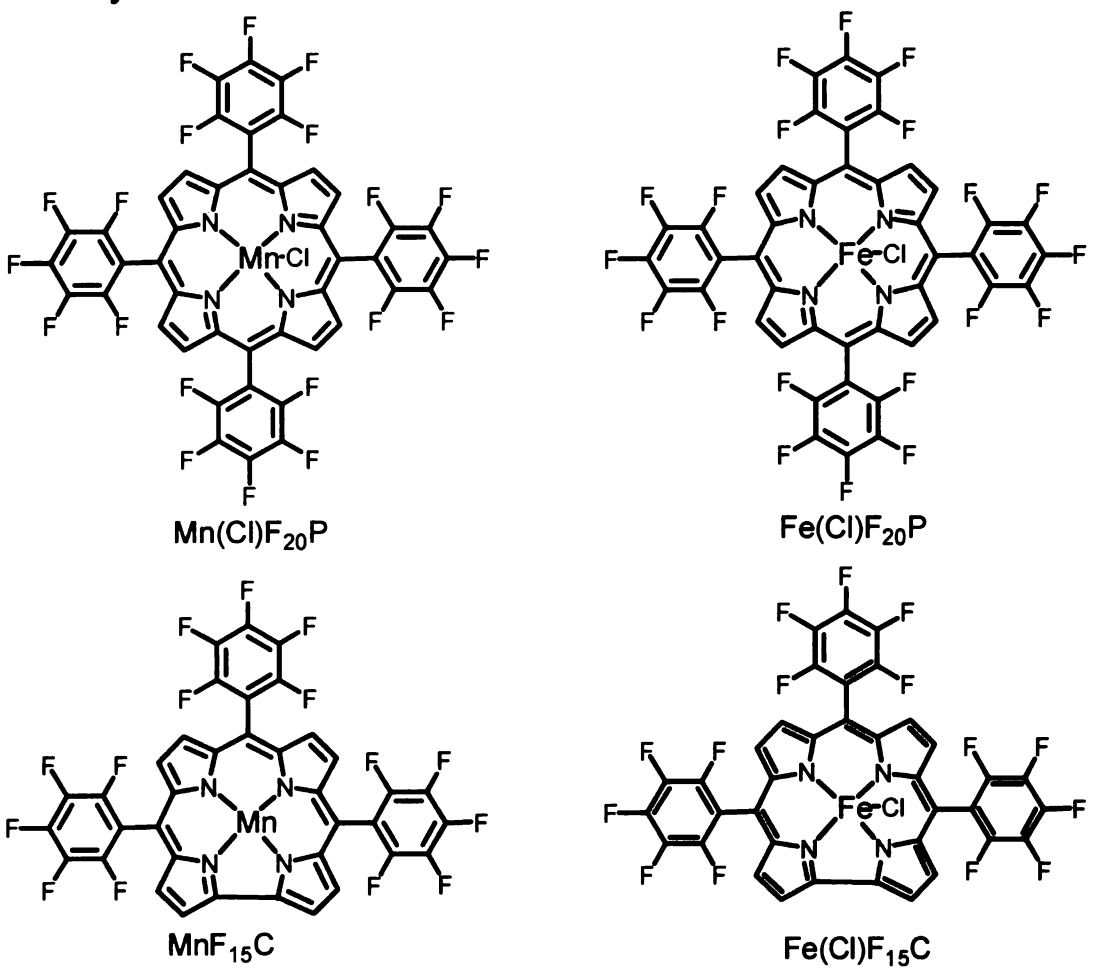

Figure 5-3. Molecular structures of catalyst for sulfide oxidation reaction.

Table 5-1. Sulfide oxidation with TBHP catalyzed by porphyrin or corrole, in the presence of 4 equivalence of imidazole.

	TON (min^{-1}) in toluene	TON (min^{-1}) in buffer	TON (min^{-1}) in hydrogel/toluene
$Mn(Cl)F_{20}P$	19.1	<0.1	2.1
$Fe(Cl)F_{20}P$	13.2	<0.1	1.8
$MnF_{15}C$	18.7	<0.1	1.6
$Fe(Cl)F_{15}C$	14.2	<0.1	1.6

Consequently, we surmised that the use of organogel as platform should provide an organic microenvironment for the less polar reactant to react while the removal of the more polar products may be facilitated by aqueous medium (Figure 5-4 and Figure 5-5).

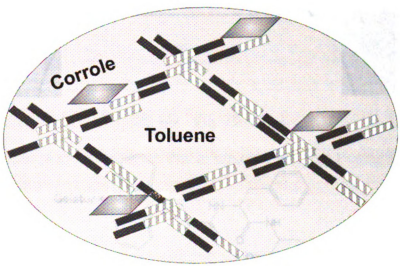

Figure 5-4. Organogel-based artificial cytochrome P-450

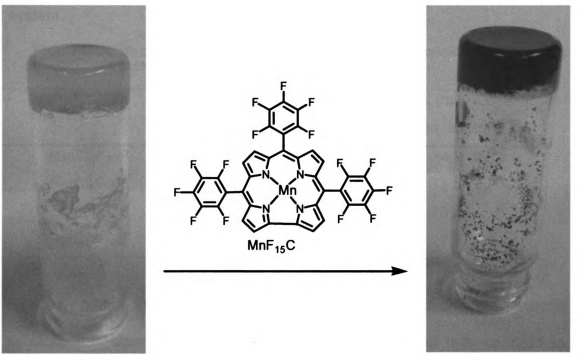

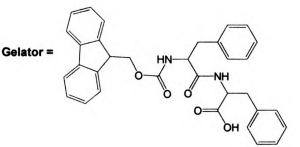

Figure 5-5: (a) Organogel of Fmoc-FF in toluene (10wt%), and (b) Organogel of Fmoc-FF and $MnF_{15}C$ (40mg:2mg) in toluene (10wt%). (This Image is presented in color)

Again, by monitoring the oxidation of methylphenylsulfide by TBHP and catalysts, we obtained the initial catalytic turn over numbers of iron and manganese porphyrin and the corrole analogs, as shown in Table 5-2. The activities of catalyst in organogel/buffer solution are slightly lower than those in

toluene solution, but are much higher than that formed in hydrogel/toluene system.

Table 5-2. Sulfide oxidation with TBHP catalyzed by porphyrin or corrole, in the presence of 4 equivalence of imidazole.

	TON (min^{-1}) in toluene	TON (min^{-1}) in organogel/buffer
$Mn(Cl)F_{20}P$	19.1	14.2
$Fe(Cl)F_{20}P$	13.2	11.5
$MnF_{15}C$	18.7	13.6
$Fe(Cl)F_{15}C$	14.2	12.7

By analyzing the product formation as a function of the reaction time in toluene solution, it is clear that sulfoxide is initially produced and then oxidized to sulfone (Figure 5-6a). Surprisingly, the Gel-buffer system produces much higher percentage of sulfone than that in toluene solution (Figure 5-6b).

(a).

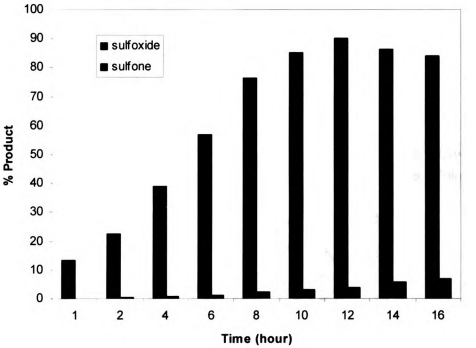

(b).

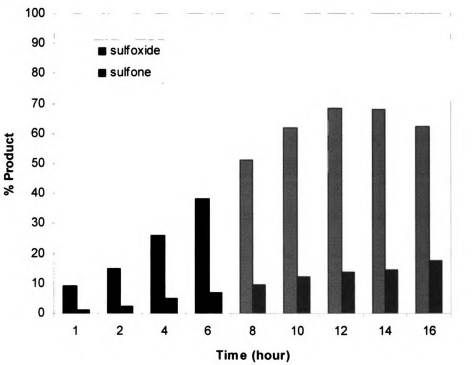

Figure 5-6: Oxidation result for oxidation of Methylphenylsulfide with one equivalent of TBHP in: (a). Toluene solution and (b). Gel-buffer.

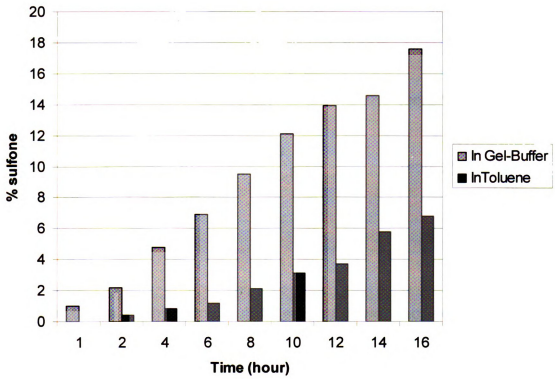

Figure 5-7: Comparison of the percentage of sulfone formation in gel-buffer and toluene solution.

By comparing the formation of sulfone in gel-buffer and in toluene systems (Figure 5-7), the result also clearly shows the formation rate is faster in gel-buffer system. This rate enhancement may be explained by the following hypothesis. In homogenous solution, the rate of sulfone formation depends on the concentration of sulfoxide.[36] Whereas in the heterogeneous gel-solution reaction, the reaction rates of sulfoxide and sulfone formation are under diffusion control, and the rates of diffusion of the reactants and products depend on their molecular size and lipophilicity. Thus, the local concentration of sulfoxide and catalyst could be higher in the gel matrix than in homogenous

solution. Moreover, the gel-matrix could slow down the bimolecular self-oxidation of the catalyst.

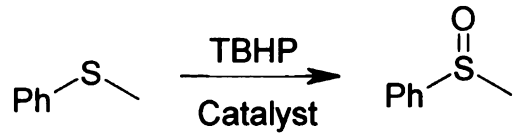

(eqn. 1)

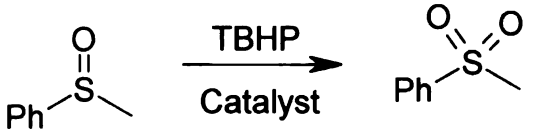

(eqn. 2)

In addition to the methylphenyl sulfide substrate, we also examined other sulfides with different structure and electronic effect. The results are consistent in that the gel-matrix significantly enhances the formation of sulfone (Figure 5-8). In addition to the sulfoxide and sulfone formed, all of these sulfide oxidations showed trace amounts of S-dealkylation side products, which are also found in other reactions involving the metal-oxo species and is consistent with the cytochrome-P450 type chemistry.

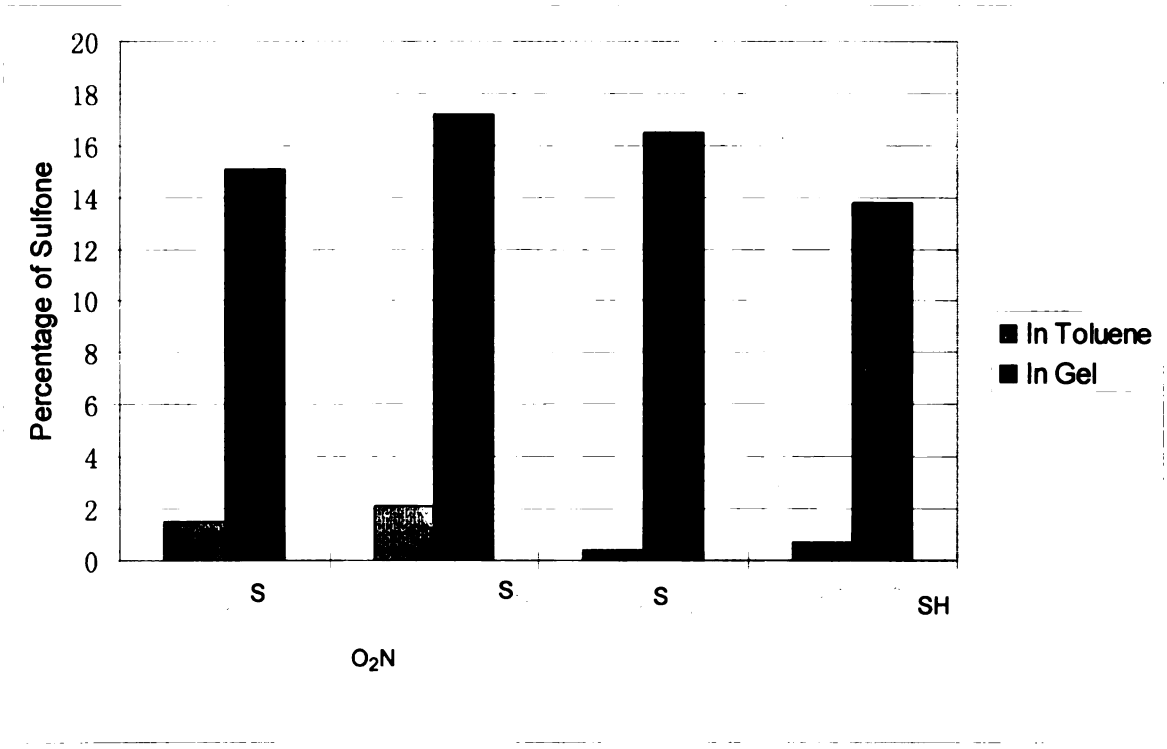

Figure 5-8. The comparison of the various sulfide oxidations in toluene and in organogel.

It has been mentioned throughout this thesis that the corrole macrocycles may be specially suited as a catalyst for oxidative reactions. This advantage may be extended further when the manganese corrole is immobilized in organogel. The Mn-corrole catalyst seems stable for extended use and can be recovered quantitatively. The reaction progress can be actually observed from the color change of organogel (Figure 5-9).

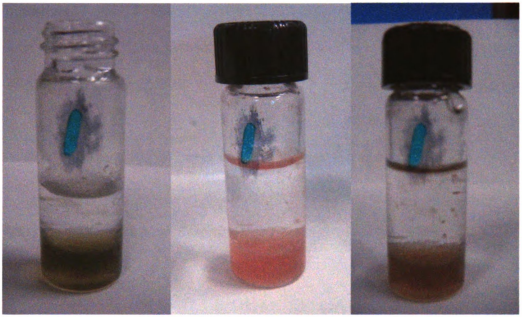

Figure 5-9: The color-change observed during sulfide oxidation. (a) upper layer: aqueous buffer (pH=7), lower layer: Organogel of Fmoc-FF and $MnF_{15}C$ (40mg:0.1mg) in toluene (10wt%). (b) After 1 hour of the addition of 20 mole ratio of TBHP. And (c) after 2 days of the addition of 100 mole ratio of PhSMe (in order to show the color change clearly, the concentration of $MnF_{15}C$ used in this figure is 20 times diluted than in usual catalysis, see experimental section). (This Image is presented in color)

In summary, we explored the reactivity of Mn-corrole imbedded in supermolecular hydrogel or organogel. While the study so far has been limited to one reaction (sulfide oxidation), the selective increase of one product (sulfone) from altering the nature of the gel goes a long way to highlight the crucial elements of the gel research, i.e. diffusion rate and local concentration. With proper designs, we believe the gel system is useful in manipulating reactivity in general and providing a new platform in particular for biomimetic materials.

5-3. Experimental

Preparation of organogelator (F-mocFF)[8]

To Fmoc-F (1.0 mmol) and N-hydroxysuccinimide (NHS, 115 mg, 1.0 mmol) were dissolved in 20 mL of $CHCl_3$, DCC (230 mg, 1.1 mmol) was added to the solution and the reaction mixture was stirred at room temperature for 2 hours. The resulting precipitate was removed by filtration, and the organic solvent was removed *in vacuo*. The residues was washed with hexane (20 mL) and ethanol (10 mLx3), subsequently. The solid was then dissolved in 30 mL of acetone, and phenylalanine (1mmol) was added. The reaction mixture was stirred at room temperature for 12 hours. The suspended solid was removed by filtration and 15mL of dil. HCl (1N) was added to the filtrate. The resulting white solid was collected and dried by freeze drier to yield F-moc-FF (80%).

General procedure of organogel formation

Fmoc-FF (40mg) was suspended in 0.5mL of toluene, the solution was heated up until all the Fmoc-FF was dissolved. The solution was then cooled down to room temperature without disturbing.

General procedure of organogel based sulfide catalysis

MnTPFC (2mg, 2.5μmol) and Fmoc-FF (40mg) was added to 0.5mL of toluene, the solution was gelated by the general procedure described above. The resulting organogel (100mg, 0.5μmol catalyst loaded) was transfer to a round-bottomed flask containing 0.5mL of buffer solution (pH=7). Sulfide

(0.5mmol) and a solution of 70% *tert*-butylhydrogen peroxide (TBHP) in H_2O (0.5mmol) was added and the solution was stirred gently. 1mL of CH_2Cl_2 was added to dissolve the gel, the amount of sulfoxide and sulfone was determined by gas chromatography.

References

1. Lee, K.Y.; Mooney, D.J. *Chem. Rev.* **2001**, *101*, 1869.

2. Terech, P., Weiss, R.G. *Chem. Rev.* **1997**, *97*, 3133.

3. Estroff, L.A.; Hamilton, A.D. *Chem. Rev.* **2004**, *104*, 1201.

4. Yang, Z.M.; Liang, G.L.; Xu, B. *Acc. of Chem. Res.* **2008**, *41*, 315.

5. Nagai, Y.; Unsworth, L. D.; Koutsopoulos, S.; Zhang, S. G. *J. Controlled Release* **2006**, *115*, 18.

6. Yang, Z. M.; Gu, H. W.; Zhang, Y.; Wang, L.; Xu, B. *Chem. Commun.* **2004**, 208.

7. Yang, Z. M.; Xu, K. M.; Wang, L.; Gu, H. W.; Wei, H.; Zhang, M. J.; Xu, B. *Chem. Commun.* **2005**, 4414.

8. Xing, B. G.; Yu, C. W.; Chow, K. H.; Ho, P. L.; Fu, D. G.; Xu, B. *J. Am. Chem. Soc.* **2002**, *124*, 14846.

9. Tiller, J.C. *Angew. Chem., Int., Ed. Engl.* **2003**, *42*, 3072.

10. Kiyonaka, S.; Sada, K.; Yoshimura, I.; Shinkai, S.; Kato, N.; Hamachi, I. *Nat. Mater.* **2004**, *3*, 58.

11. Yang, Z. M.; Liang, G. L.; Ma, M. L.; Abbah, A. S.; Lu, W. W.; Xu, B. *Chem. Commun.* **2007**, 843.

12. Kiyonaka, S.; Sugiyasu, K.; Shinkai, S.; Hamachi, I. J. Am. Chem. Soc. **2002**, *124*, 10954.

13. Flory, P. J. *Faraday Discuss.* **1974**, *57*, 7.

14. Keller, A. *Faraday Discuss.* **1995**, *101*, 1.

15. Wang, R.; Geiger, C.; Chen, L.; Swanson, B.; Whitten, D. G. *J. Am. Chem. Soc.* **2000**, *122,* 2399.

16. Sakurai, K.; Jeong, Y.; Koumoto, K.; Friggeri, A.; Gronwald, O.; Sakurai, K.; Okamoto, S.; Inoue, K.; Shinkai, S. *Langmuir* **2003**, *19*, 8211.

17. Liu, X. Y.; Sawant, P. D.; Tan, W. B.; Noor, I. B. M.; Pramesti, C.; Chen, B. H. *J. Am. Chem. Soc.* **2002**, *124,* 15055.

18. Abdallah, D.J.; Weiss, R.G. *Adv. Mater.* **2000**, *12*, 1237.

19. Shinkai, S.; Murata, K. *J. Mater. Chem.* **1998**, *8*, 485.

20. Terech, P.; Schaffhauser, V.; Maldivi, P.; Guenet, J.M. *Langmuir* **1992**, *8,* 2104.

21. Terech, P.; Pasquier, D.; Bordas, V.; Rossat, C. *Langmuir* **2000**, *16*, 4485.

22. Lin, Y.C.; Weiss, R.G. *Macromolecules* **1987**, *20*, 414.

23. Israelachvili, J. N. *Intermolecular and surface forces*, 3rd ed.; Academic Press: London, **1992**; 341.

24. Bourrel, M.; Schechter, R. S. *Surfactant Science Series*; Dekker, M.: New York, **1988**; Vol. *30*, 111.

25. Ruckenstein, E.; Nagarajan, R. *J. Phys. Chem.* **1980**, *84*, 1349.

26. Ekwall, P.; Danielsson, I.; Stenius, P. *Physical Chemistry Series One*; Kerker, M., Ed.; Butterworths: London, **1972**; Vol. 7, Chapter 4.

27. Wang, Q.G.; Yang, Z.M.; Wang, L.; Ma, M.L.; Xu, B. *Chem. Commun.* **2007**,1032.

28. Chen, P.F.; Tsai, A.L.; Wu, K.K. *J. Biol. Chem.* **1994**, *269*, 25062.

29. Lauzon, S.; Mansuy, D.; Mahy, J.P. *Eur. J. Biochem.* **2002**, *269*, 470.

30. Zhao, Y.; Schelvis, J.P.M.; Babcock, G.T.; Marletta, M.A. *Biochemistry* **1998**, *37*, 4502.

31. Chang, C.K.; Ward, B.; Young, R.; Kondylis, M.P. *J. Macromol. Sci. Chem. A* **1988**, *25*, 1307.

32. Young, R.; C. K. Chang, C.K. J. Am. Chem. Soc. **1985**, *107*, 898.

33. Wang, Q.G.; Yang, Z.M.; Ma, M.L.; Xiao, X.D.; Chang, C.K.; Xu, B. *Angew. Chem., Int., Ed. Engl.* **2007**, *46*, 1.

34. Wang, Q.G.; Yang, Z.M.; Ma, M.L.; Chang, C.K.; Xu, B. *Chem Eur. J.* **2008**, *14*, 5073.

35. Yam, F. *Mphil Thesis in Chemistry*, Hong Kong University of Science and Technology, **2004**, Chapter 2.

36. Al-Maksoud, W.; Daniele, S.; Sorokin, A.B. *Green Chem.*, **2008**, *10*, 447.

Appendix

Table A1. Crystal data and structure refinement for H_3T_3C.

Identification code	H_3T_3C	
Empirical formula	C103 H84.50 Br Fe N4	
Formula weight	1514.01	
Temperature	173(2) K	
Wavelength	0.71073 Å	
Crystal system	Triclinic	
Space group	P -1	
Unit cell dimensions	a = 14.376(5) Å	α = 96.227(5)°.
	b = 15.928(5) Å	β = 105.077(4)°.
	c = 21.479(7) Å	γ = 109.313(4)°.
Volume	4379(2) $Å^3$	
Z	2	
Density (calculated)	1.148 Mg/m^3	
Absorption coefficient	0.676 mm^{-1}	
F(000)	1583	
Crystal size	0.20 x 0.16 x 0.14 mm^3	
Theta range for data collection	1.39 to 25.00°.	
Index ranges	-14<=h<=17, -18<=k<=17, -23<=l<=25	
Reflections collected	22984	
Independent reflections	14978 [R(int) = 0.0324]	
Completeness to theta = 25.00°	97.2 %	
Absorption correction	Semi-empirical from equivalents	
Max. and min. transmission	0.9113 and 0.8766	
Refinement method	Full-matrix least-squares on F^2	
Data / restraints / parameters	14978 / 68 / 973	
Goodness-of-fit on F^2	1.303	
Final R indices [I>2sigma(I)]	R1 = 0.1178, wR2 = 0.3281	
R indices (all data)	R1 = 0.1551, wR2 = 0.3647	
Largest diff. peak and hole	0.662 and -0.374 $e.Å^{-3}$	

Table A2. Atomic coordinates (x 10^4) and equivalent isotropic displacement parameters ($Å^2$x 10^3) for H_3T_3C. U(eq) is defined as one third of the trace of the orthogonalized U^{ij} tensor.

	x	y	z	U(eq)
Fe(1)	8011(1)	3637(1)	7066(1)	49(1)
Br(1)	7157(1)	4519(1)	7549(1)	96(1)
N(1)	7000(4)	2450(3)	6842(2)	49(1)
N(2)	8495(4)	3202(3)	7809(2)	49(1)
N(3)	9331(3)	4600(3)	7291(2)	45(1)
N(4)	7646(3)	3693(3)	6153(2)	45(1)
C(1)	6103(4)	2004(4)	6298(3)	49(1)
C(2)	5466(5)	1220(4)	6481(3)	53(2)
C(3)	5990(5)	1210(4)	7108(3)	56(2)
C(4)	6952(5)	1985(4)	7332(3)	52(1)
C(5)	7828(5)	2410(4)	7903(3)	53(2)
C(6)	8250(5)	2293(4)	8553(3)	56(2)
C(7)	9170(5)	3029(4)	8854(3)	56(2)
C(8)	9326(5)	3598(4)	8393(3)	51(1)
C(9)	10093(4)	4435(4)	8433(3)	50(1)
C(10)	10079(4)	4916(4)	7910(3)	47(1)
C(11)	10809(4)	5779(4)	7930(3)	53(2)
C(12)	10522(4)	6005(4)	7335(3)	53(2)
C(13)	9595(4)	5257(4)	6933(3)	47(1)
C(14)	9032(4)	5181(4)	6271(3)	46(1)
C(15)	8135(4)	4407(4)	5895(3)	47(1)
C(16)	7584(5)	4257(4)	5214(3)	50(1)
C(17)	6734(4)	3469(4)	5069(3)	50(1)
C(18)	6766(4)	3115(4)	5651(3)	47(1)
C(19)	5998(4)	2320(4)	5718(3)	48(1)
C(20)	11008(4)	4862(4)	9058(3)	52(2)
C(21)	11749(5)	4464(5)	9201(3)	58(2)
C(22)	11635(5)	3612(5)	8775(3)	61(2)
C(23)	11590(5)	3550(6)	8119(4)	72(2)
C(24)	11613(5)	2840(5)	9052(4)	72(2)
C(25)	9367(4)	5936(4)	5925(3)	48(1)
C(26)	10345(5)	6196(4)	5793(3)	54(2)
C(27)	11155(5)	5842(4)	6046(3)	51(1)
C(28)	10960(5)	4906(4)	5993(3)	59(2)
C(30)	12179(5)	6448(5)	6349(3)	60(2)
C(31)	8692(5)	6377(4)	5694(3)	56(2)
C(32)	7715(5)	6230(4)	5879(4)	64(2)
C(33)	8936(5)	7003(4)	5301(3)	62(2)
C(34)	5020(4)	1851(4)	5132(3)	49(1)
C(35)	4109(5)	1970(4)	5138(3)	54(2)
C(36)	3247(5)	1610(4)	4553(3)	59(2)
C(37)	3965(5)	2450(4)	5723(3)	54(2)
C(38)	4631(5)	3322(4)	6072(3)	60(2)
C(39)	4449(5)	3752(5)	6606(4)	68(2)
C(40)	3574(5)	3318(5)	6783(4)	68(2)
C(41)	2904(6)	2442(5)	6435(4)	73(2)
C(42)	3095(5)	2017(5)	5912(4)	67(2)
C(43)	5049(4)	1345(4)	4557(3)	50(1)

(Table A2 continuous)

C(44)	5982(5)	1147(4)	4511(3)	53(2)
C(45)	6477(5)	754(4)	4982(3)	59(2)
C(46)	7267(5)	487(5)	4871(4)	70(2)
C(47)	7563(6)	600(5)	4315(5)	77(2)
C(48)	3276(5)	1129(4)	3987(3)	58(2)
C(49)	4185(5)	997(4)	4005(3)	55(2)
C(50)	6291(5)	1259(4)	3951(3)	60(2)
C(51)	7096(6)	990(5)	3862(4)	72(2)
C(52)	2377(5)	803(5)	3353(4)	64(2)
C(53)	1816(7)	1315(6)	3171(5)	105(3)
C(54)	1016(9)	1039(7)	2568(6)	143(6)
C(55)	12656(5)	4903(5)	9748(3)	62(2)
C(56)	12830(5)	5726(5)	10153(3)	58(2)
C(57)	12065(5)	6090(5)	10006(3)	58(2)
C(58)	13814(5)	6222(5)	10695(4)	66(2)
C(59)	14753(6)	6250(6)	10609(4)	85(2)
C(60)	11154(5)	5688(4)	9470(3)	53(2)
C(61)	10405(5)	6147(5)	9348(3)	56(2)
C(62)	10744(6)	7077(5)	9356(4)	74(2)
C(63)	9339(5)	5682(5)	9241(3)	63(2)
C(64)	8679(7)	6128(6)	9138(4)	82(2)
C(65)	11521(6)	2044(6)	8657(5)	85(2)
C(66)	11453(6)	2020(7)	8003(6)	95(3)
C(67)	11483(6)	2749(7)	7735(4)	86(3)
C(68)	12761(6)	5225(5)	6524(4)	69(2)
C(69)	12969(6)	6157(5)	6582(4)	69(2)
C(70)	10560(5)	6842(4)	5408(3)	56(2)
C(71)	9843(5)	7227(4)	5129(3)	60(2)
C(72)	10046(5)	7840(5)	4653(4)	67(2)
C(73)	9723(6)	8570(6)	4657(4)	76(2)
C(74)	7690(6)	6260(5)	6505(5)	75(2)
C(75)	6809(8)	6185(6)	6682(6)	97(3)
C(76)	5904(8)	6068(7)	6166(7)	102(3)
C(77)	5918(7)	6020(6)	5553(7)	101(3)
C(78)	6781(5)	6098(5)	5366(5)	75(2)
C(79)	10529(6)	7686(5)	4190(4)	72(2)
C(80)	10679(6)	8243(6)	3743(4)	82(2)
C(81)	10324(6)	8970(6)	3771(5)	86(3)
C(82)	9008(8)	7055(7)	9138(5)	96(3)
C(83)	10056(8)	7528(7)	9249(5)	93(3)
C(84)	751(7)	196(7)	2188(5)	111(3)
C(85)	1297(6)	-329(6)	2360(4)	83(2)
C(86)	2104(5)	-41(5)	2946(3)	66(2)
C(87)	13832(6)	6669(5)	11299(4)	72(2)
C(88)	14749(6)	7165(7)	11793(4)	85(2)
C(89)	15698(6)	7219(7)	11692(4)	90(3)
C(90)	15686(6)	6755(7)	11109(4)	94(3)
C(91)	9883(6)	9145(6)	4221(4)	81(2)
C(92)	11761(6)	4612(5)	6228(4)	69(2)
C(1S)	8990(18)	11493(17)	2875(12)	136(8)
C(2S)	8270(30)	10660(20)	2327(17)	244(18)
C(3S)	7410(20)	10820(20)	1855(18)	270(20)
C(4S)	6850(20)	10080(30)	1223(14)	260(19)
C(5S)	5720(20)	9550(30)	1166(18)	245(18)

(Table A2 continuous)

C(6S)	5200(30)	8740(20)	580(20)	300(20)
C(7S)	4110(30)	8670(40)	190(20)	289(19)
C(8S)	3820(40)	8120(40)	-534(18)	280(20)
C(10S)	6110(50)	9570(30)	7990(20)	380(40)
C(11S)	6010(30)	8580(30)	7785(15)	230(17)
C(12S)	6610(50)	8290(30)	8363(17)	340(20)
C(13S)	6960(30)	8980(30)	9009(16)	360(30)
C(14S)	7810(20)	8850(20)	9544(18)	310(20)
C(15S)	8610(20)	9750(20)	9977(14)	181(12)
C(16S)	9656(19)	9970(30)	9852(19)	187(13)
C(17S)	9700(40)	10460(60)	9280(30)	420(40)
C(21S)	4460(40)	9220(30)	830(20)	280(20)
C(22S)	4890(30)	8810(50)	350(20)	320(20)
C(23S)	4030(30)	8020(30)	-180(30)	330(20)
C(24S)	4320(50)	7880(30)	-813(19)	370(30)
C(25S)	4720(30)	7110(30)	-850(20)	380(30)
C(26S)	4180(30)	6440(30)	-1520(14)	310(20)
C(27S)	4360(20)	5550(20)	-1502(19)	218(16)
C(28S)	5330(20)	5580(20)	-1686(15)	156(10)

Table A3. Bond lengths [Å] and angles [°] for H_3T_3C.

Fe(1)-N(2)	1.868(5)
Fe(1)-N(1)	1.881(5)
Fe(1)-N(3)	1.904(5)
Fe(1)-N(4)	1.915(5)
Fe(1)-Br(1)	2.4592(14)
N(1)-C(4)	1.355(8)
N(1)-C(1)	1.401(7)
N(2)-C(5)	1.381(8)
N(2)-C(8)	1.397(7)
N(3)-C(13)	1.376(8)
N(3)-C(10)	1.391(7)
N(4)-C(15)	1.380(8)
N(4)-C(18)	1.383(7)
C(1)-C(19)	1.385(9)
C(1)-C(2)	1.446(8)
C(2)-C(3)	1.366(9)
C(3)-C(4)	1.437(8)
C(4)-C(5)	1.415(8)
C(5)-C(6)	1.429(9)
C(6)-C(7)	1.381(9)
C(7)-C(8)	1.426(9)
C(8)-C(9)	1.397(8)
C(9)-C(10)	1.425(9)
C(9)-C(20)	1.512(8)
C(10)-C(11)	1.416(8)
C(11)-C(12)	1.362(9)
C(12)-C(13)	1.439(7)
C(13)-C(14)	1.411(8)
C(14)-C(15)	1.423(8)
C(14)-C(25)	1.491(8)
C(15)-C(16)	1.422(8)
C(16)-C(17)	1.367(8)
C(17)-C(18)	1.423(8)
C(18)-C(19)	1.429(8)
C(19)-C(34)	1.517(8)
C(20)-C(21)	1.397(9)
C(20)-C(60)	1.424(9)
C(21)-C(55)	1.410(9)
C(21)-C(22)	1.486(9)
C(22)-C(23)	1.386(11)
C(22)-C(24)	1.417(11)
C(23)-C(67)	1.380(11)
C(24)-C(65)	1.394(11)
C(25)-C(31)	1.400(9)
C(25)-C(26)	1.441(9)
C(26)-C(70)	1.395(9)
C(26)-C(27)	1.462(9)
C(27)-C(30)	1.396(9)
C(27)-C(28)	1.409(9)
C(28)-C(92)	1.379(10)
C(30)-C(69)	1.363(10)
C(31)-C(33)	1.392(9)
C(31)-C(32)	1.509(10)

(Table A3 continuous)

C(32)-C(74)	1.352(11)
C(32)-C(78)	1.432(10)
C(33)-C(71)	1.390(10)
C(34)-C(35)	1.387(9)
C(34)-C(43)	1.418(9)
C(35)-C(36)	1.418(9)
C(35)-C(37)	1.496(9)
C(36)-C(48)	1.382(9)
C(37)-C(42)	1.399(9)
C(37)-C(38)	1.389(9)
C(38)-C(39)	1.399(10)
C(39)-C(40)	1.392(11)
C(40)-C(41)	1.394(10)
C(41)-C(42)	1.384(10)
C(43)-C(49)	1.376(8)
C(43)-C(44)	1.500(9)
C(44)-C(50)	1.397(9)
C(44)-C(45)	1.407(9)
C(45)-C(46)	1.403(10)
C(46)-C(47)	1.378(12)
C(47)-C(51)	1.358(11)
C(48)-C(49)	1.382(9)
C(48)-C(52)	1.510(9)
C(50)-C(51)	1.409(10)
C(52)-C(53)	1.346(11)
C(52)-C(86)	1.393(10)
C(53)-C(54)	1.400(11)
C(54)-C(84)	1.370(14)
C(55)-C(56)	1.401(9)
C(56)-C(57)	1.388(10)
C(56)-C(58)	1.478(8)
C(57)-C(60)	1.398(8)
C(58)-C(59)	1.398(11)
C(58)-C(87)	1.400(10)
C(59)-C(90)	1.396(10)
C(60)-C(61)	1.477(9)
C(61)-C(62)	1.394(10)
C(61)-C(63)	1.406(9)
C(62)-C(83)	1.390(12)
C(63)-C(64)	1.351(11)
C(64)-C(82)	1.393(13)
C(65)-C(66)	1.378(14)
C(66)-C(67)	1.344(14)
C(68)-C(92)	1.373(10)
C(68)-C(69)	1.399(11)
C(70)-C(71)	1.405(10)
C(71)-C(72)	1.507(10)
C(72)-C(73)	1.388(11)
C(72)-C(79)	1.395(11)
C(73)-C(91)	1.388(11)
C(74)-C(75)	1.387(12)
C(75)-C(76)	1.415(15)
C(76)-C(77)	1.317(15)
C(77)-C(78)	1.372(13)

(Table A3 continuous)

C(79)-C(80)	1.387(11)
C(80)-C(81)	1.414(13)
C(81)-C(91)	1.338(13)
C(82)-C(83)	1.385(13)
C(84)-C(85)	1.343(13)
C(85)-C(86)	1.380(10)
C(87)-C(88)	1.375(10)
C(88)-C(89)	1.413(12)
C(89)-C(90)	1.376(12)
C(1S)-C(2S)	1.526(18)
C(2S)-C(3S)	1.498(19)
C(3S)-C(4S)	1.529(19)
C(4S)-C(5S)	1.534(19)
C(5S)-C(6S)	1.525(19)
C(6S)-C(7S)	1.54(2)
C(7S)-C(8S)	1.569(19)
C(10S)-C(11S)	1.532(5)
C(11S)-C(12S)	1.532(5)
C(12S)-C(13S)	1.532(5)
C(13S)-C(14S)	1.528(5)
C(14S)-C(15S)	1.528(5)
C(15S)-C(16S)	1.527(5)
C(16S)-C(16S)#1	1.00(5)
C(16S)-C(17S)	1.530(5)
C(21S)-C(22S)	1.533(5)
C(22S)-C(23S)	1.529(5)
C(23S)-C(24S)	1.528(5)
C(24S)-C(25S)	1.530(5)
C(25S)-C(26S)	1.528(5)
C(26S)-C(27S)	1.528(5)
C(27S)-C(28S)	1.529(5)

N(2)-Fe(1)-N(1)	79.9(2)
N(2)-Fe(1)-N(3)	90.0(2)
N(1)-Fe(1)-N(3)	160.2(2)
N(2)-Fe(1)-N(4)	156.8(2)
N(1)-Fe(1)-N(4)	89.2(2)
N(3)-Fe(1)-N(4)	93.7(2)
N(2)-Fe(1)-Br(1)	97.76(16)
N(1)-Fe(1)-Br(1)	101.67(16)
N(3)-Fe(1)-Br(1)	96.55(15)
N(4)-Fe(1)-Br(1)	104.51(15)
C(4)-N(1)-C(1)	109.3(5)
C(4)-N(1)-Fe(1)	117.1(4)
C(1)-N(1)-Fe(1)	131.7(4)
C(5)-N(2)-C(8)	107.5(5)
C(5)-N(2)-Fe(1)	117.7(4)
C(8)-N(2)-Fe(1)	133.2(4)
C(13)-N(3)-C(10)	106.7(5)
C(13)-N(3)-Fe(1)	125.2(4)
C(10)-N(3)-Fe(1)	125.9(4)
C(15)-N(4)-C(18)	107.0(5)
C(15)-N(4)-Fe(1)	125.3(4)
C(18)-N(4)-Fe(1)	127.0(4)

(Table A3 continuous)

C(19)-C(1)-N(1)	120.2(5)
C(19)-C(1)-C(2)	132.9(5)
N(1)-C(1)-C(2)	106.8(5)
C(3)-C(2)-C(1)	107.5(5)
C(2)-C(3)-C(4)	108.2(6)
N(1)-C(4)-C(5)	112.2(5)
N(1)-C(4)-C(3)	108.2(5)
C(5)-C(4)-C(3)	139.5(6)
N(2)-C(5)-C(6)	109.0(5)
N(2)-C(5)-C(4)	110.3(5)
C(6)-C(5)-C(4)	140.6(6)
C(7)-C(6)-C(5)	107.3(6)
C(6)-C(7)-C(8)	107.8(5)
N(2)-C(8)-C(9)	118.6(5)
N(2)-C(8)-C(7)	108.4(5)
C(9)-C(8)-C(7)	132.9(6)
C(8)-C(9)-C(10)	123.9(5)
C(8)-C(9)-C(20)	119.1(6)
C(10)-C(9)-C(20)	117.1(5)
N(3)-C(10)-C(9)	124.7(5)
N(3)-C(10)-C(11)	108.8(5)
C(9)-C(10)-C(11)	126.5(5)
C(12)-C(11)-C(10)	108.6(5)
C(11)-C(12)-C(13)	106.4(5)
N(3)-C(13)-C(14)	123.9(5)
N(3)-C(13)-C(12)	109.5(5)
C(14)-C(13)-C(12)	126.6(6)
C(13)-C(14)-C(15)	123.6(5)
C(13)-C(14)-C(25)	120.2(5)
C(15)-C(14)-C(25)	116.2(5)
N(4)-C(15)-C(16)	109.5(5)
N(4)-C(15)-C(14)	124.2(5)
C(16)-C(15)-C(14)	126.3(5)
C(17)-C(16)-C(15)	106.8(5)
C(16)-C(17)-C(18)	108.1(5)
N(4)-C(18)-C(17)	108.5(5)
N(4)-C(18)-C(19)	125.5(5)
C(17)-C(18)-C(19)	126.0(5)
C(1)-C(19)-C(18)	122.4(5)
C(1)-C(19)-C(34)	120.4(5)
C(18)-C(19)-C(34)	117.1(5)
C(21)-C(20)-C(60)	120.3(5)
C(21)-C(20)-C(9)	118.6(5)
C(60)-C(20)-C(9)	120.9(6)
C(20)-C(21)-C(55)	119.2(6)
C(20)-C(21)-C(22)	121.9(5)
C(55)-C(21)-C(22)	118.8(6)
C(23)-C(22)-C(24)	118.0(7)
C(23)-C(22)-C(21)	122.6(7)
C(24)-C(22)-C(21)	119.3(6)
C(67)-C(23)-C(22)	121.2(9)
C(65)-C(24)-C(22)	119.6(8)
C(31)-C(25)-C(26)	118.8(6)
C(31)-C(25)-C(14)	119.1(5)

(Table A3 continuous)

C(26)-C(25)-C(14)	122.0(5)
C(70)-C(26)-C(25)	118.8(6)
C(70)-C(26)-C(27)	116.5(6)
C(25)-C(26)-C(27)	124.6(6)
C(30)-C(27)-C(28)	117.2(6)
C(30)-C(27)-C(26)	119.4(6)
C(28)-C(27)-C(26)	123.3(6)
C(92)-C(28)-C(27)	120.6(6)
C(69)-C(30)-C(27)	122.1(7)
C(33)-C(31)-C(25)	119.8(6)
C(33)-C(31)-C(32)	117.8(6)
C(25)-C(31)-C(32)	122.3(6)
C(74)-C(32)-C(78)	118.6(7)
C(74)-C(32)-C(31)	123.3(7)
C(78)-C(32)-C(31)	118.0(7)
C(71)-C(33)-C(31)	122.7(7)
C(35)-C(34)-C(43)	119.6(5)
C(35)-C(34)-C(19)	120.0(5)
C(43)-C(34)-C(19)	120.3(5)
C(34)-C(35)-C(36)	118.2(6)
C(34)-C(35)-C(37)	124.6(5)
C(36)-C(35)-C(37)	117.2(6)
C(48)-C(36)-C(35)	122.5(6)
C(42)-C(37)-C(38)	118.3(6)
C(42)-C(37)-C(35)	118.6(6)
C(38)-C(37)-C(35)	123.1(6)
C(39)-C(38)-C(37)	121.0(7)
C(38)-C(39)-C(40)	120.1(6)
C(39)-C(40)-C(41)	119.1(7)
C(42)-C(41)-C(40)	120.4(7)
C(41)-C(42)-C(37)	121.1(7)
C(49)-C(43)-C(34)	119.9(6)
C(49)-C(43)-C(44)	116.6(5)
C(34)-C(43)-C(44)	123.5(5)
C(50)-C(44)-C(45)	119.2(6)
C(50)-C(44)-C(43)	119.0(6)
C(45)-C(44)-C(43)	121.4(6)
C(46)-C(45)-C(44)	118.6(7)
C(47)-C(46)-C(45)	121.6(8)
C(51)-C(47)-C(46)	120.1(7)
C(49)-C(48)-C(36)	117.8(6)
C(49)-C(48)-C(52)	120.2(6)
C(36)-C(48)-C(52)	122.0(6)
C(48)-C(49)-C(43)	122.0(6)
C(44)-C(50)-C(51)	120.3(7)
C(47)-C(51)-C(50)	120.2(8)
C(53)-C(52)-C(86)	118.5(6)
C(53)-C(52)-C(48)	120.8(7)
C(86)-C(52)-C(48)	120.7(6)
C(52)-C(53)-C(54)	121.2(9)
C(84)-C(54)-C(53)	118.6(9)
C(56)-C(55)-C(21)	121.7(6)
C(57)-C(56)-C(55)	117.6(6)
C(57)-C(56)-C(58)	120.6(6)

(Table A3 continuous)

C(55)-C(56)-C(58)	121.7(6)
C(56)-C(57)-C(60)	123.3(6)
C(59)-C(58)-C(87)	118.6(6)
C(59)-C(58)-C(56)	119.7(7)
C(87)-C(58)-C(56)	121.6(6)
C(90)-C(59)-C(58)	119.7(8)
C(57)-C(60)-C(20)	117.9(6)
C(57)-C(60)-C(61)	118.8(6)
C(20)-C(60)-C(61)	123.2(5)
C(62)-C(61)-C(63)	117.5(7)
C(62)-C(61)-C(60)	120.4(6)
C(63)-C(61)-C(60)	122.1(6)
C(83)-C(62)-C(61)	121.6(8)
C(64)-C(63)-C(61)	120.4(8)
C(63)-C(64)-C(82)	122.6(8)
C(66)-C(65)-C(24)	119.4(9)
C(67)-C(66)-C(65)	121.7(8)
C(66)-C(67)-C(23)	120.0(9)
C(92)-C(68)-C(69)	119.4(7)
C(30)-C(69)-C(68)	119.8(7)
C(26)-C(70)-C(71)	122.1(6)
C(33)-C(71)-C(70)	117.3(6)
C(33)-C(71)-C(72)	121.8(6)
C(70)-C(71)-C(72)	120.8(6)
C(73)-C(72)-C(79)	118.3(7)
C(73)-C(72)-C(71)	119.6(7)
C(79)-C(72)-C(71)	122.2(7)
C(72)-C(73)-C(91)	121.5(9)
C(32)-C(74)-C(75)	123.4(9)
C(74)-C(75)-C(76)	116.5(10)
C(77)-C(76)-C(75)	120.3(9)
C(76)-C(77)-C(78)	124.2(10)
C(77)-C(78)-C(32)	116.9(9)
C(72)-C(79)-C(80)	121.1(8)
C(79)-C(80)-C(81)	117.7(8)
C(91)-C(81)-C(80)	122.2(8)
C(83)-C(82)-C(64)	117.9(8)
C(62)-C(83)-C(82)	120.1(9)
C(85)-C(84)-C(54)	121.1(8)
C(84)-C(85)-C(86)	119.8(8)
C(85)-C(86)-C(52)	120.5(8)
C(88)-C(87)-C(58)	121.7(7)
C(87)-C(88)-C(89)	119.2(8)
C(90)-C(89)-C(88)	119.4(7)
C(89)-C(90)-C(59)	121.2(8)
C(81)-C(91)-C(73)	119.2(9)
C(68)-C(92)-C(28)	120.8(7)
C(3S)-C(2S)-C(1S)	113.7(15)
C(2S)-C(3S)-C(4S)	113.3(16)
C(3S)-C(4S)-C(5S)	111.6(15)
C(6S)-C(5S)-C(4S)	111.5(15)
C(5S)-C(6S)-C(7S)	111.6(16)
C(6S)-C(7S)-C(8S)	108.9(15)
C(10S)-C(11S)-C(12S)	111.0(5)

(Table A3 continuous)

C(11S)-C(12S)-C(13S)	110.9(5)
C(14S)-C(13S)-C(12S)	111.5(5)
C(15S)-C(14S)-C(13S)	111.7(5)
C(16S)-C(15S)-C(14S)	111.8(5)
C(16S)#1-C(16S)-C(15S)	130(5)
C(16S)#1-C(16S)-C(17S)	115(5)
C(15S)-C(16S)-C(17S)	111.6(5)
C(23S)-C(22S)-C(21S)	111.4(5)
C(24S)-C(23S)-C(22S)	111.8(5)
C(23S)-C(24S)-C(25S)	111.7(5)
C(26S)-C(25S)-C(24S)	111.7(5)
C(27S)-C(26S)-C(25S)	111.8(5)
C(26S)-C(27S)-C(28S)	111.8(5)

Symmetry transformations used to generate equivalent atoms:
#1 -x+2,-y+2,-z+2

Table A4. Torsion angles [°] for H_3T_3C.

N(2)-Fe(1)-N(1)-C(4)	14.8(5)
N(3)-Fe(1)-N(1)-C(4)	75.3(8)
N(4)-Fe(1)-N(1)-C(4)	174.2(5)
Br(1)-Fe(1)-N(1)-C(4)	-81.1(5)
N(2)-Fe(1)-N(1)-C(1)	177.2(6)
N(3)-Fe(1)-N(1)-C(1)	-122.3(7)
N(4)-Fe(1)-N(1)-C(1)	-23.3(6)
Br(1)-Fe(1)-N(1)-C(1)	81.3(5)
N(1)-Fe(1)-N(2)-C(5)	-14.3(5)
N(3)-Fe(1)-N(2)-C(5)	-177.2(5)
N(4)-Fe(1)-N(2)-C(5)	-77.7(7)
Br(1)-Fe(1)-N(2)-C(5)	86.2(4)
N(1)-Fe(1)-N(2)-C(8)	-177.6(6)
N(3)-Fe(1)-N(2)-C(8)	19.5(6)
N(4)-Fe(1)-N(2)-C(8)	119.0(6)
Br(1)-Fe(1)-N(2)-C(8)	-77.1(6)
N(2)-Fe(1)-N(3)-C(13)	179.1(5)
N(1)-Fe(1)-N(3)-C(13)	120.2(7)
N(4)-Fe(1)-N(3)-C(13)	21.9(5)
Br(1)-Fe(1)-N(3)-C(13)	-83.1(4)
N(2)-Fe(1)-N(3)-C(10)	-19.9(5)
N(1)-Fe(1)-N(3)-C(10)	-78.8(8)
N(4)-Fe(1)-N(3)-C(10)	-177.0(5)
Br(1)-Fe(1)-N(3)-C(10)	77.9(5)
N(2)-Fe(1)-N(4)-C(15)	-114.5(6)
N(1)-Fe(1)-N(4)-C(15)	-176.2(5)
N(3)-Fe(1)-N(4)-C(15)	-15.8(5)
Br(1)-Fe(1)-N(4)-C(15)	81.9(5)
N(2)-Fe(1)-N(4)-C(18)	76.5(7)
N(1)-Fe(1)-N(4)-C(18)	14.8(5)
N(3)-Fe(1)-N(4)-C(18)	175.2(5)
Br(1)-Fe(1)-N(4)-C(18)	-87.0(5)
C(4)-N(1)-C(1)-C(19)	-176.1(6)
Fe(1)-N(1)-C(1)-C(19)	20.5(9)
C(4)-N(1)-C(1)-C(2)	0.8(7)
Fe(1)-N(1)-C(1)-C(2)	-162.7(4)
C(19)-C(1)-C(2)-C(3)	175.4(7)
N(1)-C(1)-C(2)-C(3)	-0.8(7)
C(1)-C(2)-C(3)-C(4)	0.6(7)
C(1)-N(1)-C(4)-C(5)	-178.8(5)
Fe(1)-N(1)-C(4)-C(5)	-12.6(7)
C(1)-N(1)-C(4)-C(3)	-0.4(7)
Fe(1)-N(1)-C(4)-C(3)	165.7(4)
C(2)-C(3)-C(4)-N(1)	-0.1(7)
C(2)-C(3)-C(4)-C(5)	177.6(8)
C(8)-N(2)-C(5)-C(6)	-1.0(7)
Fe(1)-N(2)-C(5)-C(6)	-168.3(4)
C(8)-N(2)-C(5)-C(4)	178.6(5)
Fe(1)-N(2)-C(5)-C(4)	11.3(7)
N(1)-C(4)-C(5)-N(2)	0.9(8)
C(3)-C(4)-C(5)-N(2)	-176.7(7)
N(1)-C(4)-C(5)-C(6)	-179.7(8)
C(3)-C(4)-C(5)-C(6)	2.7(15)

(Table A4 continuous)

N(2)-C(5)-C(6)-C(7)	0.9(7)
C(4)-C(5)-C(6)-C(7)	-178.5(8)
C(5)-C(6)-C(7)-C(8)	-0.4(7)
C(5)-N(2)-C(8)-C(9)	-177.4(6)
Fe(1)-N(2)-C(8)-C(9)	-12.9(9)
C(5)-N(2)-C(8)-C(7)	0.7(7)
Fe(1)-N(2)-C(8)-C(7)	165.2(5)
C(6)-C(7)-C(8)-N(2)	-0.1(7)
C(6)-C(7)-C(8)-C(9)	177.5(7)
N(2)-C(8)-C(9)-C(10)	0.3(9)
C(7)-C(8)-C(9)-C(10)	-177.2(6)
N(2)-C(8)-C(9)-C(20)	-178.8(5)
C(7)-C(8)-C(9)-C(20)	3.7(11)
C(13)-N(3)-C(10)-C(9)	-179.7(6)
Fe(1)-N(3)-C(10)-C(9)	16.3(8)
C(13)-N(3)-C(10)-C(11)	0.1(6)
Fe(1)-N(3)-C(10)-C(11)	-163.9(4)
C(8)-C(9)-C(10)-N(3)	-2.8(10)
C(20)-C(9)-C(10)-N(3)	176.3(5)
C(8)-C(9)-C(10)-C(11)	177.4(6)
C(20)-C(9)-C(10)-C(11)	-3.5(9)
N(3)-C(10)-C(11)-C(12)	0.4(7)
C(9)-C(10)-C(11)-C(12)	-179.8(6)
C(10)-C(11)-C(12)-C(13)	-0.7(7)
C(10)-N(3)-C(13)-C(14)	178.9(5)
Fe(1)-N(3)-C(13)-C(14)	-17.0(8)
C(10)-N(3)-C(13)-C(12)	-0.5(6)
Fe(1)-N(3)-C(13)-C(12)	163.6(4)
C(11)-C(12)-C(13)-N(3)	0.8(7)
C(11)-C(12)-C(13)-C(14)	-178.6(6)
N(3)-C(13)-C(14)-C(15)	-1.2(9)
C(12)-C(13)-C(14)-C(15)	178.0(6)
N(3)-C(13)-C(14)-C(25)	179.0(5)
C(12)-C(13)-C(14)-C(25)	-1.7(9)
C(18)-N(4)-C(15)-C(16)	-2.8(7)
Fe(1)-N(4)-C(15)-C(16)	-173.6(4)
C(18)-N(4)-C(15)-C(14)	175.2(5)
Fe(1)-N(4)-C(15)-C(14)	4.4(8)
C(13)-C(14)-C(15)-N(4)	7.8(9)
C(25)-C(14)-C(15)-N(4)	-172.4(5)
C(13)-C(14)-C(15)-C(16)	-174.6(6)
C(25)-C(14)-C(15)-C(16)	5.2(9)
N(4)-C(15)-C(16)-C(17)	2.7(7)
C(14)-C(15)-C(16)-C(17)	-175.2(6)
C(15)-C(16)-C(17)-C(18)	-1.5(7)
C(15)-N(4)-C(18)-C(17)	1.8(7)
Fe(1)-N(4)-C(18)-C(17)	172.4(4)
C(15)-N(4)-C(18)-C(19)	-175.7(6)
Fe(1)-N(4)-C(18)-C(19)	-5.1(9)
C(16)-C(17)-C(18)-N(4)	-0.2(7)
C(16)-C(17)-C(18)-C(19)	177.3(6)
N(1)-C(1)-C(19)-C(18)	-2.0(9)
C(2)-C(1)-C(19)-C(18)	-177.9(6)
N(1)-C(1)-C(19)-C(34)	-178.8(5)

(Table A4 continuous)

C(2)-C(1)-C(19)-C(34)	5.3(11)
N(4)-C(18)-C(19)-C(1)	-4.9(10)
C(17)-C(18)-C(19)-C(1)	178.0(6)
N(4)-C(18)-C(19)-C(34)	172.0(5)
C(17)-C(18)-C(19)-C(34)	-5.1(9)
C(8)-C(9)-C(20)-C(21)	71.0(8)
C(10)-C(9)-C(20)-C(21)	-108.1(7)
C(8)-C(9)-C(20)-C(60)	-113.4(7)
C(10)-C(9)-C(20)-C(60)	67.4(8)
C(60)-C(20)-C(21)-C(55)	-1.7(10)
C(9)-C(20)-C(21)-C(55)	173.9(6)
C(60)-C(20)-C(21)-C(22)	-178.6(6)
C(9)-C(20)-C(21)-C(22)	-3.1(10)
C(20)-C(21)-C(22)-C(23)	61.3(9)
C(55)-C(21)-C(22)-C(23)	-115.7(8)
C(20)-C(21)-C(22)-C(24)	-121.4(7)
C(55)-C(21)-C(22)-C(24)	61.6(9)
C(24)-C(22)-C(23)-C(67)	2.6(10)
C(21)-C(22)-C(23)-C(67)	180.0(6)
C(23)-C(22)-C(24)-C(65)	-1.6(10)
C(21)-C(22)-C(24)-C(65)	-179.1(6)
C(13)-C(14)-C(25)-C(31)	-118.5(6)
C(15)-C(14)-C(25)-C(31)	61.7(7)
C(13)-C(14)-C(25)-C(26)	64.5(8)
C(15)-C(14)-C(25)-C(26)	-115.3(6)
C(31)-C(25)-C(26)-C(70)	-3.6(8)
C(14)-C(25)-C(26)-C(70)	173.3(5)
C(31)-C(25)-C(26)-C(27)	175.3(6)
C(14)-C(25)-C(26)-C(27)	-7.8(9)
C(70)-C(26)-C(27)-C(30)	48.0(8)
C(25)-C(26)-C(27)-C(30)	-130.9(6)
C(70)-C(26)-C(27)-C(28)	-131.3(6)
C(25)-C(26)-C(27)-C(28)	49.8(9)
C(30)-C(27)-C(28)-C(92)	-0.7(9)
C(26)-C(27)-C(28)-C(92)	178.6(6)
C(28)-C(27)-C(30)-C(69)	0.6(10)
C(26)-C(27)-C(30)-C(69)	-178.7(6)
C(26)-C(25)-C(31)-C(33)	4.9(9)
C(14)-C(25)-C(31)-C(33)	-172.1(6)
C(26)-C(25)-C(31)-C(32)	-172.4(6)
C(14)-C(25)-C(31)-C(32)	10.6(9)
C(33)-C(31)-C(32)-C(74)	-129.5(7)
C(25)-C(31)-C(32)-C(74)	47.9(9)
C(33)-C(31)-C(32)-C(78)	47.3(9)
C(25)-C(31)-C(32)-C(78)	-135.3(6)
C(25)-C(31)-C(33)-C(71)	-0.9(10)
C(32)-C(31)-C(33)-C(71)	176.6(6)
C(1)-C(19)-C(34)-C(35)	74.6(8)
C(18)-C(19)-C(34)-C(35)	-102.4(7)
C(1)-C(19)-C(34)-C(43)	-110.2(7)
C(18)-C(19)-C(34)-C(43)	72.9(7)
C(43)-C(34)-C(35)-C(36)	-2.6(9)
C(19)-C(34)-C(35)-C(36)	172.7(6)
C(43)-C(34)-C(35)-C(37)	177.0(6)

C(19)-C(34)-C(35)-C(37)	-7.7(9)
C(34)-C(35)-C(36)-C(48)	1.6(10)
C(37)-C(35)-C(36)-C(48)	-178.0(6)
C(34)-C(35)-C(37)-C(42)	-129.9(7)
C(36)-C(35)-C(37)-C(42)	49.8(9)
C(34)-C(35)-C(37)-C(38)	52.8(9)
C(36)-C(35)-C(37)-C(38)	-127.5(7)
C(42)-C(37)-C(38)-C(39)	1.1(10)
C(35)-C(37)-C(38)-C(39)	178.4(6)
C(37)-C(38)-C(39)-C(40)	-1.9(11)
C(38)-C(39)-C(40)-C(41)	2.0(11)
C(39)-C(40)-C(41)-C(42)	-1.4(12)
C(40)-C(41)-C(42)-C(37)	0.5(12)
C(38)-C(37)-C(42)-C(41)	-0.4(11)
C(35)-C(37)-C(42)-C(41)	-177.8(7)
C(35)-C(34)-C(43)-C(49)	1.7(9)
C(19)-C(34)-C(43)-C(49)	-173.6(6)
C(35)-C(34)-C(43)-C(44)	-177.4(6)
C(19)-C(34)-C(43)-C(44)	7.3(9)
C(49)-C(43)-C(44)-C(50)	45.8(8)
C(34)-C(43)-C(44)-C(50)	-135.1(6)
C(49)-C(43)-C(44)-C(45)	-126.9(6)
C(34)-C(43)-C(44)-C(45)	52.2(8)
C(50)-C(44)-C(45)-C(46)	-0.1(8)
C(43)-C(44)-C(45)-C(46)	172.6(5)
C(44)-C(45)-C(46)-C(47)	0.0(9)
C(45)-C(46)-C(47)-C(51)	0.9(11)
C(35)-C(36)-C(48)-C(49)	0.5(10)
C(35)-C(36)-C(48)-C(52)	-175.9(6)
C(36)-C(48)-C(49)-C(43)	-1.6(10)
C(52)-C(48)-C(49)-C(43)	174.9(6)
C(34)-C(43)-C(49)-C(48)	0.5(9)
C(44)-C(43)-C(49)-C(48)	179.6(6)
C(45)-C(44)-C(50)-C(51)	-0.6(9)
C(43)-C(44)-C(50)-C(51)	-173.5(6)
C(46)-C(47)-C(51)-C(50)	-1.6(11)
C(44)-C(50)-C(51)-C(47)	1.5(10)
C(49)-C(48)-C(52)-C(53)	-139.0(9)
C(36)-C(48)-C(52)-C(53)	37.3(12)
C(49)-C(48)-C(52)-C(86)	41.7(10)
C(36)-C(48)-C(52)-C(86)	-142.0(7)
C(86)-C(52)-C(53)-C(54)	-4.0(16)
C(48)-C(52)-C(53)-C(54)	176.7(11)
C(52)-C(53)-C(54)-C(84)	6(2)
C(20)-C(21)-C(55)-C(56)	0.3(10)
C(22)-C(21)-C(55)-C(56)	177.4(7)
C(21)-C(55)-C(56)-C(57)	1.2(10)
C(21)-C(55)-C(56)-C(58)	-175.3(7)
C(55)-C(56)-C(57)-C(60)	-1.5(10)
C(58)-C(56)-C(57)-C(60)	175.1(6)
C(57)-C(56)-C(58)-C(59)	-138.3(8)
C(55)-C(56)-C(58)-C(59)	38.2(11)
C(57)-C(56)-C(58)-C(87)	41.8(11)
C(55)-C(56)-C(58)-C(87)	-141.8(8)
C(87)-C(58)-C(59)-C(90)	-3.1(13)

(Table A4 continuous)

C(56)-C(58)-C(59)-C(90)	176.9(9)
C(56)-C(57)-C(60)-C(20)	0.3(10)
C(56)-C(57)-C(60)-C(61)	-178.3(6)
C(21)-C(20)-C(60)-C(57)	1.4(9)
C(9)-C(20)-C(60)-C(57)	-174.1(6)
C(21)-C(20)-C(60)-C(61)	179.9(6)
C(9)-C(20)-C(60)-C(61)	4.4(9)
C(57)-C(60)-C(61)-C(62)	47.2(9)
C(20)-C(60)-C(61)-C(62)	-131.3(7)
C(57)-C(60)-C(61)-C(63)	-130.7(7)
C(20)-C(60)-C(61)-C(63)	50.8(9)
C(63)-C(61)-C(62)-C(83)	-1.3(11)
C(60)-C(61)-C(62)-C(83)	-179.3(7)
C(62)-C(61)-C(63)-C(64)	1.3(10)
C(60)-C(61)-C(63)-C(64)	179.3(7)
C(61)-C(63)-C(64)-C(82)	-0.7(13)
C(22)-C(24)-C(65)-C(66)	0.0(11)
C(24)-C(65)-C(66)-C(67)	0.7(12)
C(65)-C(66)-C(67)-C(23)	0.3(12)
C(22)-C(23)-C(67)-C(66)	-2.0(11)
C(27)-C(30)-C(69)-C(68)	-0.4(11)
C(92)-C(68)-C(69)-C(30)	0.3(11)
C(25)-C(26)-C(70)-C(71)	-1.8(9)
C(27)-C(26)-C(70)-C(71)	179.2(6)
C(31)-C(33)-C(71)-C(70)	-4.5(10)
C(31)-C(33)-C(71)-C(72)	174.2(6)
C(26)-C(70)-C(71)-C(33)	5.8(9)
C(26)-C(70)-C(71)-C(72)	-172.9(6)
C(33)-C(71)-C(72)-C(73)	36.6(10)
C(70)-C(71)-C(72)-C(73)	-144.8(7)
C(33)-C(71)-C(72)-C(79)	-141.7(7)
C(70)-C(71)-C(72)-C(79)	37.0(9)
C(79)-C(72)-C(73)-C(91)	-0.8(11)
C(71)-C(72)-C(73)-C(91)	-179.2(7)
C(78)-C(32)-C(74)-C(75)	-1.1(11)
C(31)-C(32)-C(74)-C(75)	175.7(7)
C(32)-C(74)-C(75)-C(76)	0.2(12)
C(74)-C(75)-C(76)-C(77)	1.2(14)
C(75)-C(76)-C(77)-C(78)	-1.7(16)
C(76)-C(77)-C(78)-C(32)	0.7(14)
C(74)-C(32)-C(78)-C(77)	0.7(11)
C(31)-C(32)-C(78)-C(77)	-176.2(7)
C(73)-C(72)-C(79)-C(80)	-0.3(11)
C(71)-C(72)-C(79)-C(80)	178.0(7)
C(72)-C(79)-C(80)-C(81)	-0.2(11)
C(79)-C(80)-C(81)-C(91)	1.9(12)
C(63)-C(64)-C(82)-C(83)	0.0(15)
C(61)-C(62)-C(83)-C(82)	0.7(14)
C(64)-C(82)-C(83)-C(62)	0.0(15)
C(53)-C(54)-C(84)-C(85)	-5(2)
C(54)-C(84)-C(85)-C(86)	3.5(18)
C(84)-C(85)-C(86)-C(52)	-1.8(14)
C(53)-C(52)-C(86)-C(85)	2.0(13)
C(48)-C(52)-C(86)-C(85)	-178.6(7)

(Table A4 continuous)

C(59)-C(58)-C(87)-C(88)	3.0(13)
C(56)-C(58)-C(87)-C(88)	-177.0(8)
C(58)-C(87)-C(88)-C(89)	-0.6(14)
C(87)-C(88)-C(89)-C(90)	-1.7(15)
C(88)-C(89)-C(90)-C(59)	1.6(16)
C(58)-C(59)-C(90)-C(89)	0.9(16)
C(80)-C(81)-C(91)-C(73)	-3.0(12)
C(72)-C(73)-C(91)-C(81)	2.5(12)
C(69)-C(68)-C(92)-C(28)	-0.4(11)
C(27)-C(28)-C(92)-C(68)	0.7(10)
C(1S)-C(2S)-C(3S)-C(4S)	166(3)
C(2S)-C(3S)-C(4S)-C(5S)	115(4)
C(3S)-C(4S)-C(5S)-C(6S)	-173(3)
C(4S)-C(5S)-C(6S)-C(7S)	-135(4)
C(5S)-C(6S)-C(7S)-C(8S)	157(5)
C(10S)-C(11S)-C(12S)-C(13S)	11(8)
C(11S)-C(12S)-C(13S)-C(14S)	-164(4)
C(12S)-C(13S)-C(14S)-C(15S)	144(5)
C(13S)-C(14S)-C(15S)-C(16S)	-109(3)
C(14S)-C(15S)-C(16S)-C(16S)#1	-115(7)
C(14S)-C(15S)-C(16S)-C(17S)	86(5)
C(21S)-C(22S)-C(23S)-C(24S)	155(5)
C(22S)-C(23S)-C(24S)-C(25S)	99(4)
C(23S)-C(24S)-C(25S)-C(26S)	131(4)
C(24S)-C(25S)-C(26S)-C(27S)	-165(4)
C(25S)-C(26S)-C(27S)-C(28S)	-90(4)

Symmetry transformations used to generate equivalent atoms:
#1 -x+2,-y+2,-z+2

Table A5. Crystal data and structure refinement for $Fe(NO)T_3C$.

Identification code	ch010408_sq	
Empirical formula	C109 H86 Fe N5 O	
Formula weight	1537.68	
Temperature	173(2) K	
Wavelength	0.71073 Å	
Crystal system	Triclinic	
Space group	P -1	
Unit cell dimensions	a = 14.204(4) Å	α = 95.963(3)°.
	b = 16.068(4) Å	β = 105.118(3)°.
	c = 21.319(5) Å	γ = 110.050(3)°.
Volume	4311.3(19) $Å^3$	
Z	2	
Density (calculated)	1.185 Mg/m^3	
Absorption coefficient	0.229 mm^{-1}	
F(000)	1618	
Crystal size	0.36 x 0.32 x 0.25 mm^3	
Theta range for data collection	1.88 to 25.26°.	
Index ranges	-17<=h<=16, -19<=k<=19, 0<=l<=25	
Reflections collected	15520	
Independent reflections	15520 [R(int) = 0.0000]	
Completeness to theta = 25.00°	99.5 %	
Absorption correction	Semi-empirical from equivalents	
Max. and min. transmission	0.7452 and 0.5544	
Refinement method	Full-matrix least-squares on F^2	
Data / restraints / parameters	15520 / 0 / 883	
Goodness-of-fit on F^2	0.839	
Final R indices [I>2sigma(I)]	R1 = 0.0688, wR2 = 0.1649	
R indices (all data)	R1 = 0.1388, wR2 = 0.1818	
Largest diff. peak and hole	0.628 and -0.453 $e.Å^{-3}$	

Table A6. Atomic coordinates (x 10^4) and equivalent isotropic displacement parameters ($Å^2$x 10^3) for $Fe(NO)T_3C$. U(eq) is defined as one third of the trace of the orthogonalized U^{ij} tensor.

	x	y	z	U(eq)
Fe(1)	7052(1)	1329(1)	7921(1)	29(1)
N(1)	7360(2)	1303(2)	8841(1)	24(1)
C(2)	8257(3)	1881(2)	9353(2)	24(1)
C(3)	8275(3)	1522(2)	9936(2)	30(1)
C(4)	7420(3)	739(2)	9785(2)	29(1)
C(5)	6852(3)	576(2)	9094(2)	24(1)
C(6)	5959(3)	-171(2)	8720(2)	24(1)
C(7)	5399(3)	-254(2)	8061(2)	27(1)
C(8)	4450(3)	-976(3)	7661(2)	33(1)
C(9)	4167(3)	-759(3)	7068(2)	36(1)
C(10)	4927(3)	96(2)	7076(2)	27(1)
N(11)	5683(2)	397(2)	7697(1)	27(1)
C(12)	4935(3)	556(3)	6555(2)	28(1)
C(13)	5700(3)	1378(3)	6602(2)	33(1)
C(14)	5848(3)	1974(3)	6152(2)	37(1)
C(15)	6759(3)	2706(3)	6465(2)	38(1)
C(16)	7191(3)	2584(2)	7108(2)	31(1)
N(17)	6534(2)	1783(2)	7185(1)	30(1)
C(18)	8076(3)	3029(2)	7687(2)	30(1)
C(19)	9020(3)	3805(3)	7920(2)	38(1)
C(20)	9534(3)	3783(2)	8546(2)	33(1)
C(21)	8923(3)	2987(2)	8716(2)	25(1)
N(22)	8030(2)	2543(2)	8172(1)	27(1)
C(23)	9028(3)	2666(2)	9288(2)	26(1)
C(24)	5612(3)	-930(2)	9066(2)	26(1)
C(25)	6291(3)	-1381(2)	9276(2)	31(1)
C(26)	7254(3)	-1227(3)	9073(2)	38(1)
C(27)	8214(3)	-1075(3)	9550(3)	54(1)
C(28)	9091(4)	-1011(4)	9364(4)	75(2)
C(29)	9034(5)	-1090(4)	8710(4)	84(2)
C(30)	8078(5)	-1228(3)	8227(3)	74(2)
C(31)	7209(4)	-1290(3)	8416(2)	49(1)
C(32)	6059(3)	-1993(2)	9666(2)	37(1)
C(33)	5139(3)	-2225(2)	9854(2)	33(1)
C(34)	4970(3)	-2833(3)	10318(2)	40(1)
C(35)	5270(3)	-3566(3)	10296(2)	49(1)
C(36)	5143(4)	-4123(3)	10750(3)	60(1)
C(37)	4710(4)	-3960(4)	11223(3)	62(1)
C(38)	4395(4)	-3241(4)	11252(2)	67(2)
C(39)	4521(4)	-2680(3)	10801(2)	54(1)
C(40)	4444(3)	-1833(2)	9596(2)	29(1)
C(41)	4659(3)	-1195(2)	9212(2)	28(1)
C(42)	3832(3)	-832(3)	8958(2)	31(1)
C(43)	2795(3)	-1451(3)	8658(2)	38(1)
C(44)	1992(3)	-1159(3)	8420(2)	49(1)
C(45)	2205(4)	-253(3)	8477(2)	55(1)
C(46)	3230(4)	369(3)	8779(2)	47(1)
C(47)	4035(3)	78(3)	9018(2)	36(1)

(Table A6 continuous)

C(48)	4022(3)	128(3)	5927(2)	33(1)
C(49)	3885(3)	-667(3)	5518(2)	36(1)
C(50)	4636(3)	-1130(3)	5674(2)	35(1)
C(51)	4267(4)	-2040(3)	5674(2)	62(1)
C(52)	4967(6)	-2476(4)	5830(3)	87(2)
C(53)	6021(6)	-1997(5)	5971(3)	100(2)
C(54)	6382(4)	-1114(5)	5959(3)	77(2)
C(55)	5708(4)	-668(3)	5811(2)	54(1)
C(56)	2995(3)	-1072(3)	4975(2)	50(1)
C(57)	2211(4)	-714(3)	4809(2)	53(1)
C(58)	1221(4)	-1217(3)	4238(2)	56(1)
C(59)	1232(4)	-1669(3)	3668(2)	60(1)
C(60)	317(4)	-2161(4)	3152(3)	81(2)
C(61)	-625(4)	-2196(4)	3218(3)	83(2)
C(62)	-650(4)	-1714(5)	3778(3)	92(2)
C(63)	268(4)	-1239(4)	4295(3)	78(2)
C(64)	2389(4)	81(3)	5206(2)	56(1)
C(65)	3269(3)	513(3)	5760(2)	42(1)
C(66)	3352(3)	1344(3)	6184(2)	44(1)
C(67)	3376(3)	2097(3)	5930(3)	57(1)
C(68)	3450(4)	2872(4)	6329(4)	79(2)
C(69)	3523(4)	2898(5)	6977(4)	81(2)
C(70)	3496(4)	2162(5)	7233(3)	73(2)
C(71)	3410(3)	1385(3)	6844(2)	51(1)
C(72)	9987(3)	3135(2)	9881(2)	28(1)
C(73)	11402(4)	1650(3)	8260(2)	51(1)
C(74)	11058(3)	2526(2)	9318(2)	28(1)
C(75)	11912(3)	2950(3)	9114(2)	42(1)
C(76)	12097(4)	2512(3)	8598(2)	52(1)
C(77)	10928(3)	3010(2)	9896(2)	31(1)
C(78)	10550(3)	1225(3)	8451(2)	46(1)
C(79)	10383(3)	1653(3)	8978(2)	37(1)
C(80)	11782(3)	3378(2)	10479(2)	32(1)
C(81)	11762(3)	3854(2)	11042(2)	31(1)
C(82)	12645(3)	4211(3)	11663(2)	40(1)
C(83)	12926(3)	5059(3)	12063(2)	47(1)
C(84)	13742(4)	5382(4)	12645(2)	67(2)
C(85)	14297(4)	4862(5)	12855(3)	84(2)
C(86)	14052(4)	4019(5)	12488(3)	90(2)
C(87)	13224(4)	3696(3)	11881(2)	66(2)
C(88)	10834(3)	3993(2)	11008(2)	34(1)
C(89)	9954(3)	3638(2)	10445(2)	29(1)
C(90)	9028(3)	3851(2)	10477(2)	29(1)
C(91)	8699(3)	3743(3)	11025(2)	40(1)
C(92)	7903(3)	4017(3)	11118(2)	52(1)
C(93)	7465(3)	4423(3)	10645(3)	51(1)
C(94)	7776(3)	4531(3)	10093(2)	49(1)
C(95)	8560(3)	4244(2)	10004(2)	38(1)
N(96)	7702(3)	740(2)	7628(2)	34(1)
O(97)	8062(3)	358(2)	7419(2)	71(1)

Table A7. Bond lengths [Å] and angles [°] for $Fe(NO)T_3C$

Fe(1)-N(96)	1.706(4)
Fe(1)-N(17)	1.881(3)
Fe(1)-N(22)	1.887(3)
Fe(1)-N(1)	1.903(3)
Fe(1)-N(11)	1.904(3)
N(1)-C(2)	1.390(4)
N(1)-C(5)	1.390(4)
C(2)-C(23)	1.406(5)
C(2)-C(3)	1.422(5)
C(3)-C(4)	1.350(5)
C(3)-H(3A)	0.9500
C(4)-C(5)	1.429(5)
C(4)-H(4A)	0.9500
C(5)-C(6)	1.384(5)
C(6)-C(7)	1.390(5)
C(6)-C(24)	1.496(5)
C(7)-N(11)	1.378(4)
C(7)-C(8)	1.419(5)
C(8)-C(9)	1.343(5)
C(8)-H(8A)	0.9500
C(9)-C(10)	1.421(5)
C(9)-H(9A)	0.9500
C(10)-N(11)	1.383(4)
C(10)-C(12)	1.397(5)
C(12)-C(13)	1.366(5)
C(12)-C(48)	1.497(5)
C(13)-N(17)	1.381(4)
C(13)-C(14)	1.428(5)
C(14)-C(15)	1.360(5)
C(14)-H(14A)	0.9500
C(15)-C(16)	1.414(5)
C(15)-H(15A)	0.9500
C(16)-N(17)	1.361(4)
C(16)-C(18)	1.416(5)
C(18)-N(22)	1.360(4)
C(18)-C(19)	1.406(5)
C(19)-C(20)	1.354(5)
C(19)-H(19A)	0.9500
C(20)-C(21)	1.421(5)
C(20)-H(20A)	0.9500
C(21)-C(23)	1.365(5)
C(21)-N(22)	1.380(4)
C(23)-C(72)	1.491(5)
C(24)-C(41)	1.402(5)
C(24)-C(25)	1.406(5)
C(25)-C(32)	1.362(5)
C(25)-C(26)	1.489(5)
C(26)-C(31)	1.376(6)
C(26)-C(27)	1.397(6)
C(27)-C(28)	1.378(6)
C(27)-H(27A)	0.9500
C(28)-C(29)	1.366(8)
C(28)-H(28A)	0.9500

(Table A7 continuous)

C(29)-C(30)	1.403(8)
C(29)-H(29A)	0.9500
C(30)-C(31)	1.371(6)
C(30)-H(30A)	0.9500
C(31)-H(31A)	0.9500
C(32)-C(33)	1.407(5)
C(32)-H(32A)	0.9500
C(33)-C(40)	1.374(5)
C(33)-C(34)	1.467(5)
C(34)-C(35)	1.384(6)
C(34)-C(39)	1.387(6)
C(35)-C(36)	1.390(6)
C(35)-H(35A)	0.9500
C(36)-C(37)	1.357(7)
C(36)-H(36A)	0.9500
C(37)-C(38)	1.376(7)
C(37)-H(37A)	0.9500
C(38)-C(39)	1.388(6)
C(38)-H(38A)	0.9500
C(39)-H(39A)	0.9500
C(40)-C(41)	1.381(5)
C(40)-H(40A)	0.9500
C(41)-C(42)	1.489(5)
C(42)-C(47)	1.375(5)
C(42)-C(43)	1.392(5)
C(43)-C(44)	1.377(5)
C(43)-H(43A)	0.9500
C(44)-C(45)	1.366(6)
C(44)-H(44A)	0.9500
C(45)-C(46)	1.383(6)
C(45)-H(45A)	0.9500
C(46)-C(47)	1.378(5)
C(46)-H(46A)	0.9500
C(47)-H(47A)	0.9500
C(48)-C(49)	1.391(5)
C(48)-C(65)	1.399(5)
C(49)-C(56)	1.371(5)
C(49)-C(50)	1.487(5)
C(50)-C(51)	1.374(6)
C(50)-C(55)	1.379(6)
C(51)-C(52)	1.394(7)
C(51)-H(51A)	0.9500
C(52)-C(53)	1.360(8)
C(52)-H(52A)	0.9500
C(53)-C(54)	1.340(8)
C(53)-H(53A)	0.9500
C(54)-C(55)	1.374(6)
C(54)-H(54A)	0.9500
C(55)-H(55A)	0.9500
C(56)-C(57)	1.403(6)
C(56)-H(56A)	0.9500
C(57)-C(64)	1.363(6)
C(57)-C(58)	1.495(6)
C(58)-C(59)	1.358(6)

(Table A7 continuous)

C(58)-C(63)	1.378(6)
C(59)-C(60)	1.375(6)
C(59)-H(59A)	0.9500
C(60)-C(61)	1.364(7)
C(60)-H(60A)	0.9500
C(61)-C(62)	1.371(7)
C(61)-H(61A)	0.9500
C(62)-C(63)	1.375(7)
C(62)-H(62A)	0.9500
C(63)-H(63A)	0.9500
C(64)-C(65)	1.380(6)
C(64)-H(64A)	0.9500
C(65)-C(66)	1.483(6)
C(66)-C(67)	1.370(6)
C(66)-C(71)	1.380(6)
C(67)-C(68)	1.390(7)
C(67)-H(67A)	0.9500
C(68)-C(69)	1.352(8)
C(68)-H(68A)	0.9500
C(69)-C(70)	1.347(8)
C(69)-H(69A)	0.9500
C(70)-C(71)	1.375(6)
C(70)-H(70A)	0.9500
C(71)-H(71A)	0.9500
C(72)-C(89)	1.399(5)
C(72)-C(77)	1.410(5)
C(73)-C(78)	1.358(6)
C(73)-C(76)	1.378(6)
C(73)-H(73A)	0.9500
C(74)-C(75)	1.376(5)
C(74)-C(79)	1.384(5)
C(74)-C(77)	1.476(5)
C(75)-C(76)	1.375(6)
C(75)-H(75A)	0.9500
C(76)-H(76A)	0.9500
C(77)-C(80)	1.390(5)
C(78)-C(79)	1.372(5)
C(78)-H(78A)	0.9500
C(79)-H(79A)	0.9500
C(80)-C(81)	1.367(5)
C(80)-H(80A)	0.9500
C(81)-C(88)	1.396(5)
C(81)-C(82)	1.462(5)
C(82)-C(87)	1.388(6)
C(82)-C(83)	1.397(5)
C(83)-C(84)	1.362(6)
C(83)-H(83A)	0.9500
C(84)-C(85)	1.366(7)
C(84)-H(84A)	0.9500
C(85)-C(86)	1.372(7)
C(85)-H(85A)	0.9500
C(86)-C(87)	1.405(6)
C(86)-H(86A)	0.9500
C(87)-H(87A)	0.9500

(Table A7 continuous)

C(88)-C(89)	1.384(5)
C(88)-H(88A)	0.9500
C(89)-C(90)	1.483(5)
C(90)-C(91)	1.374(5)
C(90)-C(95)	1.388(5)
C(91)-C(92)	1.396(6)
C(91)-H(91A)	0.9500
C(92)-C(93)	1.385(6)
C(92)-H(92A)	0.9500
C(93)-C(94)	1.368(6)
C(93)-H(93A)	0.9500
C(94)-C(95)	1.390(6)
C(94)-H(94A)	0.9500
C(95)-H(95A)	0.9500
N(96)-O(97)	1.056(4)
N(96)-Fe(1)-N(17)	102.75(14)
N(96)-Fe(1)-N(22)	104.18(14)
N(17)-Fe(1)-N(22)	79.33(13)
N(96)-Fe(1)-N(1)	104.94(14)
N(17)-Fe(1)-N(1)	151.60(13)
N(22)-Fe(1)-N(1)	87.87(12)
N(96)-Fe(1)-N(11)	100.32(14)
N(17)-Fe(1)-N(11)	88.41(13)
N(22)-Fe(1)-N(11)	154.46(12)
N(1)-Fe(1)-N(11)	92.74(12)
C(2)-N(1)-C(5)	107.1(3)
C(2)-N(1)-Fe(1)	126.6(2)
C(5)-N(1)-Fe(1)	124.7(2)
N(1)-C(2)-C(23)	125.0(3)
N(1)-C(2)-C(3)	108.4(3)
C(23)-C(2)-C(3)	126.6(3)
C(4)-C(3)-C(2)	108.3(3)
C(4)-C(3)-H(3A)	125.9
C(2)-C(3)-H(3A)	125.9
C(3)-C(4)-C(5)	107.9(3)
C(3)-C(4)-H(4A)	126.0
C(5)-C(4)-H(4A)	126.0
C(6)-C(5)-N(1)	124.1(3)
C(6)-C(5)-C(4)	127.6(3)
N(1)-C(5)-C(4)	108.3(3)
C(5)-C(6)-C(7)	124.4(3)
C(5)-C(6)-C(24)	115.8(3)
C(7)-C(6)-C(24)	119.8(3)
N(11)-C(7)-C(6)	123.7(3)
N(11)-C(7)-C(8)	108.9(3)
C(6)-C(7)-C(8)	127.3(3)
C(9)-C(8)-C(7)	107.2(3)
C(9)-C(8)-H(8A)	126.4
C(7)-C(8)-H(8A)	126.4
C(8)-C(9)-C(10)	109.0(3)
C(8)-C(9)-H(9A)	125.5
C(10)-C(9)-H(9A)	125.5
N(11)-C(10)-C(12)	125.2(3)

(Table A7 continuous)

N(11)-C(10)-C(9)	107.6(3)
C(12)-C(10)-C(9)	127.2(3)
C(7)-N(11)-C(10)	107.3(3)
C(7)-N(11)-Fe(1)	124.5(2)
C(10)-N(11)-Fe(1)	125.7(2)
C(13)-C(12)-C(10)	123.6(3)
C(13)-C(12)-C(48)	119.4(3)
C(10)-C(12)-C(48)	116.9(3)
C(12)-C(13)-N(17)	119.6(3)
C(12)-C(13)-C(14)	133.1(4)
N(17)-C(13)-C(14)	107.3(3)
C(15)-C(14)-C(13)	107.6(3)
C(15)-C(14)-H(14A)	126.2
C(13)-C(14)-H(14A)	126.2
C(14)-C(15)-C(16)	108.0(3)
C(14)-C(15)-H(15A)	126.0
C(16)-C(15)-H(15A)	126.0
N(17)-C(16)-C(15)	108.4(3)
N(17)-C(16)-C(18)	111.6(3)
C(15)-C(16)-C(18)	140.0(4)
C(16)-N(17)-C(13)	108.7(3)
C(16)-N(17)-Fe(1)	117.3(2)
C(13)-N(17)-Fe(1)	132.2(3)
N(22)-C(18)-C(19)	108.5(3)
N(22)-C(18)-C(16)	111.0(3)
C(19)-C(18)-C(16)	140.4(4)
C(20)-C(19)-C(18)	107.4(3)
C(20)-C(19)-H(19A)	126.3
C(18)-C(19)-H(19A)	126.3
C(19)-C(20)-C(21)	108.7(3)
C(19)-C(20)-H(20A)	125.6
C(21)-C(20)-H(20A)	125.6
C(23)-C(21)-N(22)	120.2(3)
C(23)-C(21)-C(20)	133.2(3)
N(22)-C(21)-C(20)	106.3(3)
C(18)-N(22)-C(21)	109.0(3)
C(18)-N(22)-Fe(1)	117.3(2)
C(21)-N(22)-Fe(1)	131.1(2)
C(21)-C(23)-C(2)	122.8(3)
C(21)-C(23)-C(72)	121.0(3)
C(2)-C(23)-C(72)	116.3(3)
C(41)-C(24)-C(25)	118.2(3)
C(41)-C(24)-C(6)	123.2(3)
C(25)-C(24)-C(6)	118.6(3)
C(32)-C(25)-C(24)	119.7(3)
C(32)-C(25)-C(26)	118.4(3)
C(24)-C(25)-C(26)	121.9(3)
C(31)-C(26)-C(27)	118.7(4)
C(31)-C(26)-C(25)	121.6(4)
C(27)-C(26)-C(25)	119.6(4)
C(28)-C(27)-C(26)	120.5(5)
C(28)-C(27)-H(27A)	119.7
C(26)-C(27)-H(27A)	119.7
C(29)-C(28)-C(27)	120.4(5)

(Table A7 continuous)

C(29)-C(28)-H(28A)	119.8
C(27)-C(28)-H(28A)	119.8
C(28)-C(29)-C(30)	119.6(5)
C(28)-C(29)-H(29A)	120.2
C(30)-C(29)-H(29A)	120.2
C(31)-C(30)-C(29)	119.7(5)
C(31)-C(30)-H(30A)	120.2
C(29)-C(30)-H(30A)	120.2
C(30)-C(31)-C(26)	121.1(5)
C(30)-C(31)-H(31A)	119.4
C(26)-C(31)-H(31A)	119.4
C(25)-C(32)-C(33)	122.8(4)
C(25)-C(32)-H(32A)	118.6
C(33)-C(32)-H(32A)	118.6
C(40)-C(33)-C(32)	116.4(3)
C(40)-C(33)-C(34)	123.1(4)
C(32)-C(33)-C(34)	120.5(4)
C(35)-C(34)-C(39)	117.9(4)
C(35)-C(34)-C(33)	121.2(4)
C(39)-C(34)-C(33)	120.9(4)
C(34)-C(35)-C(36)	121.1(5)
C(34)-C(35)-H(35A)	119.4
C(36)-C(35)-H(35A)	119.4
C(37)-C(36)-C(35)	120.2(5)
C(37)-C(36)-H(36A)	119.9
C(35)-C(36)-H(36A)	119.9
C(36)-C(37)-C(38)	119.8(5)
C(36)-C(37)-H(37A)	120.1
C(38)-C(37)-H(37A)	120.1
C(37)-C(38)-C(39)	120.3(5)
C(37)-C(38)-H(38A)	119.9
C(39)-C(38)-H(38A)	119.9
C(34)-C(39)-C(38)	120.6(5)
C(34)-C(39)-H(39A)	119.7
C(38)-C(39)-H(39A)	119.7
C(33)-C(40)-C(41)	122.6(4)
C(33)-C(40)-H(40A)	118.7
C(41)-C(40)-H(40A)	118.7
C(40)-C(41)-C(24)	120.0(3)
C(40)-C(41)-C(42)	117.1(3)
C(24)-C(41)-C(42)	122.9(3)
C(47)-C(42)-C(43)	118.6(4)
C(47)-C(42)-C(41)	123.5(3)
C(43)-C(42)-C(41)	117.9(3)
C(44)-C(43)-C(42)	120.7(4)
C(44)-C(43)-H(43A)	119.7
C(42)-C(43)-H(43A)	119.7
C(45)-C(44)-C(43)	120.2(4)
C(45)-C(44)-H(44A)	119.9
C(43)-C(44)-H(44A)	119.9
C(44)-C(45)-C(46)	119.7(4)
C(44)-C(45)-H(45A)	120.2
C(46)-C(45)-H(45A)	120.2
C(47)-C(46)-C(45)	120.2(4)

C(47)-C(46)-H(46A)	119.9
C(45)-C(46)-H(46A)	119.9
C(42)-C(47)-C(46)	120.6(4)
C(42)-C(47)-H(47A)	119.7
C(46)-C(47)-H(47A)	119.7
C(49)-C(48)-C(65)	119.3(4)
C(49)-C(48)-C(12)	121.3(3)
C(65)-C(48)-C(12)	119.3(4)
C(56)-C(49)-C(48)	119.1(4)
C(56)-C(49)-C(50)	118.4(4)
C(48)-C(49)-C(50)	122.3(3)
C(51)-C(50)-C(55)	118.4(4)
C(51)-C(50)-C(49)	120.1(4)
C(55)-C(50)-C(49)	121.5(4)
C(50)-C(51)-C(52)	120.5(5)
C(50)-C(51)-H(51A)	119.8
C(52)-C(51)-H(51A)	119.8
C(53)-C(52)-C(51)	119.5(6)
C(53)-C(52)-H(52A)	120.2
C(51)-C(52)-H(52A)	120.2
C(54)-C(53)-C(52)	120.2(6)
C(54)-C(53)-H(53A)	119.9
C(52)-C(53)-H(53A)	119.9
C(53)-C(54)-C(55)	121.4(6)
C(53)-C(54)-H(54A)	119.3
C(55)-C(54)-H(54A)	119.3
C(54)-C(55)-C(50)	120.0(5)
C(54)-C(55)-H(55A)	120.0
C(50)-C(55)-H(55A)	120.0
C(49)-C(56)-C(57)	122.7(4)
C(49)-C(56)-H(56A)	118.7
C(57)-C(56)-H(56A)	118.7
C(64)-C(57)-C(56)	116.6(4)
C(64)-C(57)-C(58)	122.9(4)
C(56)-C(57)-C(58)	120.5(4)
C(59)-C(58)-C(63)	118.9(4)
C(59)-C(58)-C(57)	121.5(4)
C(63)-C(58)-C(57)	119.5(4)
C(58)-C(59)-C(60)	121.6(5)
C(58)-C(59)-H(59A)	119.2
C(60)-C(59)-H(59A)	119.2
C(61)-C(60)-C(59)	119.1(5)
C(61)-C(60)-H(60A)	120.4
C(59)-C(60)-H(60A)	120.4
C(60)-C(61)-C(62)	120.1(5)
C(60)-C(61)-H(61A)	119.9
C(62)-C(61)-H(61A)	119.9
C(61)-C(62)-C(63)	120.1(5)
C(61)-C(62)-H(62A)	119.9
C(63)-C(62)-H(62A)	119.9
C(62)-C(63)-C(58)	119.9(5)
C(62)-C(63)-H(63A)	120.0
C(58)-C(63)-H(63A)	120.0
C(57)-C(64)-C(65)	123.0(4)
C(57)-C(64)-H(64A)	118.5

C(65)-C(64)-H(64A)	118.5
C(64)-C(65)-C(48)	119.2(4)
C(64)-C(65)-C(66)	118.6(4)
C(48)-C(65)-C(66)	122.0(4)
C(67)-C(66)-C(71)	118.1(4)
C(67)-C(66)-C(65)	120.6(4)
C(71)-C(66)-C(65)	121.3(4)
C(66)-C(67)-C(68)	120.2(5)
C(66)-C(67)-H(67A)	119.9
C(68)-C(67)-H(67A)	119.9
C(69)-C(68)-C(67)	120.4(6)
C(69)-C(68)-H(68A)	119.8
C(67)-C(68)-H(68A)	119.8
C(70)-C(69)-C(68)	119.9(6)
C(70)-C(69)-H(69A)	120.0
C(68)-C(69)-H(69A)	120.0
C(69)-C(70)-C(71)	120.5(6)
C(69)-C(70)-H(70A)	119.7
C(71)-C(70)-H(70A)	119.7
C(70)-C(71)-C(66)	120.8(5)
C(70)-C(71)-H(71A)	119.6
C(66)-C(71)-H(71A)	119.6
C(89)-C(72)-C(77)	119.0(3)
C(89)-C(72)-C(23)	121.4(3)
C(77)-C(72)-C(23)	119.4(3)
C(78)-C(73)-C(76)	119.6(4)
C(78)-C(73)-H(73A)	120.2
C(76)-C(73)-H(73A)	120.2
C(75)-C(74)-C(79)	117.8(4)
C(75)-C(74)-C(77)	118.7(3)
C(79)-C(74)-C(77)	123.5(3)
C(76)-C(75)-C(74)	120.9(4)
C(76)-C(75)-H(75A)	119.5
C(74)-C(75)-H(75A)	119.5
C(75)-C(76)-C(73)	120.1(4)
C(75)-C(76)-H(76A)	119.9
C(73)-C(76)-H(76A)	119.9
C(80)-C(77)-C(72)	118.5(4)
C(80)-C(77)-C(74)	118.4(3)
C(72)-C(77)-C(74)	123.1(3)
C(73)-C(78)-C(79)	120.2(4)
C(73)-C(78)-H(78A)	119.9
C(79)-C(78)-H(78A)	119.9
C(78)-C(79)-C(74)	121.3(4)
C(78)-C(79)-H(79A)	119.4
C(74)-C(79)-H(79A)	119.4
C(81)-C(80)-C(77)	123.7(4)
C(81)-C(80)-H(80A)	118.2
C(77)-C(80)-H(80A)	118.2
C(80)-C(81)-C(88)	116.8(3)
C(80)-C(81)-C(82)	123.7(4)
C(88)-C(81)-C(82)	119.5(4)
C(87)-C(82)-C(83)	117.5(4)
C(87)-C(82)-C(81)	120.1(4)
C(83)-C(82)-C(81)	122.4(4)

C(84)-C(83)-C(82)	122.0(4)
C(84)-C(83)-H(83A)	119.0
C(82)-C(83)-H(83A)	119.0
C(83)-C(84)-C(85)	119.6(5)
C(83)-C(84)-H(84A)	120.2
C(85)-C(84)-H(84A)	120.2
C(84)-C(85)-C(86)	121.2(5)
C(84)-C(85)-H(85A)	119.4
C(86)-C(85)-H(85A)	119.4
C(85)-C(86)-C(87)	119.0(5)
C(85)-C(86)-H(86A)	120.5
C(87)-C(86)-H(86A)	120.5
C(82)-C(87)-C(86)	120.6(5)
C(82)-C(87)-H(87A)	119.7
C(86)-C(87)-H(87A)	119.7
C(89)-C(88)-C(81)	122.3(4)
C(89)-C(88)-H(88A)	118.8
C(81)-C(88)-H(88A)	118.8
C(88)-C(89)-C(72)	119.7(3)
C(88)-C(89)-C(90)	116.4(3)
C(72)-C(89)-C(90)	123.9(3)
C(91)-C(90)-C(95)	119.2(4)
C(91)-C(90)-C(89)	118.7(4)
C(95)-C(90)-C(89)	121.7(4)
C(90)-C(91)-C(92)	121.6(4)
C(90)-C(91)-H(91A)	119.2
C(92)-C(91)-H(91A)	119.2
C(93)-C(92)-C(91)	117.9(4)
C(93)-C(92)-H(92A)	121.0
C(91)-C(92)-H(92A)	121.0
C(94)-C(93)-C(92)	121.4(4)
C(94)-C(93)-H(93A)	119.3
C(92)-C(93)-H(93A)	119.3
C(93)-C(94)-C(95)	120.0(4)
C(93)-C(94)-H(94A)	120.0
C(95)-C(94)-H(94A)	120.0
C(90)-C(95)-C(94)	119.9(4)
C(90)-C(95)-H(95A)	120.0
C(94)-C(95)-H(95A)	120.0
O(97)-N(96)-Fe(1)	176.3(4)

Table A8. Torsion angles [°] for $Fe(NO)T_3C$.

N(96)-Fe(1)-N(1)-C(2)	83.4(3)
N(17)-Fe(1)-N(1)-C(2)	-83.4(4)
N(22)-Fe(1)-N(1)-C(2)	-20.7(3)
N(11)-Fe(1)-N(1)-C(2)	-175.1(3)
N(96)-Fe(1)-N(1)-C(5)	-80.3(3)
N(17)-Fe(1)-N(1)-C(5)	112.8(3)
N(22)-Fe(1)-N(1)-C(5)	175.6(3)
N(11)-Fe(1)-N(1)-C(5)	21.1(3)
C(5)-N(1)-C(2)-C(23)	175.2(3)
Fe(1)-N(1)-C(2)-C(23)	9.1(5)
C(5)-N(1)-C(2)-C(3)	-2.4(4)
Fe(1)-N(1)-C(2)-C(3)	-168.5(2)
N(1)-C(2)-C(3)-C(4)	0.6(4)
C(23)-C(2)-C(3)-C(4)	-176.9(3)
C(2)-C(3)-C(4)-C(5)	1.3(4)
C(2)-N(1)-C(5)-C(6)	-176.0(3)
Fe(1)-N(1)-C(5)-C(6)	-9.5(5)
C(2)-N(1)-C(5)-C(4)	3.2(4)
Fe(1)-N(1)-C(5)-C(4)	169.6(2)
C(3)-C(4)-C(5)-C(6)	176.3(4)
C(3)-C(4)-C(5)-N(1)	-2.8(4)
N(1)-C(5)-C(6)-C(7)	-6.2(6)
C(4)-C(5)-C(6)-C(7)	174.9(4)
N(1)-C(5)-C(6)-C(24)	172.7(3)
C(4)-C(5)-C(6)-C(24)	-6.2(5)
C(5)-C(6)-C(7)-N(11)	1.2(6)
C(24)-C(6)-C(7)-N(11)	-177.7(3)
C(5)-C(6)-C(7)-C(8)	-176.4(4)
C(24)-C(6)-C(7)-C(8)	4.8(6)
N(11)-C(7)-C(8)-C(9)	-0.3(4)
C(6)-C(7)-C(8)-C(9)	177.6(4)
C(7)-C(8)-C(9)-C(10)	0.4(4)
C(8)-C(9)-C(10)-N(11)	-0.4(4)
C(8)-C(9)-C(10)-C(12)	178.8(4)
C(6)-C(7)-N(11)-C(10)	-177.9(3)
C(8)-C(7)-N(11)-C(10)	0.1(4)
C(6)-C(7)-N(11)-Fe(1)	19.0(5)
C(8)-C(7)-N(11)-Fe(1)	-163.0(2)
C(12)-C(10)-N(11)-C(7)	-179.0(3)
C(9)-C(10)-N(11)-C(7)	0.2(4)
C(12)-C(10)-N(11)-Fe(1)	-16.2(5)
C(9)-C(10)-N(11)-Fe(1)	163.0(2)
N(96)-Fe(1)-N(11)-C(7)	80.0(3)
N(17)-Fe(1)-N(11)-C(7)	-177.3(3)
N(22)-Fe(1)-N(11)-C(7)	-116.5(3)
N(1)-Fe(1)-N(11)-C(7)	-25.7(3)
N(96)-Fe(1)-N(11)-C(10)	-80.0(3)
N(17)-Fe(1)-N(11)-C(10)	22.7(3)
N(22)-Fe(1)-N(11)-C(10)	83.5(4)
N(1)-Fe(1)-N(11)-C(10)	174.3(3)
N(11)-C(10)-C(12)-C(13)	-0.7(6)
C(9)-C(10)-C(12)-C(13)	-179.7(4)
N(11)-C(10)-C(12)-C(48)	-178.1(3)

(Table A8 continuous)

C(9)-C(10)-C(12)-C(48)	2.8(6)
C(10)-C(12)-C(13)-N(17)	1.5(6)
C(48)-C(12)-C(13)-N(17)	178.9(3)
C(10)-C(12)-C(13)-C(14)	-177.7(4)
C(48)-C(12)-C(13)-C(14)	-0.3(6)
C(12)-C(13)-C(14)-C(15)	-180.0(4)
N(17)-C(13)-C(14)-C(15)	0.8(4)
C(13)-C(14)-C(15)-C(16)	-0.1(4)
C(14)-C(15)-C(16)-N(17)	-0.7(4)
C(14)-C(15)-C(16)-C(18)	179.6(5)
C(15)-C(16)-N(17)-C(13)	1.2(4)
C(18)-C(16)-N(17)-C(13)	-179.0(3)
C(15)-C(16)-N(17)-Fe(1)	167.3(2)
C(18)-C(16)-N(17)-Fe(1)	-12.9(4)
C(12)-C(13)-N(17)-C(16)	179.4(3)
C(14)-C(13)-N(17)-C(16)	-1.2(4)
C(12)-C(13)-N(17)-Fe(1)	16.1(5)
C(14)-C(13)-N(17)-Fe(1)	-164.5(3)
N(96)-Fe(1)-N(17)-C(16)	-86.2(3)
N(22)-Fe(1)-N(17)-C(16)	16.1(3)
N(1)-Fe(1)-N(17)-C(16)	80.8(4)
N(11)-Fe(1)-N(17)-C(16)	173.6(3)
N(96)-Fe(1)-N(17)-C(13)	76.0(4)
N(22)-Fe(1)-N(17)-C(13)	178.3(4)
N(1)-Fe(1)-N(17)-C(13)	-117.0(4)
N(11)-Fe(1)-N(17)-C(13)	-24.2(3)
N(17)-C(16)-C(18)-N(22)	-0.7(5)
C(15)-C(16)-C(18)-N(22)	178.9(5)
N(17)-C(16)-C(18)-C(19)	176.1(5)
C(15)-C(16)-C(18)-C(19)	-4.2(9)
N(22)-C(18)-C(19)-C(20)	-0.3(4)
C(16)-C(18)-C(19)-C(20)	-177.2(5)
C(18)-C(19)-C(20)-C(21)	0.4(4)
C(19)-C(20)-C(21)-C(23)	-174.7(4)
C(19)-C(20)-C(21)-N(22)	-0.3(4)
C(19)-C(18)-N(22)-C(21)	0.1(4)
C(16)-C(18)-N(22)-C(21)	178.0(3)
C(19)-C(18)-N(22)-Fe(1)	-163.8(3)
C(16)-C(18)-N(22)-Fe(1)	14.0(4)
C(23)-C(21)-N(22)-C(18)	175.4(3)
C(20)-C(21)-N(22)-C(18)	0.1(4)
C(23)-C(21)-N(22)-Fe(1)	-23.7(5)
C(20)-C(21)-N(22)-Fe(1)	161.1(3)
N(96)-Fe(1)-N(22)-C(18)	84.0(3)
N(17)-Fe(1)-N(22)-C(18)	-16.6(3)
N(1)-Fe(1)-N(22)-C(18)	-171.1(3)
N(11)-Fe(1)-N(22)-C(18)	-79.2(4)
N(96)-Fe(1)-N(22)-C(21)	-75.7(3)
N(17)-Fe(1)-N(22)-C(21)	-176.3(3)
N(1)-Fe(1)-N(22)-C(21)	29.1(3)
N(11)-Fe(1)-N(22)-C(21)	121.0(4)
N(22)-C(21)-C(23)-C(2)	0.5(5)
C(20)-C(21)-C(23)-C(2)	174.2(4)
N(22)-C(21)-C(23)-C(72)	179.9(3)

(Table A8 continuous)

C(20)-C(21)-C(23)-C(72)	-6.3(6)
N(1)-C(2)-C(23)-C(21)	6.0(5)
C(3)-C(2)-C(23)-C(21)	-176.9(3)
N(1)-C(2)-C(23)-C(72)	-173.5(3)
C(3)-C(2)-C(23)-C(72)	3.7(5)
C(5)-C(6)-C(24)-C(41)	114.2(4)
C(7)-C(6)-C(24)-C(41)	-66.8(5)
C(5)-C(6)-C(24)-C(25)	-63.4(4)
C(7)-C(6)-C(24)-C(25)	115.6(4)
C(41)-C(24)-C(25)-C(32)	-6.2(5)
C(6)-C(24)-C(25)-C(32)	171.6(3)
C(41)-C(24)-C(25)-C(26)	172.4(3)
C(6)-C(24)-C(25)-C(26)	-9.9(5)
C(32)-C(25)-C(26)-C(31)	127.2(4)
C(24)-C(25)-C(26)-C(31)	-51.4(5)
C(32)-C(25)-C(26)-C(27)	-48.4(5)
C(24)-C(25)-C(26)-C(27)	133.0(4)
C(31)-C(26)-C(27)-C(28)	-1.5(6)
C(25)-C(26)-C(27)-C(28)	174.2(4)
C(26)-C(27)-C(28)-C(29)	0.4(8)
C(27)-C(28)-C(29)-C(30)	0.6(8)
C(28)-C(29)-C(30)-C(31)	-0.5(8)
C(29)-C(30)-C(31)-C(26)	-0.6(7)
C(27)-C(26)-C(31)-C(30)	1.6(6)
C(25)-C(26)-C(31)-C(30)	-174.0(4)
C(24)-C(25)-C(32)-C(33)	2.2(6)
C(26)-C(25)-C(32)-C(33)	-176.4(4)
C(25)-C(32)-C(33)-C(40)	3.3(6)
C(25)-C(32)-C(33)-C(34)	-175.1(4)
C(40)-C(33)-C(34)-C(35)	144.2(4)
C(32)-C(33)-C(34)-C(35)	-37.6(6)
C(40)-C(33)-C(34)-C(39)	-37.1(6)
C(32)-C(33)-C(34)-C(39)	141.1(4)
C(39)-C(34)-C(35)-C(36)	-1.0(6)
C(33)-C(34)-C(35)-C(36)	177.8(4)
C(34)-C(35)-C(36)-C(37)	0.5(7)
C(35)-C(36)-C(37)-C(38)	0.2(7)
C(36)-C(37)-C(38)-C(39)	-0.3(7)
C(35)-C(34)-C(39)-C(38)	0.9(6)
C(33)-C(34)-C(39)-C(38)	-177.9(4)
C(37)-C(38)-C(39)-C(34)	-0.2(7)
C(32)-C(33)-C(40)-C(41)	-4.7(5)
C(34)-C(33)-C(40)-C(41)	173.5(4)
C(33)-C(40)-C(41)-C(24)	0.8(6)
C(33)-C(40)-C(41)-C(42)	179.4(3)
C(25)-C(24)-C(41)-C(40)	4.8(5)
C(6)-C(24)-C(41)-C(40)	-172.9(3)
C(25)-C(24)-C(41)-C(42)	-173.8(3)
C(6)-C(24)-C(41)-C(42)	8.6(5)
C(40)-C(41)-C(42)-C(47)	130.5(4)
C(24)-C(41)-C(42)-C(47)	-51.0(5)
C(40)-C(41)-C(42)-C(43)	-48.0(5)
C(24)-C(41)-C(42)-C(43)	130.5(4)
C(47)-C(42)-C(43)-C(44)	0.7(6)

(Table A8 continuous)

C(41)-C(42)-C(43)-C(44)	179.2(4)
C(42)-C(43)-C(44)-C(45)	-0.1(7)
C(43)-C(44)-C(45)-C(46)	-0.4(7)
C(44)-C(45)-C(46)-C(47)	0.4(7)
C(43)-C(42)-C(47)-C(46)	-0.7(6)
C(41)-C(42)-C(47)-C(46)	-179.2(4)
C(45)-C(46)-C(47)-C(42)	0.2(6)
C(13)-C(12)-C(48)-C(49)	112.9(4)
C(10)-C(12)-C(48)-C(49)	-69.5(5)
C(13)-C(12)-C(48)-C(65)	-69.7(5)
C(10)-C(12)-C(48)-C(65)	107.8(4)
C(65)-C(48)-C(49)-C(56)	-2.3(6)
C(12)-C(48)-C(49)-C(56)	175.0(4)
C(65)-C(48)-C(49)-C(50)	-178.2(4)
C(12)-C(48)-C(49)-C(50)	-0.8(6)
C(56)-C(49)-C(50)-C(51)	-47.0(6)
C(48)-C(49)-C(50)-C(51)	128.9(4)
C(56)-C(49)-C(50)-C(55)	132.1(4)
C(48)-C(49)-C(50)-C(55)	-52.0(6)
C(55)-C(50)-C(51)-C(52)	2.0(7)
C(49)-C(50)-C(51)-C(52)	-178.9(4)
C(50)-C(51)-C(52)-C(53)	-1.2(9)
C(51)-C(52)-C(53)-C(54)	0.0(10)
C(52)-C(53)-C(54)-C(55)	0.4(10)
C(53)-C(54)-C(55)-C(50)	0.4(8)
C(51)-C(50)-C(55)-C(54)	-1.5(7)
C(49)-C(50)-C(55)-C(54)	179.3(4)
C(48)-C(49)-C(56)-C(57)	0.4(7)
C(50)-C(49)-C(56)-C(57)	176.4(4)
C(49)-C(56)-C(57)-C(64)	1.8(7)
C(49)-C(56)-C(57)-C(58)	-175.8(4)
C(64)-C(57)-C(58)-C(59)	144.1(5)
C(56)-C(57)-C(58)-C(59)	-38.5(7)
C(64)-C(57)-C(58)-C(63)	-37.4(8)
C(56)-C(57)-C(58)-C(63)	140.1(5)
C(63)-C(58)-C(59)-C(60)	-1.1(8)
C(57)-C(58)-C(59)-C(60)	177.5(5)
C(58)-C(59)-C(60)-C(61)	-0.2(9)
C(59)-C(60)-C(61)-C(62)	2.8(9)
C(60)-C(61)-C(62)-C(63)	-4.1(10)
C(61)-C(62)-C(63)-C(58)	2.7(10)
C(59)-C(58)-C(63)-C(62)	-0.1(9)
C(57)-C(58)-C(63)-C(62)	-178.7(5)
C(56)-C(57)-C(64)-C(65)	-2.2(7)
C(58)-C(57)-C(64)-C(65)	175.3(5)
C(57)-C(64)-C(65)-C(48)	0.4(7)
C(57)-C(64)-C(65)-C(66)	-176.0(4)
C(49)-C(48)-C(65)-C(64)	2.0(6)
C(12)-C(48)-C(65)-C(64)	-175.4(4)
C(49)-C(48)-C(65)-C(66)	178.2(4)
C(12)-C(48)-C(65)-C(66)	0.8(6)
C(64)-C(65)-C(66)-C(67)	-61.1(6)
C(48)-C(65)-C(66)-C(67)	122.7(5)
C(64)-C(65)-C(66)-C(71)	119.2(5)

(Table A8 continuous)

C(48)-C(65)-C(66)-C(71)	-57.1(6)
C(71)-C(66)-C(67)-C(68)	-0.5(6)
C(65)-C(66)-C(67)-C(68)	179.7(4)
C(66)-C(67)-C(68)-C(69)	1.6(7)
C(67)-C(68)-C(69)-C(70)	-1.9(8)
C(68)-C(69)-C(70)-C(71)	1.0(8)
C(69)-C(70)-C(71)-C(66)	0.1(7)
C(67)-C(66)-C(71)-C(70)	-0.4(6)
C(65)-C(66)-C(71)-C(70)	179.4(4)
C(21)-C(23)-C(72)-C(89)	107.0(4)
C(2)-C(23)-C(72)-C(89)	-73.5(4)
C(21)-C(23)-C(72)-C(77)	-78.1(5)
C(2)-C(23)-C(72)-C(77)	101.4(4)
C(79)-C(74)-C(75)-C(76)	-1.3(6)
C(77)-C(74)-C(75)-C(76)	176.8(4)
C(74)-C(75)-C(76)-C(73)	2.7(7)
C(78)-C(73)-C(76)-C(75)	-2.0(7)
C(89)-C(72)-C(77)-C(80)	1.3(5)
C(23)-C(72)-C(77)-C(80)	-173.7(3)
C(89)-C(72)-C(77)-C(74)	-177.1(3)
C(23)-C(72)-C(77)-C(74)	7.9(5)
C(75)-C(74)-C(77)-C(80)	-51.3(5)
C(79)-C(74)-C(77)-C(80)	126.7(4)
C(75)-C(74)-C(77)-C(72)	127.2(4)
C(79)-C(74)-C(77)-C(72)	-54.8(5)
C(76)-C(73)-C(78)-C(79)	-0.1(7)
C(73)-C(78)-C(79)-C(74)	1.4(6)
C(75)-C(74)-C(79)-C(78)	-0.7(6)
C(77)-C(74)-C(79)-C(78)	-178.7(4)
C(72)-C(77)-C(80)-C(81)	0.3(6)
C(74)-C(77)-C(80)-C(81)	178.8(3)
C(77)-C(80)-C(81)-C(88)	-2.2(6)
C(77)-C(80)-C(81)-C(82)	177.5(4)
C(80)-C(81)-C(82)-C(87)	-40.7(6)
C(88)-C(81)-C(82)-C(87)	139.1(4)
C(80)-C(81)-C(82)-C(83)	140.7(4)
C(88)-C(81)-C(82)-C(83)	-39.5(6)
C(87)-C(82)-C(83)-C(84)	0.6(7)
C(81)-C(82)-C(83)-C(84)	179.2(4)
C(82)-C(83)-C(84)-C(85)	-1.2(8)
C(83)-C(84)-C(85)-C(86)	0.5(9)
C(84)-C(85)-C(86)-C(87)	0.8(10)
C(83)-C(82)-C(87)-C(86)	0.7(8)
C(81)-C(82)-C(87)-C(86)	-177.9(5)
C(85)-C(86)-C(87)-C(82)	-1.4(9)
C(80)-C(81)-C(88)-C(89)	2.7(6)
C(82)-C(81)-C(88)-C(89)	-177.1(4)
C(81)-C(88)-C(89)-C(72)	-1.2(6)
C(81)-C(88)-C(89)-C(90)	-179.2(3)
C(77)-C(72)-C(89)-C(88)	-0.9(5)
C(23)-C(72)-C(89)-C(88)	174.0(3)
C(77)-C(72)-C(89)-C(90)	176.9(3)
C(23)-C(72)-C(89)-C(90)	-8.2(6)
C(88)-C(89)-C(90)-C(91)	-47.4(5)

(Table A8 continuous)

C(72)-C(89)-C(90)-C(91)	134.7(4)
C(88)-C(89)-C(90)-C(95)	125.8(4)
C(72)-C(89)-C(90)-C(95)	-52.1(5)
C(95)-C(90)-C(91)-C(92)	0.1(6)
C(89)-C(90)-C(91)-C(92)	173.4(4)
C(90)-C(91)-C(92)-C(93)	-1.3(6)
C(91)-C(92)-C(93)-C(94)	1.8(7)
C(92)-C(93)-C(94)-C(95)	-1.0(7)
C(91)-C(90)-C(95)-C(94)	0.7(5)
C(89)-C(90)-C(95)-C(94)	-172.4(3)
C(93)-C(94)-C(95)-C(90)	-0.3(6)
N(17)-Fe(1)-N(96)-O(97)	-44(6)
N(22)-Fe(1)-N(96)-O(97)	-126(6)
N(1)-Fe(1)-N(96)-O(97)	143(6)
N(11)-Fe(1)-N(96)-O(97)	47(6)